Studies on Poly (Lactic Acid)/Chitosan based Bionanocomposites for Packaging Applications

Thesis submitted in partial fulfillment of the requirements for the degree of

DOCTOR OF PHILOSOPHY

by

AKHILESH KUMAR PAL

(Roll No. 11610723)

Department of Chemical Engineering

Indian Institute of Technology Guwahati

Guwahati – 781 039, India

April, 2017

Dedicated to my beloved

Parents

Department of Chemical Engineering
Indian Institute of Technology Guwahati

CERTIFICATE

This is to certify that the thesis entitled "**Studies on Poly (Lactic Acid)/Chitosan based Bionanocomposites for Packaging Applications"**, being submitted by **Akhilesh Kumar Pal** for the award of Ph.D. degree has been carried out by him at the Department of Chemical Engineering, Indian Institute of Technology Guwahati, under my guidance and supervision. The work documented in this thesis has not been submitted to any other University or Institute for the award of any degree or diploma.

(Dr. Vimal Katiyar)
Associate Professor
Department of Chemical Engineering
Indian Institute of Technology Guwahati
Guwahati - 781 039, India.

Acknowledgement

With great pleasure and profound sense of gratitude, I take this opportunity to express my heartfelt and sincere thanks to my learned guide Dr. Vimal Katiyar, for his valuable guidance and encouragement provided to me throughout the course of my PhD work. His great enthusiasm and extremely hard working attitude kept me inspired all through. I would like to acknowledge sincerely the support, encouragement and valuable criticism provided by my Doctoral Committee members Dr. Chandan Das, Dr. Amit Kumar and Dr. A. S. Achalkumar. I wish to place on record the use of facilities and sophisticated instruments available at Center of Excellence for Sustainable Polymers (CoE-SusPol) and Central Instruments Facility (CIF), IIT Guwahati for carrying out instrumental analysis part of my research work. I would also like to thank the heads and all authorities of the department of chemical engineering for providing me all research and analytical facilities required for my work. I am extremely thankful to the technical staff (teaching and non-teaching) of the chemical engineering department, particularly Ritumoni Kalita, Harsaraj Biswanath, Dipak Kumar Barman, Jayanta Kumar Mout, Dr. Lukumoni Borah, Debajit Borah, Pankaj Sekhar Baruah, Deep Jyoti Sinha, Sailen Das and Bhagya Boro for providing me all help and assistance for the completion of my work. My heartfelt thanks are due to Dr. Neelima Tripathi for providing me timely help and support at all times along the way. My thanks are also due to all my labmates, especially Arvind Gupta, Prodyut Dhar, Surendra Singh Gaur, Gourhari Chakraborty, Medha Mili, Monika, Narendren S, Shasanka Sekhar Borkotoky, Melaku Tesfaye, Siddharth Mohan Bhasney, Naba Kumar Kalita, Arvind Prasad, Kiran Kumar Gali, other lab members and Lakhya Dhar Boro (lab attendant) for all kinds of help and morale support made available to me in the lab. I wish

to place on record, my thankfulness to my close friends Saurabh Pandey and Pawan Kumar for boosting my morale at the difficult moments. Last but not least, from the core of my heart, I wish to acknowledge the encouragement, support and love from my parents and wife. At the end, I wish to thank sincerely one in all who helped me directly or indirectly to complete my research work. *Blessings of Almighty are always solicited*.

[Akhilesh Kumar Pal]

Abstract

Nowadays, bio-based polymers such as poly (lactic acid) (PLA) and chitosan (CH) have attracted much attention because of their environment friendliness and biodegradability. Poly (lactic acid) has proved to be the most promising biodegradable polymer which has been consumed in wide variety of applications. Due to its desirable properties such as transparency, bio-safety and compostability, it has been used in promising applications such as consumer goods, fibers, biomedicines and packaging. However, PLA has some limitations such as lower barrier properties, glass transition temperature, melting temperature and short degradation rate as compare to conventional polymers such as polyethylene terephthalate and polystyrene. Hence, it cannot be used efficiently in food packaging applications. Such limitations of PLA can be eliminated by mixing it with other biodegradable polymer which should have film forming ability. Literature survey revealed that chitosan, a biodegradable polymer, has good film forming ability with excellent barrier properties. Chitosan has been extracted from the exoskeleton of various natural resources such as crabs, lobsters, shrimps, insects etc. However, as per the literature survey, it has not been extracted from Muga silkworms till date. It is noteworthy to mention that chitosan is not compatible with PLA due to its hydrophilic nature and cannot be utilized in packaging and other applications due to non-melting behaviour. The incompatibility behaviour of PLA with chitosan has been studied by **Suyatma et al., 2004**. They have fabricated PLA/chitosan blend to check the improvement in water vapor transmission rate as well as mechanical property. The results showed an improvement in water vapor transmission rate whereas, elastic modulus and tensile strength were decreased due to agglomeration of filler. Hence, researchers have found many ways such as blending, mixing and grafting to avoid such limitations. As per the available literature, such techniques were

conducted by using various initiators, catalysts, additives and solvents in order to improve the functionalization, productivity and transformation of its nature from hydrophilic to hydrophobic. When the functionalized low/high molecular weight copolymer reacts with the matrix polymer, it may result the enhancement in physico-chemical and other properties. Various polymer film/sheet formation techniques such as solution casting, layer by layer approach, melt blending etc. have been used and the resultant polymers have shown improvements upto a good extent in their barrier and other properties. It is noteworthy to mention that the catalyst or initiators used in functionalization are toxic in nature, which cannot be permitted to use in food packaging applications. Further, some techniques such as solution casting and layer by layer approach are not industrially viable. It was also inferred that very less efforts have been made to synthesize a bio-based chitosan grafted copolymer which when blends with PLA, it disperses uniformly in the form of spherical aggregates in hydrophobic PLA matrix. The fabricated bionanocomposite films may sustain better barrier properties as compare to that of PLA, which are also comparable to that of conventional plastics used for food packaging applications. Hence, it was observed that no work has been published on: (a) extraction of chitin and chitosan from Muga silkworms (MS) (*Antheraea assamensis*), (b) synthesis of modified hydrophobic chitosan grafted copolymer using lactic acid, (c) use of chitosan based copolymer in PLA for food packaging applications using solution casting as well as melt extrusion techniques.

As a result, the present doctoral work is mainly focused on food packaging application. In this research work, chitin and chitosan are extracted upto ~8 and ~7 wt% respectively from Muga silkworms and well characterized. Degree of deacetylation is found in the range of 77-97%. Further, chitosan is used as a filler in PLA matrix to fabricate poly (lactic acid)/chitosan based

biocomposite films for food packaging application. However, the semicrystalline biocomposite films are not found suitable for same application due to reduction in mechanical strength and increment in water vapour transmission rate due to agglomeration. Moreover, chitosan has been chosen for functionalization with lactic acid due to have reactive amine group. Polycondensation reaction has been used for grafting of lactic acid oligomer on chitosan backbone with the help of conventional heating and microwave heating methods. As a result, it is found that lactic acid oligomer binds selectively at amine group of chitosan, which is also proved with the help of various analyses such as FTIR and NMR. Further, the formulated chitosan copolymer is used as a filler in PLA matrix for the fabrication of PLA/CH-*g*-OLLA bionanocomposite films with the help of various techniques such as solution casting and melt extrusion. The results shows that the glass transition temperature has been reduced more than 18 °C as compare to that of pristine PLA. However, the mechanical properties have been found comparable with PLA except its elongation, which has been improved significantly. The oxygen gas permeability of pristine PLA has been reduced upto ~90.4% with the increment of 5 wt% in filler loading. Further, non-isothermal degradation and isothermal crystallization kinetics of pristine PLA and its bionanocomposite films have been performed in order to check their rate of degradation and crystal growth respectively. Finally, it has been observed that the fabricated PLA/CH-*g*-OLLA bionanocomposite films can be one of the best alternatives in food packaging application.

Contents

List of Figures

List of Tables

Nomenclature

Abbreviations

ASTM	American society for testing and materials
ATR	Attenuated total reflectance
C	Solution concentration
C*	Chroma
CA	Contact angle
CH	Chitosan
CH-*g*-OLLA	Chitosan-*graft*-oligo(l-lactic acid)
D	Diffusion coefficient
d	Interlayer spacing
DA%	Degree of acetylation
DD%	Degree of deacetylation
DMA	Dynamic mechanical analysis
DSC	Differential scanning calorimetry
E	Young's modulus
e	Film thickness
EDX	Energy dispersive X-ray spectroscopy
FDA	Food and drug administration
FESEM	Field emission scanning electron microscopy
FTIR	Fourier transform infrared spectroscopy
F-W-O	Flynn-wall-ozawa
G	Growth rate
GPC	Gel permeation chromatography

ΔH_m	Enthalpy of melting
ΔH_{cc}	Enthalpy of cold crystallization
I_{cr}	Crystallinity index
K-A-S	Kissinger-Akahira-Sunose
LA	Lactic acid
M_n	Number average molecular weight
M_v	Viscosity average molecular weight
M_w	Weight average molecular weight
MS	Muga silkworms
NMR	Nuclear magnetic resonance
OLLA	Oligomer of l- lactic acid
P	Oxygen permeability
PBAT	Poly(butylene adipate-co-terephthalate)
PBSA	Polybutylene succinate
PC	Polycarbonate
PCL	Polycaprolactone
PE	Polyethylene
PEA	Polyesteramide
PEG	Poly (ethylene glycol)
PHA	Polyhydroxyalkanoates
PLA	Poly (lactic acid)
PLA/CH	Poly (lactic acid)/chitosan
PLA/CH-*g*-OLLA	Poly (lactic acid)/chitosan-*graft*-oligo (l-lactic acid)

POM	Polarized optical microscopy
PP	Polypropylene
PTT	Poly(trimethylene terephthalate)
RBF	Round bottom flask
S	Solubility coefficient
SEM	Scanning electron microscopy
$t_{1/2}$	Half-time
TEM	Transmission electron microscopy
TGA	Thermogravimetric analysis
TG-FTIR	Hyphenated thermogravimetric-Fourier transform infrared spectroscopy
WVP	Water vapour permeability
WVTR	Water vapour transmission rate
XRD	X-ray diffractometry

Notations

A	Pre-exponential factor
E_a	Activation energy
K	Avrami kinetic constant
R	Universal gas constant
T_g	Glass transition temperature
T_o	Onset degradation temperature
T_{cc}	Cold crystallization temperature

T_m	Melting temperature
T_P	Peak temperature
T_{max}	Maximum temperature
T_{off}	Offset temperature

Greek letters

α	Degree of conversion
θ	Diffraction angle
β	Heating rate
η	Intrinsic viscosity
σ	Ultimate tensile strength
ε	Elongation at break

Chapter 1
Introduction

The chapter briefly describes about bio-based, non-toxic and biodegradable polymers. The benefits, limitations and applications of bio-based polymers over petroleum based products are highlighted. The chapter also provides general overview of the origin, chemical structure, properties, challenges and applications of bio-based polymers and polysaccharides. The chapter mainly focuses on various aspects of poly (lactic acid) and chitosan. The chapter also presents literature survey on bio-based materials such as poly (lactic acid) and polysaccharide chitosan. Some major outcomes reported so far on extraction, modification and utilization of chitosan in packaging and other applications are highlighted. The objective of the thesis is fabrication of bionanocomposite film fabrication by utilizing chitosan and poly (lactic acid) as precursors using solution casting as well as melt extrusion techniques.

1.1. Background and context

The use of plastic in packaging currently consumes about 66.5% of all plastic production. About half of this amount is used in food packaging which is largely dominated by petrochemical derived plastics. Conventional smaller and regular food packaging plastics typically thrown to the fields which does not degrade and due to smaller in size, waste disposable management is a critical concern **[Tang et al., 2012]**. Further, such kind of conventional packaging does not meet increasing demands in society for sustainability and environmental safety. Plastics are crucial part of our day to day life and as per current situation, it is very difficult to survive without plastics. It is noteworthy to mention that most of the plastics are being developed using fossil based feedstocks such as petroleum products, which took millions of years for its conversion inside the earth crust from dead plants, which means the conventional plastics are not from renewable resources. In conclusion, revolution of our industrial development leads to the value added plastics and

its products. Therefore, it is essential to possibly recycle such plastics instead of incineration, which leads to more carbon footprint to our ecological system for millions of years. However, if such plastics are not recycled through efficient waste disposal mechanism, can leads to the landfills and enhance more solid waste related hazards. However, synthetic plastics can be replaced by bio-based precursors, which reduce the carbon footprint and leads to degrade plastic products within stipulated time period. As per the standards, plastics may be considered as degradable plastic, if it is clearly evident that bio-based and biodegradable plastics have unique advantage of leaving low carbon foot-print and approximately no solid waste hazards due to its degradation and 90% of its carbon content is converted into CO_2 in 180 days. In this class, there are various polymer resins, which comes under the class of biodegradable plastics and produce commercially worldwide. These include poly (lactic acid) (PLA), poly (hydroxyalkanoate) (PHA), poly (ε-caprolactone) (PCL) and other polysaccharide based thermoplastics. However, among all, PLA is most versatile plastic having glass transition temperature (T_g) of ~55-60 ºC depending on the molecular weight of PLA. Mechanical properties of the plastic are comparable with some of the conventional plastics such as polyethylene (PE), polystyrene (PS), polypropylene (PP) with improved gas barrier properties. Hence, biodegradable plastics such as PLA, PCL, poly (hydroxybutyrate) (PHB) have potential to replace the commodity plastics. Among these, PLA produced by enantiomeric lactic acid, which metabolized into human body, have significant applications in biomedical areas including orthopedic fixation devices and implants, due to having glass transition temperature higher than room temperature and high OTR, which makes it suitable for biomedical applications as well as stringent food packaging. Further above polymers have lower heat stability temperature, hence, can't be used under mechanical load at elevated temperature. PLA is a bio-based thermoplastic polyester derived from renewable resources

such as corn, starch, sugarcane, etc. **[Rasal et al., 2010]**. There are two existing methods for manufacturing PLA from lactic acid. The first method uses lactide as an intermediate stage and second method is direct polymerization of lactic acid. PLA can be used in variety of applications such as packaging, drug delivery, tissue engineering, biomedical etc. Some limitations of PLA are its poor toughness, slow degradation rate, hydrophobicity etc.

Food packaging is used to protect food from the environment and to maintain the food quality for certain time interval. Different materials such as glass, metal, paper and plastics are used in food packaging. Plastics have good material properties and low cost, so they are preferred over other packaging materials. Plastics can be either made by addition polymerization or condensation polymerization of hydrocarbons which originate from the petrochemical industries. To overcome the limitations of biodegradable plastics, the development of modern techniques is going on, so that improved barrier, thermal and mechanical properties can be achieved. Chemical modification of biopolymers is a one modern technique in which different biopolymers with plasticizers and modifiers are mixed together to increase different properties. A number of bio-based plastics e.g. PLA, polyethylene terephthalate (PET), poly trimetylene terphthalate (PTT), PP, PE, PHA, poly butylene succinate (PBS) and poly propylene carbonate (PPC) are commercially available. The structures of commercially available polymers are shown in Figure 1.1. But all the bio-based plastics are not biodegradable at different levels such as PP, PE, PET, PTT and polyamides. The rest plastics (PLA, PHA, PBS and PPC) are biodegradable, environmental friendly and low carbon foot-print bioplastics having less dependency on petroleum products. These plastics are the most promising candidates for future applications **[Peelman et al., 2013]**. The growth of biodegradable plastics demand reached up to 15% annually till 2015 and the percentage of biodegradable plastics (used for packaging) has grown upto 66.5% till 2016 as shown in Figure 1.2.

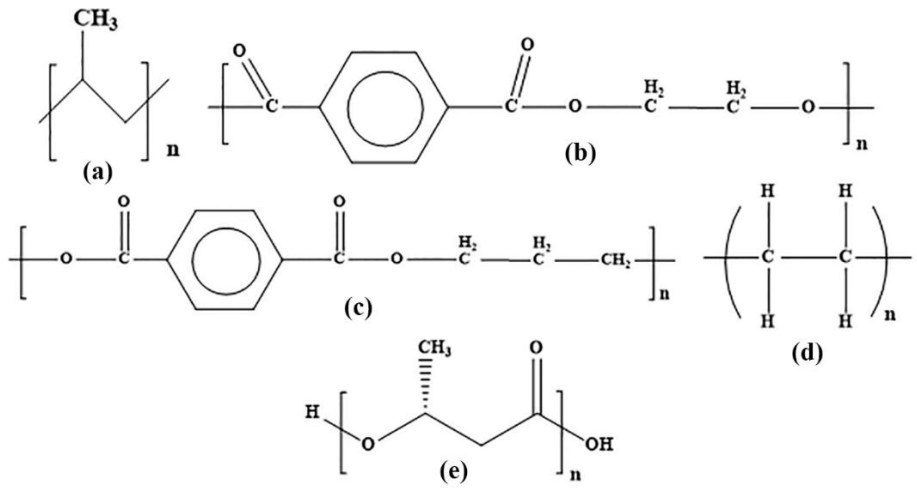

Figure 1.1. Different structures of bio-based Polymers; (a) Polypropylene, (b) Polyethylene terephthalate, (c) Polytrimethyl terephthalate, (d) Polyethylene and (e) Polyhydroxyalkanoates.

The advantages of using bioplastics in packaging show the improvement of strength, stiffness, oxygen barrier, moisture barrier, resistance to food component attack and flexibility, which has increased its consumption in global market.

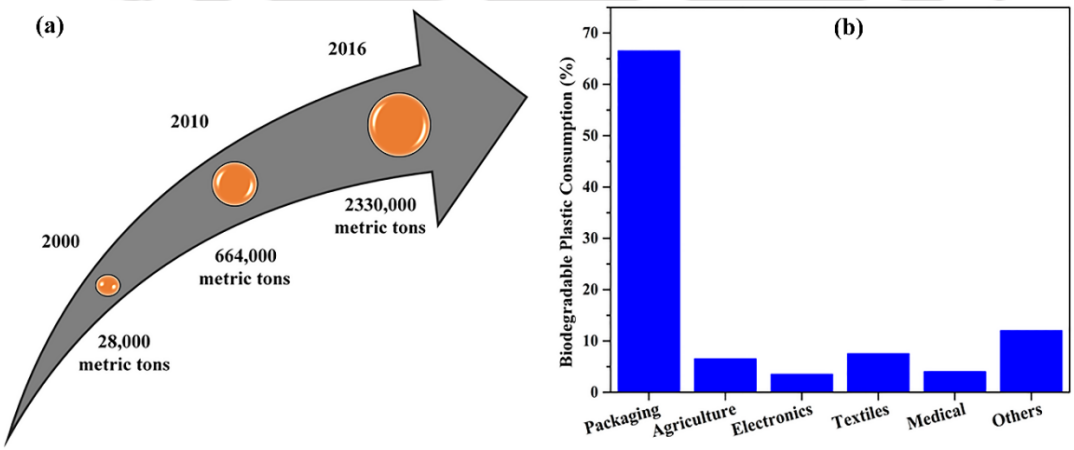

Figure 1.2. (a) Increment in demand of biodegradable plastics and (b) Global consumption of biodegradable plastics **[http://www.plastemart.com/Plastic-Technical-Article.asp?LiteratureID=1958&Paper=biodegradable-plastics-demand-to-grow-15-percent-annually-to-2015]**.

1.1.1. Poly (lactic acid)

Lactic acid based polymer i.e. poly (lactic acid) is a synthetic environment friendly polymer which is obtained from natural resources like corn, sweet potato, sugar feedstock, wheat, maize and waste products from food or agriculture industry by fermentation etc. **[Bocchini et al., 2010]**. It belongs to the family of aliphatic polyesters. The monomer unit of poly (lactic acid) is 2-hydroxy propionic acid. It is biodegradable, non-toxic and hydrophobic in nature. It has enormous potential to substitute a wide variety of conventional fossil fuel based packaging plastics and have been demonstrated to be even commercially viable. The following Figure 1.3 shows natural resources of lactic acid, its chemical structure and polymerization routes. The formation of PLA is possible either by direct polycondensation or ring opening polymerization of lactic acid **[Lunt, 1998]**. It is a biodegradable polymer with a reasonable shelf life for a wide variety of consumer products, such as food packaging films, paper coatings, moulded articles and fiber applications **[Datta et al., 1995]**. It is observed that PLA degrades slowly by simple hydrolysis of the ester bond to convert into harmless, natural products like CO_2 and H_2O **[Drumright et al., 2000]**. Hence, it could be a functional and economical replacement to the large amount of existing non-biodegradable plastics, used in the worldwide. According to the available literature, the degradation time in the environment is of the order of six months to two years **[Ohara et al., 2003]**. Lactic acid is polymerized by bulk polycondensation to yield a viscous, brittle and glassy material (molecular weight up to 10,000 Da). The molecular weight actually depends on the various polymerization conditions. Presence of water in the prepared material is the reason for low molecular weight polymer. Various unwanted side chain reactions such as transesterification, ester exchange and backbiting equilibrium reactions come in picture due to the low concentration of reactive end groups which favours the formation of lactide as byproduct **[Garlotta, 2002]**.

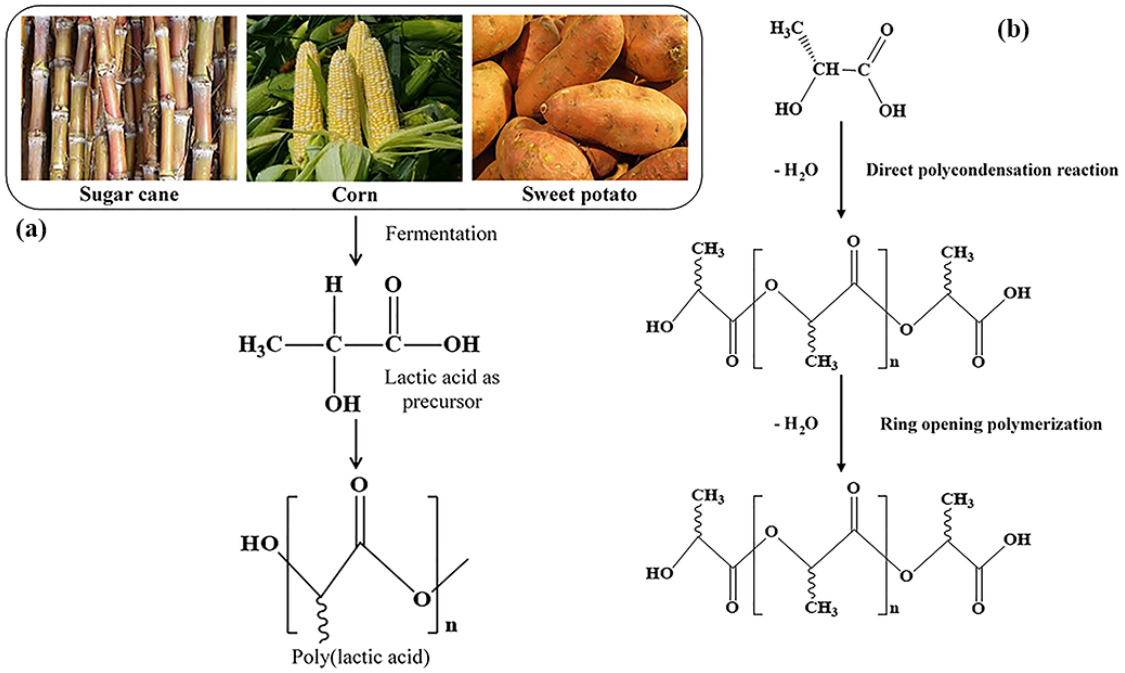

Figure 1.3. (a) Natural resources of lactic acid and (b) various routes of lactic acid polymerization.

1.1.1.1. Properties of poly (lactic acid)

Poly (lactic acid) is eco-friendly in nature because it is derived from renewable natural resources. It is biodegradable, recyclable and compostable. It does not produce carcinogenic effect in local tissues i.e. biocompatible and non-toxic. It has better thermal processability than other conventional bio-based polymers. It requires 25-55% less energy for production than the petroleum based polymers **[Rasal et al., 2010]**. High molecular weight PLA is a glossy, colourless, stiff and thermoplastic in nature. Its properties are similar to polystyrene. PLA is a semicrystalline polymer and shows all the different phases at different temperatures like T_g, cold crystallization temperature (T_{cc}) and melting temperature (T_m). These temperatures are very much dependent on the isomers of PLA. All the characteristic temperatures decrease with increase in content of D-isomer. Amorphous PLA is prepared from meso- or rac-lactide. The melting temperature enthalpy for pure PLA is estimated in the range between 93 J/g and 148 J/g **[Lunt, 1998; Miyata et al., 1998]**.

The mechanical properties of PLA are significantly influenced by its molecular weight and degree of crystallinity. The variation in these two controlling properties can change the behaviour of PLA from soft and elastic nature to stiff and high strength nature. However, after annealing of the same PLA, the crystallinity and the impact resistance increase due to the crosslinking effects in the crystalline region. The tensile strength of PLA depends on the stereoregularity of the chain **[Nakagawa et al., 2003]**. Solubility is an important property for proper dispersion of PLA in any solvent. Solubility depends on polymer molecular weight and degree of crystallinity. Crystalline PLA is only soluble in benzene and chlorinated solvents. On the other hand, Amorphous PLA is soluble in most organic solvents such as benzene, acetonitrile, chlorinated solvents, tetrahydrofuran and dioxane.

1.1.1.2. Limitations of poly (lactic acid)

The demand for biodegradable polymers such as PLA with excellent material properties is increasing very rapidly. However, some limitations such as lower thermal and mechanical properties (as required for engineering applications) of PLA restrict it for some specific applications only. PLA is not suitable for high strength, high performance and high temperature applications, due to its weak mechanical properties and low heat deflection temperature. The oxygen transmission rate (OTR) is an important parameter for a good quality food packaging. PLA has lower OTR range than PET so barrier properties of PLA is not as good as PET. The degradation time of PLA is short so it is not applicable for engineering applications **[Carrasco et al., 2010]**. The improvement in PLA properties such as ultimate tensile strength, storage modulus, flexural modulus and elongation at break can be possible, when mixed with layered silicates. A lot of literature is available for poly (lactic acid)/clay nanocomposite (PLACN) with montmorillonite (MMT), synthetic mica and smectite clays in order to improve the mechanical, barrier and physicochemical properties **[Chang et al., 2003]**.

1.1.1.3. Applications of poly (lactic acid)

There are a wide range of applications of PLA based on the material properties and manufacturing processes. The major applications of PLA are in food packaging and biomedical materials **[Inkinen et al., 2011]** as shown in Figure 1.4. Lactic acid can also be utilized in various applications such as buffering agent, acidic flavouring agent, acidulant and bacterial inhibitor in many processed foods **[Garlotta, 2002]**.

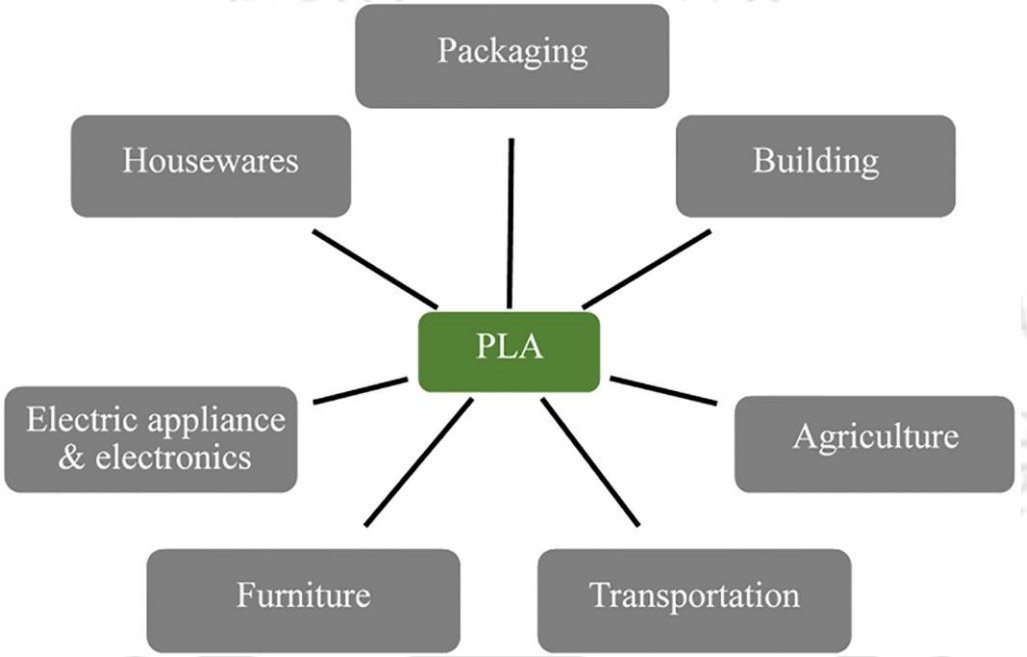

Figure 1.4. Poly (lactic acid) utilization in various applications.

1.1.2. Chitosan

Chitin and chitosan (CH) are promising, versatile and highly bioactive polysaccharides, which exist in the category of biomaterials. Chitin, a second most abundant polysaccharide after cellulose in nature, is nitrogenous polysaccharide, rigid and inelastic, which is extracted from the internal structure and exoskeleton of invertebrates such as shellfish, lobsters, insects and many more **[Dash et al., 2011; Nemtsev et al., 2004; Paulino et al., 2006]** as shown in Figure 1.5(a). Primarily, it is a composition of

2-amino-2-deoxy-D-glucose units, which is a derivative of cellulose. The only difference between cellulose and chitin is the presence of acetamide (-$NHCOCH_3$) functional group in place of -OH group at C2 position. Chitin exists in three types of polymorphs i.e. α-chitin, β-chitin and γ-chitin. The only difference in all three chitins is the arrangement of polymer chains as shown in Figure 1.5(b). Approximately, ten billion tons of chitin is produced every year from crustaceans, molluscs, algae, insects and fungus. Chitosan is a copolymer of two monomers i.e. D-glucosamine (DG) and N-acetyl-D-glucosamine (NADG) **[Zhao et al., 2011]**. Basically, shells are the waste material for seafood lovers. Around 40-50% part of seafood is only shells and shells are having enormous amount of chitin. Chitin is extracted from the shells by two methods i.e. biological method and chemical method. The extracted amount of chitin is less by biological method than chemical method so chemical method is preferred for chitin extraction. Chitosan is extracted from chitin by deacetylation process. Chitin is not completely converted in to chitosan and it depends on degree of deacetylation (DD%). If the DD% is higher, chitosan part is more and vice versa. On the other hand, higher DD% gives lower molecular weight chitosan and vice versa. The conversion of chitosan from chitin depends on distinct parameters such as deacetylation time, temperature and alkali concentration. If deacetylation time is more, conversion will be more. The main difference in chitosan and chitin is the functional group situated at carbon-carbon of the monomeric unit. Chitin is the most available natural polymer after cellulose and the solubility and reactivity of chitosan is greater than chitin because of presence of free amine groups in chitosan **[Tang et al., 2007]**. Chitosan is approved as a food additive by Food and Drug Administration (FDA) as it is found to be non-toxic after oral administration in human being. In an in vitro condition, chitosan degrades by the enzymes, such as chitosanase,

lysozyme and papain and under in vivo condition, it is degraded by lysozyme **[Nair et al., 2007]**.

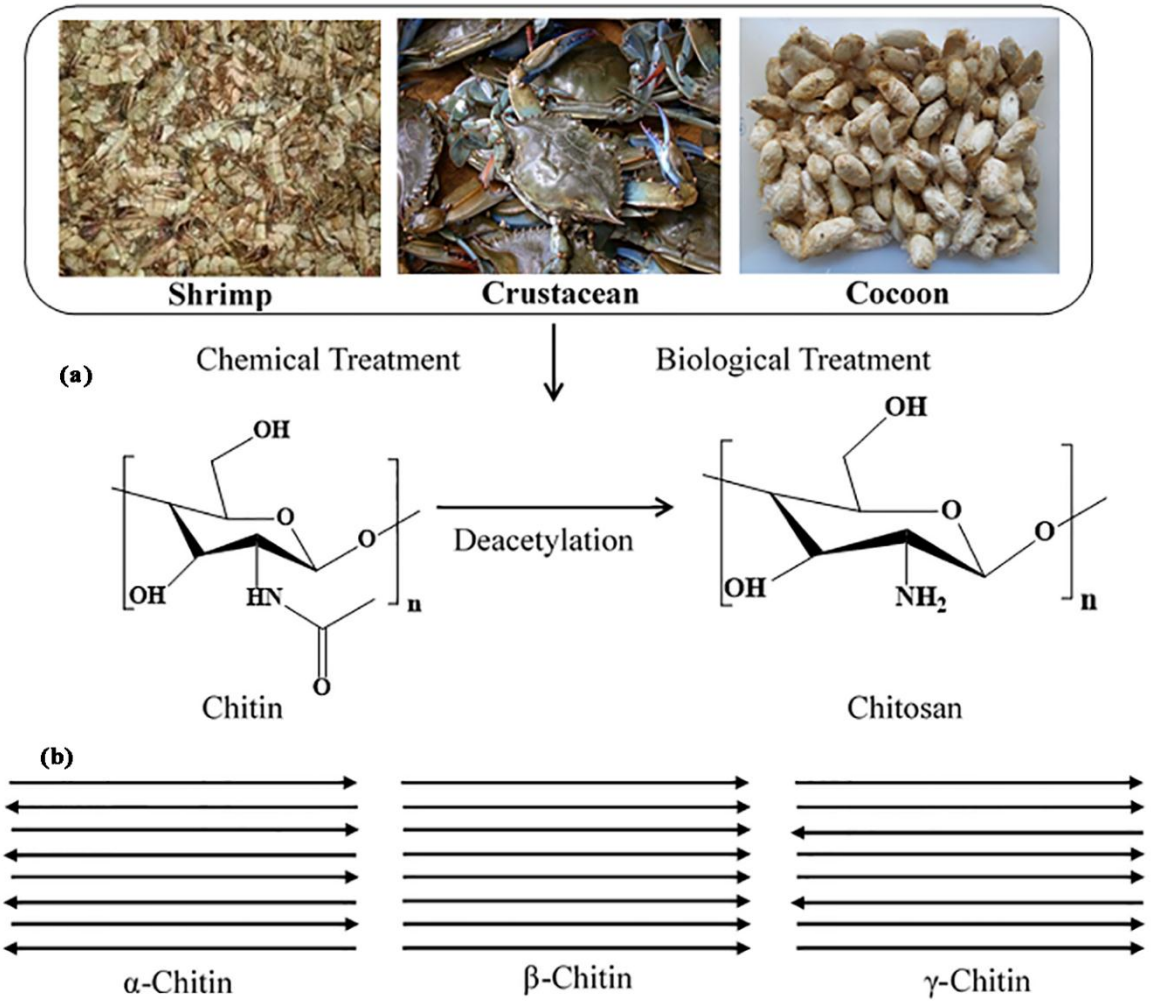

Figure 1.5. (a) Natural resources of chitosan and (b) various polymorphs of chitin.

1.1.2.1. Properties of chitosan

The most important properties of chitosan are solubility, flexibility, polymer conformation and viscosity. These properties are different for chitin and chitosan. DD% is very important to check the solubility of chitosan. If the degree of deacetylation is more than 50% then it is confirmed that the prepared polymer is chitosan and it is soluble in acidic solvent and if the DD% is less than 50% or degree of acetylation (DA%) is higher than 50% then it is

chitin and it is insoluble in acidic conditions **[Balazs et al., 2007]**. Actually, DD% and DA% are opposite to each other. Basically, Chitosan is hydrophilic in nature. It is soluble in weak acidic solutions. It is not soluble in chlorinated and organic solvents. Chitosan is highly reactive than chitin because of having a versatile amino group at C2 position. It is also a good proton conducting biopolymer electrolyte. The versatility of chitosan is only based on the reactive amino group. If the pH is high, chitosan is insoluble because chitosan's amines are deprotonated and reactive at high pH (>6.5) as shown in Figure 1.6. On the other hand, chitosan is soluble at low pH (<6) because it is protonated at low pH and converts in to NH_3^+ **[Dash et al., 2011]**.

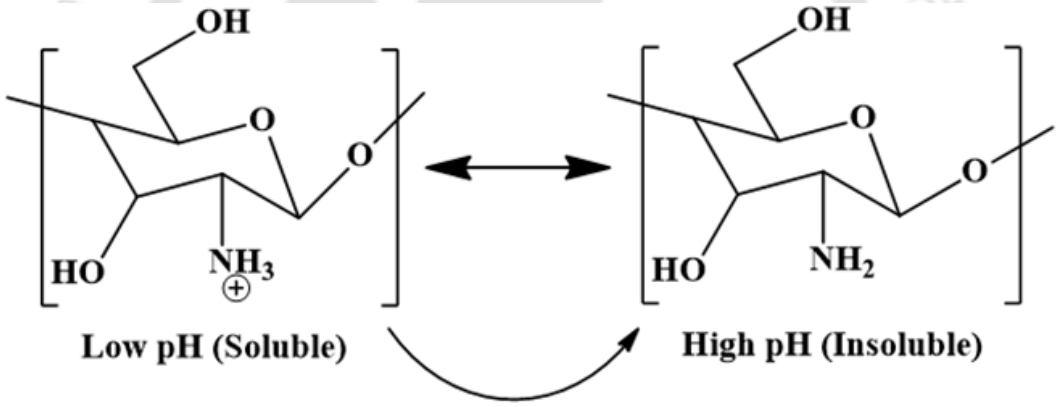

Figure 1.6. Schematic diagram of chitosan versatility **[Dash et al., 2011]**.

1.1.2.2. Limitations of chitosan

Chitosan has versatile properties that's why it is applicable in different fields. It has film forming ability and sustain very high gas barrier properties. On the other hand, it has some limitations. An existing limitation of chitosan is that it shows poor mechanical and weak water resistance in the presence of water and humidity because it is hydrophilic in nature. These properties can be improved by adding plasticizers and salt, cross linking of polysaccharides, use of suitable solvent, chemical modification of hydroxyl groups, change

in pH, the addition of different polysaccharides and blending with other polymers. The other drawback is its solubility because it is dissolved only in acidic medium. The film forming ability of chitosan can't be utilized without the addition of plasticizer or sufficient modifier due to its brittleness **[Baskar et al., 2009; Dash et al., 2011; Feng et al., 2012]**.

1.1.2.3. Applications of chitosan

Chitosan, a versatile biopolymer, is very much used in several manufacturing and industrial processes such as textile, agriculture, medical, pharmaceutical, waste water treatment, food packaging and food process **[Adlim et al., 2004]** as shown in Figure 1.7. The vast applications of chitosan are such as Food Packaging, film former capability, drug delivery, hydrogel, wound healing, beauty products, antioxidant agent, antimicrobial agent, filler in tablets, pharmaceutical applications, coating material, plant protection, natural seed treatment, plant growth enhancer, ecologically friendly biopesticide substance, water filtration, fining agent in winemaking, diluent, muco adhesive polymer, permeation enhancer, disintegrating agent. Chitosan nanoparticles show different properties like good biocompatibility, stability, biodegradability and due to these properties it is used as good drug carrier. One advantage of having small size is that it passes from biological barriers in vivo such as the blood-brain barrier **[Ali et al., 2011]**. Many bioadhesive and drug delivery systems based on chitosan nanoparticles are under process. On the other hand, it is also very much used in tissue engineering for developing drug delivery devices and as scaffolds. Solubility is one important property of chitosan due to which it is fabricated in too many forms like gels, microspheres, nanospheres **[Nair et al., 2007]**. Chitosan has some applications in fuel cells field also. It is used for structural reorganization of tight junction associated proteins which is the result of its interaction with the cell membrane so it also has the ability to act as a permeation enhancer. As discussed earlier, chitosan has high chemical reactivity which is very useful factor for cancer therapy **[Nair et al., 2007]**. One

composite material is also exist which is made of chitosan and silver. It shows higher antibacterial and antimicrobial activity and the work is going on to improve these kinds of properties. One advantage is also there that the chitosan composites are economical and efficient **[Lin et al., 2011]**.

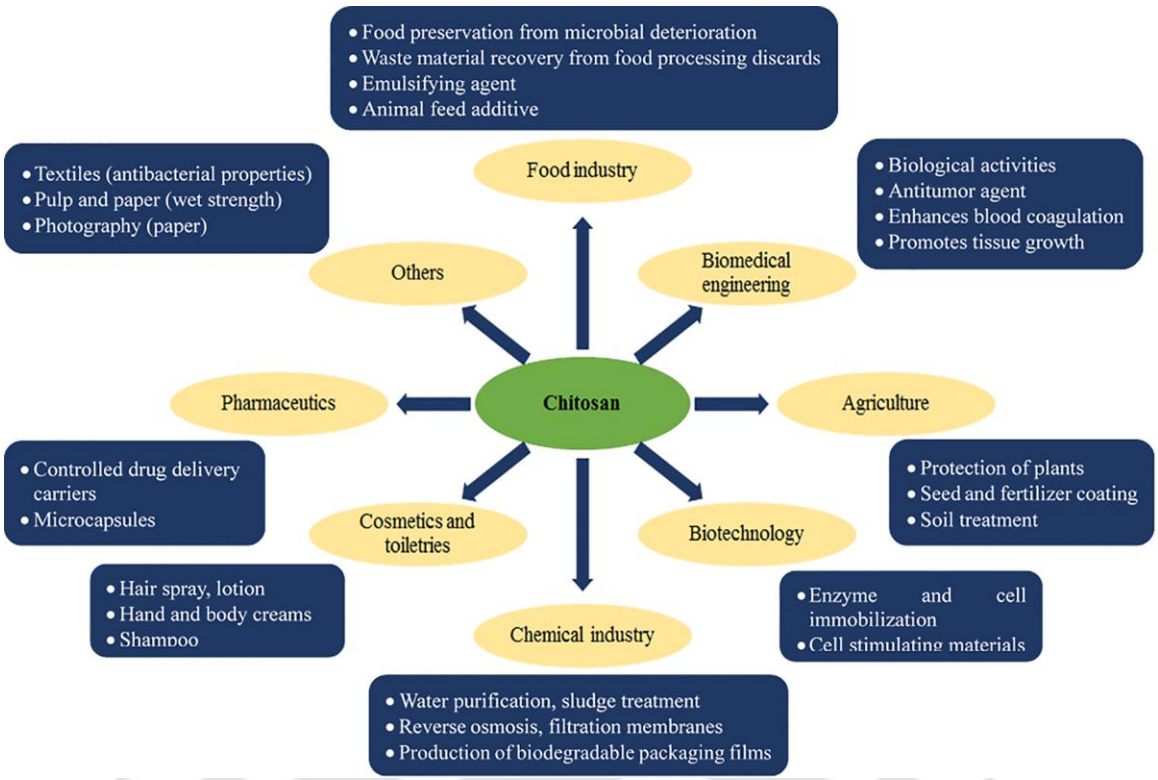

Figure 1.7. Various applications of chitosan.

1.1.3. Degree of deacetylation

Degree of deacetylation is defined as the removal of acetyl group from a molecule. It is also defined as the mole fraction of deacetylated units in the polymorph chain. Various methods are available to calculate DD% such as ^{1}H-NMR spectroscopy, IR-spectroscopy, potentiometric titration, UV-spectroscopy, conductometric titration, colloidal titration and enzymatic methods **[Alvarenga et al., 2010]**. UV spectroscopy and ^{1}H-NMR spectroscopy are very costly techniques and others like IR-spectroscopy, potentiometric titration,

colloidal titration and enzymatic methods are cheap methods. These methods can be performed in laboratory so these methods are preferred for calculating DD%. According to the ASTM standard, ^{1}H-NMR spectroscopy is considered as a reference technique for DD% analysis **[Jiang et al., 2003]**. Degree of deacetylation is the most important parameter for the variation in chemical, physical and biological properties of chitosan sample **[Balazs et al., 2007]** as mentioned in Table 1.1.

Table 1.1. Relation between properties and structural characteristics **[Dash et al., 2011]**.

S. No.	Property	Structural characteristic (DD%)
1	Solubility	↑
2	Crystallinity	↓
3	Biodegradability	↓, ↓ Molecular weight
4	Viscosity	↑
5	Biocompatibility	↑
9	Antimicrobial	↑
10	Permeation enhancing effect	↑
11	Antioxidant	↑, ↓ Molecular weight

↑- Directly proportional to property, ↓ - Inversely proportional to property.

1.2. Literature Review

Production of packaging materials represents one field with a particular high potential for meeting the challenges of combining "green" approaches with nanotechnology. Plastic can be produced from renewable sources such as fermentation products (e.g. lactic acid) from agricultural crops and wastes, starch, plant oils, cellulose, gelatin and chitosan **[Fomin and Guzeev, 2001]**. These plastics are usually biodegradable and if incinerated

often produce less toxic gases than plastic produced from fossil fuels such as PP, PS, PET and poly(vinyl chloride) (PVC) **[Garlotta, 2002]**. Unfortunately, properties such as brittleness, low thermal stability, high gas permeability etc. restrict the use of bioplastics in many applications. However, by introduction of 1-5% nanofillers to the bioplastic, the chemical and physical properties can be strongly improved **[Abdollahi et al., 2012]**. Natural and cheap layer silicates (clays) can be used as nanofillers, however, biopolymer as nano fillers can also be used, such as cellulose nanocrystals, chitosan nanoparticle, sucrose ester, etc. **[Katiyar and Nanavati, 2011]**. The scientific challenge is to obtain the optimal dispersion and interactions between the nano-fillers and the biopolymer, due to strong intermolecular forces between nano particles.

Packaging for food serves several purposes; it preserves quality and freshness, provides consumer appeal and facilities for storage and distribution. Modified atmosphere packaging (MAP) involves a non-atmospheric gas mixture of usually nitrogen, carbon dioxide and oxygen that is favorable to chemical and microbiological stability of food **[Haugaard et al., 2003]**. Packaging films used for MAP demand high barrier properties as the modified atmosphere should be retained throughout the shelf life of the product (from few days to months) and permeation often constitutes the rate limiting step for deteriorative oxygen consuming processes and drying of foods **[Garlotta, 2002]**. At present, only films made of a combination of two or more petrochemical based synthetic polymers, can ful-fill these demands **[Mukund et al., 2007]**. The use of alternative biodegradable materials from renewable sources (bio-packaging materials) have been relatively limited due to their poor barrier properties, microbiological instability and high price **[Mukund et al., 2007]**. Chitin and chitosan are efficient biopolymers which can be extracted from various natural animal based resources as shown in Table 1.2. The highest yield (%) of extraction is obtained from marine sources.

Table 1.2. Extraction of chitin from various natural animal based resources **[Synowiecki et al., 2003; Abdou et al., 2008; Paulino et al., 2006; Nemtsev et al., 2004; Liu et al., 2012 and Mohammed et al., 2013]**.

Name	Extracted Chitin (%)
Marine Sources	
Squid Pens	46.23
Pink Shrimp (P. durarum)	34.02
Indian White Shrimp (P. indicus)	30
Brown Shrimp (P. aztecus)	29.5
Mussel Shell	21.32
Crab Shell	16.68
Crayfish Shell	15.46
Cuttlefish pens	6.12
Insect Sources	
Honey Bee (Apis mellifera)	23-32
Beetle (Holotrichia parallela)	15
Silkworm (Bombyx mori)	2-4
Microbial Sources	
Aspergillus niger	42
Histoplasma capsulatum	25.8 – 26.4
Aspergillas phoenicis	23.7
Penicillium chrysogenum	19.5 – 42
Trichoderma viridis	12 – 22
Blastomyces dermatidis	13
Paracoccidioides brasiliensis	11

Chen et al., 1996 have extracted 90% deacetylated chitosan from alkali treatment of chitin (from red shrimp waste). Gel permeation chromatography and viscometric method can be used to calculate number average and viscosity average molecular weight, which affects the thermal, mechanical and permeation properties of chitosan membrane i.e. enthalpy, maximum melting temperature, tensile strength and elongation of the membranes, flow rates of permeate and water. Various properties such as thermal and mechanical obtained from high molecular weight chitosan are higher except permeability. The applications of such kind of membranes are in medicines, biotechnology areas, membrane separation, chemical engineering and food processing. For the case of membrane separation, selectivity is the most important parameter and the factors affecting are membrane pore size, thickness, annealing treatment, swelling index, molecular weight, membrane making condition, charge effect, chain flexibility etc. Chitosan membrane is very useful for artificial kidney and drug delivery system. Chitosan is basically hydrophilic in nature and blend with different hydrophilic compounds to form chitosan membrane with improved properties e.g. chitosan-poly (vinyl pyrolidine) membrane, chitosan-poly (vinyl alcohol) membrane, chitosan-cellulose membrane. The tensile strength of prepared membrane decreases with decrease in molecular weight.

Fattah et al., 2007 has also prepared chitosan with different degree of deacetylation having microsphere size. They have also fabricated three dimensional chitosan matrices which are used for bone tissue engineering applications as they have suitable pore size, porosity and mechanical properties. According to this paper, chitosan is prepared with thermomechanochemical techniques by changing the applied pressure and NaOH solution concentration and used different techniques for characterization i.e. elemental analysis, viscosity measurements, thermal analysis, x-ray diffraction and proton nuclear magnetic resonance. The fabrication of chitosan microsphere and 3-D chitosan matrices is done by

ionotropic gelation method and sintered microsphere technique respectively. Compressive modulus of sintered microsphere matrix and human cancellous bone is in the range of (662.26±54.53) MPa and (10-2000) MPa respectively, which confirms that such types of microspheres are very much useful for bone tissue engineering applications. Three dimensional, biocompatible and biodegradable polymeric scaffold are used as a temporary extracellular matrix for initial cell attachment and subsequent tissue formation in many tissue engineering methods. The polymeric scaffold should be porous with interconnected pore networks so that cell growth, metabolic waste and nutrients transport will be more. Natural polymers like type I collagen, hyaluronic, chitosan and synthetic polymers like poly (lactic acid), poly glycolic acid, their copolymers like poly(lactic acid-glycolic acid) are used for scaffolding material. But such kinds of polymers degrade after a certain period of time due to stressed region at the contact surface. Natural biopolymer chitosan is also used for wound healing and cartilage tissue engineering.

There are many factors which influence the antimicrobial activity of chitosan films. The factors are pH, intrinsic factors, chitosan-metal complex, sorption and bactericides properties. The antimicrobial activity of chitosan based films decreases with increasing pH. This is because of hurdle effect of the acid stress on the bacterial cells. Chitosan has the ability to bind the bacterial cell wall with electrostatic interaction. On the other hand, good antimicrobial activity is found in average molecular weight chitosan i.e. less than 10 kDa. However, very low molecular weight of chitosan has very less or no antimicrobial activity. There are different types of chitosan-polysaccharides based films and chitosan-protein based films which are mainly used in food industries. The films are chitosan-topioca starch based edible films and coatings, hydroxypropyl methylcellulose edible films with chitosan, chitosan/pectin laminated films with lactic acid. The chitosan-protein based films are round scad protein-chitosan based films, chitosan-whey protein films, fish gelatin-chitosan films.

1.2.1. Permeability

Permeability is the most important parameter to characterize the film's suitability for food packaging and other applications. Permeability is defined as a steady-state property that describes the extent to which a permeating substance dissolves and then the rate at which it diffuses through a film, with a driving force related to the difference in concentration of that substance between the two sides of the film. Gas permeabilities of edible films and coatings depend on several factors such as the integrity of the film, the ratio between crystalline and amorphous zones, the hydrophilic-hydrophobic ratio and the polymeric chain mobility; the interaction between the film-forming polymer and the presence of a plasticizer or other additives are also important factors in film permeability **[Souza et al., 2009]**. Permeability is mainly three types in food packaging applications i.e. oxygen permeability, carbon dioxide permeability and water vapour permeability.

The vast applications of chitosan also depends on degree of deacetylation and permeability. However, the hydrophilic nature of chitosan restricts its utilization in various aspects, which can be conquered by functionalized it with other hydrophobic or hydrophilic polymers. The functionalization of chitosan with various synthetic and biodegradable polymers has received greater attention to overcome its limitations and increase their utilization to enhance various physicochemical and biological properties. The functionalization of chitosan can be performed using physical and chemical methods. However, chemical modification is more stable and productive than the physical modification **[Sashiwa and Aiba, 2004]**. **Wang et al., 2007** have prepared quaternized chitosan nanocomposite using montmorillonite (MMT) (modified by cetyl trimethyl ammonium bromide) by a simple solution mixing method however, toxic nature of such modifier were not addressed by them. Whereas, **Kabiri et al., 2007** avoided commercially modified nanoclays, as they were worried about its toxic in nature so it is not suitable for

bio applications. The preparation of polymer clay nanocomposite (PCN) was done by the use of nanoclay. PCN is mainly prepared by cation exchange reaction between cationic intercalants and clay. According to **Rhim et al., 2006**, chitosan based nanocomposite films are prepared by solvent casting method. Different nanocomposite films have been prepared by using four types of nanoparticles i.e. an organically modified montmorillonite (Cloisite 30B), an unmodified montmorillonite (NaMMT), a nano-silver and an Ag-zeolite (Ag-ion). These nanoparticles are dispersed homogeneously throughout the chitosan polymer matrix in the entire nanocomposite films except the nano-silver incorporated film. Basically, intercalation affects the barrier and mechanical properties of chitosan films. According to the results obtained from this literature, tensile strength was increased upto 16% and water vapor permeability (WVP) decreased by 25-30%. **Tang et al., 2008**, have demonstrated that only 0.4 wt% carbon nanotubes increased its young's modulus and tensile strength by 124% and 171% respectively. According to **Wu et al., 2006**, chitosan is also used with biodegradable PLA and MMT nanocomposites prepared by solution mixing process. In this process, PLA polymer is mixed with organically modified montmorillonite (m-MMT). This mixture is first treated with n-cetyl trimethyl-ammonium bromide (CTAB) cations and then modified by biodegradable chitosan. It is done to increase the compatibility between the PLA and m-MMT. The silicate layers have been swelled during the process. On the basis of XRD and TEM analysis, the swellable silicate layers are randomly intercalated to PLA matrix. Dynamic mechanical analysis and TGA explain about the mechanical and thermal stability of PLA/m-MMT nanocomposites from which significant improvements in storage modulus and 50% loss in temperature than those of neat PLA matrix were observed.

1.2.2. Chitosan in food packaging applications

Chitosan can form impermeable film for oxygen and carbon dioxide. However, it is very sensitive to water vapour permeation due to its hydrophilic nature. **Suyatma et al., 2004** have fabricated thin biodegradable films of PLA and chitosan blends by solution mixing and film casting for improving water vapour barrier properties as well as mechanical properties. The results showed that water vapour barrier properties has been improved by incorporation of PLA in to chitosan. Whereas, water sensitivity, tensile strength and elastic modulus are decreased due to phase separation between PLA and chitosan. The final conclusion was that the chitosan is incompatible with PLA solution because of absence of interaction between PLA and chitosan. **Niamsa et al., 2009** has prepared pure chitosan films using lactic acid as a solvent in place of acetic acid by solution casting method. They have used different molecular weight chitosan and different concentration of lactic acid with L- and DL- forms. Intermolecular bonds are observed between lactic acid and chitosan film matrices. Free amino and amide groups of chitosan and chitin interacts with carbonyl groups of lactic acids. They have proved that there is an effect of solvent on the mechanical properties like tensile strength decreases and percent elongation increases for lactic acid. Flexibility and wettability of chitosan film depends on the ratio of both L- and DL- lactic acid. The plasticization effect is higher in case of L- lactic acid than the DL- lactic acid. On the other hand, film transparency is not effected by different lactic acid ratios.

Souza et al., 2009 has fabricated fully biodegradable and environmentally friendly chitosan coatings to provide additional protection during transportation for foodstuffs by edible films and coatings in the presence of moderate electric field. The different properties like water vapor, oxygen, carbon dioxide, colour, opacity and solubility in water were tested in different electric field strengths. The electric field strengths (100 V/cm and higher) show statistically significant effects and correlation is maintained between water vapor, oxygen

and carbon dioxide permeability and field strength. The observed improvement in the functional properties of films with an effect of electric field can improve food shelf life and reduce water loss, oxygen and carbon dioxide exchange.

Park et al., 2012 have casted poly (lactic acid) films and used biodegradable and biocompatible natural chitosan or chitosan/clay nanocomposites as coating material for improvement in barrier properties. The results exhibit significant reduction in oxygen transmission rate (OTR) and water vapour transmission rate (WVTR) values in the case of chitosan and chitosan/clay nanocomposite coatings, which confirms excellent oxygen-barrier properties as compare to that of pristine PLA films. WVTR value of neat PLA film (thickness=20 μm) was measured as 556 g/m^2.day. However, WVTR value for PLA films (thickness=20 μm) coated with chitosan (thickness=2 μm) and with chitosan/clay nanocomposite were found as 515 and 431 g/m^2.day. Oxygen permeability (OP) value of neat PLA films (thickness=20 μm) was measured as 736 cc/m^2.day, which has reduced upto 99.5% by the addition of chitosan/clay nanocomposite coating with same thickness.

Hirvicorpi et al., 2011 have developed a thin (20 nm) non-toxic polyelectrolyte multilayer (PEM) film, which was made from PLA coated with the mixture of chitosan and sodium alginate followed by the deposition of a thick (25 nm) Al_2O_3 layer. Water vapor barrier properties of PLA films are enhanced due to double coating (PEM+ Al_2O_3) as mentioned in Table 1.3.

Svagan et al., 2012 have extruded PLA film followed by coating its surface with alternate layers of MMT and CH using layer-by-layer (LBL) approach as shown in Figure 1.8. The average OP value of coated PLA film with 70 bilayers was about 0.255×10^{-2} ml.mm/m^2.day.kPa at 20% RH and the average OP value of neat PLA film was 17.68×10^{-2} ml.mm/m^2.day.kPa. At 50% RH conditions, the OP was increased slightly to

0.635×10^{-2} ml.mm/m^2.day.kPa and that of neat PLA film was 16.70×10^{-2} ml.mm/m^2.day.kPa. As a result, the oxygen permeability of PLA films with 70 bilayers are reduced by 99 and 96% at 20 and 50% RH conditions respectively. For multilayer structures on PLA films, the advantage of LBL process is that the optical clarity remains very close to that of neat PLA film but slight decrease in transmittance with the increasing number of bilayers.

Table 1.3. WVTR & contact angle (CA) values of PLA and various coated PLA films.

S. No.	Film	WVTR (g/m^2.day)	CA(˚)
1	PLA	53 ± 4	73 ± 2
2	PLA + PEM	106 ± 7	76 ± 4
3	PLA + Al_2O_3 (25 nm)	33 ± 6	48 ± 1
4	PLA + PEM + Al_2O_3 (25 nm)	25 ± 9	98 ± 4

Arnon et al., 2014 have developed carboxymethyl cellulose (CMC) and chitosan bilayer edible coating, which can be used for preserving various citrus fruits such as 'Navel' oranges, 'Or' and 'Mor' mandarins, and 'Star Ruby' grapefruit. The CMC/chitosan bilayer coating has increased fruit firmness. The bilayer does not show any effect on acidity levels and juice total soluble solids. Apart from this, flavour quality of mandarins has been deteriorated and weight loss has not prevented effectively. It is expected that on adding specific lipid components, water vapour barrier properties may enhance.

Bie et al., 2013 have fabricated antimicrobial films with the blend matrix of poly (lactic acid)/starch/chitosan by extrusion process. The dynamic contact angle analysis has shown that starch enhances the hydrophobic property of the blends so that water can immerse in to the blends. Without using a suitable compatibilizer, starch and PLA are

bonded physically which shows that starch/chitosan aggregations present only at the centre of the blend films. Without compatibilizer, the thermal and mechanical properties also decrease but having good release rate. In this matrix, PLA and starch act as slow-releasing device and chitosan as antimicrobial agent. It has been observed that this blend matrix can also be used for foods, such as meat, having high water activity.

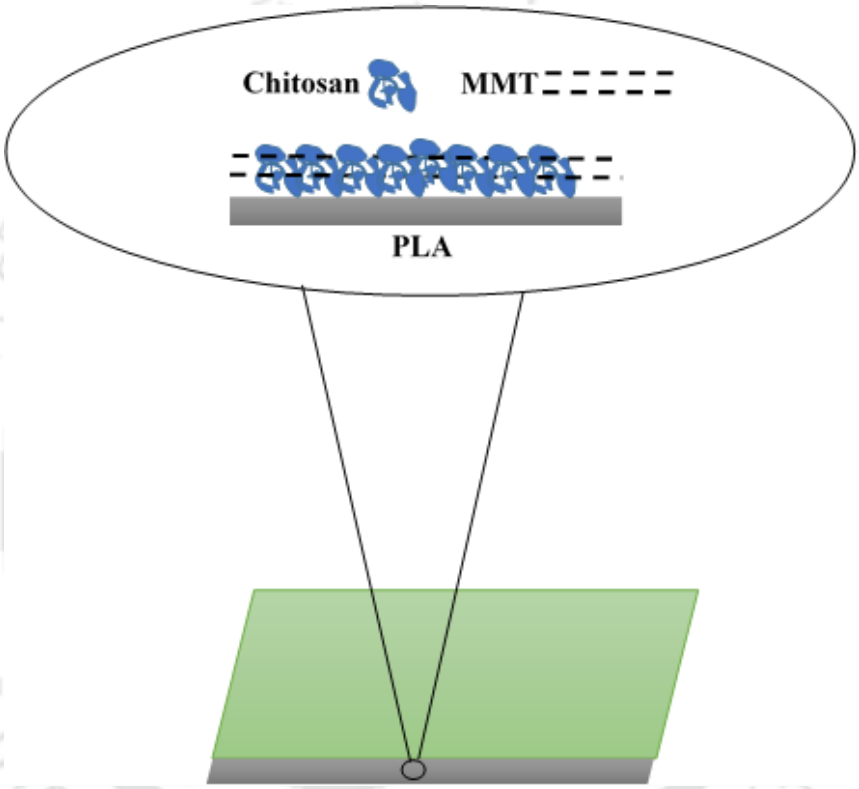

Figure 1.8. Multilayer MMT/chitosan coated PLA film **[Svagan et al., 2012]**.

Bonilla et al., 2013 have developed chitosan-PLA composite films by the extrusion process to measure the physicochemical characteristics and antimicrobial activity. Enhancement of substantial antimicrobial activity has been observed with the addition of chitosan particles because chitosan also acts as an antimicrobial agent. Crystallization temperature of composite films has been increased because of presence of chitosan particles. However, the reduction in mechanical resistance, water vapour barrier and extensibility of the composite

films have been observed due to the incompatibility of chitosan with PLA matrix. On the other hand, elongation at break values for PLA/chitosan films with grinded chitosan particles and neat PLA films are approximately same. Optical transparency has been reduced for composite films, which contributes to inhibit lipid oxidation in food system.

Erdohan et al., 2013 have prepared films from PLA and olive leaf extracts (OLE) using solvent casting method and antimicrobial effect has been observed against *Staphylococcus Aureus*. All the prepared films are transparent and homogeneous without insoluble particles. A slight improvement in elongation of PLA films has been observed by increasing PLA concentration. WVP and elongation have increased whereas, tensile strength has decreased with increasing ethanol concentration in PLA films. It is noteworthy to mention that WVP has been reduced with OLE incorporation in PLA films and degradation rate has been increased. However, tensile property has been reduced and water absorption has been increased with an increase in OLE content.

Boonfaung et al., 2011 have mixed distinct plasticizers such as polypropylene glycol (PPG), poly(ethylene glycol-ran-propylene glycol) (PEPG), dioctyl phthalate (DOP), Tributyl citrate (TBC) and Adipic acid in PLA to overcome the limitations such as rigidity and brittleness using twin screw extruder. Only PPG has shown improved results in the form of improved elongation at break with reduced Young's modulus and tensile strength.

Goncalves et al., 2013 have incorporated α-tocopherol (AT), butylated hydroxytoluene (BHT) and tert-butylhydroquinone (TBHQ) in PLA to improve the gas barrier and antioxidant properties. AT is a natural antioxidant whereas, BHT and TBHQ are synthetic antioxidants. The improvement in properties is dependent on the quantity of antioxidants and compatibility of antioxidants with the polymer matix.

Gonzalez et al., 2013 have prepared PLA and isolated soy protein (ISP) bilayer films, which improves transparency and mechanical properties as compare to that of pristine ISP

films. Antifungal agent (natamycin) and antibacterial agent (thymol) have been added to ISP layer to inhibit bacterial growth, mold and yeast.

Kaur et al., 2013 have developed nano-biobased film from starch containing cadmium sulphide (CdS) and gold (Au) nanoparticles in the range of 25-100 nm. Drastic improvement in the mechanical properties has been observed as compare to that of pure starch films. The work has been done to synthesize nanoparticles which contains in biodegradable starch films. The produced starch films containing Au nanoparticles are UV-visible active. It has been discovered that stabilization of glycerol coated CdS nanoparticles have improved properties than only starch coated Au nanoparticles.

Khwaldia et al., 2014 have coated paper by caseinate and caseinate/chitosan bilayer. Various properties have been analysed w.r.t. its coating weight, caseinate contents and coating application methods. WVP has been decreased as compare to that of pure caseinate coating. Better flexibility, appearance and adhesion between cellulosic substrate have been observed after coating with caseinate/chitosan bilayer, which may be used in paper packaging materials.

Croisier et al., 2013 have demonstrated that chitosan based materials have wide applications in tissue engineering in the form of 2D-scaffolds as films and fibers, 3D-scaffolds as gels and sponges and wound healing applications.

Armentano et al., 2013 have added nano-fillers such as layered silicates and cellulose nano-whiskers in PLA for the drastic improvement in the critical properties in packaging and tissue engineering.

Choi et al., 2013 have demonstrated the improvement in plasticization effect of PLA after grafted with low molecular weight acrylated-poly ethylene glycol (PEG) by reactive blending. Elongation at break has increased by ~380%. However, glass transition temperature and young's modulus have decreased by more than 20 °C and 66%

respectively. The ductility has also been improved for such grafted blend of poly (lactic acid).

Duan et al., 2013 have fabricated various PLA based nanocomposite films by adding nanoclays with the help of melt compounding followed by compression moulding. As a result, the interlayer spacing has been increased from 1.84 to 3.4 nm and the intercalation of MMT layered silicate has been confirmed by TEM and XRD analysis. The WVTR has decreased up to 40% by the addition of nanoclays in PLA matrix.

Findenig et al., 2012 have used highly hydrophilic and permeable cellulose films as a substrate for the preparation of water vapour barrier coatings, made of polyelectrolyte/clay multilayers using LBL technique. Polyethylene imine (PEI) or 2-hydroxy-3-triethylammonium propyl chloride starch (HPMA starch) has been used as a polyelectrolyte with MMT clay and improved barrier properties have been observed by the application of only five bilayers of PEI and MMT on each side of the cellulose film. Up to 68% reduction in WVTR has been observed by the deposition of 40 PEI/MMT bilayers on cellulose films. On the other hand, only 32% reduction in WVTR has been observed by using HPMA starch films as a substrate.

Fortunati et al., 2013 have used modified cellulose with PLA matrix for active food packaging. The combination of surfactant modified cellulose nanocrystals and silver nanoparticles have been used as a matrix modifier. As a result, the barrier properties of produced nanocomposite films have been improved by the addition of surfactant modified cellulose nanocrystals (s-CNC) and silver nanoparticles due to the proper dispersion of fillers. WVP enhances approx. 60% by the addition of 5 wt% of s-CNC and 1wt% of Ag nanoparticles.

Gu et al., 2013 have utilized LBL approach for the preparation of alternate layers of sodium alginate and polyethyleneimine (PEI) on biaxially oriented poly (lactic acid). The OTR

analysis has been performed after 30 ALG/PEI layers on PLA films and almost 99.8% reduction in OTR values has been observed as compare to that of uncoated PLA films. The tensile strength has also improved slightly and optical clarity is very close to the Neat PLA films.

Laufer et al., 2012 have also used LBL approach to prepare thin films or coatings by alternate layers of positively charged chitosan with two different pH levels (pH 3 and 6) and anionic MMT clay nanoplatelets on PLA film substrate. Polystyrene films and silicon wafers can also be used as substrate. The oxygen permeability (P) has been reduced by four order of magnitude after 30 bilayers of chitosan and clay on PLA film with the same coating system, but only ten bilayers have been used on a flexible polyurethane foam to increase the flame retardant property. As a result, the melting of polyurethane foam has been completely stopped after such coatings and 52% reduction has been observed than that of uncoated control. The reduction in oxygen barrier and increment in flame retardant property are due to the brick wall nanostructure, which provides highly tortuous path. Such nano-coatings will be really helpful to improve the quality of food packaging system.

Laufer et al., 2013 have coated PET films with chitosan, carrageenan (CR) and MMT clay by LBL technique. Ten trilayers of CH/MMT/CR have been prepared on PET film and the observed reduction in OP is an order of magnitude under dry conditions. The reduction in OP has been improved by two orders of magnitude under the same conditions only by incorporating one extra layer of chitosan on PET substrate i.e. a quadlayer film of CH/CR/CH/MMT in place of trilayer film. The improvement in oxygen barrier property is due to the presence of nano-brick wall structure and strong attraction amongst the oppositely charged polysaccharides.

Leceta et al., 2013 have compared the properties of two different packaging systems i.e. a commercial food packaging film based on PP and a new biodegradable CH based film. The

environmental load of chitosan based films has been observed for food packaging and compared with the environmental load of polypropylene films. The included stages in life cycle of food packaging are material extraction, film manufacture and end of life. As a results, it is found that CH based films have less impact than PP films in carcinogens and in fossil fuels impact categories. The carcinogenic environmental load is due to the end of life stage while fossil fuels impact is due to the extraction of PP. it is noteworthy to mention that higher environmental load for chitosan films has been observed in respiratory inorganics, land use and minerals categories. The final conclusion is that PP based films have exhibited higher environmental impact than chitosan based films. The environmental load related to chitosan based films will be reduced in future after optimization of processing and additives consumption.

Li et al., 2013 have used two biopolymers i.e. chitosan and cellulose nanocrystals as coating layers on amorphous PET films using LBL technique to improve the oxygen barrier properties of coated films. The PET substrate has been coated up to thirty bilayers of chitosan and cellulose nanocrystals. The observed oxygen permeability values have been reduced up to 94% as compare to that of uncoated control film. Finally, it is concluded that such nanocomposite films have highly improved gas barrier properties and can be a promising candidate in food and drug packaging applications.

Martelli et al., 2013 have extracted banana puree from over ripe peeled bananas and developed banana puree films in the presence of plasticizers such as pectin and glycerol. Chitosan nanoparticles have been used as a reinforcement material in banana puree films. As a results, pectin and glycerol have improved elongation and hand-ability of films. The improvement in mechanical and WVTR have been observed due to the incorporation of chitosan nanoparticles as compare to that of pure puree films. The WVTR value has been

reduced up to 21% and 38% in films with and without pectin. Microscopic observation confirmed a denser matrix after incorporation of chitosan nanoparticles.

Olabarrieta et al., 2001 have fabricated blends of chitosan with poly caprolactone and whey-protein-isolate (WPI) with PCL by solution mixing and film casting technique. The purpose of this research is to increase water vapour resistivity and oxygen resistivity by adding hydrophobic and biodegradable PCL into chitosan and WPI matrix. According to the results, the WVTR values of chitosan/PCL films have been reduced up to 90% by adding only 18.3 vol% of PCL in to pure chitosan films. The shape of the PCL particles has been observed ellipsoidal. This drastic reduction in WVTR values is due to the geometrical blocking of the diffusing water molecules and a reduction in the swelling of the matrix. However, the reduction in WVTR value for WPI/PCL films is not higher than chitosan/PCL films but still significant. The observed WVTR has been reduced up to 70% for WPI/PCL films by the addition of 16.8 vol% PCL in to pure WPI films. In this case, the fibre-shaped particles has been observed and shows good miscibility between WPI and PCL components.

Ozkoc et al., 2009 have prepared poly (lactic acid) as well as poly (lactic acid) with poly ethylene glycol films as control films using melt intercalation method. PEG has been used as a plasticizer. A laboratory scale compounder is used which has been connected to a microcast film device. Different variations (0, 3 and 5%) of organoclay (Closite 30B) has been added in to the PLA films and PLA/PEG films in order to prepare nanocomposite films. The d-spacing between interlayer of clay has been increased and weak peak has been observed at 2˚ and 5˚ which indicates that most of the clay is intercalated or partially exfoliated due to shear forces during processing and diffusion of polymer chains through the clay galleries. PLA/PEG/Clay films have promoted the exfoliation of the clays due to the low molecular weight than PLA. The glass transition temperature has been improved

for PLA/3% clay films due to the restriction of the mobility of the polymer chains. The cold crystallization temperature has been reduced for PLA/PEG and PLA/PEG/Clay films because PLA crystallization has been preferred in the presence of organo-clay. Clay incorporation into PLA or PLA/PEG films enhances the degree of crystallinity up to 8%. The strength of the nanocomposite films has not been affected with the addition of 3% clay into neat PLA. However, it enhances the modulus of the films. The biodegradation rate has been reduced for the PLA/PEG, PLA/PEG/clay and PLA/clay films due to hydrophilicity and crystallinity of the films.

Pantani et al., 2013 have fabricated novel PLA/zinc oxide (ZnO) nanocomposite films by melt compounding using twin screw extruder. The surface of rod like nanoparticles of zinc oxide has been treated by silanization before mixing in PLA to obtain a better dispersion and to limit the reduction in molecular weight of PLA. According to the results, the prepared films are amorphous in nature. The activation energy of PLA/ZnO (3%) films was found to be greater than the neat PLA film which indicates that the difficulty of travelling molecules has been improved than the neat PLA film. On the other hand, the crystallinity of PLA/ZnO films has been improved by increasing the nanofiller loading. The opacity is a very important parameter for packaging applications. The opacity of PLA/ZnO films has been increased up to 10% by adding 3% ZnO in to Neat PLA films. In the case of mechanical properties, the rigidity of PLA/ZnO films has been increased slightly and tensile stress of the same films has been decreased slightly.

Peng et al., 2013 have prepared chitosan films in the presence of antioxidants such as green tea extracts (GTE) and black tea extracts (BTE) by solution casting method. The purpose of mixing GTE and BTE into chitosan is to check the effect of tea extracts on physical, structural and antioxidant properties of chitosan based films. The results suggest that the apparent viscosity has reduced after incorporation of tea extracts into chitosan film due to

the weak hydrogen bonding, which results from the interaction between tea extracts and chitosan. The WVP value for chitosan/GTE (2%) film has decreased up to 62.1% as compare to that of neat chitosan film. Water content has also decreased with the incorporation of tea extracts due to the breaking of hydrogen bonds of chitosan-water matrix during interaction between tea extracts and chitosan. The solubility and swelling degree of chitosan films have been improved significantly with incorporation of tea extracts due to the strong interaction between chitosan and tea extracts which decreases the degree of cross linking of intermolecular chain in the matrix. In the case of mechanical properties, the tensile strength and elongation at break have been reduced upto 17.5% and 84.5% respectively with the addition of low concentration of tea extracts (0.5%) in to chitosan films. The DPPH (1, 1-diphenyl-2-picrylhydrazyl) redical scavenging activity of chitosan/tea extracts films has been observed at around 94.9%.

Rhim et al., 2013 have developed various films such as neat agar film, neat k-carrageenan film, agar/k-carrageenan blend film, agar/k-carrageenan/clay (Closite® Na^+) nanocomposite film, neat PLA film, PLA/nanocomposite double layer film and PLA/nanocomposite triple layer film in the presence of glycerol to check the optical, mechanical, barrier and thermal properties. The results shows that the blend films and nanocomposite films have higher yellowness due to the presence of k-carrageenan and inclusion of the nanoclays respectively. The transmittance of blend films is higher as compare to that of nanocomposite films due to the presence of the intercalated nanoparticles in the polymer matrix. PLA films have high transparency due to have polar nature. The transmittance of the multilayer films has been increased due to the presence of transparent PLA layers. A strong adhesion between multilayers has been observed without using any adhesive or surface modification. The outer PLA layer has worked as solvent-borne adhesive and middle nanocomposite layer has worked as water-borne adhesive. This

adhesiveness comes from strong hydrogen interaction with carbonyl groups in PLA and hydroxyl groups in carbohydrates. The mechanical strength of nanocomposite films has increased by 40% as compare to that of blend film. The tensile strength of laminated double and triple layer films has been improved 38% and 17% respectively. The WVP values of nanocomposite films have been decreased up to 20% due to the dispersion of silicate layers in polymer matrix with large aspect ratio. The multilayer films have shown drastic improvement in water vapour barrier properties up to 20 folds as compare to that of composite films. The OTR values for PLA are 650 times higher than that of nanocomposite films. However, OTR values are drastically reduced for laminated double and triple layer films. The water solubility and water uptake ratio (WUR) have been decreased for laminated films due to the hydrophobic nature of PLA. The WUR has been reduced up to 960 and 100% for double and triple layer films respectively than that of nanocomposite film.

Schreiber et al., 2013 have fabricated neat chitosan films in the presence of antioxidants to improve the functionality. The chitosan/gallic acid and gallic acid-*graft*-chitosan films have also been prepared to check the required properties for food packaging application. Grafting is an important parameter in order to improve food packaging properties. According to the results, grafted chitosan has higher DPPH scavenging ability (90%) and reducing power (0.51) than that of non-grafted chitosan. Gallic acid has been grafted on chitosan at C_2, C_3 and C_6 positions. C_2 position has referred to amide bond with amino group. C_3 and C_6 positions have referred to formation of ester bond. Grafting efficiency depends on the degree of deacetylation so according to the results, chitin has much lower level of total phenolics content and antioxidant activity than that of chitosan. No significant change has been observed for chitosan with 100% DDA and 80% DDA. It means that only a certain extent of amino groups and available hydroxyl groups have grafted with gallic

acid. Grafting time is also an important parameter. The prepared sample in 1.5 h has shown lower total phenolics content, DPPH scavenging ability and reducing activity than that of prepared sample in 6 h grafting time. No difference has been observed in total phenolics content, DPPH scavenging ability and reducing activity between 6 h and 24 h grafting time. The puncture strength has also been observed for chitosan films and found higher than that of low density polyethylene bags.

Soares et al., 2013 have used thermo-presser machine to fabricate thermoplastic starch (TPS), PLA and TPS/PLA sheets. TPS/PLA sheets have been coated with glutaraldehyde cross-linked chitosan by two different methods i.e. spraying and immersion. The TPS/PLA sheets have shown good processability during molding, good handle-ability and homogeneous appearance without cracks. A continuous covering of chitosan has been observed on the surface of coated or uncoated TPS/PLA films irrespective from the coating method. The continuous sheet prepared from immersion is more irregular than that of spray coating. The immersion favours water diffusion into starch matrix, which modifies the surface appearance of the sheet. The water solubility of coated TPS/PLA films with cross-linked chitosan has been observed to be less than that of uncoated sheets. In the case of barrier properties, the coated TPS/PLA films with cross-linked chitosan has higher barrier properties produced by spraying method. WVP of spray coated TPS/PLA films has also been reduced up to 35% than that of uncoated films.

Tenn et al., 2013 have fabricated two series of PLA based nanocomposites using hydrated C30B clay (C30B-h) and dehydrated C30B clay (C30B-d) by melt compounding technique. Different variations have been taken for PLA/C30B-h and PLA/C30B-d in order to observe the effect on thermal, mechanical, barrier and other properties with the addition of nanoclay platelets in to PLA matrix. The coexistence of exfoliation, intercalation and aggregation structures have been observed in the nanocomposite films. Better degree of dispersion has

been observed in PLA/C30B-h films. The crystallinity of the nanocomposite films has been changed slightly due to the nucleating effect induced by the nanoclays. The water and barrier properties have been improved for nanocomposite films but hydrated C30B clay has shown better water and barrier properties due to the presence of water molecules induced in C30B clay. In same way, water in C30B clay has contributed better dispersion and orientation of nanoparticles in to the PLA matrix.

Vasile et al., 2013 have prepared low density polyethylene (LDPE)-chitosan composites by melt processing technique after incorporation of chitosan or chitosan sodium montmorillonite clay nanaocomposites (CHnano) with and without Irganox 1076 as a synthetic antioxidant and vitamin E (VE) as a natural antioxidant. Young modulus has been improved slightly with chitosan addition and around 11% with chitosan nanocomposites addition into LDPE matrix. Improved oxidation induction period has been observed by addition of vitamin E in the LDPE matrix. The antimicrobial and thermal properties have been improved with the addition of both chitosan nanocomposites and vitamin E in to LDPE matrix due to the increase in surface charge and synergistic effect. In such a way, the obtained new materials have good inhibition activity against different bacteria such as *L. monocytogenes, E. coli* and *S. enteritidis*. Such kind of films can be used for food packaging applications after the incorporation of above additives in to the natural products without affecting human health.

There is another positive point of chitosan that it can be used for gas barrier in food packaging application. It can prevent oxygen to enter into the plastic packaging film. Many different types of additives are added into the biopolymer films to improve food quality, minimize microbial growth and extend shelf life. The additives may be antioxidants, antimicrobials, colours, antifungal agents and nutrients. So chitosan is used and its properties (physical, mechanical and barrier) are enhanced by incorporating nanoclays and

additives. Pulp fiber chitosan sheet **[Gallstedt et al., 2006]**, montmorillonite nanoclay and rosemary essential oil interaction with chitosan **[Abdollahi et al., 2012]**, chitosan coated grease proof paper **[Kjellgren et al., 2006]**, chitosan coated polyethylene **[Kurek et al., 2012]**, nanomultilayer coating of pectin and chitosan **[Medeiros et al., 2012]**, hydroxypropyl methylcellulose edible films with chitosan/tripolyphosphate nanoparticles **[Moura et al., 2009]**, paper based minerals by chitosan coating are the applications of chitosan in packaging.

Another alternative of food packaging is edible packaging which is used for protection and increment of food shelf life and food quality. Edible packaging is defined as a packaging like a film, a sheet, a thin layer or a coating which is an integral part of a food and is eaten with. Edible packaging or coating is made directly or apply on foods but it should be as tasteless as possible in order not to be detected during the consumption of the edible packaged food products **[Debeaufort et al., 1998]**. Some properties like barrier to gas, vapours and solutes of edible packaging are same as that of plastic films. Edible films or coatings have to fulfil some requirements such as good sensory qualities, high barrier and mechanical efficiencies, enough biochemical, physico-chemical and microbial stability, free of toxics and safe for health and non-polluting to be a good packaging films. Figure 1.9 shows some selective properties of edible packaging and coatings. The water barrier efficiency of films is the most desirable property to retard the surface dehydration of fresh or frozen products to avoid caking in food powder or the loss of crispness in dried cakes. The control of gas exchanges particularly oxygen should be there for better control of ripening of fruits or significantly reduce the oxidation of oxygen sensitive foods. Aroma and flavour should also be retained in the packed food for a long time by controlling the organic vapour transfer. One of the most interesting applications of edible films and coatings is their use inside a composite food to control mass transfers between the different

compartments of the product. The effect of light and ultra-violet light that involves radical air reactions in foods could be reduced. Light penetration also affects the efficiency of the film so it can be controlled by the addition of pigments or light absorbers.

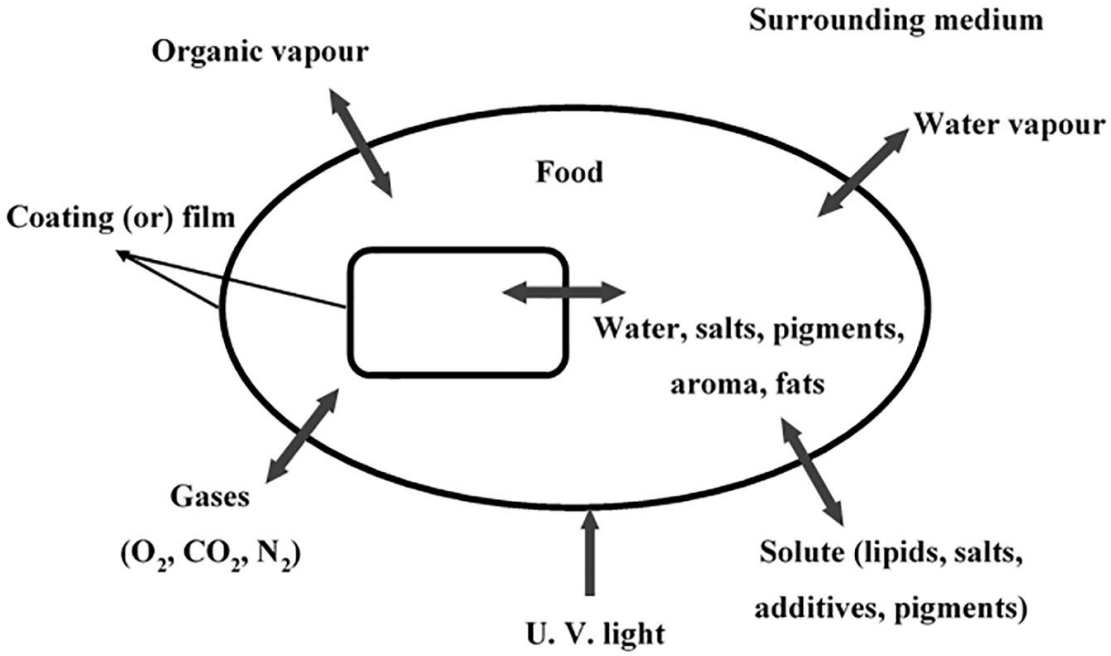

Figure 1.9. Functions of edible films and coatings **[Debeaufort et al., 1998]**.

Edible coatings are very promising systems for the future improvement of food quality and preservation during processes and storage. Indeed, they could be used where plastic packaging can't be applied i.e. they can separate several compartments within a food. Edible packaging is an intelligent packaging because they are active, selective and have infinite potential to use. Edible films and coatings are prepared by using natural polymers obtained from agricultural productions such as animal and vegetable proteins, gums, and lipids. Their cost is 10 to 50-fold higher than those of PE or PP films, but remains within the same range as of complex, multi-layered, or active plastic films. However, their cost is not a handicap to their development because quantities used are very low, and they are

especially applied for very specific goals in value-added food products. Thus, the knowledge of edible polymers and that of plastic materials should be used synergistically for the development of new applications, new biodegradable materials, and new environmental approaches. Consequently, both biodegradable plastic and edible packagings potentiality appear to be a successful key for tomorrow's food packaging **[Debeaufort et al., 1998]**.

It is concluded from the above discussion that various methods such as LBL approach, solution casting and edible packaging may enhance the required properties in food packaging applications. However, the excess use of chemicals in the form of plasticizer, binder and antioxidant is always harmful to the human health. All the above discussed processes are not industrially viable except extrusion. Hence, the other industrially viable path has to find out for the functionalization and combining two or more polymers followed by extrusion. In this direction, researchers have found that 'grafting' can be a potential technique to functionalize and combining two or more polymers, which can be further used in various applications. **Wang et al., 2013** has synthesized chitosan-*graft*-polycaprolactone (CH-*g*-PCL) with the help of green reaction media i.e. 1-ethyl-3-methylimidazolium acetate (EMIMAc) using ring opening polymerization in the presence of stannous octoate ($Sn(Oct)_2$) as a catalyst under controlled reaction conditions and feed ratios. The grafting content of polycaprolactone on both -OH and $-NH_2$ groups of chitosan is reached upto 630%. The synthesized copolymer is highly advantageous as it has the properties of both reactant polymers. **Zhou et al., 2013** has synthesized self-aggregated nanoparticles (~200 nm) of poly (lactic acid)-*graft*-chitosan (PLA-*g*-CH) copolymer via protection-*graft*-deprotection reaction for its potential use in ocular delivery of amphotericin B. The problems related to therapeutic gaps has been overthrown with the help of amphotericin B-loaded nanoparticles based on PLA-*g*-CH (AmB/PLA-*g*-CH).

Yao et al., 2003 has developed cytocompatible graft copolymer using chitosan and L-lactic acid with the help of grafting onto amino groups. The crystalline structure of chitosan is disturbed by grafting due to the randomly arranged side chains after the substitution of $-NH_2$ group. The cell growth rate is faster on grafted copolymer than that of chitosan as confirmed by the static cultivation of *invitro* fibroblast, which is continuously decreased with an increase in feed ratio.

1.3. Summary of the literature review

The shelf-life of fresh and processed vegetable and meat products, defined as the maximum length of the time that the product can be stored without deterioration to the point where it is not fit for consumption, is an increasingly important consideration because retailers and the consuming public expect a long product shelf-life and good quality. Meanwhile, the public expects a diverse range of safe high-quality packaging products to be available which can provide lowest possible gas barrier and water barrier in order to keep the freshness of food for long time and hence higher shelf life. As penetration of oxygen through packaging introduce oxidative discoloration processes as well as the microbial growth, responsible for food quality loss.

In order to find an optimum solution, there has been an increasing interest in the use of bioplastics in food packaging. As an example, PLA manufactured from corn starch as a starting material, has entered markets for packaging of salads, delicatessen items and other food products in a number of European and North American markets. PLA has also been introduced to the beverage packaging market in the form of injection blow-molded water bottles.

1.4. Motivation

Completely Green packaging has commercial interests worldwide as it can be manufactured from combination of renewable resources such as agriculture crop wastes in case of PLA, abundantly available marine chitin feedstock. It has the potential to meet environmental and health requirements along with required necessary packaging properties such as high gas barrier, mechanical and thermo-physical properties.

1.5. Aims and objectives

The aim of current research is to develop PLA/chitosan based food packaging films with necessary gas barrier, mechanical and thermal properties to overcome the limitation of conventional bio-based PLA so far. It can be achieved by using new polymer formulations. Hence, PLA/chitosan copolymer will be synthesized which may reduce oxygen transmission rate when dispersed in extruded PLA matrix. Nano-scale reinforcement of chitosan particles may improve mechanical and thermo-physical properties of PLA. This novel formulation may produce bionanocomposite film by solution casting and melt extrusion technique, which can provide cost effective single process production of films.

In order to achieve the overall aims, the objectives (as shown in Figure 1.10) are outlined as follows:

1. To gain an in depth understanding about the consumed biodegradable polymers such as poly (lactic acid) and chitosan, their properties, limitations and processing techniques.
2. To extract chitin and chitosan from unexplored natural resource i.e. Muga silkworms (*Antheraea assamensis*) and their detailed characterization.
3. To fabricate poly (lactic acid)/chitosan biocomposite films using poly (lactic acid) and chitosan as matrix and filler respectively by solution casting technique followed by detailed characterization.

4. To synthesize chitosan-*graft*-oligo (l-lactic acid) copolymer using condensation polymerization reaction and detailed characterization in order to calculate its degree of grafting and uniform dispersion in hydrophobic polymers.
5. To fabricate poly (lactic acid)/chitosan-*graft*-oligo(l-lactic acid) bionanocomposite films using solution casting technique at lab scale for the development of a new generation of green packaging followed by its comprehensive characterization.
6. To fabricate and characterize poly (lactic acid)/chitosan-*graft*-oligo(l-lactic acid) bionanocomposite films using melt extrusion technique at pilot scale in order to check its industrial viability.
7. Non-isothermal degradation behaviour of poly (lactic acid)/chitosan based films using various isoconversional and model fitting methods in order to analysis their reuse.
8. Isothermal crystallization behaviour of poly (lactic acid)/chitosan based films to observe the crystal growth with the variation in filler loading.

The environmental pollution caused by the massive use of non-degradable plastics, has increased the research on biodegradable films as potential packaging materials. In a similar way, proposed biodegradable films can be used to pack food products to reduce loss of moisture, to restrict absorption of oxygen, to improve mechanical properties, to provide physical protection or to offer an alternative to the commercial packaging materials. In the present study, PLA/chitosan based biodegradable films will be developed and tested for packaging application. The study is expected to develop new generation green packaging films for industrial and commercial use for a wide range of food products.

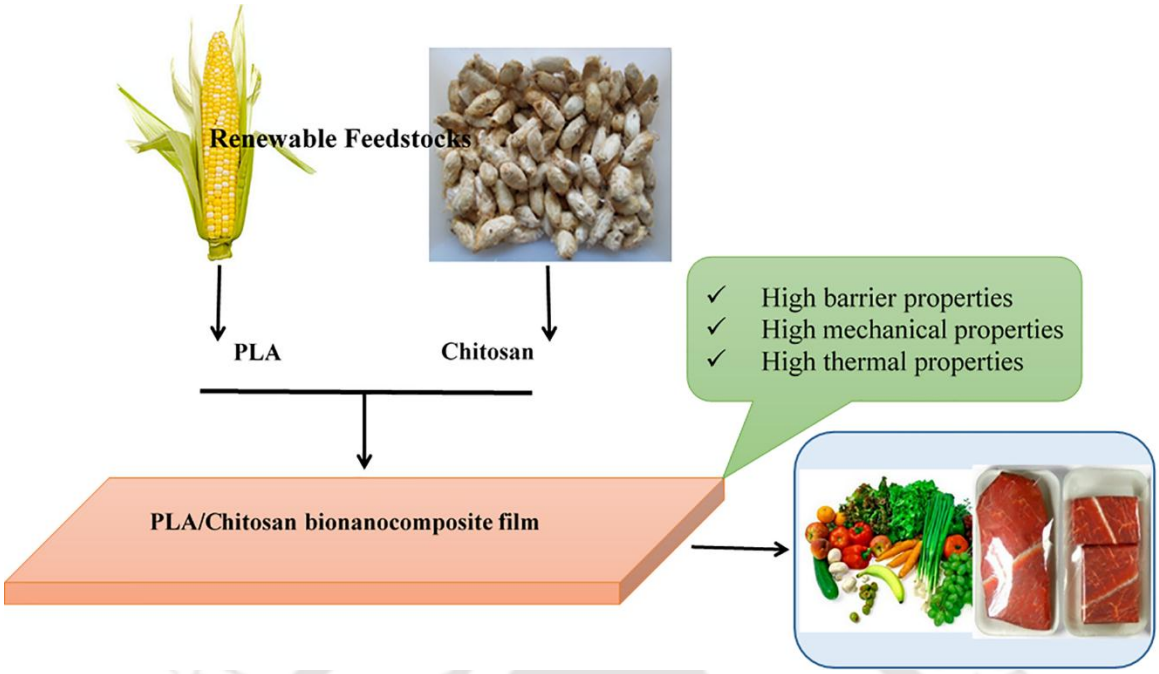

Figure 1.10. Objective of the present research work.

1.6. Details of improved technology to be developed

The production of monolayer packaging films using biopolymers such as poly (lactic acid) in combination with other biopolymer such as chitosan which will subsequently yield necessary packaging properties such as higher gas barrier, mechanical and thermo-physical properties. It can be achieved by using new polymer formulation consist of combination of Chitosan/OLLA copolymer, a highly viscous material with network structure morphology useful for reduction in gas transport properties. The antimicrobial properties of the chitosan will also inhibit microbial growth when added in biopolymer films and therefore it extends the shelf life of the food.

Based on the objectives mentioned in section 1.6, further enclosed chapters are organized as follows:

The chapter two explains about the utilization of polymers and other chemicals with detailed protocols for various experiments performed in this research work. The extraction

of chitosan, synthesis of bio-based copolymer and films fabrication procedures followed by distinct analytical methods are discussed. Details on the calculation methodology for converting raw experimental data into appropriate domain are also presented. The characteristic properties for analyzing the samples are also determined.

The chapter three focuses on extraction of chitin from Muga silkworms and its conversion into chitosan by chemical treatment process. The extracted amount of chitin and chitosan from MS were obtained ~8 and ~7 wt%, respectively. Potentiometric titrations, conductometric titrations, elemental analysis, proton nuclear magnetic resonance (^{1}H-NMR) and Fourier transform infrared spectroscopy (FTIR) analyses were employed to calculate the degree of deacetylation (DD%) of chitosan and found as 77%±2, 81%±1.8, 82%±2.4, 97.77%±0.3 and 82%±1.8 respectively. The deacetylation process of chitin showed pseudo-first order reaction kinetics and activation energy was estimated as ~15.5 kJ/mole. The extracted chitosan showed higher crystallinity and improved thermal stability with respect to chitosan extracted from other marine sources.

The chapter four reveals the fabrication of poly (lactic acid)/chitosan based biocomposite films (PLA/CH) by solution casting technique. All the regular peaks of PLA and CH are observed in biocomposite films by FTIR analysis. XRD analysis confirms the regular lattice arrangement of PLA chains in PLA/CH films. DSC analysis of films reveals that the glass transition temperature, cold crystallization temperature and melting temperature were reduced up to 1.9, 4.6 and 3.2 ºC respectively with the increase in chitosan concentration due to the plasticizing effect of short polymer chains of PLA. Phase separation between PLA and chitosan was also observed by FESEM analysis.

The chapter five elucidates the investigation on chitosan-*graft*-oligo(l-lactic acid) copolymer (CH-*g*-OLLA) for its use in packaging application. The monomer lactic acid is used to graft on chitosan backbone by conventional heating and microwave heating

methods. However, microwave heating method is selected for further investigations. The hydrophilic chitosan is grafted with *insitu* grown lactic acid oligomer. The grafting at NH_2 groups in chitosan backbone with oligo-(L-lactic acid) (OLLA) chains is confirmed by FTIR and NMR analyses. Other analyses such as SEM, TEM and contact angle measurements support uniform dispersion of chitosan in OLLA due to effective grafting reaction. The prepared copolymer is found to be amorphous in nature which was proved by XRD and DSC analyses due to unavailability of crystallization peak and broad peak of heat of fusion.

The chapter six demonstrates the utilization of synthesized CH-*g*-OLLA, a nano-amphiphilic molecule, as a nano-filler for improvement in multiple properties of PLA films, essential for stringent food packaging applications. FTIR analysis shows the presence of amide-ester bond at 1539 cm^{-1} which confirms the structural grafting of OLLA chains with chitosan molecules. Prepared PLA/CH-*g*-OLLA bionanocomposite films appear with uniform dispersion of nano-amphiphilic CH-*g*-OLLA molecules with self-assembled micelles having size as low as ~20 nm and as high as ~150 nm with core-shell morphology in PLA matrix. This nano-filler is found very effective towards significant reduction in oxygen permeability (P) by ~10 folds due to the reduction in solubility of oxygen molecules and improvement in crystal nucleation density due to availability of nano-nucleating sites. The glass transition temperature of bionanocomposites is decreased by more than 18 °C with increase in CH-*g*-OLLA loading which indicates the improved plasticization characteristics of PLA matrix.

The chapter seven focuses on the successful utilization of CH-*g*-OLLA as a nano-filler in PLA matrix to fabricate PLA/CH-*g*-OLLA bionanocomposite films by co-rotating twin screw compounder cum cast film extrusion technique (distinctly advantageous over conventional solution casting) at bench scale as well as semi-pilot scale and are

demonstrated for its application in food packaging with improved oxygen barrier properties. The number average and weight average molecular weights of PLA are reduced ~23% and ~15% respectively with an increase in filler loadings. It is meaningful to mention that the degradation temperature of PLA/CH-*g*-OLLA bionanocomposite films is still above than the required processing temperature of control films, which makes the PLA/CH-*g*-OLLA bionanocomposite films suitable for industrial scale production. The best fitted theoretical models with the experimental data for mechanical modeling of extruded PLA/CH-*g*-OLLA samples are foam and modified foam models, Nicolais-Narkis model and modified Mitsuishi model. The permeability and solubility of oxygen across the PLA film are significantly reduced upto ~90.4 and ~95.7% with increase in filler upto 5 wt%. Further, the lamination technique is used to fabricate a bilayer of extruded PLA and PLA/CH-*g*-OLLA bionanocomposite films at ~90 ºC with improved storage modulus (~86%) and elongation (~490%) as compare to that of pristine PLA.

The chapter eight describes about the non-isothermal degradation behaviour of PLA/CH biocomposite and PLA/CH-*g*-OLLA bionanocomposite films. Non-isothermal degradation kinetics, proposed by Kissinger, Kissinger-Akahira-Sunose, Flynn-Wall-Ozawa and Augis & Bennett models, are utilized to estimate the activation energies (E_a) for PLA, which are 254.1, 260.2, 257.0 and 259.1 kJ/mol respectively. The evolved gaseous products like hydrocarbons, carbon dioxide, carbon monoxide and cyclic oligomers are successfully identified with TG-FTIR analysis in the case of PLA/CH-*g*-OLLA bionanocomposite films.

The chapter nine demonstrates the effect of CH and CH-*g*-OLLA nano-filler on the crystallization behaviour of solution casted PLA films, which is also equally important for the improvement in multiple properties essential for stringent food packaging applications. In the case of CH-*g*-OLLA nano-filler, the improvement in crystal nucleation density of

PLA films was observed after the addition of CH-*g*-OLLA in various proportions, which was due to the availability of newly generating nano-nucleating sites. The crystallization kinetics suggests non-three dimensional truncated spherical structures, which is controlled by the combination of thermal and athermal instantaneous nucleations. POM analysis suggested that the spherulite growth of PLA is improved significantly with the addition of CH-*g*-OLLA.

The chapter ten highlights the major inferences drawn from the doctoral work and an outlook for future studies.

Chapter 2
Materials and Methods

This chapter explains about the utilization of polymers and other chemicals with detailed protocols for various experiments performed in this research work. The extraction of chitosan, synthesis of copolymer and films fabrication procedures followed by distinct analytical methods are discussed. Details on the calculation methodology for converting raw experimental data into appropriate domain are also presented. The characteristic properties for analyzing the samples are also determined.

2.1. Materials

Muga silkworm (MS) cocoons were supplied by Regional Muga Research Station, Central Silk Board, Assam, India. Cocoons were stored in a cool place before use. Commercial chitosan (medium molecular weight, degree of deacetylation >70%), L-lactic acid (20% assay), acetic acid (≥ 99.7%), deuterated water, deuterated acetic acid and deuterated chloroform were obtained from Sigma Aldrich, India. Poly (lactic acid) (2003D, D-lactic acid: 1.4%, L-lactic acid: 98.6%, granules form, density of 1.24 g/cm^3, melt flow index: 0.73 g/min at 210 °C) with number average molecular weight (M_n) of ~150,000 Da and weight average (M_w) of ~200,000 Da, respectively was supplied by Natureworks®, USA. Chloroform (analytical grade, Assay min. 99%, density (at 20 ºC) 1.474-1.480 g/mL), n-toluene (~99.8%, density at 20 ºC: 0.866-0.8679 g/mL), ethyl acetate (analytical grade, extrapure, ~99.5%, density at 20 ºC: 0.899-0.901 g/mL), hydrochloric acid, sodium hydroxide, acetone and sodium chloride were procured from SISCO research laboratories (SRL Chemicals, India). HPLC grade chloroform, HPLC grade water and glycerol were purchased from Merck (India). HPLC grade water was utilized in water vapor transmission rate (WVTR) studies. Acetone (~99%, density at 20 ºC: 0.790-0.792 g/mL), dichloromethane (~99%, density at 20 ºC: 0.791-0.793 g/mL) and methanol (~99%, density at 20 ºC: 0.790-0.793 g/mL) were received from Fisher Scientific, India. Lab made chitosan

(CH) (DD% >77% and viscosity average molecular weight: 44 kDa) was extracted from Muga silkworms (*Antheraea assamensis*) and utilized as a filler in this research work. Millipore water (Metrohm, ELIX 3) was used as a solvent to dissolve chitosan and to perform solubility experiments and also to perform contact angle measurements of film samples. All the above chemicals were used without any further purification.

2.2. Methods

2.2.1. Extraction of chitin

Initially, MS were isolated from the cocoons and chopped into small pieces. The pieces were washed multiple times using normal tap water to remove dirt, dry flash and other impurities. Further, the material was dried overnight in vacuum oven at 60 ºC. The dried sample was ground using mixer grinder and resulting powder was treated with 1 M HCl solvent in a proportion of 10 mL (HCl)/g of dry powder for 20 min at 100 ºC during demineralization step, as shown in Figure. 2.1. After demineralization, the solution was filtered, thereafter, several washing with millipore water, the excess acid was removed and dried in vacuum oven till it reached to the constant weight. The demineralized MS powder was treated with 1 M NaOH solution (10 mL (NaOH)/g of dry powder) for 24 h at 80 ºC in deproteinization step. The obtained solution was appeared black in colour. After filtration, the residue was washed several times with millipore water to remove excess NaOH, colour and froths. Finally, the residue was dried in vacuum oven at 60 ºC to constant weight. The decolouration of deproteinized MS powder was done with acetone at room temperature for 24 h. The washed powder was filtered and dried in vacuum oven at 80 ºC until constant weight. The obtained chitin powder was brown in colour which was further characterized.

2.2.2. Deacetylation process

In the deacetylation process, the extracted chitin sample was treated with 40% NaOH solution using chitin to solvent ratio of 1:10. The deacetylation of chitin was carried out at four different temperatures (60, 80, 100 and 110 ºC) at 4, 6, 8 and 10 h for each temperature in order to understand the kinetics of the deacetylation. After deacetylation reaction, reaction mixture was washed several times with millipore water till it reached to the neutral pH~7. Finally, the filtered residue was dried at 60 ºC in vacuum oven until it reaches to the constant weight. The schematic flowchart of complete extraction process is shown in Figure 2.1.

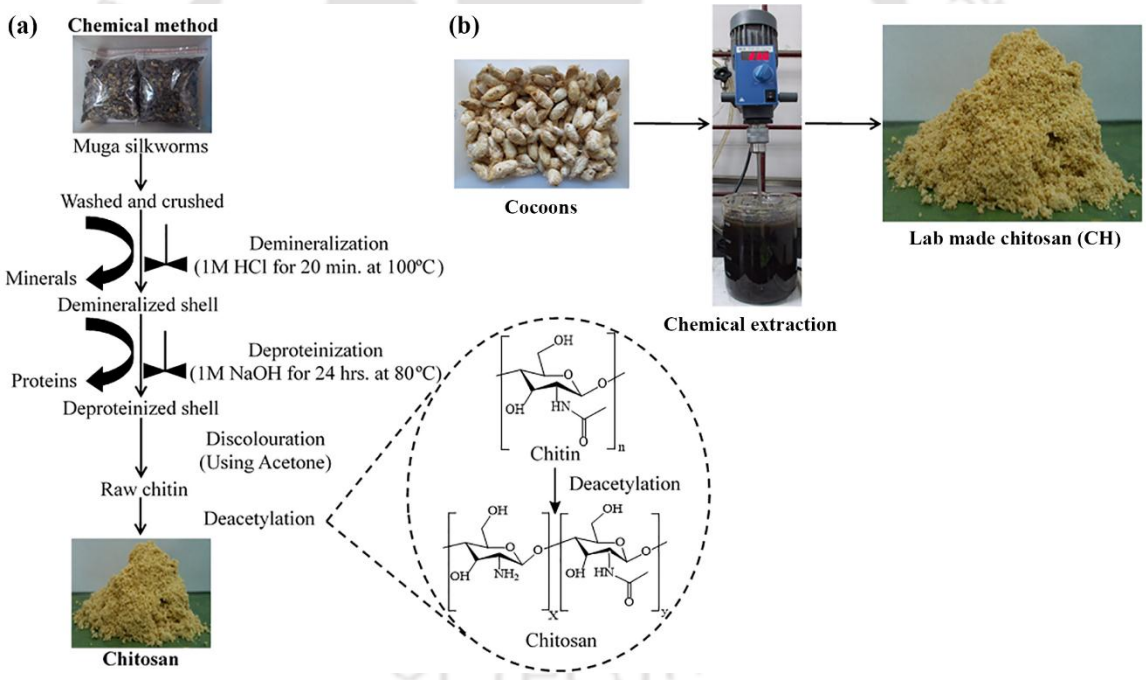

Figure 2.1. (a) Chemical extraction of chitin and its conversion to chitosan by deacetylation and (b) Overall experimental representation.

2.2.3. PLA/CH biocomposite films preparation

PLA and PLA/CH films were prepared by solution casting method. In this method, 2 g of PLA was mixed with 50 mL chloroform and a homogeneous solution was prepared by stirring it at room temperature. For the preparation of PLA/CH biocomposite films, PLA was mixed with different CH loading of 1, 3 and 5 wt% in chloroform followed by stirring for 6 h at room temperature. The solutions were sonicated in digital sonicator at room temperature for 2 h to reduce particle size and increase dispersion of CH in PLA. The prepared solutions were poured on Teflon petri dishes and dried for 12 h in fume hood. The films were peeled off and kept in vacuum oven at 40 ºC for 12 h for further drying to remove the bound and unbound solvent completely from the films. The thickness of all the film samples was measured by digital coating thickness meter (make: indi, model: indi6156). Five different positions at each sample was chosen randomly for thickness measurement. The average thickness was calculated with standard deviation. The fabricated films were shown in Figure 2.2.

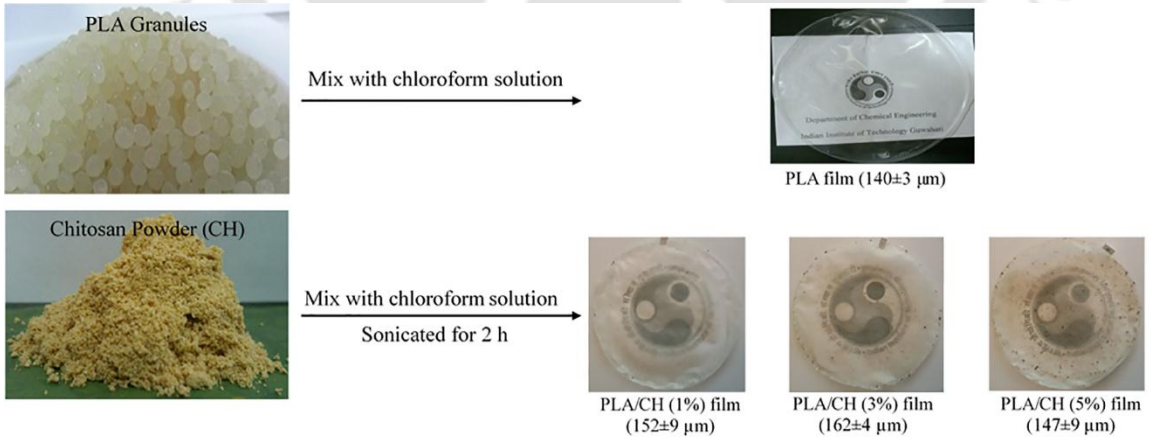

Figure 2.2. PLA/CH biocomposite films fabrication by solution casting technique.

2.2.4. Synthesis of chitosan-*graft*-oligo l-lactic acid (CH-*g*-OLLA) by conventional heating technique

Initially, 25 g of lactic acid (LA) was taken in a three neck reactor and was heated at 150 °C under Ar (inert) gas environment. Gradually, 10, 20 and 30 % (wt/wt) of CH was added under constant stirring rate (~400 rpm) for modification using polycondensation reaction in absence of catalyst. In argon (Ar) atmosphere, the solution was heated for 120 min at 150 °C. Thereafter, vacuum was applied for next 120 min. During initial 60 min, the vacuum inside the reactor raised from 100 to 0.1 mbar and afterwards it was maintained at 0.001 mbar. Finally, vacuum was broken using inert gas. The water as condensate and other byproducts were collected in an ice-cooled trap which was connected in series with condenser as shown in Figure 2.3. The prepared material (modified chitosan) was stored in a sealed vial for further use. The oligo-(L-lactic acid) (OLLA) was also prepared from LA under identical operating conditions.

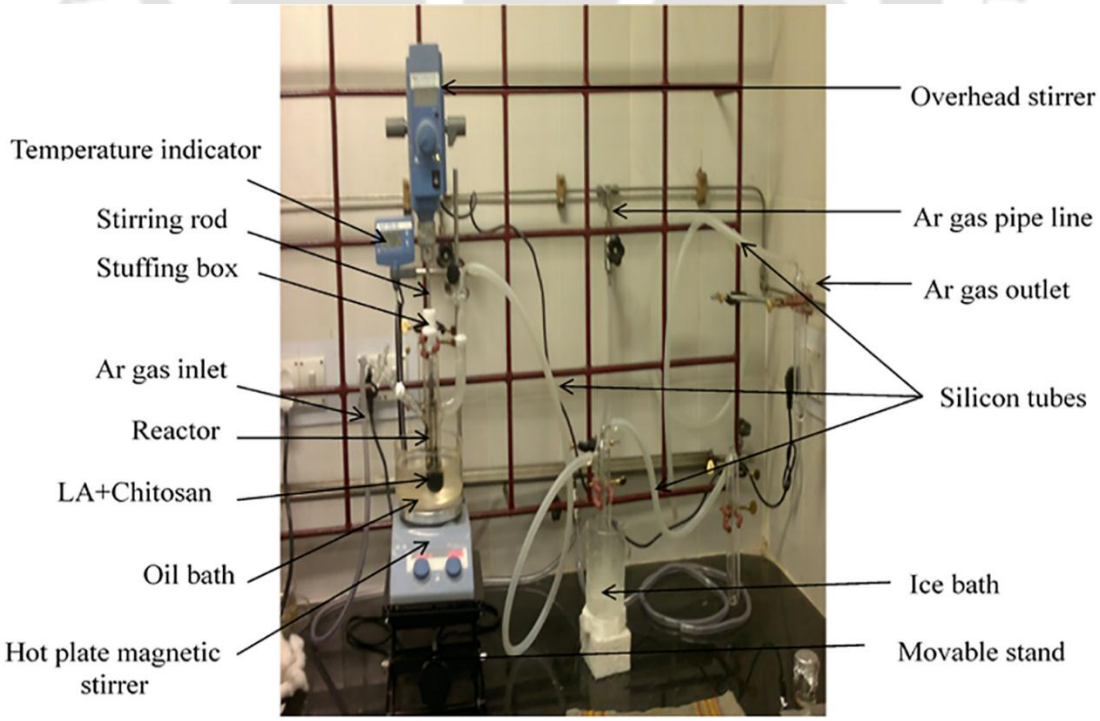

Figure 2.3. Conventional heating setup to synthesize CH-*g*-OLLA.

OLLA was efficiently grafted on chitosan backbone using conventional heating method, which has been checked via solubility test. However, microwave heating method may be preferentially used over conventional heating because it may produce the products with higher yield, less power consumption and less reaction time. Hence, microwave heating method was also performed and the prepared CH-*g*-OLLA copolymer was used in further research.

2.2.5. Synthesis of CH-*g*-OLLA by microwave assisted *insitu* condensation polymerization technique

Lactic acid was thoroughly mixed with various concentrations of chitosan such as 10%, 20% and 30% (wt/wt%) in round bottom flask (RBF) before the synthesis. The mixture was kept in RBF for 12 h at room temperature to complete soaking of LA into chitosan as shown in Figure 2.4(b). The prepared soaked mixture was kept in microwave under N_2 atmosphere. Microwave heating was used to achieve higher reaction rate and high product yield. Microwave assisted *insitu* condensation polymerization reaction was performed for the preparation of CH-*g*-OLLA copolymer in microwave at 110 °C for 30 min at 240 watts under 'convection cum microwave' mode as shown in Figure 2.4(a). A heating belt with a set temperature of ~100 °C, was connected between RBF and condensor to avoid condensation of unbound water and other byproducts during reaction. After completion of the reaction, microwave was stopped and inert atmosphere was removed. A highly viscous product of dark brown color was obtained due to the grafting of LA on chitosan backbone as shown in Figure 2.4(c). The calculated M_n and M_w values of CH-*g*-OLLA were 1400 Da and 3000 Da respectively. This grafted product is now soluble in chloroform. OLLA was also prepared by the same technique having M_n value of ~2000 Da.

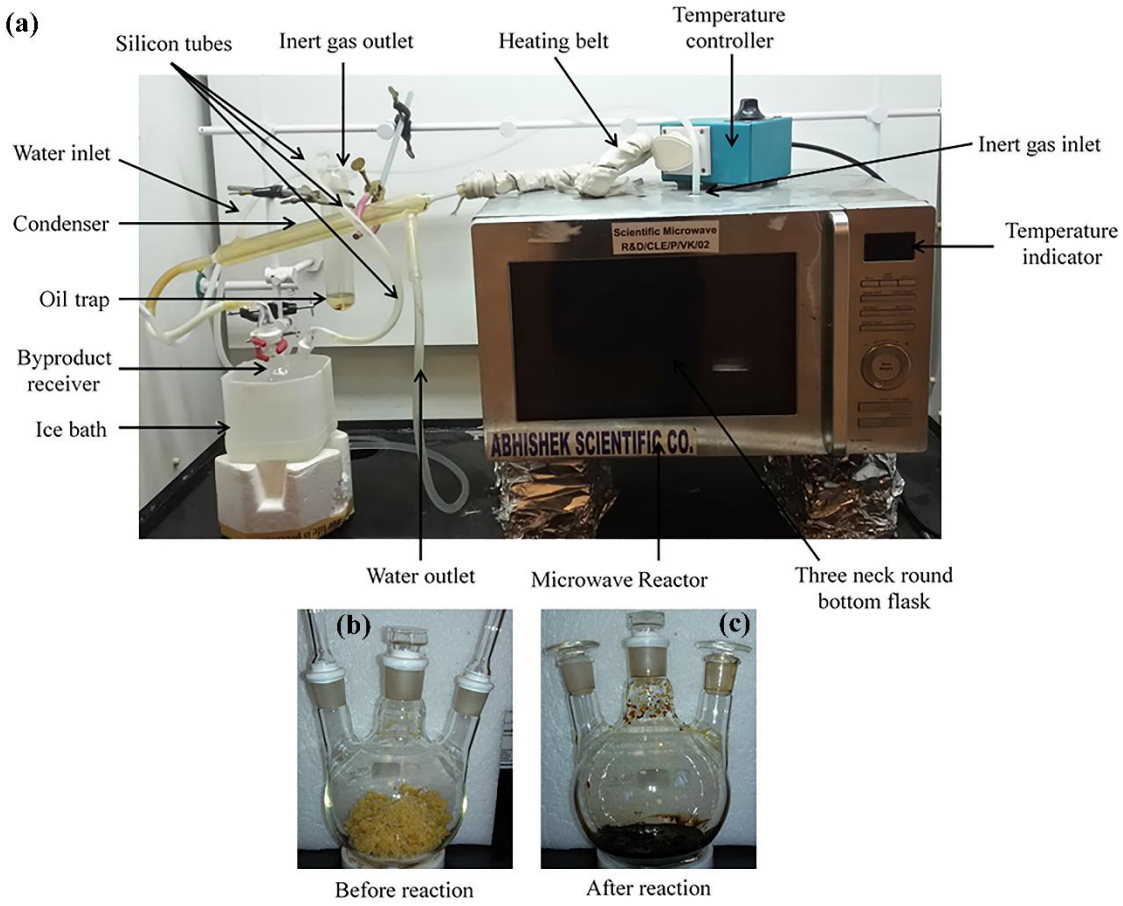

Figure 2.4. (a) Microwave setup to synthesize CH-*g*-OLLA, (b) chitosan before reaction and (c) chitosan after reaction.

The yield (%), percentage conversion (%), grafting efficiency (%), percent grafting (%) and percent homopolymer (%) in CH-*g*-OLLA copolymer were calculated by Eqs. 2.1, 2.2, 2.3, 2.4 and 2.5 respectively **[Singh et al., 2006; Pandey and Mishra, 2012]**.

$$\text{Yield (\%)} = \left(\frac{W_1}{W_0 + W_2}\right) \times 100 \quad (2.1)$$

$$\text{Percent conversion (\%)} = \left(\frac{W_1}{W_0}\right) \times 100 \quad (2.2)$$

$$\text{Grafting efficiency (\%)} = \left(\frac{W_1 - W_0}{W_2}\right) \times 100 \quad (2.3)$$

$$\text{Percent grafting (\%)} = \left(\frac{W_1 - W_0}{W_0}\right) \times 100 \quad (2.4)$$

$$\text{Percent homopolymer (\%)} = 100 - \text{Grafting efficiency} \quad (2.5)$$

Where, W_0, W_1 and W_2 denote the weight of neat chitosan, weight of copolymer and weight of lactic acid respectively. The CH-*g*-OLLA copolymer prepared by the combination of lactic acid and 30 wt% chitosan have been used for further research work.

2.2.6. PLA/CH-*g*-OLLA bionanocomposite films preparation

In this study, three different types of polymer films such as PLA, chitosan and PLA/CH-*g*-OLLA bionanocomposite films were prepared by solution evaporation technique. Chloroform was used as a solvent for PLA and PLA/CH-*g*-OLLA films. 1% (wt/wt) acetic acid solution was used for dissolution of chitosan. PLA/CH-*g*-OLLA films were prepared by using CH-*g*-OLLA as a nano-filler. A known quantity of PLA granules and CH-*g*-OLLA was mixed together in chloroform under stirring (500 rpm) at ambient conditions for six hours and after solvent evaporation, PLA or PLA/CH-*g*-OLLA bionanocomposite films were prepared. The different amounts of PLA and CH-*g*-OLLA were taken in such a way that all the films contain the following compositions of PLA/CH i.e. 100/0, 99/1, 97/3, 95/5 and 0/100 (wt/wt%). These compositions were termed as PLA, PLA/CH-*g*-OLLA (1%), PLA/CH-*g*-OLLA (3%), PLA/CH-*g*-OLLA (5%) and chitosan films. Further, a known quantity of medium molecular weight chitosan was dissolved in 1% (wt/wt) acetic acid solution under stirring (800 rpm) at ambient conditions for 12 h. After complete dissolution of chitosan, the solution was left for 12 h for the removal of bubbles. All the prepared solutions were poured into Teflon petri dishes and dried for 12 h at ambient conditions in fume hood. After drying, the films were peeled off and put into the vacuum oven at 40 ºC for 12 h for complete removal of bound and unbound solvent. All obtained films were stored in a desiccator at room temperature for further analysis. The images of PLA and bionanocomposite film were incorporated in Figure 2.5. The higher loadings of nano-filler such as 6, 8, 9 and 12 wt% cannot be used because the higher

loadings of nano-filler in polymer matrix forms agglomeration, which reduces the physico-chemical, mechanical and barrier properties. However, it is equally important to observe the variation in PLA matrix after the addition of nano-filler at lower loadings such as 1 wt%. Lower loadings of nano-filler may disperse uniformly in PLA and results the increment in various properties.

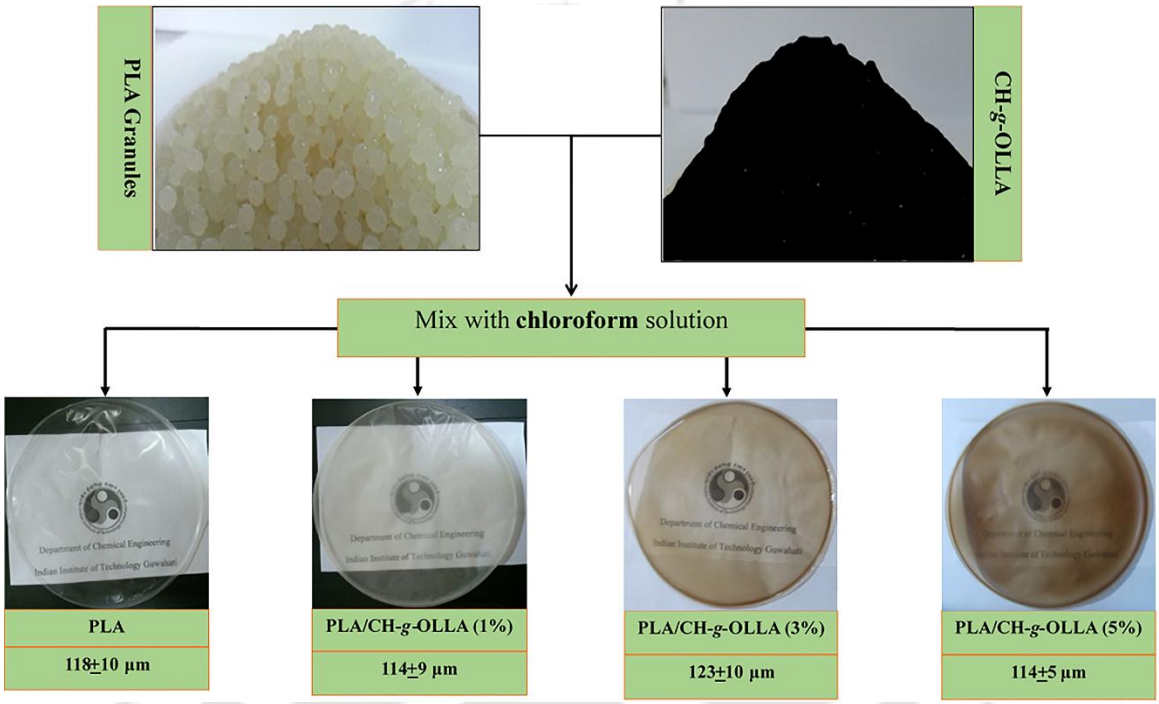

Figure 2.5. Fabricated PLA and PLA/CH-*g*-OLLA bionanocomposite films by solution casting technique.

2.2.7. Melt-blended PLA/CH-*g*-OLLA bionanocomposite films

PLA granules and CH-*g*-OLLA nano-filler were dried at 40 ºC in vacuum oven for 12 h to eliminate the residual moisture content. Subsequently, CH-*g*-OLLA was dissolved in acetone followed by vacuum filtration using ~450 µm pore size filter paper to remove the undissolved part. Further, the vacuum dried PLA granules were dipped into CH-*g*-OLLA/acetone solution for uniform dispersion of filler. The prepared mixture was

vacuum dried at 60 ºC for 12 h to remove the available acetone. The various proportions such as 1, 3 and 5 wt% of CH-*g*-OLLA was mixed with PLA granules (~8 g), which are termed as PLA/CH-*g*-OLLA (1%), PLA/CH-*g*-OLLA (3%) and PLA/CH-*g*-OLLA (5%) bionanocomposites. Neat PLA granules were used to fabricate the control film. Neat PLA and various proportions of mixtures were melt extruded in a co-rotating twin screw extruder (Haake Minilab II, ThermoFisher Scientific) at the processing temperature of 190 °C and screw speed of ~100 rpm. Neat PLA and PLA/CH-*g*-OLLA bionanocomposites were received in the form of long strips of dimension ~5×0.5 mm^2 (width×thickness) as products as shown in Figure 2.6.

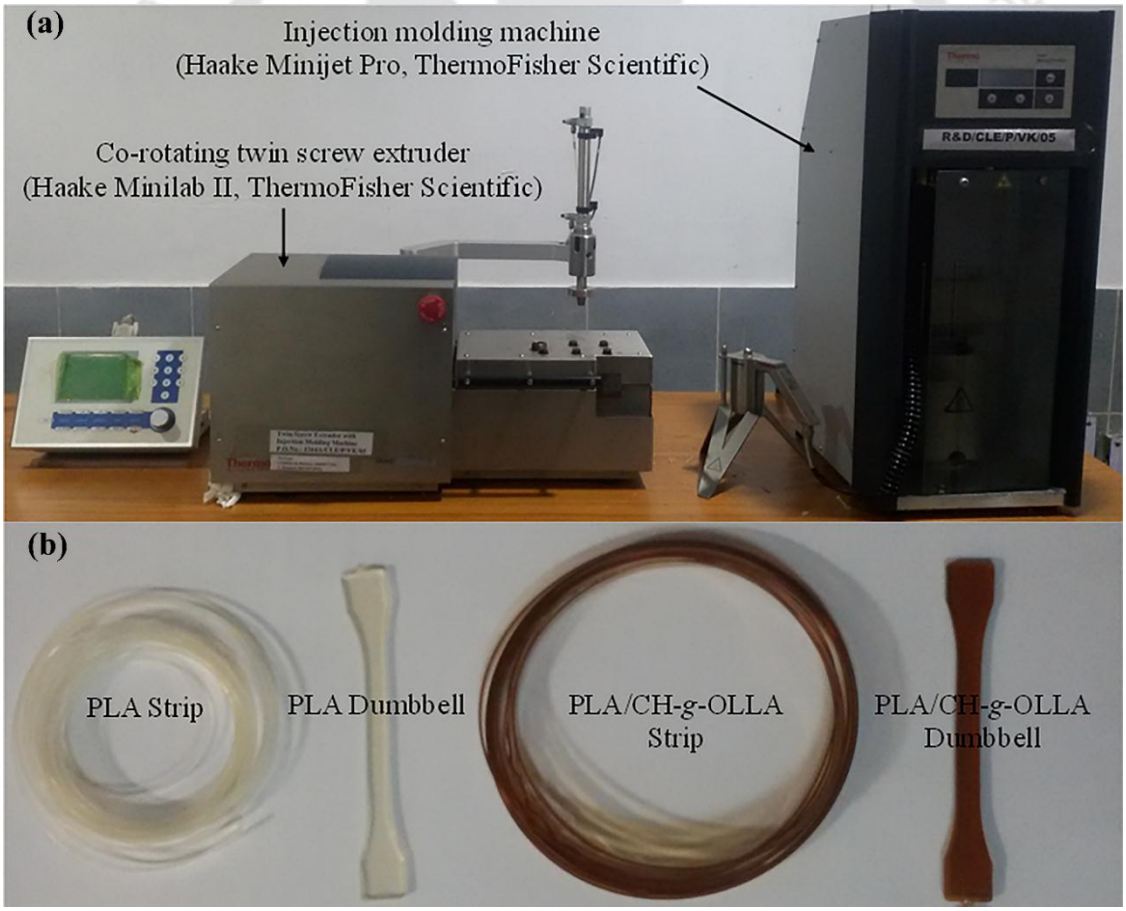

Figure 2.6. (a) Co-rotating twin screw extruder and injection molding machine and (b) Fabricated PLA strip, PLA dumbbell, PLA/CH-*g*-OLLA strip and PLA/CH-*g*-OLLA dumbbell.

The dumbbells (ISO527-2-1BA) of neat PLA granules and prepared various PLA/CH-*g*-OLLA mixtures were fabricated using injection molding machine (Haake Minijet Pro, ThermoFisher Scientific) at 190 °C and feeding pressure of ~4 bar. The mold temperature was maintained at ~70 °C. The prepared samples were stored in desiccator for further analysis. The volume fraction of filler (CH-*g*-OLLA) (Φ_f) in PLA matrix was calculated with the help of Eq. 2.6 **[Singla et al., 2016]**.

$$\Phi_f = \frac{\frac{W_f}{\rho_f}}{\frac{W_f}{\rho_f} + \frac{W_{PLA}}{\rho_{PLA}}} \quad (2.6)$$

Where, W_f, W_{PLA}, ρ_f and ρ_{PLA} represent the weight of filler (g), weight of PLA matrix (g), density of filler (g/cm^3) and density of PLA matrix (g/cm^3) respectively.

2.2.8. Melt-extruded PLA/CH-*g*-OLLA bionanocomposite films

Various proportions of PLA granules and CH-*g*-OLLA nano-filler (1, 3 and 5 wt%) were prepared by the same procedure as mentioned in section 2.2.7 and subsequently transformed into nicely dispersed films. Every batch of granules was charged into a hopper, which was further transported into a barrel (diameter: ~24 mm) of twin-screw extruder having L/D ratio of 42:1 (Boolani Engineering Corporation, India). The material was charged into primary volumetric feeder of the extruder at the screw speed of ~250 rpm. The temperature profile was sequentially fixed in five zones including die heads. The temperature profile for neat PLA granules into Film conversion was fixed from 170-190 °C across the five zones with a temperature difference of 5 °C and the set temperatures of die zones were 195, 200, 202 and 202 °C respectively. Similarly, the temperature profile for PLA/CH-*g*-OLLA bionanocomposite granules was also sequentially set from 160-180 °C across the five zones with a temperature difference of 5 °C and also for die zones was set from 185-195 °C with the same temperature difference. The molten form of PLA and PLA/CH-*g*-OLLA was discharged from the die

(width: ~15 cm) at ~1.9 mL/min. The extruded PLA and its bionanocomposite films were passed through a highly polished and chilled turning roll, which were annihilated on the contact side of the film as shown in Figure 2.7. Further, the films were transferred to a second roll for cooling on the other side. The melt extruded films were passed through the rollers at ~2 m/min in order to obtain the thickness of ~200±12 µm and finally rolled on to a winder at ~60 rpm. A nice brown colour films with homogeneously dispersed CH-*g*-OLLA were observed for further analysis. The gel content (%) in melt extruded PLA/CH-*g*-OLLA bionanocomposite films was calculated by dissolving the known amount of films in chloroform at 500 rpm for 12 h. The dissolved solutions were filtered by 0.2 µm size filter paper to extract the undissolved gel content. The filtered solution was vacuum dried at 60 °C to evaporate the solvent. The gel yield (%) was calculated by Eq. 2.7 **[Dhar et al., 2016]**.

$$\text{Gel yield } (\%) = \frac{W_{gel}}{W_{initial}} \times 100 \qquad (2.7)$$

Where, W_{gel} and $W_{initial}$ are defined as weight of final dry gel and weight of melt extruded bionanocomposite films respectively.

2.2.9. Lamination of PLA with PLA/CH-*g*-OLLA bionanocomposite films

Lamination of melt extruded PLA with PLA/CH-*g*-OLLA bionanocomposite films were performed at an optimized heating temperature of ~90 ºC and roller's speed was maintained at ~1 mm/sec as shown in Figure 2.8. The rollers were heated with the attached heating element and operated at zero gap to produce maximum shear force during lamination. Both the films were arranged over each other and passed between the rollers at above mentioned conditions. After passing through the heated rollers, the films were again passed between the two rollers at atmospheric conditions to produce the uniform laminated stretched films.

Figure 2.7. Pilot plant scale production of PLA/CH-*g*-OLLA bionanocomposite films; (a) twin screw extruder for lab and industrial scale film processing, (b) PLA granules coated with CH-*g*-OLLA, (c) PLA/CH-*g*-OLLA bionanocomposite film passing through rotating drums, (d) Processing of PLA/CH-*g*-OLLA bionanocomposite film, (e) extruded PLA film and (f) extruded PLA/CH-*g*-OLLA bionanocomposite film.

Similarly, the laminations were also performed by using extruded PLA film at ~100 ºC. IITG institute logo was sandwiched in between PLA and PLA/CH-*g*-OLLA bionanocomposite films as a reference.

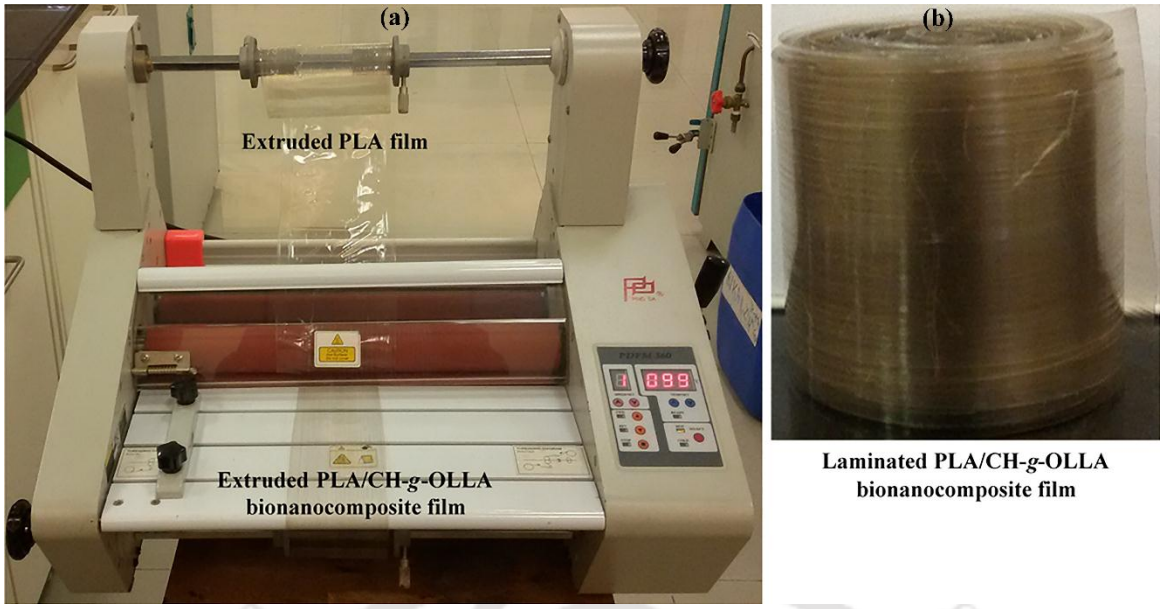

Figure 2.8. Lamination process for PLA with PLA/CH-*g*-OLLA bionanocomposite film; (a) laminator operated at 1 mm/sec and ~90 ºC and (b) laminated PLA/CH-*g*-OLLA bionanocomposite film.

2.3. Analytical instrumentation and characterizations

2.3.1. Solubility test

Solubility is the easiest technique to confirm the conversion of hydrophilic nature into hydrophobic and vice versa. Solubility determination for pure chitosan, OLLA and CH-*g*-OLLA copolymer was carried out at room temperature by adding ~1 mg of polymer in 1 mL of various organic and inorganic solvents such as water, acetic acid, methanol, chloroform, dichloromethane, acetone, n-toluene, and ethyl acetate, which was followed by stirring for 6 h at 500 rpm using a magnetic agitation.

2.3.2. Fourier transform infrared spectroscopy (FTIR)

Infrared spectroscopic analysis was carried out for extracted chitin, chitosan, LA and CH-*g*-OLLA copolymer samples using Fourier transform infrared spectrometer (Shimazdu, IR Affinity-1) at room temperature to interpret the present functional groups. The samples were prepared by uniformly mixing them with KBr in 100:1 ratio. Whereas,

IR spectra of PLA, chitosan, PLA/CH biocomposite films, solution casted PLA/CH-*g*-OLLA bionanocomposite films and melt extruded PLA/CH-*g*-OLLA bionanocomposite films were evaluated using Fourier transform infrared spectrometer (Perkin Elmer, Frontier) attached with attenuated total reflectance (ATR) attachment under dry air at room temperature. The films were dried at 80 ºC for 2 h before analysis. A small piece of each film was placed on the ATR crystal surface made of zinc selenide. The software named IRsolution was used for analysis. The FTIR spectrum was taken in a transmittance mode. The analysis was executed in the range of 4000 cm^{-1} to 600 cm^{-1} for 20 consecutive scans at a 2.0 cm^{-1} resolution **[Rinaudo, 2006; Rasal et al., 2010]**. The DD% of extracted chitosan powder was calculated by using Eq. 2.8 **[Baskar and Kumar, 2009]**.

$$DD\% = 97.67 - \left(26.486\frac{A_{1655}}{A_{3450}}\right) \quad (2.8)$$

Where, A_{1655} and A_{3450} are the absorbance values at wavenumber 1655 cm^{-1} and 3450 cm^{-1} respectively.

2.3.3. X-ray diffractometry (XRD)

The XRD measurements of chitin, chitosan powder (obtained at 80 ºC after 4, 6, 8 and 10 h), PLA/CH biocomposite films, solution casted PLA/CH-*g*-OLLA biocomposite films and melt extruded PLA/CH-*g*-OLLA biocomposite films were performed by X-ray diffractometer (Bruker, D8 Advance, Germany) equipped with θ-θ goniometer and Ni-filtered Cu Kα radiation (λ = 1.54 Å). The diverging and receiving slits were operated at 40 kV and 40 mA. The 2θ range for the analysis was chosen from 3º to 40º with a continuous scan speed and increment of 2 sec/step and 0.05º/sec respectively. The samples were annealed at 80 ºC for 2 h before analysis. The crystallinity index (I_{cr}) of chitin and chitosan powder was calculated from the intensity of the peaks at 2θ≈20º and 2θ≈16º. In the case of chitin and chitosan powder, the peak at 2θ≈20º showed maximum intensity

which has [110] lattice plane (I_{110}) and peak at 2θ≈16° showed minimum intensity (I_{am}), which signifies amorphous diffraction. The interlayer spacing (d) and I_{cr} were calculated by Eq. 2.9 and 2.10 **[Sagheer et al., 2009]**.

$$d = \frac{\lambda}{2\sin\theta} \tag{2.9}$$

$$I_{cr} = \left(\frac{I_{110} - I_{am}}{I_{110}}\right) \times 100 \tag{2.10}$$

Where, λ is the wavelength of incident radiation. θ is half of the Bragg's angle corresponding to the crystalline peak. However, the crystallinity index of PLA/CH-*g*-OLLA bionanocomposite film samples was calculated by inbuilt Topaz software in XRD, which is based on Eq. 2.11.

$$I_{Cr} = \frac{\text{Area of crystalline peaks}}{\text{Area of crystalline peaks} + \text{Area of amorphous peaks}} \times 100 \tag{2.11}$$

2.3.4. Gel permeation chromatography (GPC)

The molecular weights (number average molecular weight (M_n) and weight average molecular weight (M_w)) and polydispersity index (PDI) of synthesized CH-*g*-OLLA copolymer and extruded PLA/CH-*g*-OLLA bionanocomposite films were evaluated using gel permeation chromatography technique (Shimadzu LC-20A system, Shimadzu, Japan) fitted with two PLgel 5 µm mixed D columns (Agilent, U.K.) in series, which was working with an eluent (HPLC grade chloroform) at 1 mL/min and sample injection volume of ~40 mL. The system was calibrated with a wide molecular weight range of polystyrene (PS) standards. The samples (~30 mg) were solubilized in HPLC grade chloroform (~1 mL) followed by filtration using Whatman filter papers (0.2 µm) before analysis.

2.3.5. Optical polarimetry

The self-calibrated AUTOPOL II (Rudolph Research Laboratory, U.S.A.) was utilized to measure the optical and specific rotation of extruded PLA and PLA/CH-*g*-OLLA bionanocomposite films by dissolving ~20 mg film sample in 20 mL chloroform. The

analysis was performed at a wavelength of 589 nm. After vigorous stirring at 800 rpm for 6 h, the prepared solutions were filtered using 0.45µm Whatman filter paper to eliminate the effect of interference of chitosan particles during optical measurements.

2.3.6. Elemental analysis

Carbon, hydrogen and nitrogen contents of extracted chitin and chitosan (obtained at 80 ºC after 10 h) were measured by using CHNS Elemental Analyzer Eurovector EA3000. The sample was heated at 600 ºC for 1 h and the residual weight was calculated to find out the quantity of inorganic materials. Elemental analysis was also used for estimation of DD% of chitosan samples. The Eq. 2.12 was used to calculate the DD% **[Baskar and Kumar, 2009]**.

$$\mathrm{DD\%} = \left(1 - \frac{\frac{\mathrm{C}}{\mathrm{N}} - 5.145}{6.861 - 5.145}\right) \times 100 \qquad (2.12)$$

Where, $\frac{\mathrm{C}}{\mathrm{N}}$ is referred as carbon/nitrogen ratio of chitin and chitosan samples.

2.3.7. Nuclear magnetic resonance spectroscopy (NMR)

^{1}H-NMR spectra was obtained for extracted chitosan (obtained at 80 ºC after 10 h), OLLA and CH-*g*-OLLA copolymer by using Bruker Ascend^{TM}600 NMR spectrometer. Chitosan sample was prepared by dissolving 5 to 10 mg/mL of chitosan in 2% deuterated acetic acid in D_2O solution depending on the solubility of the sample. However, OLLA and CH-*g*-OLLA were dissolved in deuterated chloroform ($CDCl_3$) followed by filtering with 0.2 µm size syringe filter before analysis. After dissolution, approximately 1 mL of sample was transferred to NMR tube for analysis. The spectra of samples were recorded in the spectral range of 0 to 10 ppm. According to ASTM F2260-03 standard, NMR spectroscopy is the most reliable characterization technique for DD% calculation.

Hence, Eq. 2.13 was used for DD% calculation **[Sagheer et al., 2009]**.

$$DD\% = \frac{H1 - D}{H1 - D + \frac{H - Ac}{3}} \times 100 \quad (2.13)$$

Where, $H1 - D$ is the integral at δ = 3.17 ppm, corresponding to the proton of the CH group connected to the nitrogen moiety of the deacetylated monomer unit and $H - Ac$ is the integral at δ=1.88 ppm, corresponding to the three protons of the acetyl group.

In the case of synthesized CH-*g*-OLLA, graft branch length of OLLA on chitosan backbone was calculated by Eq. 2.14 **[Kannan et al., 2010]**.

$$\text{Graft branch length} = \frac{\text{Peak intensity at 5.1 ppm}}{\text{Peak intensity at 4.2 ppm}} \quad (2.14)$$

^{13}C NMR analysis of OLLA and CH-*g*-OLLA copolymer was carried out by using Bruker Ascend^{TM}600 NMR spectrometer and compared for interpreting the modification and grafting in chemical structure.

2.3.8. Potentiometric titration

In this method, 0.2 g of dried chitosan (obtained at 80 ºC after 10 h) was dissolved in 20 mL of 0.1 M HCl solution. After 30 min of continuous stirring, 25 mL of millipore water was added and stirred till chitosan dissolved completely. The solution was then titrated with 0.1 M NaOH solution. The graph was plotted and two inflection points were obtained. The values of DA% and DD% were calculated by Eqs. 2.15 and 2.16 **[Czechowska-Biskup et al., 2012]**.

$$DA\% = 2.03\frac{V2 - V1}{m + 0.0042(V2 - V1)} \quad (2.15)$$

$$DD\% = 100 - DA\% \quad (2.16)$$

Where, m = dry weight of chitosan (g), $V2 - V1$ = difference in NaOH volume between the two inflection point (mL), 2.03 is the coefficient resulting from the molecular weight

of chitin monomer and 0.0042 is the coefficient resulting from the difference in molecular weight between the chitin and chitosan monomer units.

2.3.9. Conductometric titration

The chitosan sample (obtained at 80 ºC after 10 h) was dissolved in 0.054 M HCl by stirring at room temperature and titrated with 0.165 M NaOH. The value of conductance was recorded after stabilization and plotted against the volume of titrant added. The DD% was calculated by Eq. 2.17 **[Alvarenga et al., 2010]**.

$$\mathrm{DD\%} = \frac{[\mathrm{base}] \times (\mathrm{V2} - \mathrm{V1}) \times 161}{\mathrm{m}} \qquad (2.17)$$

Where, [base] is the concentration of NaOH (M), V1 and V2 are the volumes of NaOH (mL), 161 is the molar mass of the monomer and m is the amount of sample (mg).

2.3.10. Differential scanning calorimetry (DSC)

Various thermal states such as glass transition temperature, cold crystallization temperature and melting temperature of PLA/CH biocomposite and melt extruded PLA/CH-*g*-OLLA bionanocomposite films were carried out using differential scanning calorimeter (Netzsch, DSC 204 F1 Pheonix, Germany) in the temperature range of 25 to 180 ºC at a scanning rate is 5 ºC/min by the application of two heating and one cooling cycles under nitrogen gas flow rate of 60 mL/min. Similarly, the thermal behaviour of solution casted PLA/CH-*g*-OLLA bionanocomposite films (~5-6 mg) was examined using differential scanning calorimeter (DSC 1, Star^{e} System, METTLER TOLEDO, Switzerland) under nitrogen atmosphere with flow rate of 50 mL/min. Two thermal cycles were applied for analysis in which, first cycle was from -25 ºC to 220 ºC at a scanning rate of 5 ºC/min followed by isothermal condition for two min at 220 ºC and further cooling from 220 ºC to -25 ºC with the same scan rate. The isothermal condition was maintained at 180 ºC for 2 min after the completion of first cycle. The second cycle was repeated same as that of first cycle. The instrument was pre-calibrated with Indium standards using platinum based

crucible. Enthalpy of cold crystallization (ΔH_{cc}) and enthalpy of melting (ΔH_m) are also calculated to develop the better understanding about the polymeric system. For isothermal crystallization kinetics, the film samples were heated from 25 to 180 ºC at a scanning rate of 10 ºC/min followed by holding the temperature for 2 min to remove the thermal history. In addition, the sample was cooled until 110 ºC at a cooling rate of 50 ºC/min and maintained this isothermal condition for 1 h. Further, the samples were cooled up to 25 ºC very rapidly at 50 ºC/min.

2.3.11. Thermogravimetric analysis (TGA)

TGA analysis was performed to examine the thermal stability of chitin, chitosan (obtained at 80 ºC after 10 h), OLLA, CH-*g*-OLLA copolymer by using TGA instrument (TGA-4000, Perkin Elmer, USA). Approximately, 6 mg of sample was heated from 30 to 700 ºC at a heating rate of 10 ºC/min under nitrogen atmosphere with a flow rate of 10 mL/min. However, TGA analysis of PLA, chitosan, PLA/CH biocomposite films and solution casted PLA/CH-*g*-OLLA bionanocomposite films has been performed to find out the thermal degradation temperature and E_a by other thermogravimetric analyser (Libra TG 209, Netzsch). The non-isothermal degradation kinetics for PLA/CH biocomposite films was done in the temperature range of 30 ºC to 600 ºC at different heating rates from 5 ºC/min to 20 ºC/min. However, the temperature range was selected from 35 to 650 °C at a heating rates of 2, 5 and 10 °C/min under inert atmosphere with a flow rate of 50 mL/min for solution casted PLA/CH-*g*-OLLA bionanocomposite films.

2.3.12. Hyphenated thermogravimetric-Fourier transform infrared spectroscopy (TG-FTIR)

Hyphenated TG-FTIR analysis of PLA, CH and PLA/CH-*g*-OLLA bionanocomposite films (~6 mg) was carried out using thermogravimetric analyzer (TGA4000, Perkin-Elmer, U.S.A.) coupled with Fourier transform infrared spectrophotometer (Perkin-Elmer, U.S.A.)

in a temperature range of 30 to 700 °C at a rate of 5 °C/min under the flow of N_2 gas at 20 mL/min. The isothermal condition was maintained at 700 °C for 1 min. TGA was coupled with FTIR by an interface line having gas transfer tube and gas cell. The interphase line was heated up to 250 ºC to avoid condensation of the evolved gases. The evolved gases from TG instrument was passed through the interphase line and detected by FTIR spectrophotometer.

2.3.13. Polarized optical microscopy (POM)

The spherulitic morphology, growth rate (G) and nucleation in PLA and PLA/CH-*g*-OLLA bionanocomposite films were measured using polarized optical microscope (Eclipse LV100N POL, Nikon Co., Japan) equipped with a Linkam TST350 hot stage (Linkam Scientific Instrument) at isothermal condition. The sample (~2 mg) was sandwiched between two cover slides and melted at 180 °C for two min to obtain a thin slice. The slice was transferred to a hot stage and heated upto 200 °C at a heating rate of 20 °C/min followed by isothermal condition for five min to erase the thermal and mechanical history. Afterwards, the sample was cooled to 110 °C at a cooling rate of 20 °C/min and maintained the isothermal condition for 1 h (until complete crystallization). The spherulitic morphology was recorded in the crystallization process using a stationary digital camera.

2.3.14. Scanning electron microscopy (SEM)

SEM images of extracted chitin, chitosan (obtained at 80 ºC after 10 h), OLLA, CH-*g*-OLLA copolymer and solution casted PLA/CH-*g*-OLLA bionanocomposite samples were analyzed by scanning electron microscope (1430vp, LEO, U.S.A.), operated at a voltage of 10 kV with 15 mm working distance. A small amount of dried sample was mounted at aluminium stubs over carbon tape. Further, a thin gold layer was coated on the samples under vacuum using sputter coater (SC7620, Quorum) to increase the conductivity of the samples. The energy dispersive X-ray spectroscopy (EDX) analysis of synthesized

CH, OLLA and CH-*g*-OLLA copolymer was carried out using the same instrument at same settings.

2.3.15. Field emission scanning electron microscopy (FESEM)

FESEM analysis of PLA, PLA/CH biocomposite films, solution casted PLA/CH-*g*-OLLA bionanocomposite films and melt extruded PLA/CH-*g*-OLLA bionanocomposite films was performed by field emission scanning electron microscope (Sigma, Zeiss) for examining the variation in surface morphology of PLA films with an increase in filler loadings. Small piece of film samples was mounted at aluminium stubs over double sided carbon tape and ~10 nm gold-palladium coating was done under vacuum by using sputter coater (SC7620, Quorum). The analysis was performed at 1.50 kV with ~5 mm working distance.

2.3.16. Transmission electron microscopy (TEM)

The morphological investigation of CH-*g*-OLLA copolymer, solution casted PLA/CH-*g*-OLLA bionanocomposite films and melt extruded PLA/CH-*g*-OLLA bionanocomposite films was carried out at nano scale using transmission electron microscope (JEM-2100, JEOL, USA), operated at an accelerating voltage of 200 kV. The samples were dissolved in HPLC grade chloroform followed by stirring the solution for 2 h for uniform dispersion. The filtered solutions were drop casted on carbon coated grids (Tedpell, USA) and dried overnight at 60 °C before the analysis. The dimension of dispersed particles was measured by ImageJ software. The end to end distance & radius of gyration (R_g) of OLLA chains were calculated by Material Studio 7.0 software (Biovia, USA) using Forcite module.

2.3.17. Contact angle measurements (CA)

The contact angle analysis of synthesized CH-*g*-OLLA copolymer was carried out using contact angle analyzer (GmbH DSA25, KRUSS, Germany) with ~4 µL drop volume of millipore water at 23±1 °C by sessile drop method. The liquid drop was injected on the

samples by a syringe (fitted above the sample holder). The samples were prepared by dissolving the polymer in chloroform solvent and poured the solution on glass slide. Further, the samples were dried overnight at ~60 °C in vacuum oven. During analysis, the droplet geometry was captured with the help of camera, placed in front of the sample holder. The contact angle analysis of PLA/CH biocomposite films was performed at same conditions using millipore water. The surface hydrophobicity of PLA and its bionanocomposite films is a critical property in food packaging applications as the packed food is stored in high humidity conditions. The contact angles of PLA/CH-*g*-OLLA bionanocomposite films (fabricated from minicompounder) were measured using same instrument at similar conditions. In this case, two different liquids such as millipore water and glycerol were used for contact angle measurements. The contact angles were measured only after the stabilization of the droplet on the samples and the measurement was replicated for five times (for each measurement a new spot was selected) and the average values were reported with standard deviation.

2.3.18. Viscosity average molecular weight

Intrinsic viscosity (η) measurement of chitosan (extracted at 80 ºC after 10 h) was performed by Ubbelohde viscometer at room temperature (25±1 ºC). A solvent mixture of 0.02 M acetic acid and 0.1 M sodium chloride was used to dissolve chitosan with five different concentrations from 0.001 to 0.010 g/mL. Intrinsic viscosity (mL/g) was calculated using the Huggins Eq. 2.18 **[Moura et al., 2011]**.

$$\frac{\eta_{sp}}{C} = [\eta] + k[\eta]^2 C \qquad (2.18)$$

Where, $\frac{\eta_{sp}}{C}$ is the reduced viscosity in mL/g, η_{sp} is the relation between viscosity of the polymer in solution and the solvent (dimensionless), C is the concentration of the solution in g/mL and k is a constant valid for each polymer (dimensionless).

The viscosity average molecular weight (M_v) of chitosan was calculated by using Mark-Houwink-Sakurada Eq. 2.19 **[Moura et al., 2011]**.

$$[\eta] = kM_v^{\alpha} \quad (2.19)$$

Where, k = 1.81×10^{-3} mL/g and α = 0.93

The average value of three replicates was calculated for intrinsic viscosity and viscosity average molecular weight calculation.

2.3.19. Ash content

Chitosan (extracted at 80 ºC after 10 h) ash content was estimated through combustion process using a constant weight crucible. The empty crucible was placed in muffle furnace (Reico, India) at 600±5 ºC for 30 min and subsequently the residue, cooled upto room temperature, was used for weight measurement. For real time ash analysis, 1 g of chitosan sample was treated under the identical conditions and thereafter the weight of the ash was measured followed by the calculation of ash content using Eq. 2.20 **[Yuan et al., 2011]**.

$$\text{Ash}\% = \frac{W_2 - W_0}{W_1 - W_0} \times 100 \quad (2.20)$$

Where, W_0 is the constant weight of silica crucible, W_1 is the weight of chitosan sample with crucible and W_2 is the weight of ash with crucible.

2.3.20. Mechanical properties

The uni-axial mechanical properties of PLA/CH biocomposite films, solution casted PLA/CH-*g*-OLLA bionanocomposite films and injection molded dumbbells of PLA and PLA/CH-*g*-OLLA bionanocomposites were measured using universal testing machine (Kalpak instruments and controls, KIC-2-050-C), equipped with 500 N load cell with a cross-head speed of 50 mm/min at room temperature. The dimension of film samples was based on ASTM D882 standard. The pre-analysis conditioning of test samples was done at 25±5 ºC and 50±5% relative humidity (RH) for 48 h. The ultimate tensile strength (σ), was calculated by the ratio of peak load and cross-sectional area of the sample. The elongation

at break (ε) was calculated by the ratio of elongation at the fracture point and the initial length of specimen followed by multiplication by 100. The values of Young's modulus (E) was determined from the slope of stress-strain curves. Three samples of each combination were tested, analyzed and reported the average values with standard deviation.

2.3.21. Dynamic mechanical analysis (DMA)

The thermo-mechanical analysis of solution casted PLA, PLA/CH biocomposite films and PLA/CH-*g*-OLLA bionanocomposite films (dimension: 5 mm×5 mm×0.5 mm) was carried out by using dynamic mechanical analyzer (Netzsch, DMA242) under tensile mode at an operating frequency of one hertz. The analysis was conducted at a dynamic force of two newton under constant strain amplitude of 20 µm. The test was performed in the temperature range of 25-110°C at a heating rate of 5°C/min for PLA/CH biocomposite films. However, DMA was operated in the temperature range of 25-120 °C at a heating rate of 3 °C/min for PLA/CH-*g*-OLLA bionanocomposite films.

2.3.22. Shore hardness test

The shore hardness test of melt blended PLA and PLA/CH-*g*-OLLA bionanocomposite strips were carried out using Durometer (GGR-30, Hiroshima) based on ASTM D2240 at atmospheric conditions. The average hardness value was reported by performing the measurement at five different positions in each composition.

2.3.23. Water vapor transmission rate (WVTR)

WVTR test was performed to measure the WVTR×e values of PLA, solution casted PLA/CH biocomposites films using water vapor permeability tester (PERMATRAN-W® 1/50G, Mocon, USA) based on ASTM E398-03. The test samples were conditioned at 25±1 ºC and 50% RH for 48 h prior to analysis. Temperature is an important parameter in determining accurate transmission rates. The increment or decrement in transmission rates is 4 to 6 %/ºC. The test was performed in continuous mode at 37.8±0.5 ºC and atmospheric

pressure. The permeant side and dry side RH% was maintained at 100 and 5% respectively. Pure nitrogen (~99.9%) was purged at a line pressure of 30 to 35 psig. The film samples (test area: 50 cm^2) was exposed to 95% RH approximately for 5 h. The analysis was performed in triplicate and the average results were reported with standard deviation. Further, the water vapour permeability (WVP) of melt extruded PLA/CH-*g*-OLLA bionanocomposite films (test area = 50 cm^2) was measured with the same instrument at similar operating conditions at 50% RH.

2.3.24. Oxygen transmission rate (OTR)

OTR test of solution casted PLA/CH-*g*-OLLA and melt extruded PLA/CH-*g*-OLLA bionanocomposite films was performed to measure the amount of oxygen passed across the films samples using oxygen permeability tester (OX2/231, Labthink International, China) following ASTM D3985 standard. In the case of solution casted PLA/CH-*g*-OLLA bionanocomposite films, the analysis was performed in a temperature range of 15 to 45±0.1 ºC and 0% RH to study the impact of operating temperature on oxygen permeability. However, the analysis was performed at 25±0.1 ºC and 0% RH in the case of melt extruded PLA/CH-*g*-OLLA bionanocomposite films. The films (~50 cm^2) were fixed between upper and lower diffusion chambers. Argon gas (purity: 99.999%) was injected in both upper and lower chambers with flow rates of 20 and 10 mL/min respectively for purging. The conditioning of film samples was done with the use of temperature controller (TC-01, Labthink) at 25±0.1 ºC and humidifier system at 0% RH enclosed in permeability tester during the time of purging. After the completion of zero test, the analysis was started by injecting high purity oxygen (>99.999%) in the upper diffusion chamber at a flow rate of 20 mL/min whereas, argon gas was injected in the lower diffusion chamber at a flow rate of 10 mL/min at prescribed operating conditions. Analysis completion time was considered ~6 h so as to reach steady state value. The oxygen volumetric flow rate per unit area of the

film and per time (cc/m^2.day) was monitored continuously until steady state was reached and can be measured by Eq. 2.21 **[Dhar et al., 2015]**.

$$\mathrm{OTR}\ (t) = \frac{Pp}{l}[1 + 2\sum_{n=1}(-1)^n \exp(-\frac{D^2 n^2 t}{l^2})] \quad (2.21)$$

Where, P, p and l are oxygen permeability, oxygen partial pressure and film thickness respectively. The percentage reduction in OTR values of different nanocomposite films was calculated by the formula as shown in Eq. 2.22 **[Arrieta et al., 2014; Ambrosio-Martin et al., 2014; Burgos et al., 2013; Re et al., 2014]**.

$$\text{Percentage reduction} = \frac{\text{Initial value} - \text{Final value}}{\text{Initial value}} \times 100 \quad (2.22)$$

Where, OTR value of PLA film (control) and solution casted PLA/CH-*g*-OLLA films were taken as initial and final values respectively. The value of half-time ($t_{1/2}$) was defined as the time at which OTR reached 50% of its steady state value. The diffusion coefficient (D) of oxygen gas in bionanocomposite films was calculated by Eq. 2.23, which was derived by normalizing Fick's second law as shown in Eq. 2.21.

$$D = \frac{l^2}{7.199\ t_{1/2}} \quad (2.23)$$

The solubility coefficient (S) of oxygen gas in bionanocomposite films was calculated by Eq. 2.24.

$$P = D \times S \quad (2.24)$$

Three replicates of each sample were tested.

Gas permeability values in terms of Arrhenius expression

A better understanding was developed about the effect of variation in temperature on gas transport properties of bionanocomposite films by Arrhenius expression as shown in Eq. 2.25.

$$P = P' e^{\frac{-E_P}{RT}} \quad (2.25)$$

Where, P′, E_P, R and T are pre-exponential factor (cc.mm/m^2.day), permeation activation energy (kJ/mol), universal gas constant (8.3145 J/mol.K) and absolute temperature (in K) respectively.

2.3.25. Optical Properties

The values of psychometric chroma coordinates such as lightness (L*; 0 = black, 100 = white), a*(+a* = redness, -a* = greenness) and b*(+b* = yellowness, -b* = blueness) of melt extruded PLA and PLA/CH-*g*-OLLA bionanocomposite films were detected using colour measurement spectrophotometer (Datacolor 550, Datacolor Technology Suzhou Co., Ltd, China), based on ISO 9001:2008 standard. The instrument was calibrated using white and green calibration standards (serial no. 8812351) at 23.8 ºC and 46% RH before analysis. The reference values of L*, a* and b* were measured as 90.70, -0.30 and 4.65 respectively. The illuminated area of film samples was lesser than the exposed area to avoid edge effects. Five specimens of each film sample were used for the analysis and the average values are reported. The colour difference (ΔE) values were determined by using Eq. 2.26 **[Hafsa et al., 2016]**.

$$\Delta E = [\Delta L^{*2} + \Delta a^{*2} + \Delta b^{*2}]^{\frac{1}{2}} \quad (2.26)$$

The Chroma (C*) value is defined as relative purity or saturation of a colour and is determined by using Eq. 2.27 **[Rotabakk et al., 2006]**.

$$C^{*} = [a^{*2} + b^{*2}]^{\frac{1}{2}} \quad (2.27)$$

2.3.26. Transparency

The solution casted PLA and PLA/CH-*g*-OLLA bionanocomposite films were cut in the form of strips (25 mm x 15 mm) to perform transparency analysis over the entire range from 250-1100 nm by using ultraviolet-visible (UV-Vis) spectrophotometer (Lambda 25, Perkin Elmer). Each sample was repeated three times and average value was taken into account.

Chapter 3

Extraction and Characterization of Chitosan from Muga Silkworms (*Antheraea assamensis*)

This chapter focuses on extraction of chitin from Muga silkworms (MS) and its conversion into chitosan by chemical treatment process. The extracted amount of chitin and chitosan from MS were obtained ~8 and ~7 wt%, respectively. Potentiometric titrations, conductometric titrations, elemental analysis, ^{1}H-NMR and FTIR analyses were employed to calculate the degree of deacetylation (DD%) of chitosan (extracted at 80 ºC after 10 h) and found as 77%±2, 81%±1.8, 82%±2.4, 97.77%±0.3 and 82%±1.8 respectively. The deacetylation process of chitin showed pseudo-first order reaction kinetics and activation energy was estimated as ~15.5 kJ/mole. The extracted chitosan (at 80 ºC after 10 h) showed higher percentage crystallinity and improved thermal stability with respect to chitosan extracted from other marine sources.

3.1. Introduction

Chitin is a second natural polysaccharide with a long-chain polymer of *N*-acetyl glucosamine, a derivative of glucose **[George et al., 2011; Jiang et al., 2014; Liu et al., 2012]**. It is one of the components of exoskeletons of crabs, lobsters, shrimps, fungi and insects **[Abdou et al., 2008; Paulino et al., 2006; Synowiecki and Al-Khateeb, 2003]**. It is inflexible, hard and nitrogenous polysaccharide **[Abdou et al., 2008]**. Its role in forming the exoskeleton in invertebrates is similar to that of cellulose in plants which gives rigidity to the cells. Chitin may also be described as cellulose with one hydroxyl group on each monomer, replaced with an acetyl group. This allows an increase in hydrogen bonding between adjacent polymers, giving chitin-polymer matrix an increased strength. Chitin is extracted from raw materials by two methods. One is chemical method and the other one is biological method. The chemical method is preferred due to higher yield of chitin, cost effectiveness and lesser time consumption than biological method. All the other impurities like dust, dry flesh, minerals, proteins and other soluble & insoluble components have been removed during the process. The highest yield of chitin (46% from squid pens) has been obtained from marine sources and the lowest one (2.3% from *Saccharomyces gutulata*) is from microbial sources **[Abdou et al., 2008; Liu et al., 2012; Paulino et al., 2006; Synowiecki and Al-Khateeb, 2003]**.

Chitosan is hydrophilic in nature and a bio-adhesive which readily binds to negatively charged surfaces such as mucosal membranes. It has a large number of applications in various fields such as packaging, agriculture, food, cosmetics, textiles, pharmaceutical, biomedical and refinement of industrial effluents **[Abdou et al., 2008; Alvarenga et al., 2010]**. The amine group at C-2 position has unique properties which helps chitosan consumption for a large number of applications as shown in Figure 3.1. Chitosan is insoluble in water, organic and inorganic solvents but soluble in acidic medium

such as acetic, nitric, phosphoric and hydrochloric acids. It shows biocompatible and biodegradable properties, so it is used in various medical applications. It has been used to make cotton membranes for wound dressing which gradually wear off with time as the wound heals. Based on its antimicrobial and non-toxicity, it is extensively used in the food processing and pharmaceutical industries. The chelating property makes it useful in heavy metal ions removal in wastewater treatment **[Dutta et al., 2004]**. Chitin and chitosan are fungistatic in nature. Chitosan is compatible with lots of biologically active components incorporated in cosmetic products. Substances absorbing the harmful UV radiations can be easily covalently linked with chitosan amino group. Chitosan and hair are complementary owing to the kind of charge they carry; hair being negatively charged and chitosan is positively charged. Therefore, chitosan can be used in shampoos, rinses, hair colourants, hair sprays and tonics. Medicinally, chitosan has a large number of advantages but it also has some disadvantages. Chitosan, made from the shells of sea animals like crabs, lobsters and prawns, may not be suitable for people who are allergic to sea food, should take precautions before using chitosan based medicinal products. Consumption of chitosan supplement may make our body less likely to absorb other fat soluble vitamins like A, D and E **[Dutta et al., 2004; George et al., 2011; Kannan et al., 2010; Paulino et al., 2006; Synowiecki et al., 2003]**.

In the present study, Muga silkworms have been used as a raw material. It is one of the typical worms belonging to the insect family and is found in the north eastern region (Assam) of India. Its biological name is *Antheraea assamensis*. It produces the famous "Muga Silk" which is known for its glossy fine texture and durability. The insect's exoskeleton is shell-like, thus containing sufficient amount of chitin. Chitin to chitosan conversion has been done by deacetylation technique. The DD% has been calculated by using potentiometric titration, conductometric titration, elemental analysis, FTIR and ^{1}H

NMR analysis. ^{1}H NMR has been considered the most reliable technique for DD% calculation but potentiometric titration is the easiest and cheapest technique that can be performed in lab without using any costly instruments. The deacetylation kinetics has also been carried out in order to know the mechanism. The novelty of this work is to explore a new, economic and easily available natural source of chitosan which is abundantly available in the north eastern region of India.

3.2. Results and discussion

3.2.1. Chitin extraction and chitosan conversion

The dried MS was grinded and the amount estimated as ~25 wt% of raw muga silkworm. After demineralization, the amount of dried sample was obtained ~17 wt% as per the process mentioned in Figure 3.1.

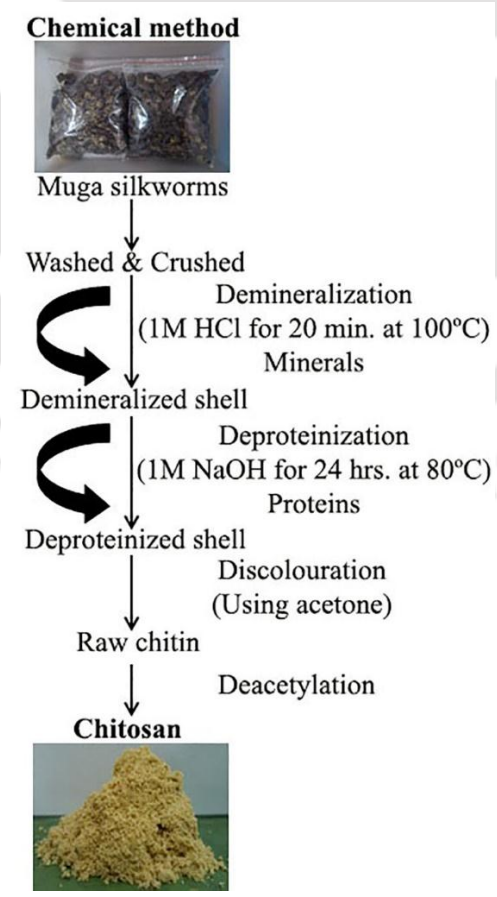

Figure 3.1. Schematic representation of chitosan extraction from Muga silkworms.

The weight loss was attributed to the removal of catechols, Ca, Mg, K and other water soluble impurities. After deproteination, the amount of dried sample was estimated as ~8 wt%. The weight loss was observed due to the removal of proteinaceous elements, pigments, lipids and other organic materials. To remove colour, the dried powder was mixed with acetone for 24 h however, the weight loss in this step was found negligible and the extracted dry chitin powder was found ~8 wt% on dry weight basis of raw MS. Whereas, the extracted chitosan percentage after deacetylation process was found ~7 wt% on dry weight basis of raw MS.

3.2.2. Attenuated total reflectance-Fourier transform infrared spectroscopy (ATR-FTIR)

In chitin sample, the absorption band at 1651 cm^{-1} shows the vibration of amide I band ($C = O$ stretching) which confirms that the extracted powder sample after discoloration is chitin as shown in Figure 3.2(a). The other absorption band is observed at 1557 cm^{-1} in chitin sample which shows the vibrations of amide II band ($N - H$ stretching). The associated reason is that some part of chitin may be already converted into chitosan during alkali treatment. FTIR spectra of chitosan (extracted at 80 ºC) is recorded for different time (up to 10 h) interval during deacetylation process. For different chitosan samples, one band is observed in the range of 1555 to 1557 cm^{-1} which denotes the vibrations of amide II band ($N - H$ stretching) and confirms that the deacetylated samples are chitosan. The vibration of amide I band at 1651 cm^{-1} in chitin sample has shifted towards higher wavenumber i.e. in the range of 1654 to 1658 cm^{-1} for different deacetylated samples which indicates the more amorphous nature of chitosan samples than that of chitin. The band in the range of 1620 to 1622 cm^{-1} is attributed to the stretching of $C - N$ vibration of the superimposed $C = O$ group. The absorption band at 1307 cm^{-1} to 1311 cm^{-1} corresponds to the formation of $CO - NH$ group. Whereas, the band at 1375 to 1377 cm^{-1} corresponds to the symmetrical

deformation of the CH_3 group in all the samples. The intensity of all above mentioned peaks is diminishing due to the deacetylation process which confirms the change in the amount of bonds in the samples. The DD% of chitosan samples are calculated by using Eq. 2.8 and observed as 66%±1.5, 68%±1.7, 70%±0.9 and 82%±1.8 at different deacetylation time i.e. 4, 6, 8 and 10 h, respectively. The DD% value increases with increasing deacetylation time as shown in Figure 3.2(a). The broad absorption band at 3450 cm^{-1} corresponds to OH^{-1} group. While, the absorption band at 3260 cm^{-1} to 3275 cm^{-1} corresponds to intermolecular hydrogen bond to acetamide vibration as shown in Figure 3.2(b).

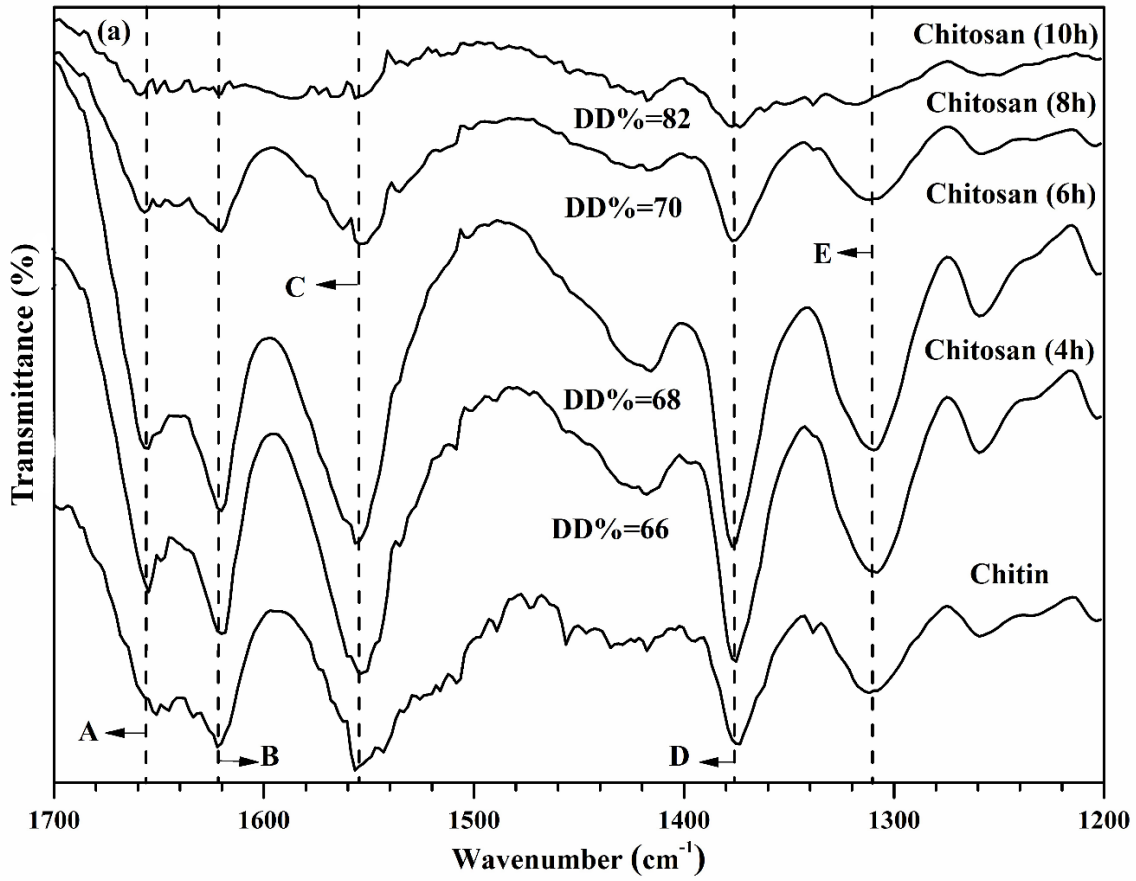

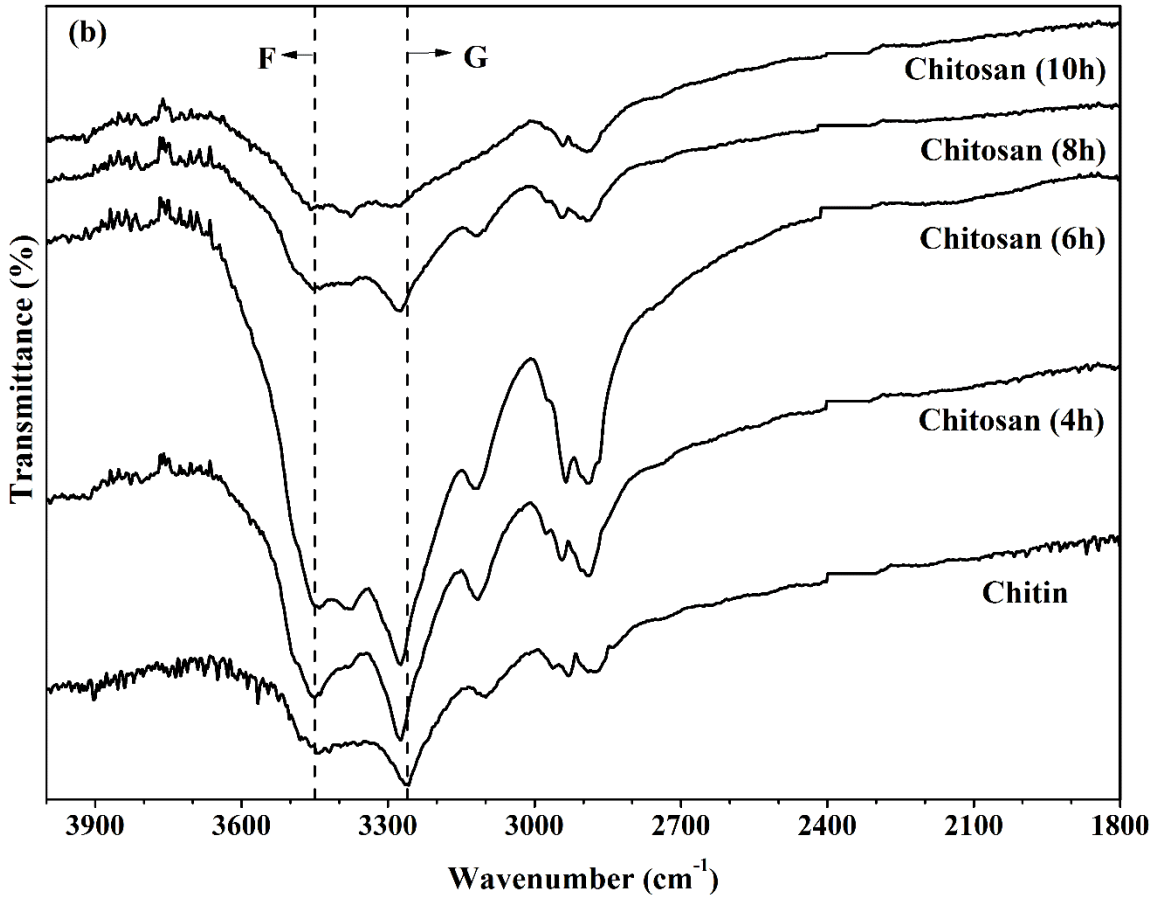

Figure 3.2. FTIR analysis of chitin and chitosan (a) in the range of 1200 to 1700 cm^{-1} (A=1654-1658 cm^{-1}; B=1620-1622 cm^{-1}; C=1555-1557 cm^{-1}; D=1375-1377 cm^{-1}; E=1307-1311 cm^{-1}) and (b) in the range of 1800 to 4000 cm^{-1} (F=3450 cm^{-1}; G=3260-3275 cm^{-1}).

3.2.3. X-ray diffractometry (XRD)

Crystallinity index and d-spacing of chitin and chitosan (extracted at 80 ºC) were shown in Figure 3.3. The orthorhombic unit cells of chitin and chitosan with diffraction planes of [0,2,0], [1,1,0] and [1,0,1] were observed in line with the literature **[Liu et al., 2012; Zhang et al., 2000]**. From the results, chitin sample shows well resolved acute reflections at 9.1º and 19.1º with minor reflections at 12.6º and 26.3º as shown in Figure 3.3. These sharp reflections show crystalline nature of chitin but the intensity of

these reflections is low which indicates the semicrystalline nature of chitin. Whereas, the same two peaks were observed for different deacetylated chitosans (obtained at 80 ºC after 4, 6, 8 and 10 h) in the range of 2θ≈9.5º to 10.2º and 2θ≈19.7º to 20.05º. The observed peaks are broad, less resolved and also shift to higher 2θ values. It shows reduced crystallinity of chitin after deacetylation which concludes that chitosan has more amorphous nature than chitin. The peaks in the range of 9.1º to 10.2º represent d-spacing in the range of 8.6 Å to 9.7 Å due to the incorporation of bound water molecules into the crystal lattice of chitin and chitosan. The peaks in the range of 19.1º to 20.05º corresponds d-spacing in the range of 4.4 Å to 4.6 Å. The interlayer spacing value decreases once the chitin transform into chitosan due to the reduction in bound water molecules. The I_{cr} value of chitin was ~84% whereas, 70-82% was observed in chitosan. The I_{cr} value for different deacetylated chitosans was different due to the penetration of alkali into the chitin crystallites. This penetration breaks the acetyl groups to modify the lattice arrangement of the chitin molecules **[Baskar and Kumar 2009]**. I_{cr} also depends on DD% and decreases with increase in deacetylation time as shown in Figure 3.3, which shows more amorphous nature of chitosan than that of chitin. In the present work, I_{cr} for chitin was found 84% which shows the highly crystalline nature of extracted chitin from MS than that of other silkworms and insects. It is reported in the literature that chitins from larva cuticles and silkworms (*Bombyx mori*) have much lower crystallinity (only 54 and 58% respectively). The reason of low crystallinity is due to the presence of low molecular weight catechol that remains in the insect chitin **[Liu et al., 2012]**. **Abdou et al., 2008** were extracted chitin and chitosan from different marine sources and obtained percentage crystallinity is 66%, 48.9%, 43.15%, 41.78%, 40.99% and 36.43% for brown shrimp, pink shrimp, cuttlefish pens, squid pens, crab shells and crayfish shells, respectively.

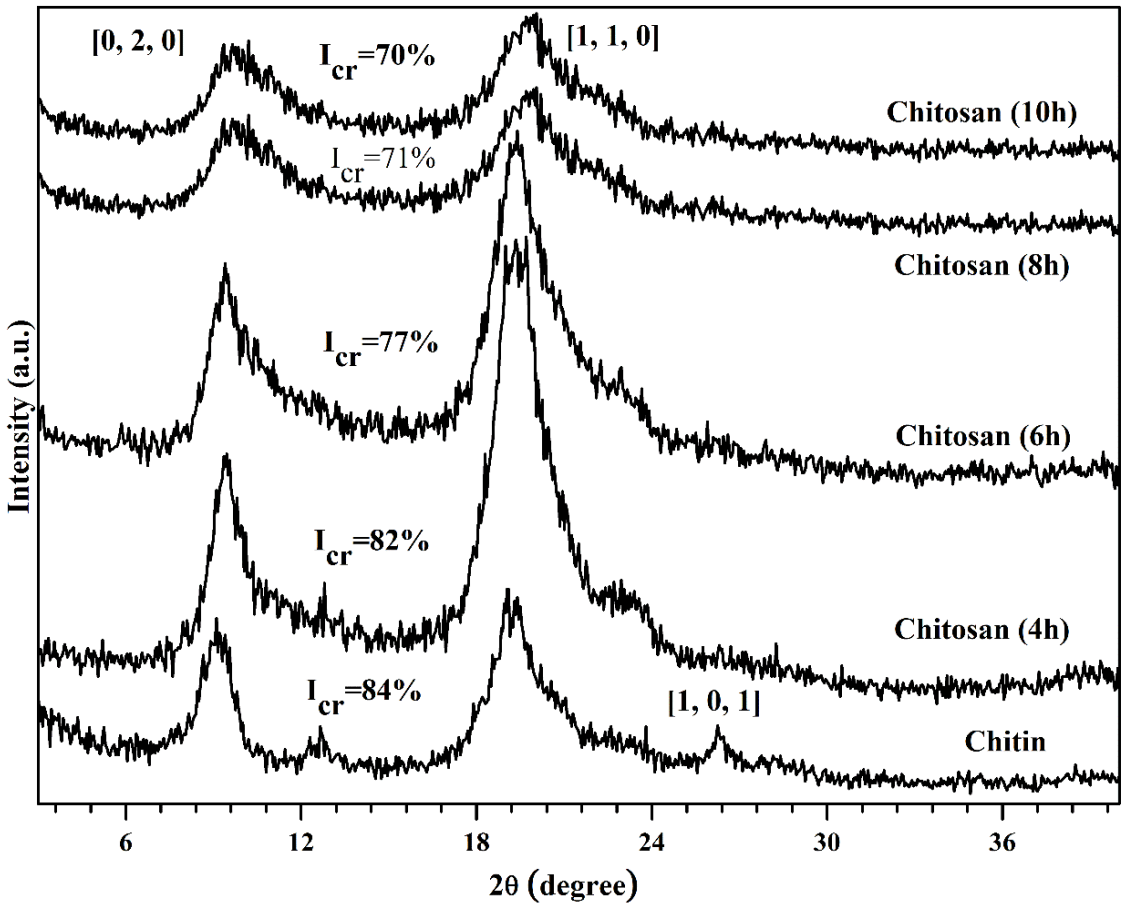

Figure 3.3. XRD analysis of extracted chitin and chitosan from Muga silkworms.

3.2.4. Elemental analysis

Elemental analysis was used to measure the elemental composition (C, H and N%) of chitin, chitosan and DD%. The average percentage of N, H and C% for chitin were observed as 6.48, 6.18, and 42.92% respectively. Whereas, the average percentage of N, H and C% for chitosan (obtained at 80 ºC after 10 h) were detected as 6.32, 6.21 and 34.42% respectively. On comparing the elemental compositions of chitin and chitosan, it shows a small difference in N and H% but a considerable difference in C% due to the conversion of amide group to amine group during deacetylation. So, the C% is mainly responsible for DD% and calculated as 82%±2.4 by Eq. 2.12.

3.2.5. Nuclear magnetic resonance (^{1}H-NMR) spectroscopy

The peak at 1.88 ppm indicates the three protons of the acetyl group (H-Ac) in glucosamine unit and at 3.17 ppm shows the proton of the CH group connected to nitrogen moiety of acetylated glucosamine unit (H1-D) as shown in Figure 3.4. In the spectrum of extracted chitosan (obtained at 80 ºC after 10 h), all the other non-anomeric protons have peaks in the range of 3.5 to 4.0 ppm. These non-anomeric protons have similar electron densities and the peaks partially overlap each other in the given spectral range. The resolution of the other protons was low and often overlapped with the signals of the solvent (4.7 to 4.9 ppm for D_2O/2.03 ppm for CD_3COOD). The slight shift in position of the peaks may be due to the working temperature. The DD% was calculated as 97.77%±0.3 by the given formula in Eq. 2.13.

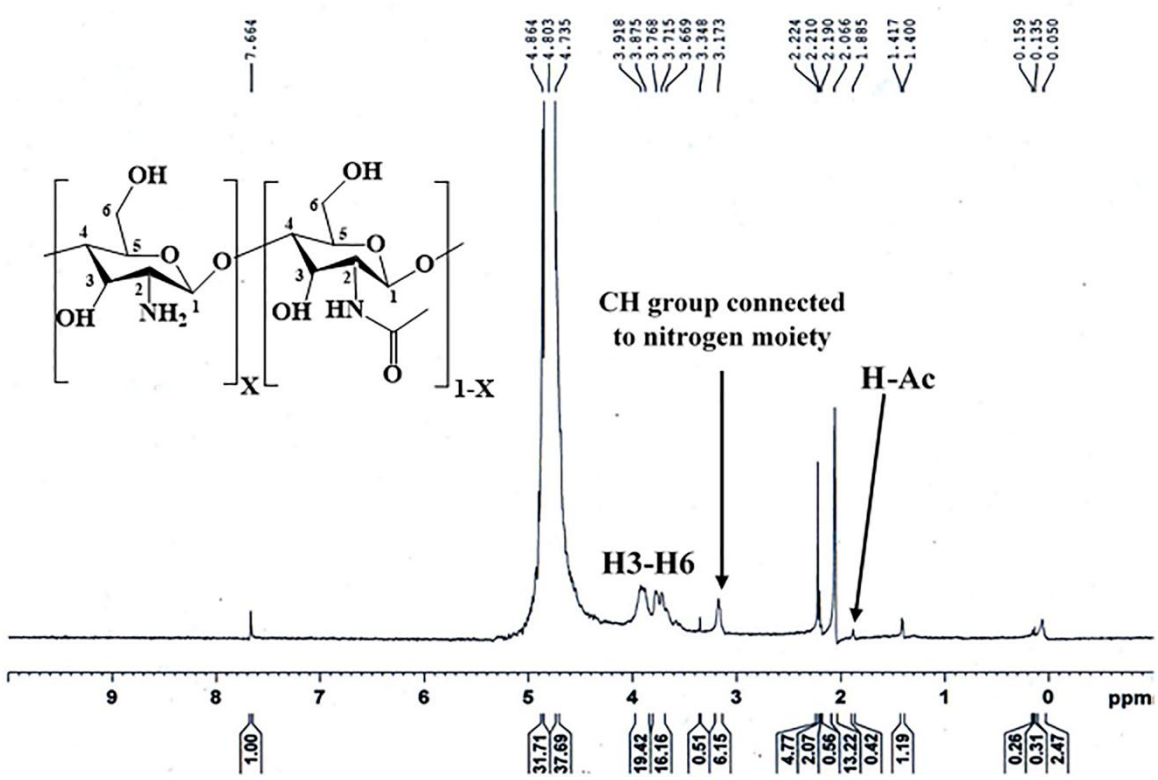

Figure 3.4. ^{1}H-NMR spectra of extracted chitosan (obtained at 80 ºC after 10 h).

3.2.6. Potentiometric titration

The graph was plotted for pH derivative against the volume of NaOH added where two inflection points were obtained as shown in Figure 3.5. The first inflection point corresponds to the neutralization of HCl and the second to the neutralization of the ammonium ions of chitosan (obtained at 80 ºC after 10 h). The difference between two inflection points gives the amount of amine groups present in chitosan. The DD% value was 77%±2 as calculated by Eq. 2.15 and 2.16.

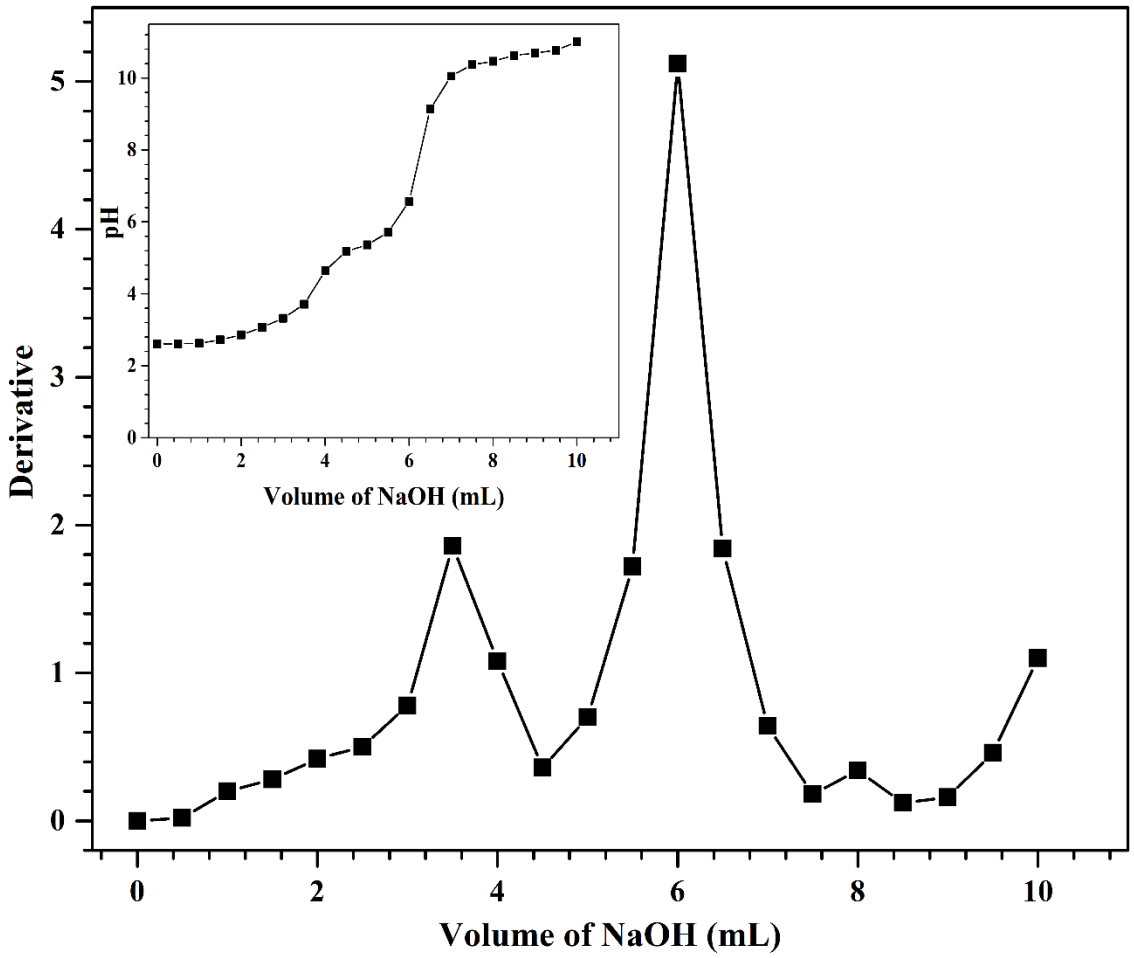

Figure 3.5. Determination of DD% of chitosan (obtained at 80 ºC after 10 h) by potentiometric titration.

3.2.7. Conductometric titration

The conductivity graph was appeared with three distinct line segments, as shown in Figure 3.6. The first segment line corresponds to the neutralization of excess HCl present in the solution whereas second shows the neutralization of the ammonium group present in the chitosan (obtained at 80 ºC after 10 h). The third segment line relate to the excess base present in the sample. The two points were found by the intersection of the three lines and the difference between the two points corresponds to the amount of NaOH required to neutralize the amine group. Using Eq. 2.17, DD% was calculated as 81%±1.8 which was in close agreement with the values calculated by FTIR, ^{1}H-NMR, elemental analysis and potentiometric titration.

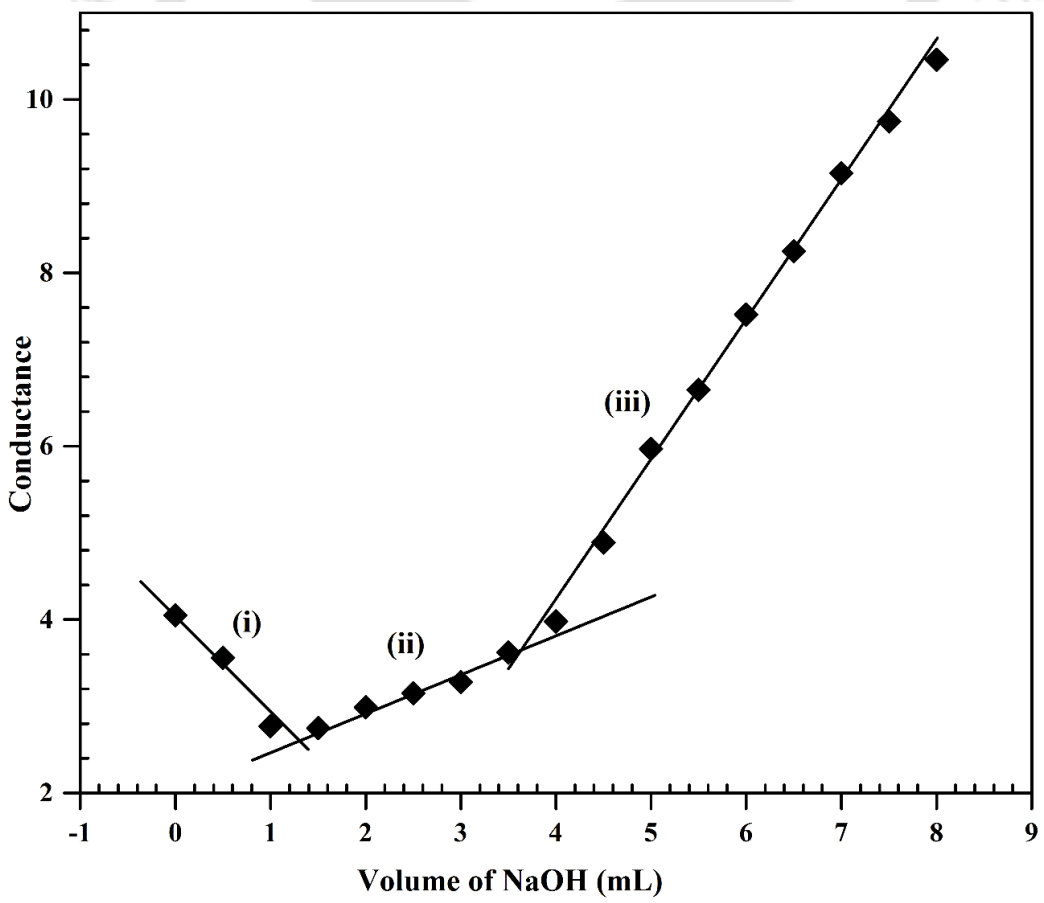

Figure 3.6. Determination of DD% of chitosan (obtained at 80 ºC after 10 h) by conductometric titration.

3.2.8. Deacetylation reaction pathway

Deacetylation occurs when chitin reacts with sodium hydroxide and subsequently the carbonyl carbon gets polarized. The OH^- ions in solution attach with the carbon of amide group and form an intermediate which converts into NH^- ions and acetic acid by rearrangement of electrons. Protons from acetic acid react with NH^- ions and forms NH_2. The reaction pathway of amide to amine conversion is shown in Figure 3.7.

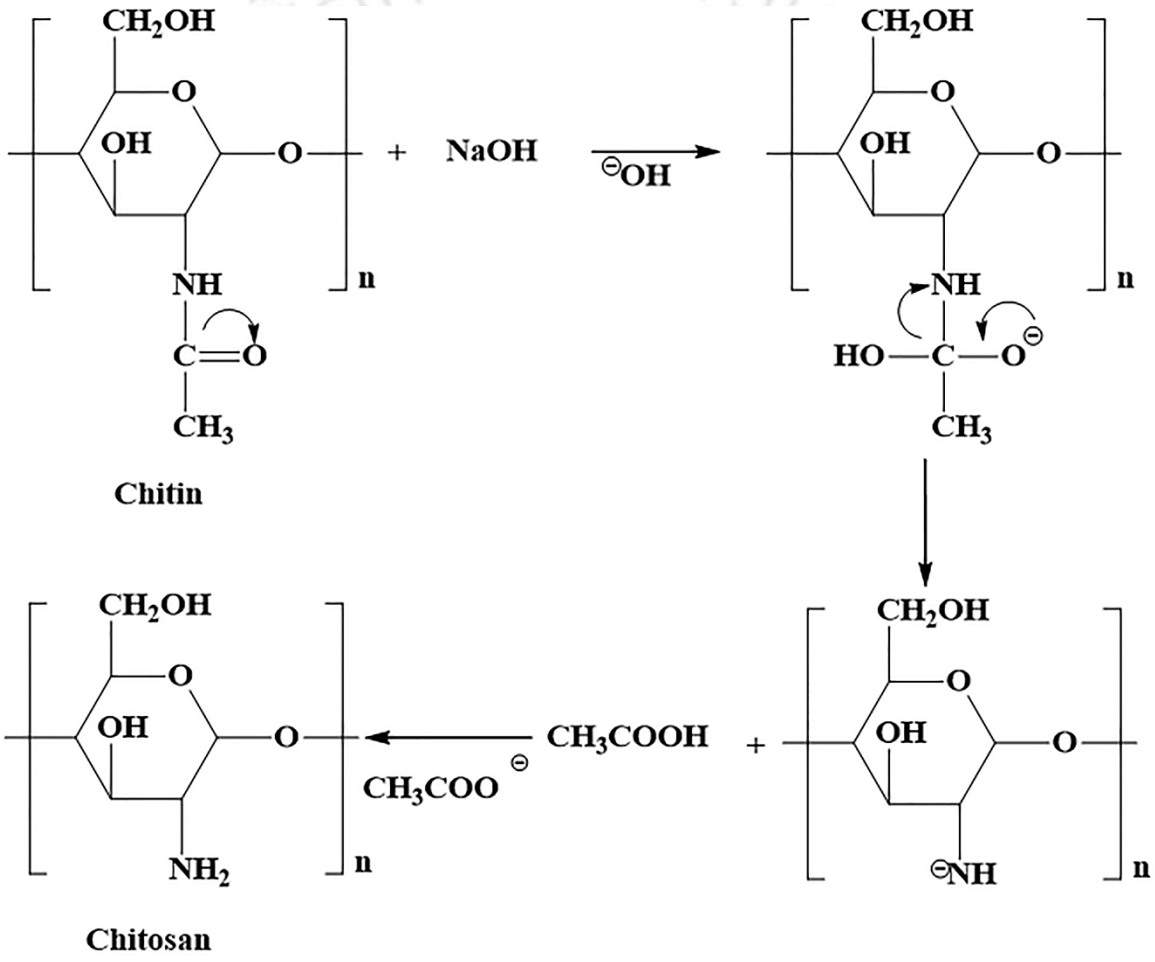

Figure 3.7. Reaction pathway for conversion of chitin to chitosan during deacetylation.

3.2.9. Multistage deacetylation kinetics

The deacetylation of chitin to chitosan is a process that depends on the reaction temperature and time. Reactions were carried out at 60, 80, 100 and 110 ºC; and the samples were collected after 4, 6, 8 and 10 h. The DD% was required for deacetylation kinetics and the values obtained by the potentiometric titration were used for the kinetic analysis. The rate of deacetylation is directly proportional to the concentration of the acetamide pendent group, hence, a pseudo-first order reaction rate Eq. 3.1 was adopted.

$$kt = \ln \frac{a}{a - x} \tag{3.1}$$

Where, k is rate constant, a is the concentration of the original acetamide group and x is the concentration of the amine group at time t. Here, $\frac{a}{a-x}$ is proportional to (1-DD). The value of ln (1-DD) was plotted as a function of time and the value of the rate constant k was generated from the slope of plot. The linear relation ($R^2 > 0.9$) was observed between ln(1-DD) and time corresponds to the pseudo-first order reaction. Arrhenius law was used to determine the activation energy as a slope of the plot of ln(k) versus reciprocal of absolute temperature as shown in Eq. 3.2.

$$\ln \frac{k2}{k1} = -\left(\frac{E}{R}\right)\left(\frac{1}{T2} - \frac{1}{T1}\right) \tag{3.2}$$

Where, k1 and k2 are the rate constants at temperatures T1 and T2 (K) respectively, E is the activation energy (J/mole) and R is the universal gas constant (8.314 J/mole K) **[Yaghobi and Hormozi, 2010; Alvarenga et al., 2010; Kasaai, 2010]**.

The deacetylation reaction was carried out at 60, 80, 100 and 110 ºC to study the deacetylation kinetics of the process and samples were collected after 4, 6, 8 and 10 h. The DD% of chitosan samples was calculated by potentiometric titration as shown in Table 3.1 which concludes that DD% increases with increase in deacetylation temperature, time and alkaline concentration.

Table 3.1: Degree of deacetylation at different temperatures calculated by potentiometric titration.

Deacetylation time (h)	Degree of deacetylation		
	80 ºC	**100 ºC**	**110 ºC**
4	28±1.4	31±1.1	34±0.7
6	43±1.2	48±1.4	69±0.8
8	63±0.9	71±0.8	82±1.2
10	77±2	84±1.6	89±1.9

The conversion of chitin to chitosan was negligible at lower temperatures (<80 ºC) which indicates that deacetylation process is highly temperature dependent and favorable at higher temperatures. **Yaghobi et al., 2010** was also found the same behavior of DD% increment with change in temperature, time and alkali concentration. The graph of –ln(1-DD) versus reaction time (t) was plotted as shown in Figure 3.8(a). The calculated rate constants were 0.1921, 0.287 and 0.2946 hr^{-1} at 80, 100 and 110 ºC, respectively. Using Arrhenius equation (Eq. 3.2), the activation energy was calculated as 15.5 kJ/mol as shown in Figure 3.8(b). Similar results were found by some other researchers also **[Yaghobi and Hormozi, 2010; Tolaimate et al., 2000]**.

3.2.10. Thermogravimetric analysis (TGA)

TGA plots of chitin and chitosan (obtained at 80 ºC after 10 h) are shown in Figure 3.9. First broad peak for both chitin and chitosan was observed as endothermic peak which appeared at ~100 ºC. The peak corresponds to evaporation or loss of water present in the sample because of strong affinity of water in polysaccharides which implies that they may be easily hydrated in presence of moisture. The second endothermic peak appeared in the range of 264 ºC to 428 ºC which corresponds to thermal degradation and decomposition of both the samples. The onset (T_{on}) and offset (T_{off}) temperatures for chitin and chitosan were

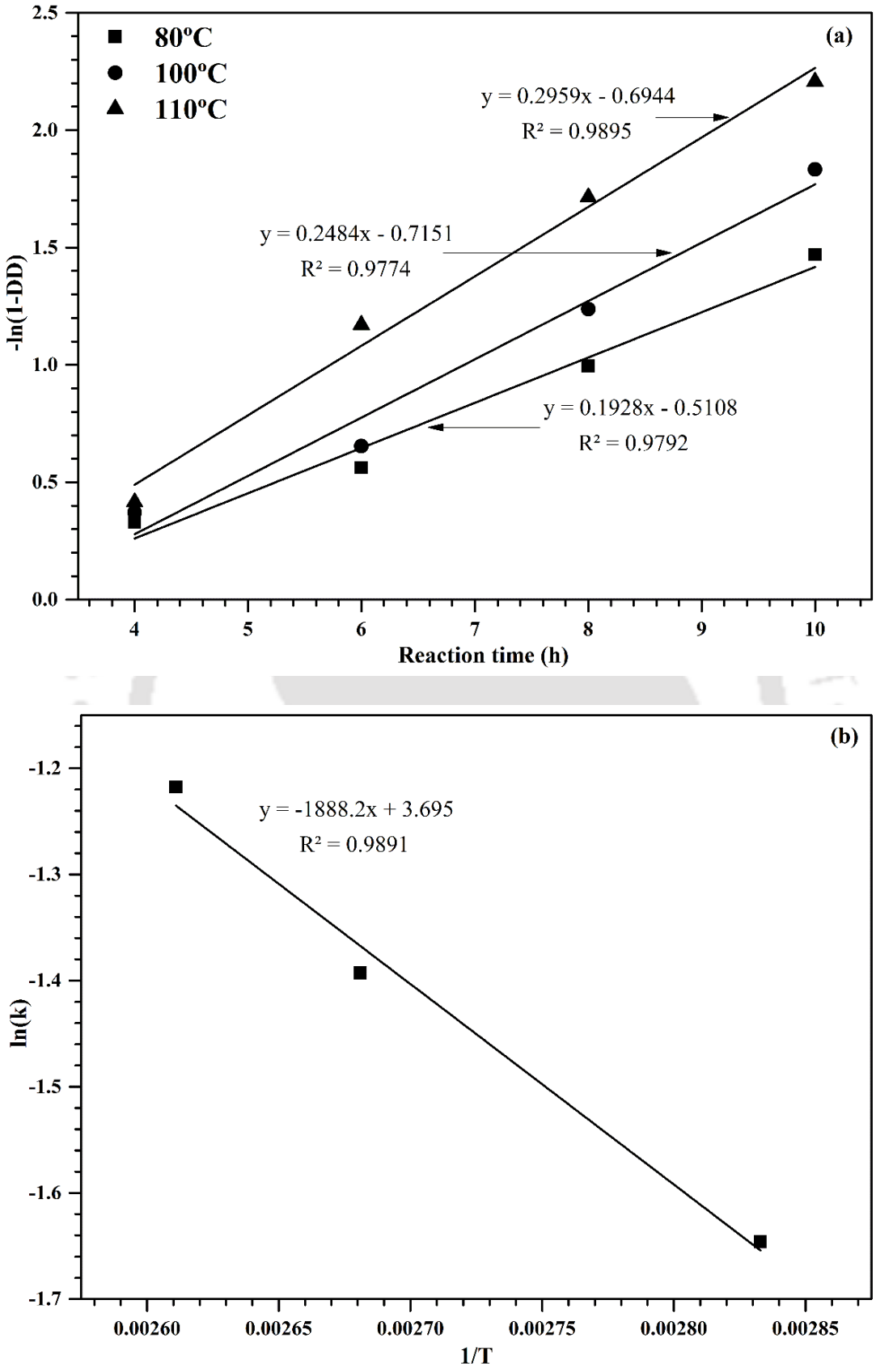

Figure 3.8. (a) -ln(1-DD) vs. reaction time (t) at different temperatures for potentiometric titration and (b) ln(k) vs. 1/T.

comparable which were ~265 ºC and ~428 ºC, respectively. The peak temperature (T_p) of chitin (381 ºC) was higher than that of chitosan (362 ºC). Thermal degradation in the saccharide backbone was observed by dehydration of the saccharide rings. As observed in Figure 3.9, chitin has higher thermal stability than chitosan. **Abdou et al., 2008** extracted chitin and chitosan from different marine sources and found the second endothermic peak at 372 ºC for chitin and 303 ºC for chitosan. **Sagheer et al., 2009** also extracted different chitins from marine sources and found the second endothermic peaks below 350 ºC. Hence, it confirmed that the chitin and chitosan extracted from MS have higher thermal stability than those from other sources.

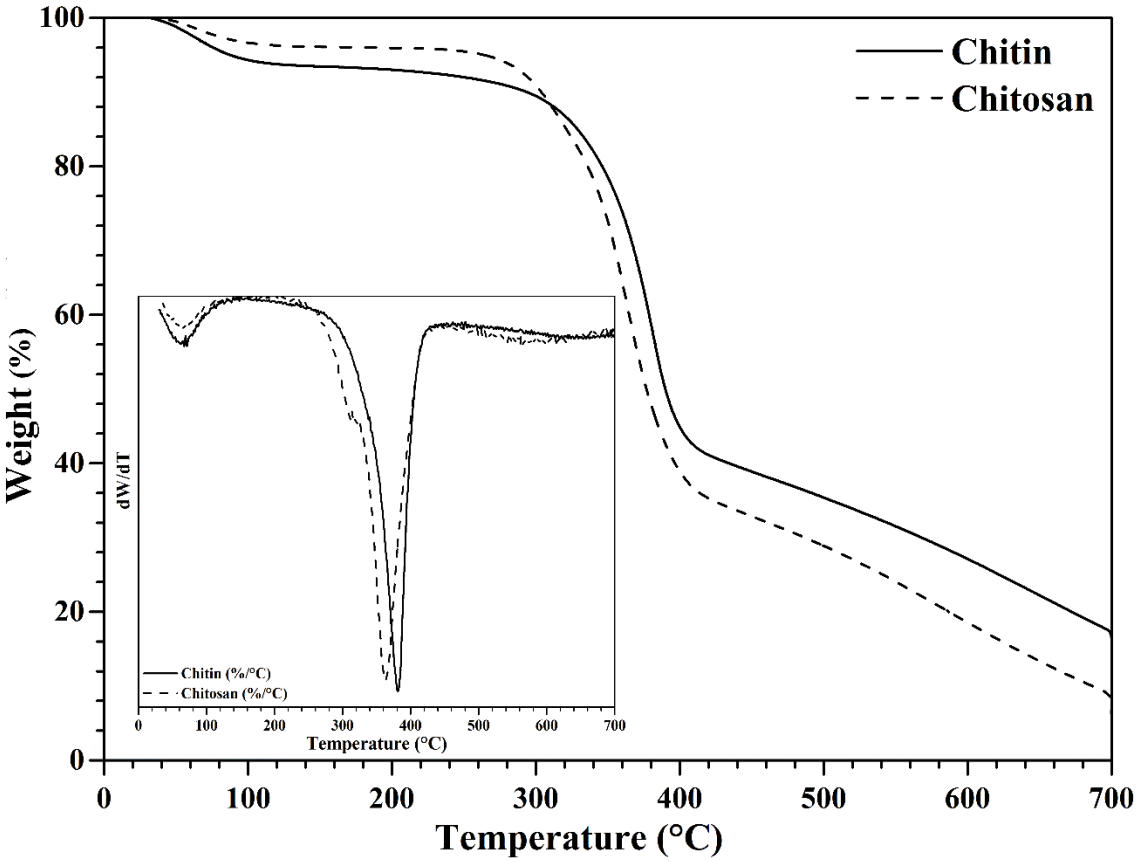

Figure 3.9. TGA and DTG curves of chitin and chitosan (obtained at 80 ºC after 10 h).

3.2.11. Scanning electron microscopy (SEM)

The SEM images exhibit surface morphology of chitin and chitosan (obtained at 80 ºC after 10 h) samples extracted from MS. A uniform, dense and lamellar microfibrillar crystalline structure in chitin was observed as shown in Figure 3.10. Flakes kind of structure, having rough and irregular shapes with different size, was observed in chitosan instead of microfibrils part, which confirmed more amorphous nature of chitosan than chitin as shown in Figure 3.10(b).

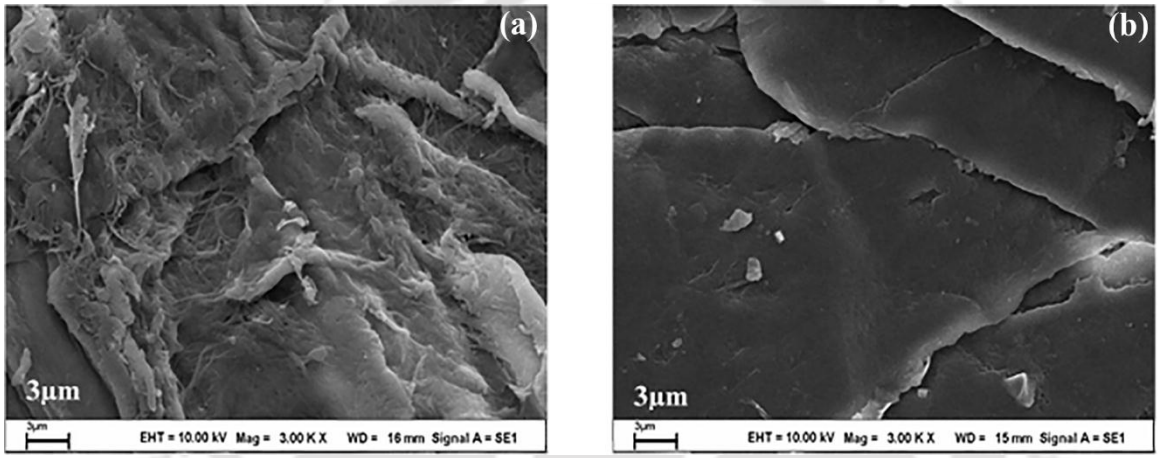

Figure 3.10. SEM images of (a) chitin and (b) chitosan (obtained at 80 ºC after 10 h).

3.2.12. Viscosity average molecular weight

The intrinsic viscosity and viscosity average molecular weight (M_v) of extracted chitosan (obtained at 80 ºC after 10 h) were calculated at room temperature (25±1 ºC) by Ubbelohde viscometer. Intrinsic viscosity was calculated as 37.54 mL/g by Huggins analogy as mentioned in the form of Eq. 2.18. The M_v of chitosan (obtained at 80 ºC after 10 h) was calculated as ~44x10^3 Da by intrinsic viscosity values used in Mark-Houwink-Sakurada analogy as mentioned in the form of Eq. 2.19. Similar results were found by other researchers **[Abdou et al., 2008; Fattah et al., 2007; Kasaai et al., 2000; Ocloo et al., 2011]**. NaOH concentration affects chitin molecular weight during

deacetylation. The higher concentration of NaOH (approx.70%) should not be preferred because it attacks on the backbone of chitosan. According to **Ocloo et al., 2011**, the extracted chitosan with lower molecular weight has better antibiotic, antioxidant, antifungal and plant growth promoting properties than that with higher molecular weight **[Ocloo et al., 2011]**.

3.2.13. Ash content

The ash content in extracted chitosan (obtained at 80 ºC after 10 h) was calculated as 0.18%. The negligible amount of ash content in chitosan shows its purity. According to **Liu et al., 2012**, the ash content of chitin and chitosan is an indication of the effectiveness of the method used for removal of inorganic materials and other impurities.

3.3. Summary

The efficiency of chitin extraction from MS and chitosan production by deacetylation has been studied in detail. Chitin has been extracted by deminaralization followed by deproteinization reaction. The yield of chitin extraction is 7 to 8% (dry weight basis) of the raw MS. Deacetylation technique has been used to convert chitin to chitosan for different deacetylation time and temperature. The yield of chitosan production is 87% (dry weight basis). Deacetylation process is highly time and temperature dependent. Chitosan conversion from chitin is not favourable at lower temperatures. It has been calculated by various methods such as potentiometric titration, conductometric titration, FTIR, elemental analysis, ^{1}H-NMR and found in the range of 77 to 87%. Deacetylation kinetics has also been studied by using pseudo-first order reaction and activation energy is found to be 15.5 KJ/mole. FTIR, XRD, elemental analysis, ^{1}H-NMR, potentiometric titrations, conductometric titrations, TGA, SEM, viscosity average molecular weight and ash content have been carried out to characterize chitin and chitosan. The peaks at 1654 to 1658 cm^{-1} and 1555 to 1557 cm^{-1} of FTIR study confirm the presence of chitin and partially

deacetylated chitosan due to presence of amide I band ($C = O$ stretching) and amide II band ($N - H$ stretching) respectively. XRD shows semicrystalline nature of chitin and chitosan. Chitin has higher I_{cr} (84%) than chitosan (70%). I_{cr} decreases with increasing deacetylation time. TGA analysis shows higher thermal stability of chitin than that of chitosan. SEM analysis shows a uniform dense structure with lamellar microfibrillar crystalline structure in chitin. Intrinsic viscosity and viscosity average molecular weight of chitosan have been calculated at 25±1 ºC and found 37.5 mL/g and 44×10^3 Da respectively. Finally, we conclude that the extracted chitosan has higher crystallinity and thermal stability than other chitosans, extracted from different marine sources.

Chapter 4

Fabrication and Characterization of Poly (Lactic Acid)/Chitosan Biocomposite Films

This chapter reveals the fabrication of poly (lactic acid)/chitosan (CH) based biocomposite films (PLA/CH) by solution blending of PLA with CH. Chitosan was extracted successfully from Muga silkworms via chemical treatments. All the regular peaks of PLA and CH are observed in biocomposite films by FTIR analysis. XRD analysis confirms the regular lattice arrangement of PLA chains in PLA/CH films. These peak intensities were reduced with chitosan loading which suggests the increment in amorphous nature of biocomposite films. DSC analysis reveals that the Glass transition temperature (T_g), cold crystallization temperature (T_{cc}) and melting temperature (T_m) are reduced up to 1.9, 4.6 and 3.2 ºC respectively with the increase in CH concentration due to the plasticizing effect of short polymer chains of PLA. The increment in water vapour permeability of PLA/CH biocomposite films is preferable for cell proliferation and cell attachment in biomedical applications.

4.1. Introduction

Recently, the use of bio-polymers and its modification with tailored and controlled properties have attracted more attention to overcome the existing limitations of conventional polymers in various applications. In the recent time, the development of new, greener and sustainable products from abundant natural resources are increased in order to reduce the environmental hazards and to provide substitutes of fossil based polymers. In the bio-based category, chitosan, a cationic polysaccharide, limits its applications due to the restricted solubility. However significant interest has been generated among the researchers to minimize such limitations and explore more insights about its characteristics such as non-toxic, biocompatible and easily acceptable in biomedical areas. Chitosan can be available in many forms such as flakes, micro-particles, whiskers, nano-particles, gels etc. It is a promising candidate of the twenty-first century with some of the unique material properties such as chemical reactivity, solubility, film forming ability, antimicrobial, antioxidant, anti-fungal, interesting optical properties and biodegradability **[Vasile et al., 2013]**. It cannot be used as packaging material due to its hydrophilicity. Hence, chitosan can be promoted as a filler with biodegradable, non-toxic, hydrophobic polymers such as PLA. PLA is a linear aliphatic thermoplastic polyester which is non-toxic, biodegradable, bio-compatible and hydrophobic in nature and can be used at industrial scale worldwide **[Wu and Wu, 2006; Tsai et al., 2010; Tripathi and Katiyar, 2016]**. Several studies are available related to the interaction between PLA and chitosan. The dispersion of chitosan in various polymeric systems depends on the nature of the matrix material. For example, **Suyatma et al., 2004** processed PLA with chitosan and prepared the blends to investigate water vapour transmission rate (WVTR) and mechanical properties. WVTR properties were improved due to the addition of hydrophobic PLA whereas, mechanical properties were reduced due to the absence of proper dispersion of PLA solution with

chitosan. **Bujang et al., 2013** prepared chitosan biocomposite films by incorporating various concentrations of lactic acid and glycerol. As a result, negligible improvement in WVTR was observed by adding 2% lactic acid with different concentrations of glycerol. Whereas, a linear gradual improvement was observed in WVTR values by reducing lactic acid concentration and increasing glycerol concentration. The mechanical properties were reduced for the same concentrations of chitosan biocomposite films. **Leceta et al., 2013** developed environmentally friendly chitosan films by adding various concentrations of glycerol for packaging applications. The improved transparency and flexibility with a slight increment in hydrophilic character make it possible to be used in food packaging applications.

In the present research work, PLA and synthesized chitosan from Muga silkworms in lab were utilized as matrix and filler materials respectively to prepare PLA/CH biocomposite films using solution casting approach. The effect of chitosan polymeric chains on crystal structure, thermal and degradation behaviour, surface morphology and water vapour barrier properties of PLA films were studied in detail.

4.2. Results and discussion

4.2.1. Fourier transform infrared spectroscopy (FTIR) with ATR

The allocation of various functional groups, present in PLA and PLA/CH biocomposite films can be confirmed by FTIR analysis as shown in Figure 4.1. The absorption bands at 754 cm^{-1} and 1385 cm^{-1} correspond to $C-H$ bending in PLA and PLA/CH biocomposite films. The absorption band at 867 cm^{-1} is observed in PLA, which denotes $(-C-C-)$ stretching. This peak is shifted towards higher wave number and located at 869 cm^{-1} in PLA/CH biocomposites. The absorption bands positioned at 1082 cm^{-1} and 1180 cm^{-1} dedicated to $(-C-O-)$ stretching in PLA and its biocomposite films. The absorption band at 1453 cm^{-1} is observed in PLA which corresponds to $-CH_3$ bending of PLA. This peak

is also shifted towards higher wave number and positioned at 1457 cm^{-1} in biocomposite films. More importantly, a sharp and intense peak is detected at 1749 cm^{-1} for both PLA and biocomposite films which represents $-C=O$ stretching vibrations. Furthermore, the strong vibrations of amide I band ($C=O$ stretching) and amide II band ($N-H$ bending) are observed at 1652 cm^{-1} and 1558 cm^{-1} in PLA/CH biocomposite films. The intensity of these peaks is less than that of the peak obtained at 1749 cm^{-1}, which resembles that a small amount of chitosan is present in PLA/CH biocomposite films in the form of filler and also the degree of deacetylation of the present chitosan is not 100%. It suggests that some amount of chitin is also present in PLA/CH biocomposite films.

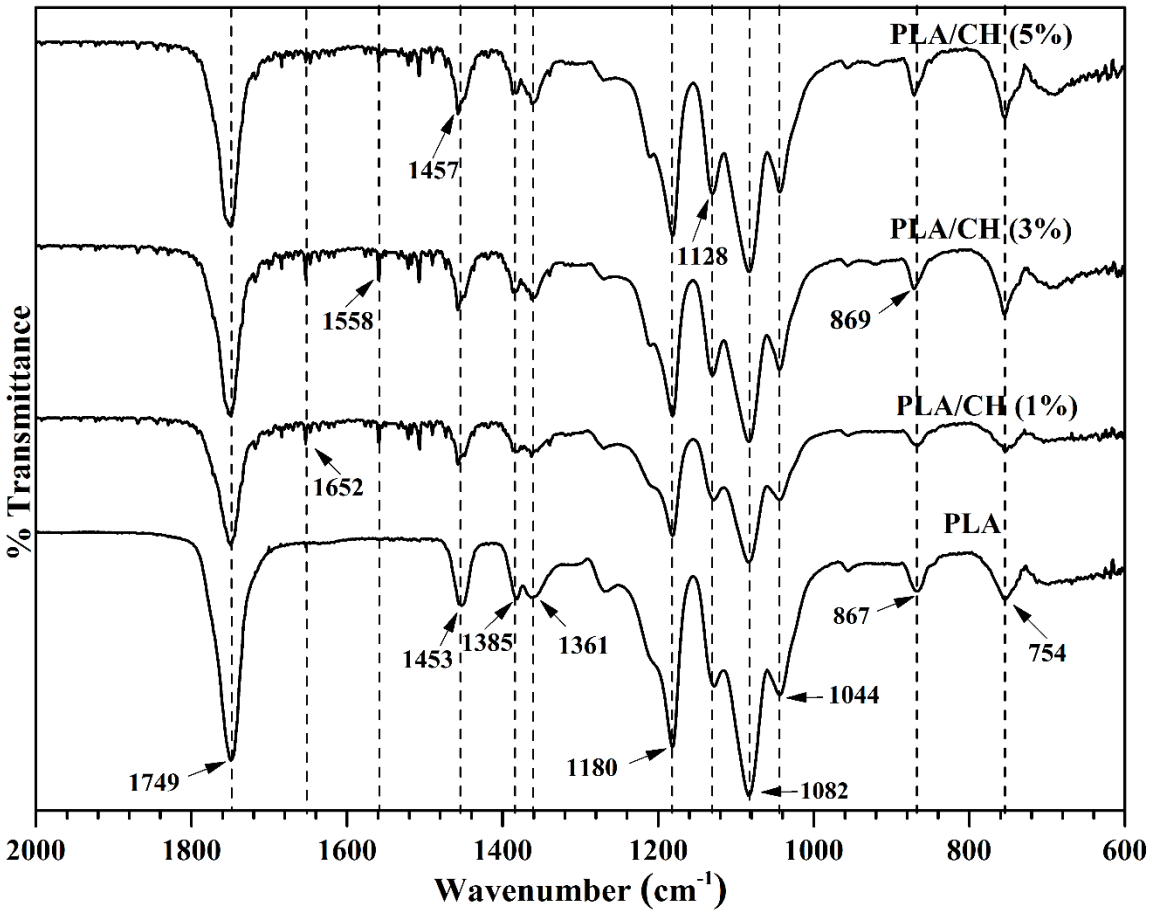

Figure 4.1. FTIR spectra of PLA and PLA/CH biocomposite films.

4.2.2. X-ray diffraction analysis (XRD)

The crystallographic analysis of PLA shows a sharp crystalline peak at 16.7º (2, 0, 0) which corresponds to α crystalline form of PLA as shown in Figure 4.2. The reflection pattern [2, 0, 0] shows the typical orthorhombic crystal structure of PLA. The XRD spectra of PLA also shows three more [0, 1, 0], [2, 0, 3] and [0, 1, 5] reflection peaks at 14.8º, 19º and 22.4º respectively. These reflection peaks also correspond to the combined effect of α and β crystalline form. Hence, it is confirmed from the above discussion that the solution casted PLA films are semicrystalline in nature.

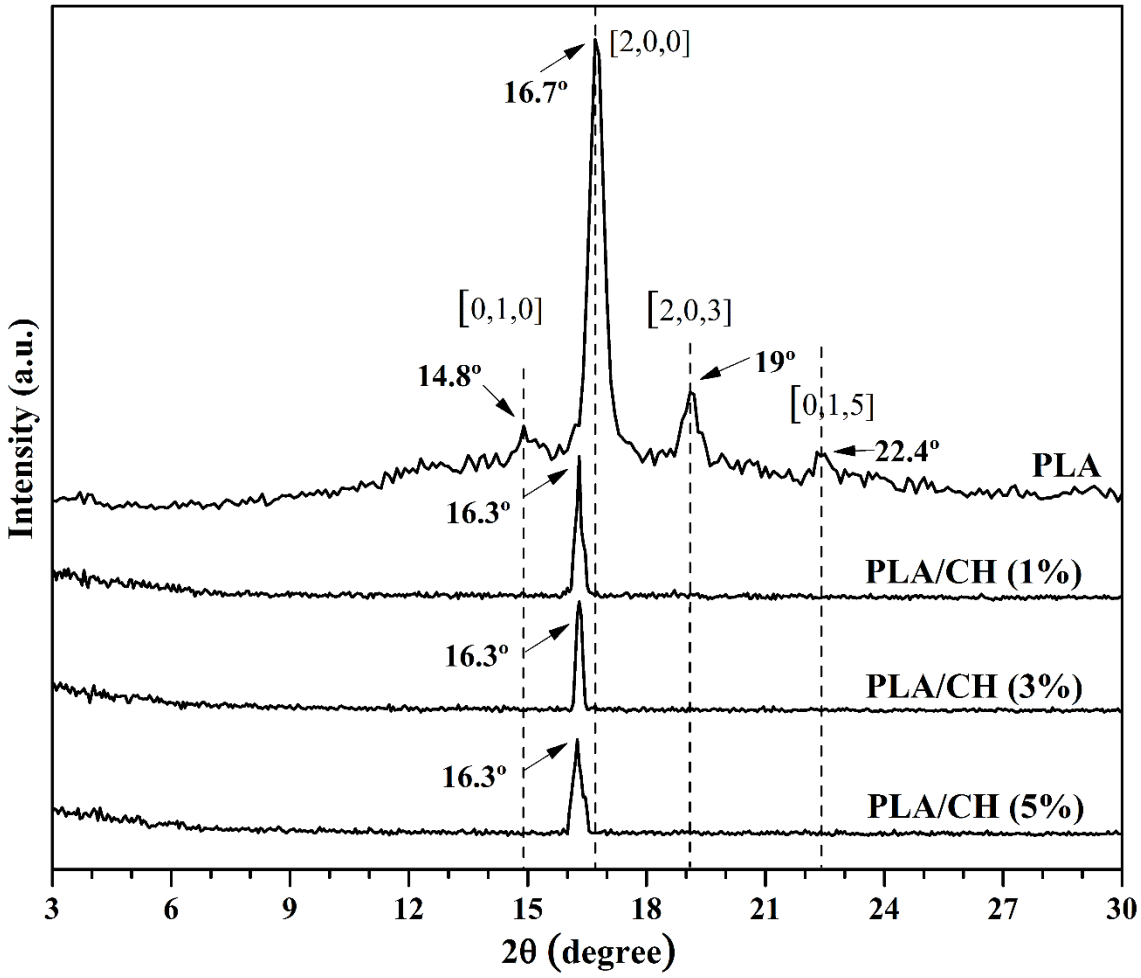

Figure 4.2. XRD diffractographs of the fabricated PLA and its biocomposite films.

PLA/CH biocomposite films only exhibit one sharp peak at 16.3º (2, 0, 0) with less intensity as compared to PLA. The slight reduction in 2θ value concludes that some of the nano-sized Muga silkworm chitosan particles intercalated in PLA matrix and increased its interlayer spacing. Rest of the peaks disappeared from XRD spectra of PLA/CH biocomposite films, which signifies the increment in amorphous nature. The intercalation of chitosan in the ordered structure of PLA may also responsible for the reduction in crystalline nature. Hence, the XRD results illustrate that PLA/CH biocomposite films are semi-crystalline in nature.

4.2.3. Differential scanning calorimetry (DSC)

DSC analysis was carried out with two thermal cycles as mentioned in section 2.3.10. The first heating cycle is highly recommended for the removal of physically & chemically bonded moisture, processing defects and also to erase the polymer thermal history. The various thermal behaviours such as glass transition, cold crystallization and melting of PLA and PLA/CH biocomposite films are studied from the second heating thermograms at a heating rate of 5 ºC/min as shown in Figure 4.3. The glass transition temperature (T_g) value of PLA is found at 59.3 ºC which is continuously reduced up to 57.4 ºC with an increase in CH loading. This reduction of ~1.9 ºC is due to the effect of CH which slightly enhance the degradation of PLA by stimulating the formation of shorter chain segments **[Valapa et al., 2015]**. A minor reduction (~0.11 J/g.K) in heat capacity at constant pressure (C_p) is detected with an increase in filler loading. It suggests that the required amount of heat becomes less to raise the unit temperature with the addition of CH in PLA matrix. It happens due to the increment in the ease of the movement of shorter polymer chains in PLA/CH biocomposites, experiencing less obstruction from adjacent longer polymer chains. The cold crystallization temperature (T_{cc}) of PLA is observed at 114.3 ºC which is close to T_{cc} values, suggested in literature **[Tripathi and Katiyar, 2016;**

Valapa et al., 2014]. A slight reduction of up to 4.6 ºC in T_{cc} values are observed in PLA/CH biocomposite films because the addition of CH assists the diffusion rate which leads to the faster migration of polymer chains to the nucleus surface. The sharpness of the cold crystallization peaks increases with an increase in filler loading, suggests that the rate of crystallization becomes faster to that of PLA due to the homogeneous nucleation effect [**Valapa et al., 2014**]. PLA and PLA/CH biocomposite films exhibit sharp, unimodal endothermic melting peaks at 150.4, 149, 149 and 147.2 ºC respectively, which clearly suggests the presence of α crystalline form of PLA.

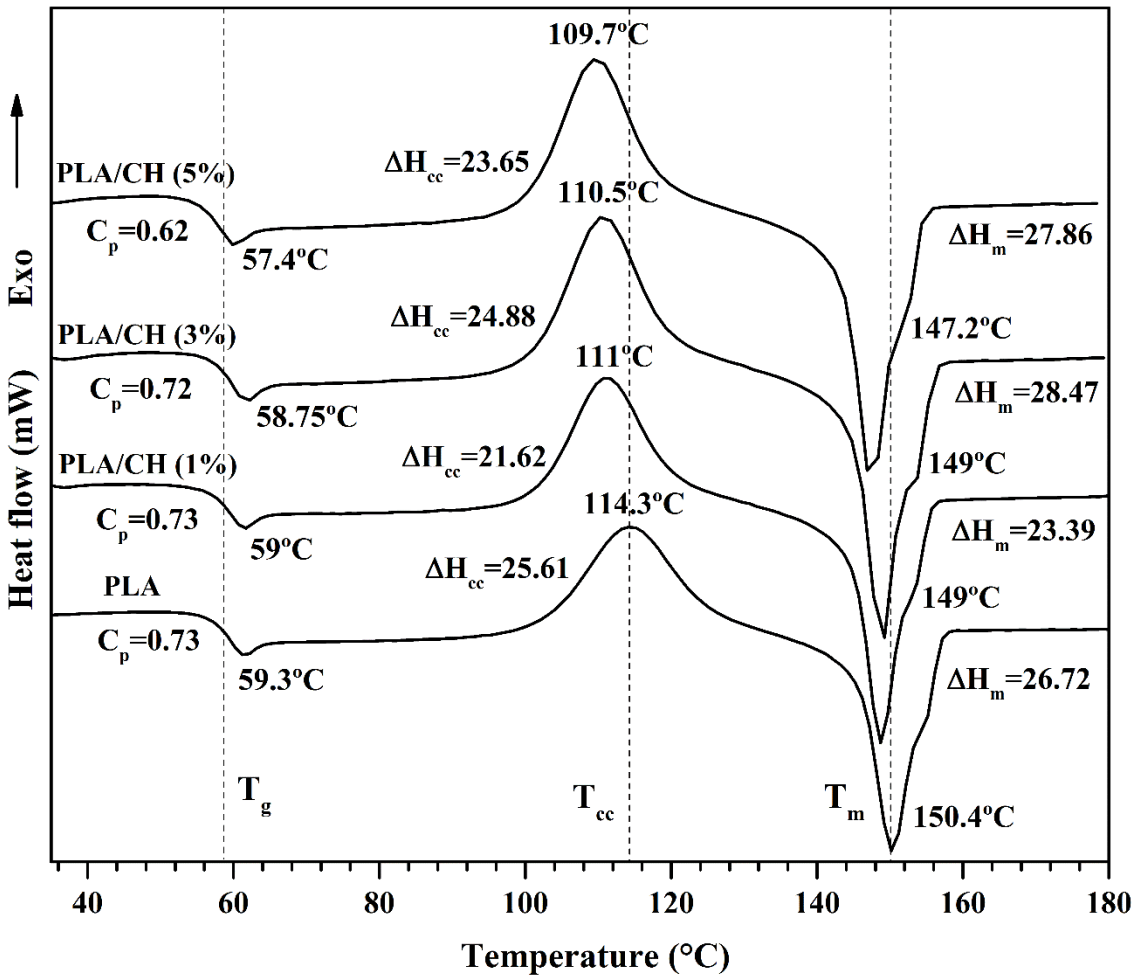

Figure 4.3. DSC thermograms of PLA and PLA/CH biocomposite films (second heating) at 5 ºC/min.

A slight reduction (up to ~3.2 ºC) in T_m values of PLA/CH biocomposite films is noticed due to the reduction in thermal stability of PLA in the presence of CH. It also signifies that the molecular weight of PLA reduces with the incorporation of CH as a filler.

4.2.4. Thermogravimetric analysis

Thermal decomposition behaviour of PLA and PLA/CH biocomposite films is measured by TGA analysis under N_2 atmosphere as shown in Figure 4.4(a) & (b). One sharp degradation peak in the temperature regime of ~302.4-390.7 ºC is observed in PLA due to the intra-molecular trans-esterification as mentioned in Figure 4.4(a). Whereas, the two significant weight loss peaks are clearly observed in PLA/CH biocomposite films in which the first weight loss peak is observed in the temperature regime of ~58-152 ºC. It is attributed to the evaporation of absorbed moisture due to the hydrophilic nature of CH. The second weight loss peaks in PLA/CH biocomposite films are totally responsible for polymer degradation, which are observed in the temperature regime of ~294-389 ºC. The peak temperature (T_p) value is highest i.e. 366.6 ºC in PLA film, which reduces continuously up to 2.7 ºC with an increase in filler loading. The onset degradation temperature (T_{on}) and offset degradation temperature (T_{off}) of biocomposite films reduce up to 8 ºC and 5.2 ºC respectively in the same fashion as shown in Table 4.1. This one step degradation can be clearly visible in the first derivative curves of PLA and PLA/CH biocomposite films as shown in Figure 4.4(b). This thermal stability reduction in biocomposite films corresponds to the breakage of longer PLA chains into shorter chains due to the presence of CH in PLA matrix and also due to the increment in acidic sites produced during the partial degradation of CH in PLA matrix. Hence, the filler promotes the thermal degradation of PLA. The increment in short polymeric chains can also deform the crystal structure that can reduce the crystallinity of the film samples which supports the XRD analysis.

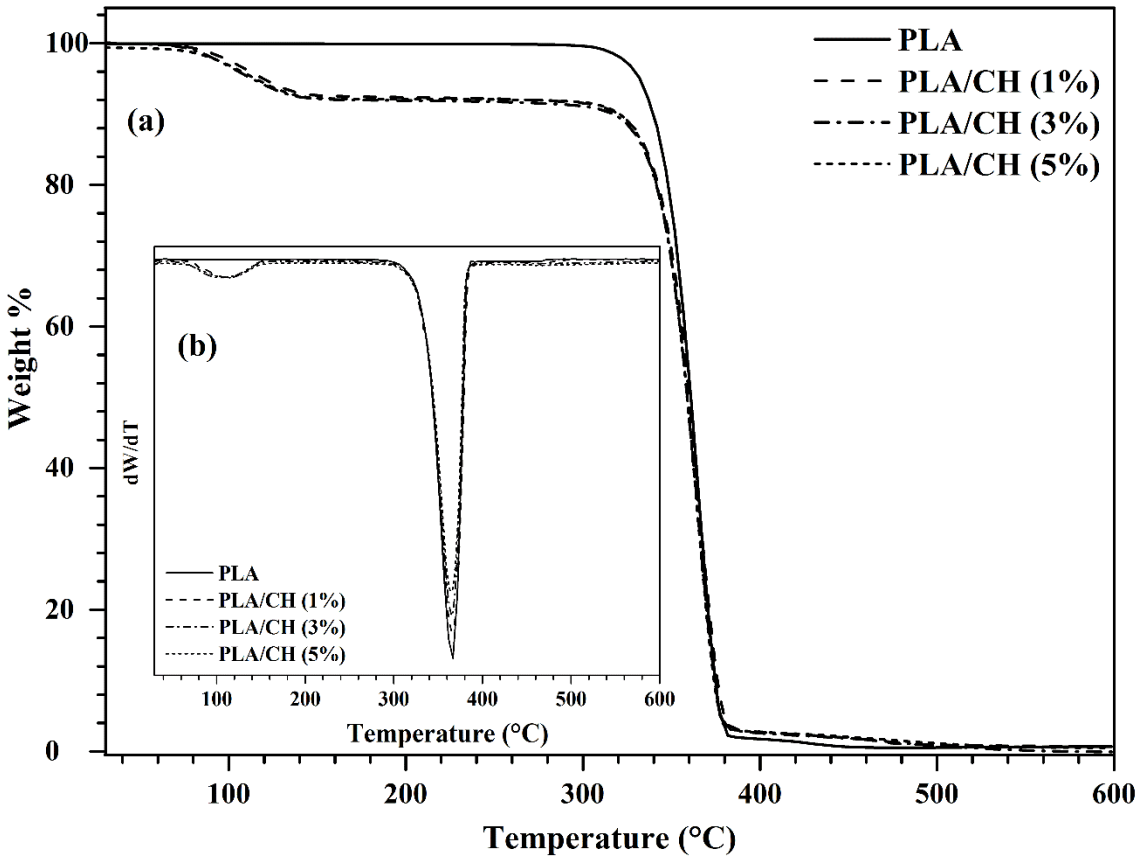

Figure 4.4. (a) TGA and (b) DTG profiles for PLA and PLA/CH biocomposite films at a heating rate of 10 ºC/min.

Table 4.1: Measured temperature values corresponds to the thermal behaviour of PLA and PLA/CH biocomposite films.

Sample Name	Sample thickness (µm)±Std. Dev.	CH loading (wt%)	TGA		
			T_{on} (ºC)	T_p (ºC)	T_{off} (ºC)
PLA	140±3	-	302.4	366.6	390.7
PLA/CH (1%)	152±9	1	297.1	364.8	388.9
PLA/CH (3%)	162±4	3	297.1	364.8	388.9
PLA/CH (5%)	147±9	5	294.4	363.9	385.5

4.2.5. Surface morphology

FESEM analysis of PLA film shows a smooth surface without any defects. Whereas, the irregular defects of chitosan in PLA matrix are observed in PLA/CH biocomposite films, which are more intense with increase in filler concentration as shown in Figure 4.5. The arrows indicate the irregular macro and microparticles of chitosan presence in PLA matrix. The size of the chitosan particles also increases with an increase in filler loading.

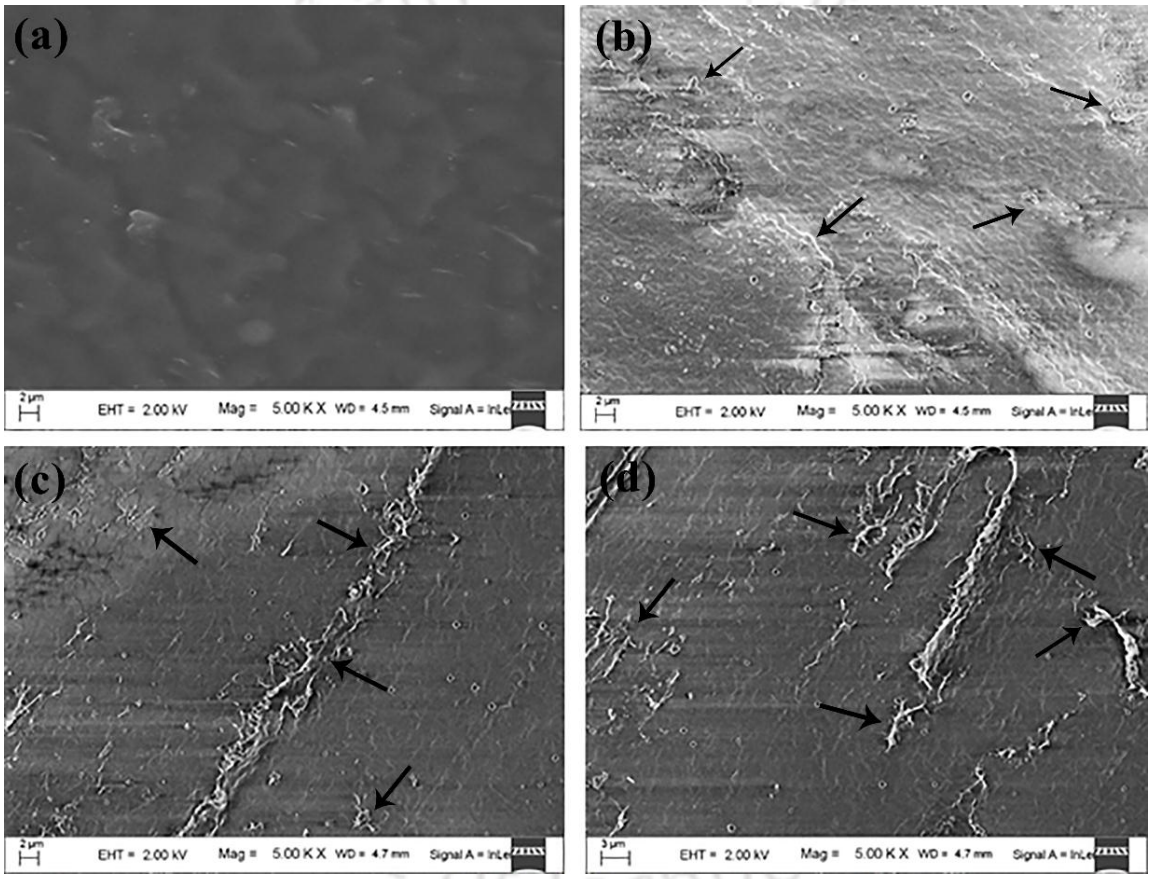

Figure 4.5. FESEM micrographs of (a) PLA, (b) PLA/CH (1%), (c) PLA/CH (3%) and (d) PLA/CH (5%).

Further, some agglomeration of chitosan particles also occurs at the higher concentrations in PLA/CH biocomposite films, which matches with the referred literature **[Ferreira et al., 2014]**. Hence, the other properties such as thermal, mechanical and

transparency can reduce due to the above-discussed reasons. It is noteworthy to mention that the physicochemical properties of such films may reduce, but still it can be useful in various applications due to the antibacterial, antifungal and antimicrobial properties of chitosan.

4.2.6. Contact angle measurements

It is well known that the contact angle values depend on several parameters such as polymer architecture, surface roughness, chemical functionality, polymer crystallinity, surface charges including sample preparation techniques. Contact angle measurements are carried out for PLA and PLA/CH biocomposite films to analyze the effect of filler on the wettability as shown in Figure 4.6. The contact angle value of PLA is measured as ~90.1º, which is close to the values of available literature **[Ferreira et al., 2014; Yuan et al., 2008]**. The contact angle values of PLA decrease continuously and found as ~80.5º, ~77.2º and ~70º with an increase in chitosan concentration i.e. 1, 3 and 5% respectively.

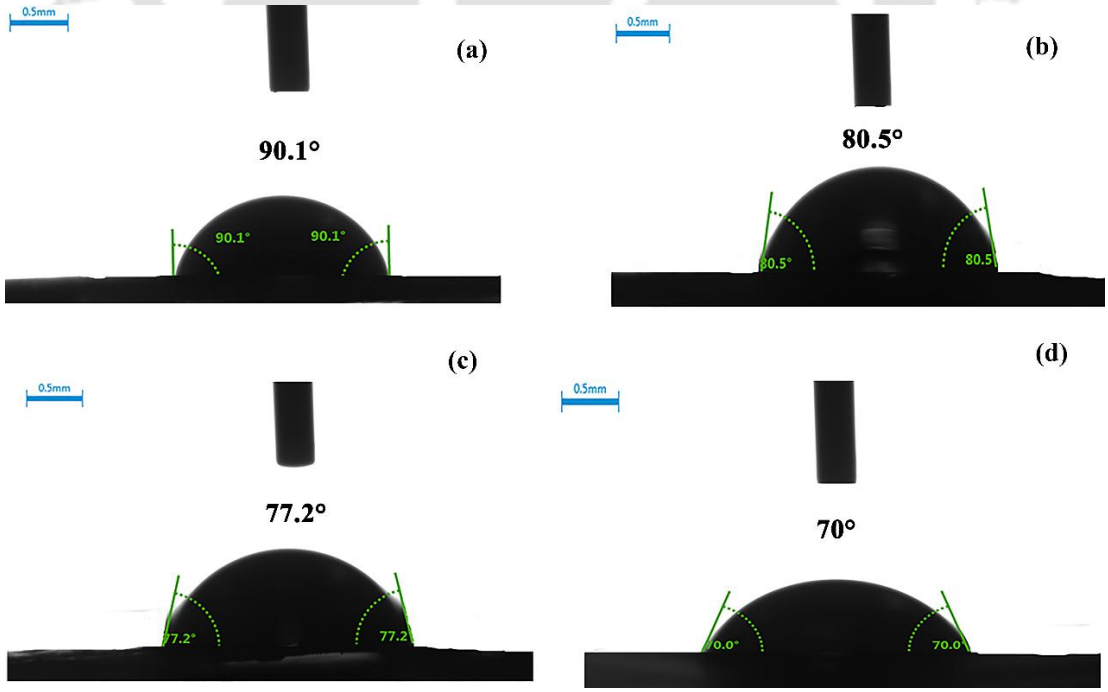

Figure 4.6. Contact angle measurement of (a) PLA, (b) PLA/CH (1%), (c) PLA/CH (3%) and (d) PLA/CH (5%) biocomposite films.

Other researchers also analyzed the same behaviour of surface wettability for PLA/chitosan blend composition. The presence of free OH groups of chitosan on the surface of the film and surface roughness absorb water, which increases the surface wettability and the prepared PLA/CH biocomposite films become less hydrophobic to that of PLA. This increment in surface wettability is highly required for cell proliferation and cell growth in biomedical applications.

4.2.7. Mechanical properties

The mechanical properties analysis was carried out for PLA and PLA/CH biocomposite films and UTS, %ε and Young's modulus are calculated and plotted as shown in Figure 4.7. The UTS of PLA film is calculated as 37.45±4.2 MPa, which is close to the values calculated in various literature **[Suyatma et al., 2004; Rhim et al., 2009]**. The tensile strength of PLA/CH biocomposite films is reduced from 37.45±4.2 to 12.2±0.9 MPa i.e. 67.42% with the increase in CH loading. The associated reason of significant reduction in tensile strength is the presence of chitosan in PLA matrix, which breaks the longer chains of PLA into shorter chains and this phenomenon increases with increase in filler concentration. The shorter polymer chains tend to align faster than the longer polymer chains during the tensile test and have less chain entanglement effect which leads to the reduction in tensile strength. The phase separation is also observed in PLA/CH biocomposite films, which is also responsible for the reduction in mechanical properties. The % E of composite films is reduced drastically from 8.89±0.5 to 5.01±0.1 MPa i.e. 43.64% with an increase in filler loading due to the brittle nature of chitosan as shown in Figure 4.7(b). The particle volume fraction and their interactions with PLA matrix also affect the film extensibility. Young's modulus of PLA/CH biocomposite films is also following the same pattern as that of UTS and %E. It is decreased from 557.2±15 to

248±9 MPa continuously with an increase in filler loading up to 5 wt% as shown in Figure 4.7(c).

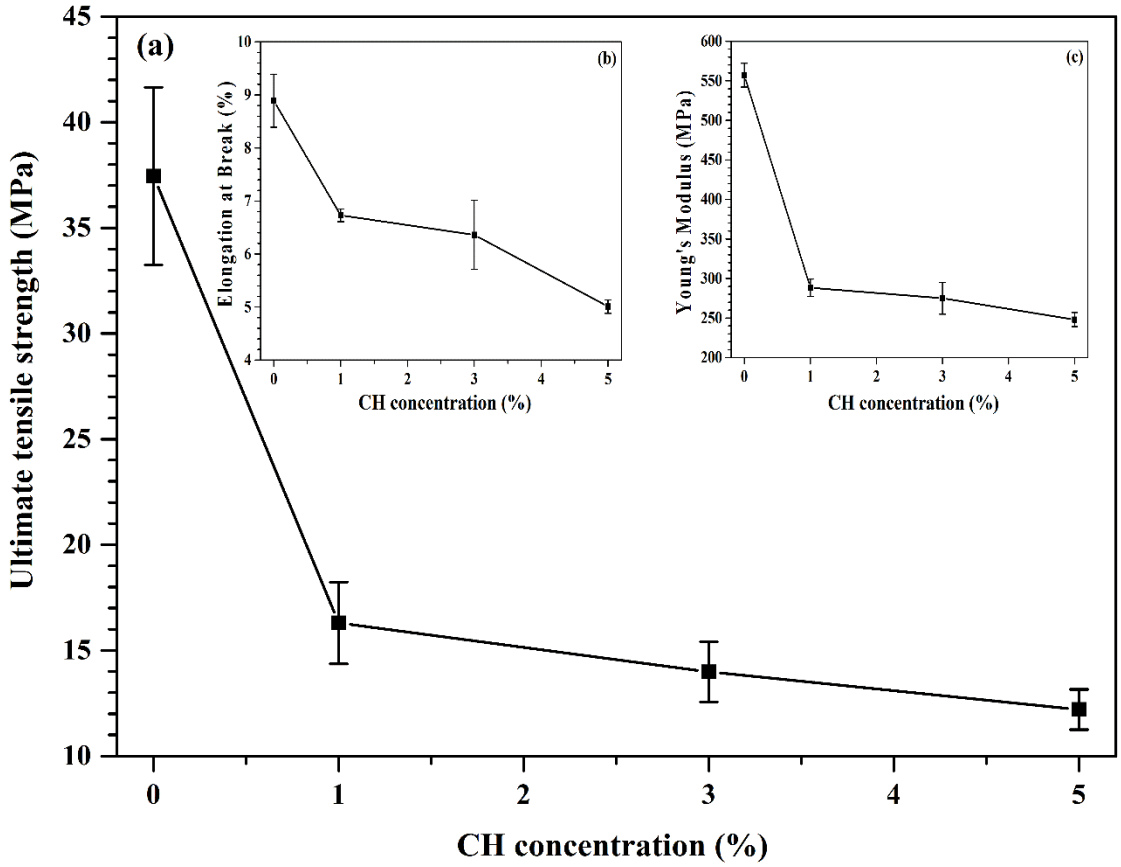

Figure 4.7. Variation in (a) Ultimate tensile strength, (b) Elongation at break and (c) Young's modulus of PLA films at different wt% of CH loading.

4.2.8. Dynamic mechanical analysis (DMA)

DMA is a feasible technique to calculate three important properties of the polymer such as storage modulus (E′), loss modulus (E″) and damping factor (tan δ). E′ is responsible for the hardness of the polymer and elastically stored energy during the deformation process. Whereas, tan δ is the measure of dissipated energy during the deformation process. The value of temperature corresponds to the maximum of the tan δ peak can provide T_g value. In this regards, the variation in E′ and tan δ are measured for PLA and PLA/CH

biocomposite films. It can be observed from Figure 4.8(a) that E′ decreases with an increase in filler concentration. The most expected reason for the reduction is the increasing concentration of chitosan, which is amorphous in nature and may result in the reduction in elastic behaviour of final composition. The reduction in E′ may also be possible due to the α-relaxation of chitosan. The variation in tan δ with respect to temperature is also observed for PLA biocomposite films as shown in Figure 4.8(b). It is concluded that the maximum peak temperature i.e. T_g slightly decreases with an increase in chitosan concentration due to the increment in the amorphous region of PLA in PLA/CH biocomposite films, which is also supported by XRD analysis. The hydrophilic behaviour of chitosan fraction can easily absorbs moisture from the atmosphere, which can also reduce the plasticization effect of PLA.

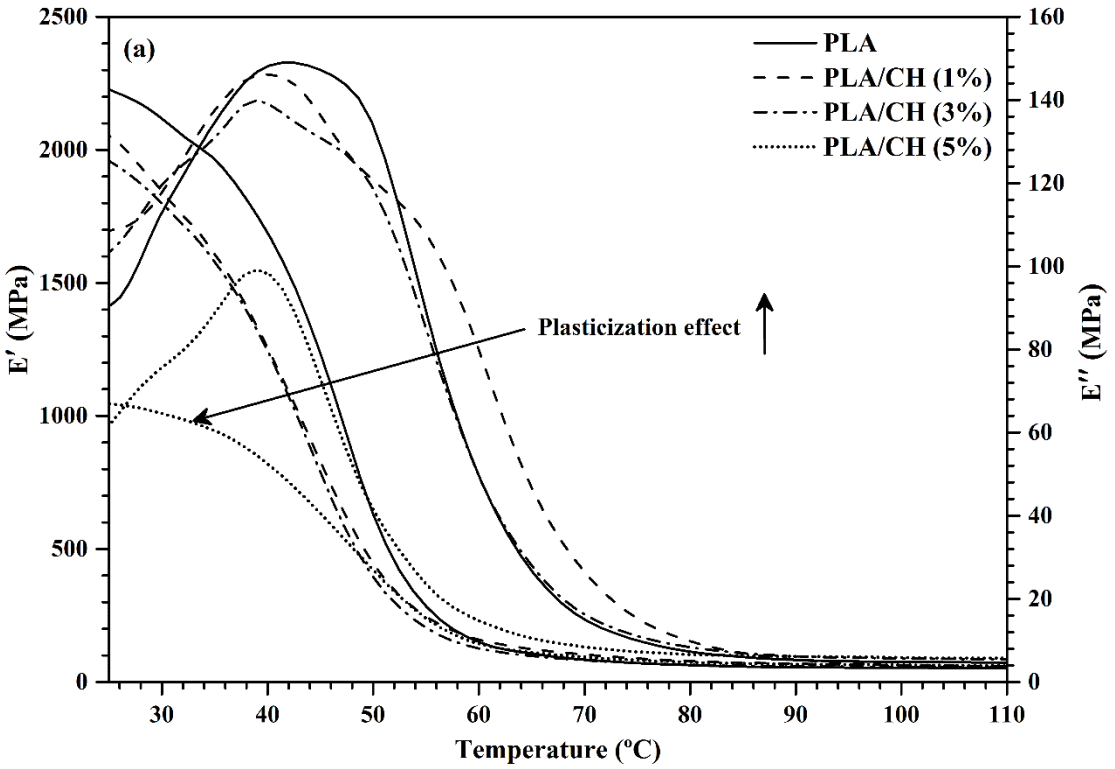

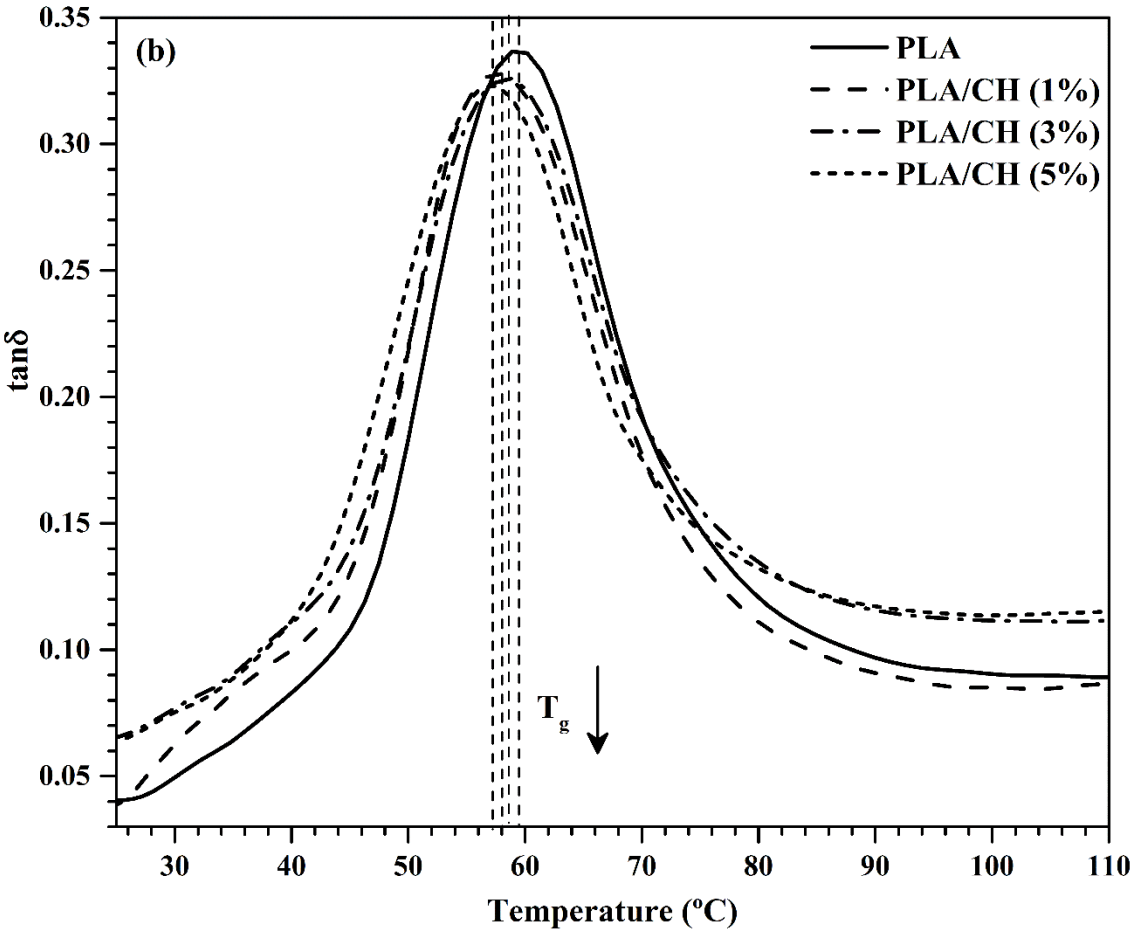

Figure 4.8. Variation in (a) storage modulus and (b) damping factor of PLA films at different wt% of CH loadings.

4.2.9. Water vapour transmission rate (WVTR)

The water vapour transmission rate is also a critical property for food packaging. The WVTR×e values are calculated at the operating conditions of 37.8±0.5 ºC and 95% RH for PLA, PLA/CH (1%), PLA/CH (3%) and PLA/CH (5%) biocomposite films as shown in Figure 4.9. The WVTR×e value of PLA film is calculated as 7.2±0.1 cc.mm/m^2.day, which is close to the values reported in various literature **[Dhar et al., 2015]**. Significant increments such as ~9.7, ~28.8 and ~52.4% in WVTR×e values are observed in the case of PLA/CH (1%), PLA/CH (3%) and PLA/CH (5%) films respectively. This happens due to the significant reduction in polymer crystallinity and dispersibility with an increase in filler

concentration. The agglomeration at higher loadings is also observed in PLA/CH films, which is also responsible for increment in WVTR×e values. One strong reason behind the significant increment in WVTR×e values is the presence of active hydrophilic sites due to the excess availability of OH groups in chitosan which imparts hydrophilicity when comes in contact with moisture or water. This kind of moisture absorbing capacity of films is highly required in such packaging in which moisture is helpful to preserve the material inside. The increasing water uptake capacity of PLA/CH biocomposite films can provide the most suitable environment for cell culture growth, cell attachment and cell proliferation with respect to that of PLA films because the cell growth and cell proliferation are very much dependent on the hydrophilicity of the surface and bulk.

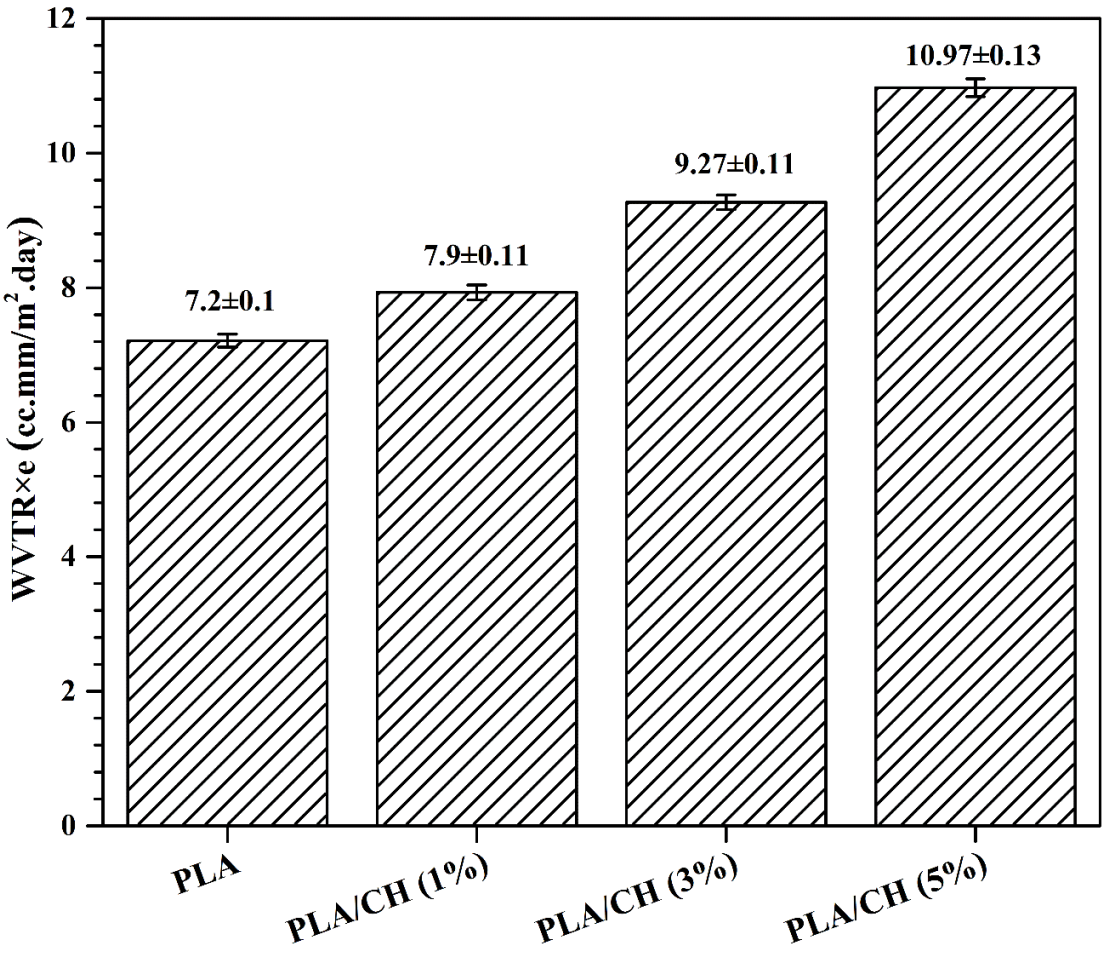

Figure 4.9. Water vapour barrier properties of PLA and its biocomposite films.

4.3. Summary

Poly (lactic acid) and chitosan extracted from Muga silkworms were utilized as matrix and filler respectively for the preparation of various compositions of PLA/CH biocomposite films by solution casting technique. The prepared films were of uniform thickness, which were thoroughly analyzed by structural, thermal, surface, mechanical and barrier properties. In FTIR analysis, all the regular peaks were observed at their respective positions for PLA and chitosan in PLA/CH biocomposite films. XRD analysis confirmed that the prepared films are semicrystalline in nature. The intensity of the peaks reduced with an increase in filler concentration. The thermal behaviour of the films was also reduced due to the phase separation phenomena which was confirmed by the surface morphology. FESEM analysis proved that the present chitosan particles were of micron size, which formed agglomeration at higher concentration. The mechanical properties and transparency of the films were significantly reduced by incorporating chitosan in PLA matrix. The water vapour transmission rate of PLA/CH biocomposite films was increased slightly due to the hydrophilic nature of chitosan. The Isothermal crystallization kinetics of PLA and PLA/CH biocomposite films showed homogeneous nucleation.

Chapter 5
Synthesis and Characterization of Chitosan-*Graft*-Oligo (L-Lactic Acid) Copolymer

The chapter elucidates the investigation on chitosan-graft-oligo(l-lactic acid) copolymer (CH-g-OLLA) for its use in packaging application. The monomer lactic acid is used to graft on chitosan backbone by conventional heating and microwave heating methods. However, microwave heating method is selected for further investigations. The hydrophilic chitosan is grafted with insitu grown lactic acid oligomer. The grafting at NH_2 groups in chitosan backbone with oligo-(L-lactic acid) (OLLA) chains is confirmed by FTIR and NMR analyses. Other analyses such as SEM, TEM and contact angle measurements support uniform dispersion of chitosan in OLLA due to effective grafting reaction. The prepared copolymer is found to be amorphous in nature which was proved by XRD and DSC analyses due to absence of crystallization peak and broad peak of heat of fusion.

5.1. Introduction

Recently, much attention has been delivered for the modification of existing polymers with bio-based polymers to improve the performance and its utilization along with the reduction in polymer wastes. Synthesis is a unique tool which is used for the modification of polymers. Grafting is one of the promising methods among all other methods for synthesis of polymers. Chitosan is widely used in packaging applications due to its biodegradability, non-toxic and film forming ability. This property was utilized by **Khan et al., 2012** and they have fabricated biodegradable films using chitosan as matrix and nano-crystalline cellulose (NCC) as filler in the range of 1-10 wt% by solution casting method. It was observed that the improvement of ~26% was noticed in ultimate tensile strength as compare to that of pristine chitosan film by adding 5% (w/w) of NCC. Chitosan/NCC films have demonstrated an optimum reduction of ~27% in water vapor permeability (WVP) as compare to that of neat chitosan, which is really required for packaging. Chitosan was also used to prepare chitosan/tripolyphosphate nanoparticles (CH-TPP) by ionic gelation method and blend with hydroxypropyl methylcellulose (HPMC) to prepare edible films by solution casting method. The available pores in HPMC matrix were collapsed by adding chitosan nanoparticles, which improved WVP, tensile properties and thermal properties. The WVP of HPMC films was reduced upto 26% with the incorporation of CH-TPP nanoparticles **[Moura et al., 2009]**. Various other examples for properties enhancement by adding chitosan are grease-proof paper with chitosan coating **[Kjellgren et al., 2006]**, pulp fiber-chitosan sheets **[Gallstedt and Hedenqvist, 2006]**, biodegradable rice starch/chitosan films **[Bourtoom and Chinnan, 2008]**, chitosan/layered silicate nanocomposite films **[Oguzlu and Tihminlioglu, 2010]**, chitosan-starch films loaded with silver nanoparticles **[Yoksan and Chirachanchai, 2010]** and corn starch/chitosan composite films **[Garcia et al., 2006]**. In all above cases, it was observed that the presence

of chitosan has enhanced barrier and other properties of various conventional and bio-based polymers. However, the physico-chemical properties of polymers are improved by the addition of chitosan, the hydrophilic nature of chitosan is the real drawback, which inhibits its contribution in packaging applications. Hence, the modification of existing bio-based polymers has attracted much attention of researchers to overcome its limitations and it can be achieved by using different techniques such as copolymerization, grafting, grafting cum condensation polymerization or ring opening polymerization etc. Among various modification techniques, grafting has received significant attention which can be achieved using various intermediates including free radical, ions, photo-initiated grafting, plasma induced grafting and enzymatic grafting **[Bhattacharya et al., 2004]**. Whereas, photochemical grafting can be processed by two ways i.e. with sensitizer and without sensitizer **[Kubota et al., 2001]**. The newest developed technique is enzymatic grafting, which performs with the help of enzyme. In this method, the enzymes behave as initiator to perform chemical grafting. For example, tyrosinase has the capability to transform phenol into o-quinone, which further reacts with chitosan under non-enzymatic conditions and form grafted copolymer **[Chen et al., 2000]** as shown in Figure 5.1. Hence, there are various advantages of grafting such as the transformation in hydrophilicity/hydrophobicity of polymers, enhanced thermal stability, improved mechanical and barrier properties etc.

Chitosan is highly used to fabricate tough, clean and flexible films with low oxygen permeability and can be used in the form of edible packaging to enhance the food shelf life due to its $–NH_2$ group present at C2 position. It is noteworthy to mention that chitosan can't be utilized as individual packaging due to its hydrophilic nature and is incompatible with hydrophobic polymers such as PLA which leads to phase separation, subsequently reduces its mechanical and thermal properties **[Suyatma et al., 2004]**. Chitosan can be easily

modified due to the availability of hydroxyl and amino groups to overcome the limitation of compatibility with PLA and other hydrophobic polymers.

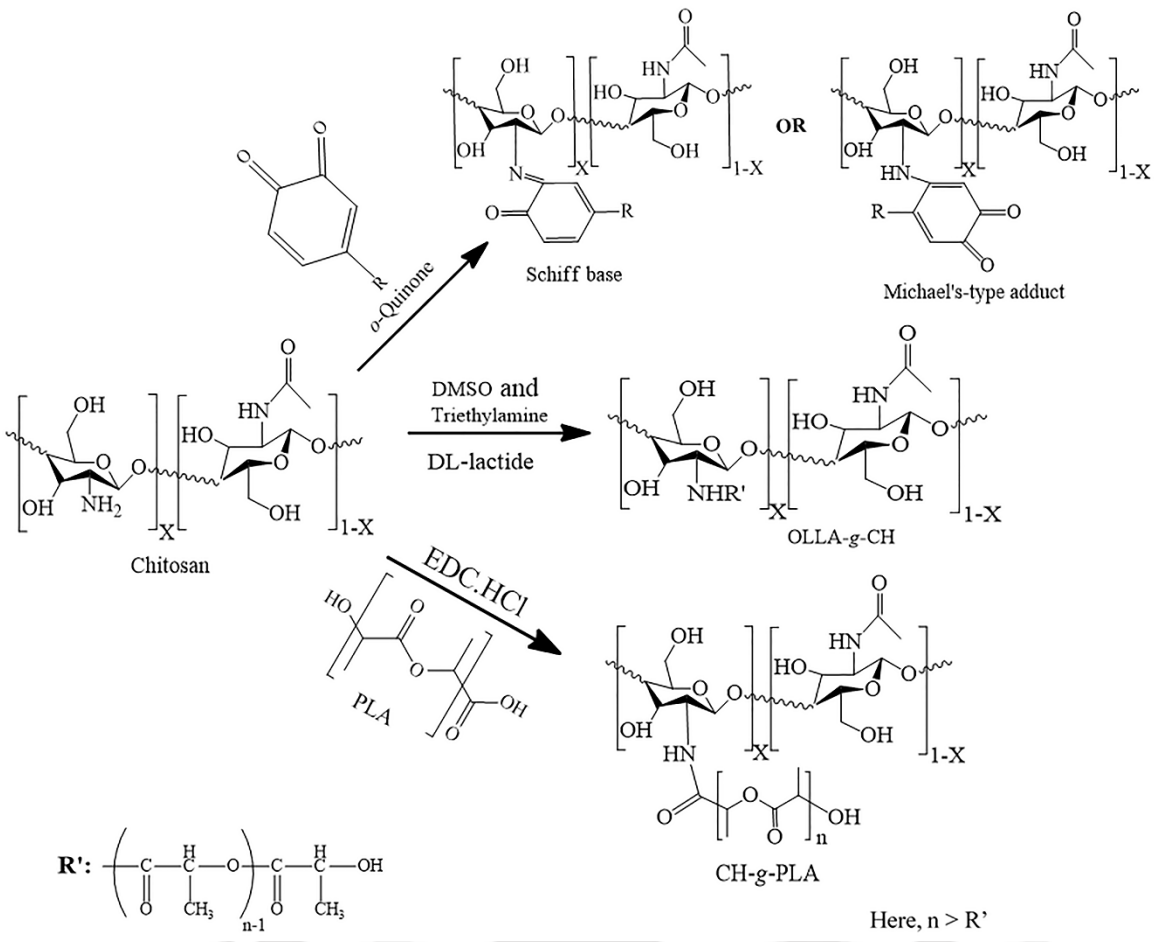

Figure 5.1. Different routes for surface modifications of chitosan.

Several attempts have been taken to modify chitosan with other conventional and bio-based polymers by using catalysts/initiators which work as a bridge between two polymers **[Ganji and Abdekhodaie, 2010; Liu et al., 2008]**. **Li et al., 2008** and **Zhou et al., 2013** have developed an amphiphilic graft copolymer using hydrophilic chitosan and hydrophobic poly (L-lactic acid) (PLLA) by protection-*graft*-deprotection mechanism. In this reaction mechanism, the monomer unit of PLLA reacts with the available hydroxyl groups on phthaloylchitosan (PHCS) in the presence of homogeneous system i.e

N,N-dimethylformamide (DMF) solvent. The grafted copolymer disperses in the form of solid and hollow spherical micelles in aqueous solutions and should be non-toxic due the use of biodegradable reactants. Chitosan has been modified with PLA to form PLA-*graft*-chitosan (PLA-*g*-CH) nanoparticles to load a drug called amphotericin B by dialysis method for ocular delivery. It was projected that the therapeutic gaps in ocular drug delivery can be conquered with the help of distinct structure of PLA-*g*-CH. Similarly, **Li et al., 2012** has developed a chemical conjugation method for the synthesis of chitosan-*graft*-PLA (CH-*g*-PLA) with low degree of grafting by using 1-ethyl-3-(3-dimethylaminopropyl) carbodiimide (EDC) and N-hydroxy-succinimide (NHS) as mediators for coupling reaction as mentioned in Figure 5.1. The molecular weight and amount of PLA can easily tune the chain length of grafted polymer. The grafted copolymer i.e. CH-*g*-PLA exhibits tunable hydrophilicity, hydrophobicity, solubility, thermal stability, biodegradability and self-assembling behaviour, which can be utilized in various applications such as food packaging, drug delivery and tissue engineering. The biodegradable chitosan is also grafted with other polymers such as poly(*p*-dioxanone) (PDO) and form chitosan-*graft*-poly(*p*-dioxanone) copolymer (CGP) in the presence of a catalyst i.e. stannous octoate ($SnOct_2$) by a well-known ring opening polymerization, which is highly used in drug delivery **[Liu et al., 2008]**. **Schreiber et al., 2013** has studied the antioxidant activity of pristine chitosan and gallic acid grafted chitosan films for their use in food packaging application. The grafting of gallic acid on chitosan backbone was performed in the presence of EDC and NHS. An improved 2,2-diphenyl-1-picrylhydrazyl (DPPH) scavenging i.e. 89.5% has been observed in gallic acid-*graft*-chitosan films in comparison to that of pristine chitosan, which is highly appreciable for its use in multifunctional packaging applications. Chitosan can be modified not only by high molecular weight polymers but also with the low molecular weight polymers such as

oligo (l-lactic acid) based on its use in particular application. **Yao et al., 2003** has synthesized low molecular weight oligo (l-lactic acid)-*graft*-chitosan copolymers (CH-*g*-OLLA) with the help of 1,6-hexanediol, dimethylsulfoxide (DMSO) and acetic anhydride. The molecular weight of CH-*g*-OLLA varies from ~600-5000 Da with the variation in side chain length. The prepared copolymer can be widely used in packaging, tissue engineering and drug delivery. Further, **Wu et al., 2005** also prepared polymeric micelles of graft copolymer based on amphiphilic chitosan and DL-lactide in the presence of triethylamine and DMSO (as shown in Figure 5.1), which can be an appropriate option for improving gas barrier properties of packages, entrapment of drugs and their controlled release.

From the above discussion, it is quite clear that biodegradable chitosan can be easily modified with various polymers in the presence of different initiators by using numerous grafting techniques. Although, the used polymers are biodegradable and non-toxic, the initiators are hazardous and toxic in nature, which is also not acceptable in the cases of packaging and medical applications.

This research work is primarily focused on the synthesis and characterization of chitosan-*g*-oligo (l-lactic acid) (CH-*g*-OLLA) copolymer of higher solubility in organic solvents, low crystallinity and low molecular weight using conventional and microwave assisted condensation polymerization reaction for grafting of lactyl units on CH backbone without the consumption of any catalyst or additive. Grafting, molecular weight, thermal behavior, contact angle and surface morphology have been properly characterized by FTIR, NMR, XRD, GPC, TGA, SEM and TEM.

5.2. Results and discussion

5.2.1. Solubility test

Solubility of CH, OLLA and CH-*g*-OLLA copolymer are evaluated in a series of organic and inorganic solvents as shown in Table 5.1. It clearly shows the successful modification of chitosan and its conversion into CH-*g*-OLLA, which also indicates the conversion of hydrophilic nature of chitosan into hydrophobic by grafting of OLLA side chains on chitosan backbone via *insitu* condensation polymerization. Pure chitosan swells in water and soluble in acetic acid solution. Whereas, OLLA and CH-*g*-OLLA (30%) is not soluble in water. It is noteworthy to mention that CH-*g*-OLLA (30%) copolymer is partially soluble in acetic acid solution due to the existence of free OH groups on chitosan backbone. So, CH-*g*-OLLA (30%) copolymer also exhibits amphiphilic nature. The amphiphilic CH-*g*-OLLA (30%) copolymer also soluble in other solvents such as chloroform, dichloromethane, acetone, methanol and ethyl acetate.

Table 5.1: Solubility of CH, OLLA and CH-*g*-OLLA copolymer in various solvents.

S. No.	Solvents	CH	OLLA	CH-*g*-OLLA (30%)
1	Water	+	--	No
2	1% acetic acid	++	--	+
3	Chloroform	--	++	++
4	Dichloromethane	--	++	++
5	Acetone	--	-	++
6	Methanol	--	++	++
7	Ethyl acetate	--	++	++

'+' denotes slightly soluble, '++' denotes strongly soluble, '-' denotes insoluble and '--' denotes strongly insoluble.

It is due to the random distribution of OLLA side chains which disturbs the regular arrangement of chitosan backbone and engage with the NH_2 groups of chitosan. Hence, the improved solubility of CH-*g*-OLLA copolymer expands the utilization of chitosan in various applications.

5.2.2. Calculation of grafting parameters

Oligo(l-lactic acid) is efficiently grafted on chitosan backbone with the help of microwave assisted *in-situ* polycondensation reaction and a good yield of prepared copolymer (CH-*g*-OLLA) is obtained after the completion of the reaction. Both lactic acid and chitosan are hydrophilic in nature hence, initially, the grafting phenomena takes place in an aqueous medium and the present water in the system absorbs microwave energy. The polar behaviour of water generates dielectric heating of the reaction medium. It is also reported in literature that the Gibbs free energy reduces during the activation of reaction in microwaves **[Pandey and Mishra, 2012]**. These two factors are responsible for the quick conversion of lactic acid and chitosan into ion radicals. These radicals react with water and generate free hydroxyl radicals. The available free radicals in the system promote homopolymerization, which is the faster reaction to that of copolymerization and grafting. Hence, lactic acid free radicals can attached together and start to form OLLA chain. The OLLA chain grows until it attaches with the other such chain. The OLLA chains may attach with the most electronegative functional groups i.e. NH_2 in chitosan chain to perform grafting. The various grafting parameters such as yield (%), percent conversion (%), grafting efficiency (%), percent grafting (%) and percent homopolymer were calculated as ~51.6, ~266.6, ~40, ~150 and ~60% respectively.

5.2.3. Fourier transform infrared spectroscopy (FTIR)

The grafting phenomena of OLLA polymeric chains on chitosan backbone is corroborated in FTIR analysis as shown in Figure 5.2(a) & (b). The regular characteristic peaks of OLLA are detected at 1720 cm^{-1}, 1454 cm^{-1}, 1375 cm^{-1}, 1207 cm^{-1}, 1121 cm^{-1}, 1041 cm^{-1} and 870 cm^{-1} which attributed to the $-C=O$ stretching, $-CH_3$ bending, $-CH-$ bending for symmetric and asymmetric deformation, $(C-O-C)$ asymmetric stretching, $C-OH$ side group vibrations and $-C-C-$ stretching respectively as shown in Figure 5.2(a). These regular peaks are also presented in CH-*g*-OLLA (30%) copolymer. It is noteworthy to mention that few FTIR peaks are shifted towards higher wave number values which are positioned at 1745 cm^{-1}, 1382 cm^{-1}, 1128 cm^{-1} and 1092 cm^{-1} due to the development of new inter-molecular hydrogen bonds. However, the shifting of peaks towards higher wave number values can also be possible due to the dark brown colour of CH-*g*-OLLA copolymer. The regular characteristic peaks of chitosan powder are also detected at 1545 and 1640 cm^{-1} which attributed to the strong $-N-H$ bending vibrations of secondary amides and $-C=O$ stretching vibrations of primary amides respectively. These peaks with reduced intensity are also observed in CH-*g*-OLLA (30%) filler which correspond to the grafting of OLLA chains on chitosan backbone. The FTIR peak at 1545 cm^{-1} in chitosan powder is shifted towards higher wavenumber value and positioned at 1550 cm^{-1} in CH-*g*-OLLA (30%) copolymer which supported the structural differences in CH-*g*-OLLA (30%) copolymer. One additional new peak at 1539 cm^{-1} is detected in CH-*g*-OLLA (30%) sample which confirmed the amide ester linkage $(-OCONH-)$ of chitosan with repeat units of LA **[Byun et al., 2010]**. The peak at 1539 cm^{-1} is the proof of structural modification in chitosan backbone. As a result of grafting, the growth of OLLA polymeric chains on chitosan backbone is shown in Figure 5.5 in the form of reaction.

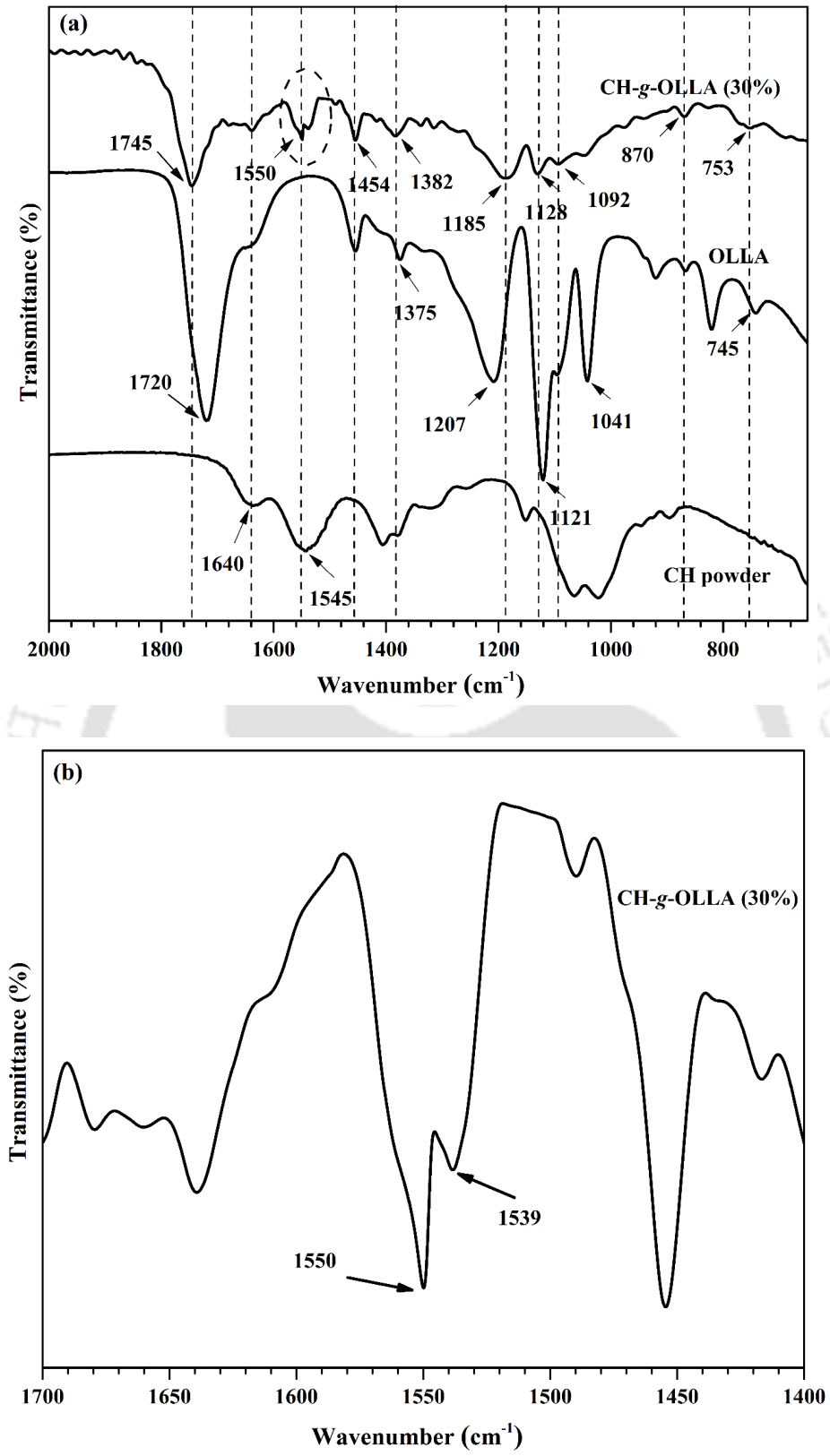

Figure 5.2. (a) FTIR spectra of chitosan powder, OLLA and CH-*g*-OLLA (30%) copolymer in the range of 650-2000 cm^{-1} and (b) FTIR spectra of CH-*g*-OLLA (30%) copolymer in the range of 1400-1700 cm^{-1}.

5.2.4. ^{1}H-Nuclear magnetic resonance (^{1}H-NMR)

The structural details of chitosan, OLLA and CH-*g*-OLLA copolymer are compared in terms of peaks position and their shifting as shown in Figure 5.3. Firstly, the ^{1}H-NMR spectra of chitosan exhibits the regular peaks at 7.66, 4.80, 3.17, 3.71, 3.76, 3.87, 3.91 and 1.88 ppm, which denote two protons attached with nitrogen at C2 position, H1 proton, CH group connected to nitrogen moiety, H3, H4, H5, H6 protons and NHAc respectively. The main peaks of OLLA are obtained at 5.13, 1.56 and 1.24 ppm, which represent -CH protons of OLLA, -CH_3 protons of OLLA and -CH_3 protons of hydroxylated OLLA respectively as shown in Figure 5.3(b). It is noteworthy to mention that the graft copolymer (CH-*g*-OLLA) shows the signals of chitosan as well as OLLA, which means that both chitosan and OLLA are present in the sample. The peaks are positioned at 4.95, 2.05, 1.52 and 1.25 ppm, which exhibit H1 proton of glucosamine ring (GlcN), NHAc, -CH_3 protons of lactyl units at terminal groups and -CH_3 protons of hydroxylated lactyl units at terminal groups respectively as mentioned in Figure 5.3(c). Similar results were obtained by **Espadin et al., 2014, Luckachan et al., 2006 and Bhattarai et al., 2006** in the preparation of graft copolymer using lactic acid and chitosan. The new peaks observed at 5.1 and 4.2 ppm are attributed to the terminal -CH protons of branched lactyl units and terminal -CH protons of hydroxylated lactyl units respectively. Similar results are retrieved by **Wu et al., 2005** during the synthesis of chitosan-polylactide graft copolymer. The obtained results in this study indicate that CH-*g*-OLLA copolymer is made up of chitosan backbone with attached OLLA side chains at NH_2 group. The peak at 7.66 ppm, which presents in chitosan spectra, is completely disappeared in CH-*g*-OLLA NMR spectra. It confirms the complete consumption of proton (attached with nitrogen at C2 position) by the replacement of OLLA chains. On the basis of ^{1}H-NMR analysis, the proposed reaction pathway of synthesized CH-*g*-OLLA is displayed in Figure 5.5.

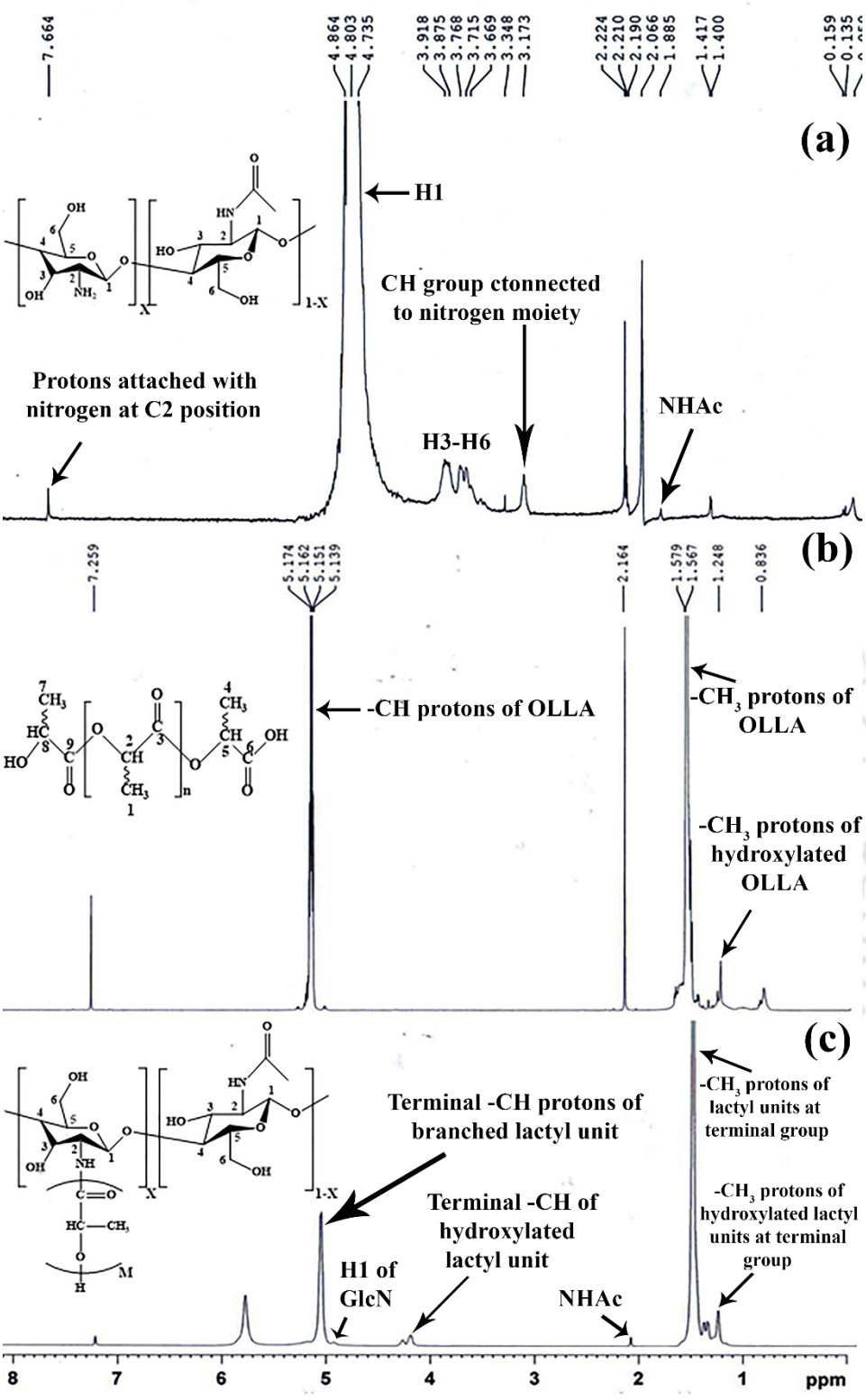

Figure 5.3. ^{1}H-NMR analysis of (a) chitosan, (b) OLLA, (c) CH-*g*-OLLA (30%) copolymer.

5.2.5. Carbon-13 nuclear magnetic resonance (^{13}C-NMR)

^{13}C-NMR analysis is performed to identify the grafting of OLLA chains on chitosan backbone. In the spectra of OLLA, the sharp peaks are detected at 16.73 and 16.81 ppm, which confirm the presence of methyl regions. The NMR peaks at 69.18 and 69.60 ppm denote methane signals. However, the carbonyl peak (-CO) is positioned at 169.77 ppm as shown in Figure 5.4(a). Similar peaks positions for low molecular weight PLA were also observed by **Lan and Lv_2008**. A well know triplet for $CDCl_3$ is identified in the range of 77-77.44 ppm for both OLLA and CH-*g*-OLLA copolymer. ^{13}C-NMR spectra of CH-*g*-OLLA copolymer has demonstrated various peaks at 16.84, 20.29, 66.94 and 69.26 ppm which attribute to the presence of a1, a2, b1 and b2 type carbons of attached OLLA respectively as shown in Figure 5.4(b). The other peaks at 175.21 and 169.81 ppm signify the availability of d1 and d2 type carbons, which represent carbonyl region of linked OLLA. The various carbons i.e. C2, C3, C4, C5 and C6 of glucosamine ring in chitosan are located at 69.34, 69.39, 72.68, 69.60 and 66.78 ppm respectively. Two more peaks named as d1-C2 and d2-C2 are observed at 179.08 and 174.41 ppm which explain about the interaction between carbonyl carbons of d1 and d2 with the available carbon at C2 position in chitosan backbone. Hence, it is proved that the grafting of OLLA chains on chitosan backbone takes place preferentially at $–NH_2$ group.

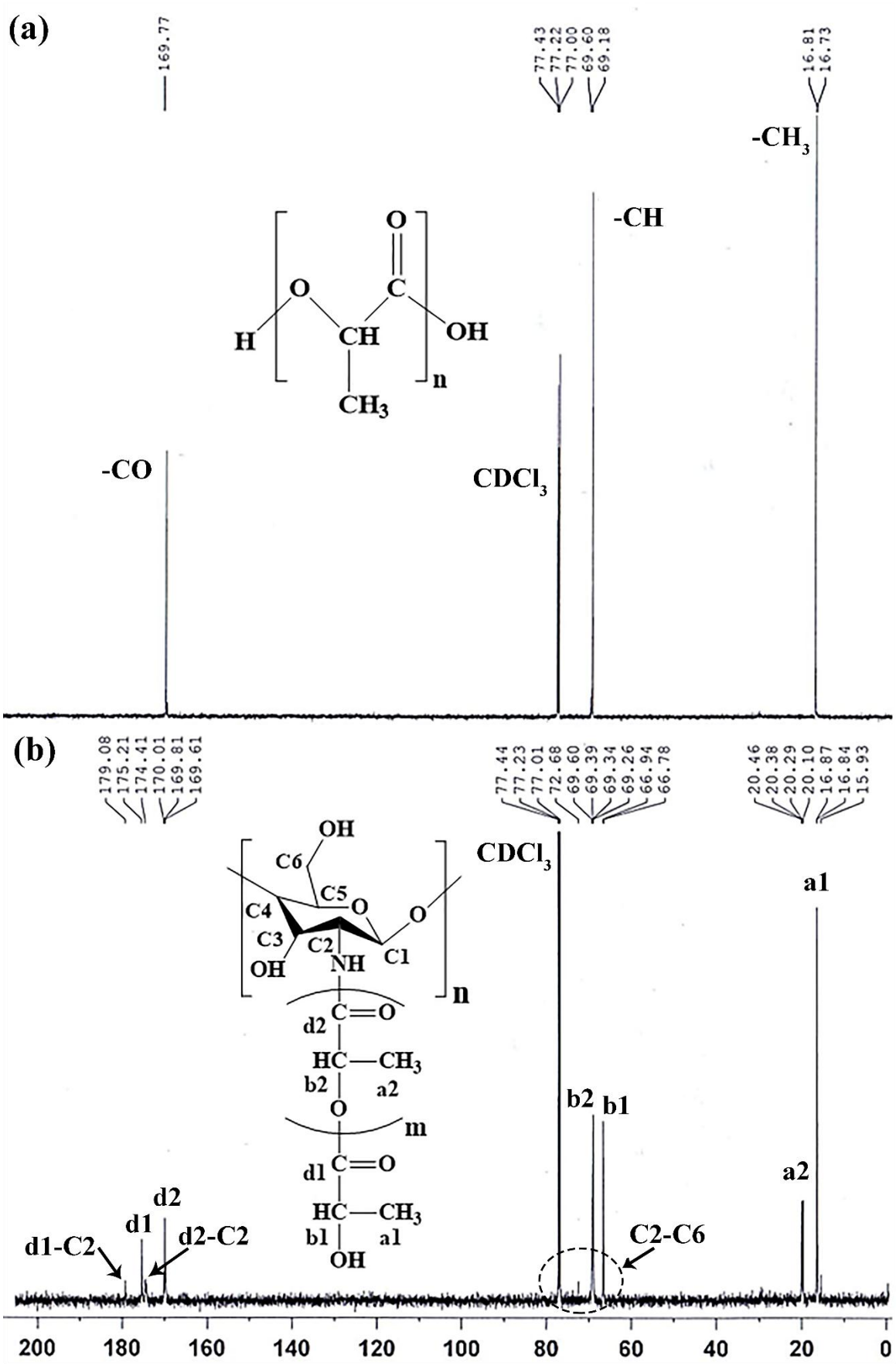

Figure 5.4. ^{13}C NMR spectra of (a) OLLA and (b) CH-*g*-OLLA (30%) copolymer.

As per ^{1}H-NMR and ^{13}C-NMR analyses, the proposed reaction pathway is as shown in Figure 5.5.

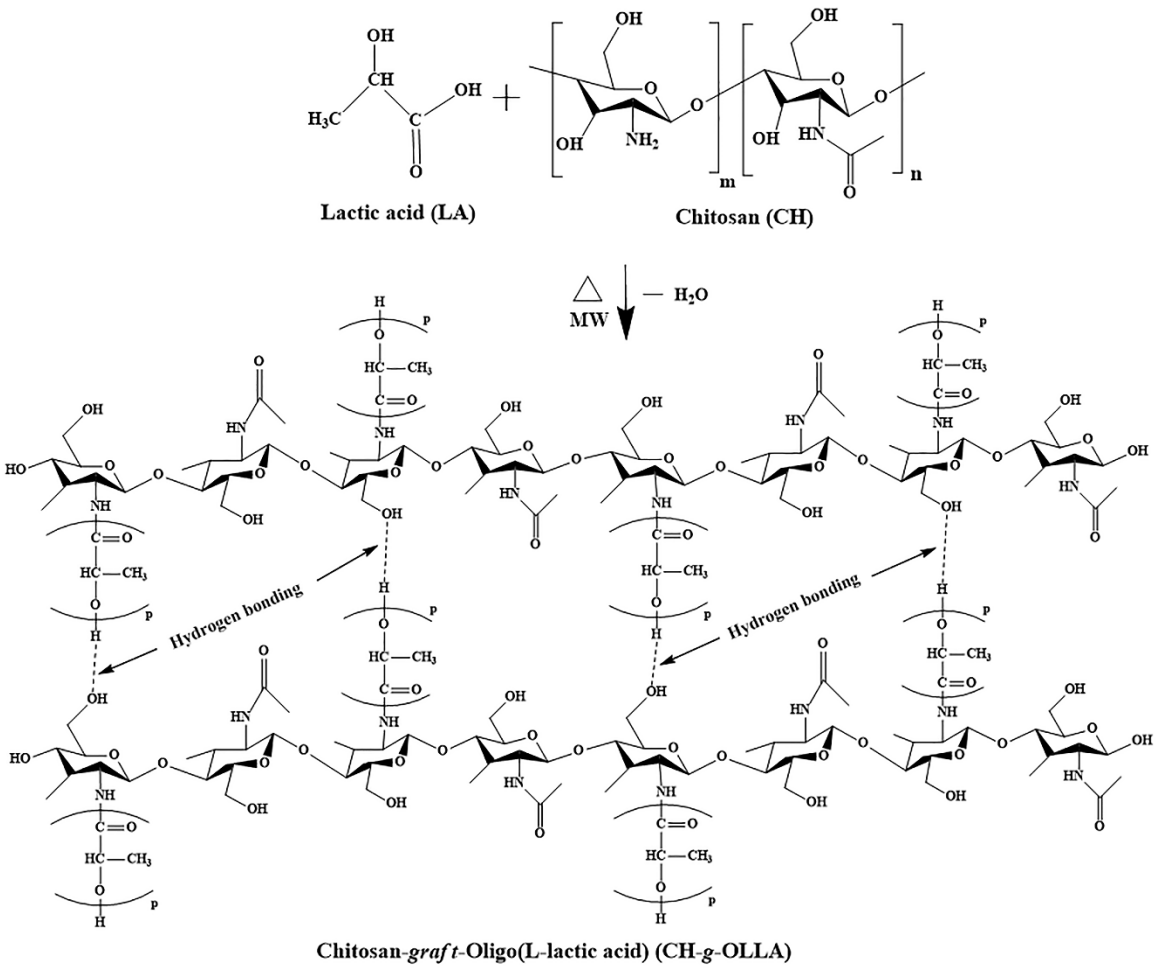

Figure 5.5. Proposed reaction pathway for the synthesis of CH-*g*-OLLA using microwave assisted *insitu* polycondensation reaction.

5.2.6. X-ray diffraction (XRD)

Two diffraction peaks at 2θ = 10.2° and 20° are observed in chitosan with orthorhombic crystals having diffraction planes of [0,2,0] and [1,1,0] respectively as shown in Figure 5.6. No peaks are detected in OLLA and CH-*g*-OLLA (30%) copolymer, which is explained by the significant reduction in hydrogen bonding capability of chitosan after grafting because hydroxyl functional groups are occupied by OLLA chains. It increased the molecular

mobility of polymeric chains. Hence, the crystalline phase of chitosan powder is destroyed after grafting and CH-*g*-OLLA (30%) became amorphous in nature.

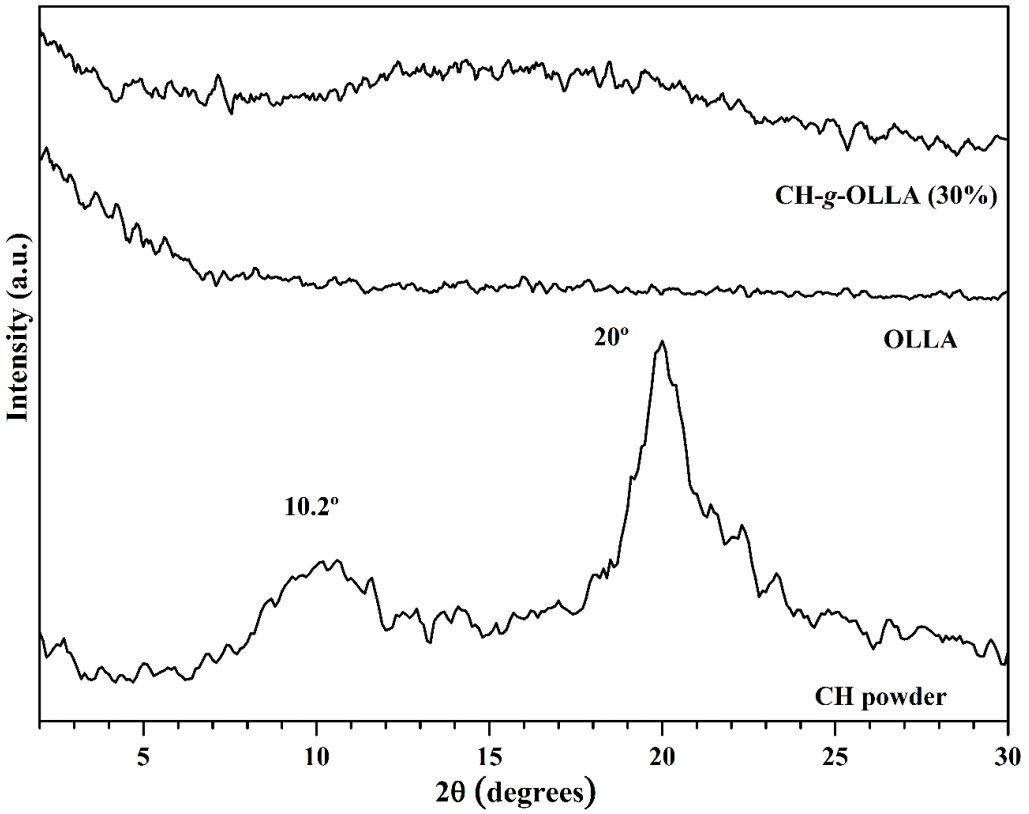

Figure 5.6. XRD analysis of chitosan powder, OLLA and CH-*g*-OLLA (30%) copolymer.

5.2.7. Differential scanning calorimetry (DSC)

DSC thermograms of neat chitosan, OLLA and CH-*g*-OLLA (30%) copolymer are observed during second heating cycle at a heating rate of 5 °C/min as shown in Figure 5.7. The first scanning rate (both heating and cooling cycles) with isothermal condition at 180 °C for 2 min were performed in order to remove the thermal and processing history of the samples. In Figure 5.7, no T_c and T_m peaks are observed in all the samples, which suggests that either amorphous segment does not crystallize itself or they do not have well-ordered hard domain (arranged molecular chains).

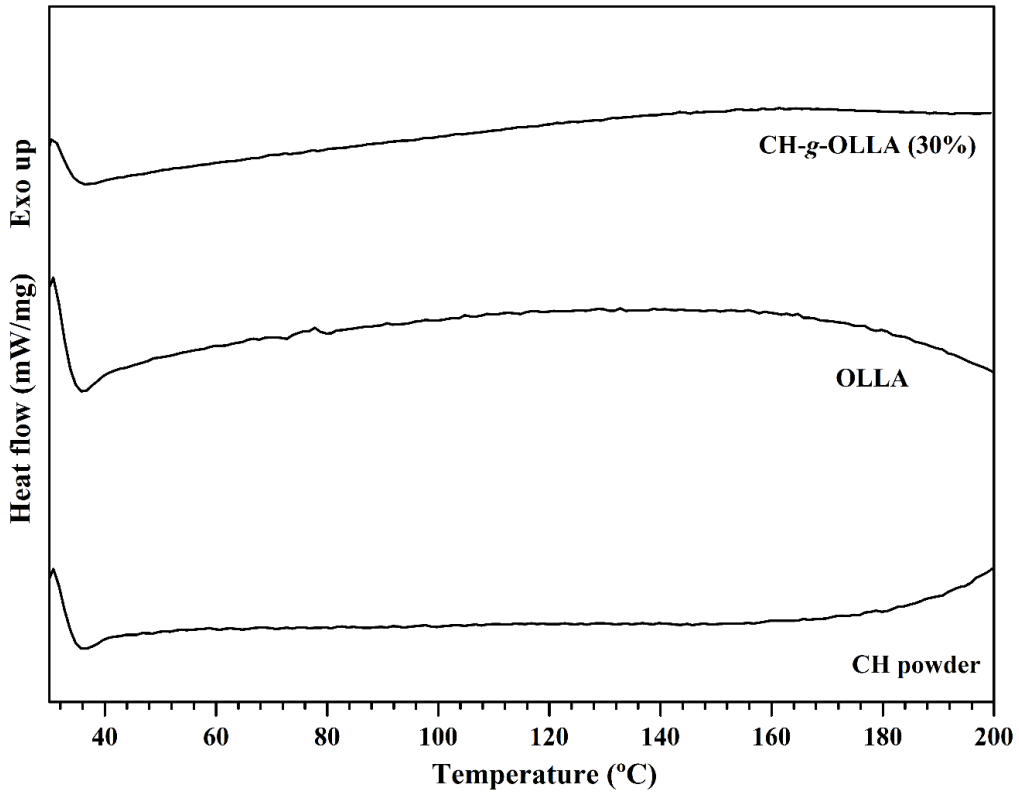

Figure 5.7. Second heating cycle of DSC analysis for chitosan powder, OLLA and CH-*g*-OLLA (30%) copolymer at a heating rate of 5 °C/min.

5.2.8. Thermogravimetric analysis (TGA)

Two significant peaks of thermal degradation are observed at different temperature ranges for chitosan powder as shown in Figure 5.8. The first broad peak is detected in the temperature range of 40-125 °C, which is associated with the evaporation of moisture because chitosan has a strong affinity of moisture due to the presence of hydroxyl groups in its polymer chain. The removal of moisture is not observed in OLLA and CH-*g*-OLLA samples which confirmed the significant reduction in hydrophilicity and its conversion into hydrophobic nature. The second peak is positioned in the temperature range of 235-403 °C, which is attributed to the breakdown of saccharide rings. The maximum degradation temperature is observed at 312 °C, which is higher than the degradation temperature of OLLA and CH-*g*-OLLA. The second prominent degradation peak is noticed in the

temperature range of 81-298 °C and 140-372 °C for OLLA and CH-*g*-OLLA respectively. It showed the reduction in thermal stability due to the availability of less active sites on chitosan backbone and also the presence of low molecular weight OLLA side chains. The single degradation peak in CH-*g*-OLLA (30%) also confirmed the grafting of OLLA on chitosan. It is noteworthy to mention that two degradation peaks of OLLA are acquired at 197 °C and 265.5 °C due to the presence of lactide units in a small amount.

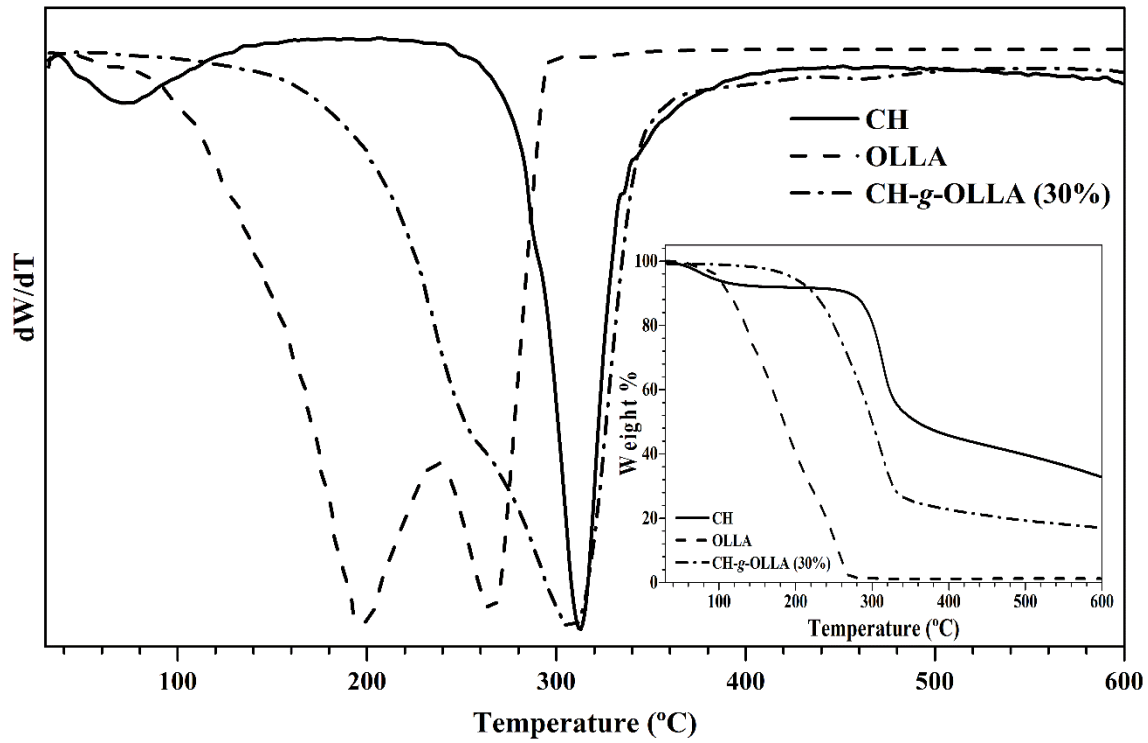

Figure 5.8. TGA analysis for chitosan powder, OLLA and CH-*g*-OLLA (30%) copolymer at a heating rate of 10 °C/min.

5.2.9. Scanning electron microscopy (SEM)

A clear difference in surface & bulk morphology of chitosan, OLLA and CH-*g*-OLLA (30%) copolymer is observed as shown in Figure 5.9(a), (b) and (c) respectively. The roughness and unevenness of the CH and OLLA surfaces are observed in the micrographs. Whereas, CH-*g*-OLLA (30%) copolymer shows smooth surface with uniformly distributed

spherical chitosan particles in OLLA matrix. Uniformly distributed spherical chitosan particles are of various sizes due to the aggregation of polymeric micelles.

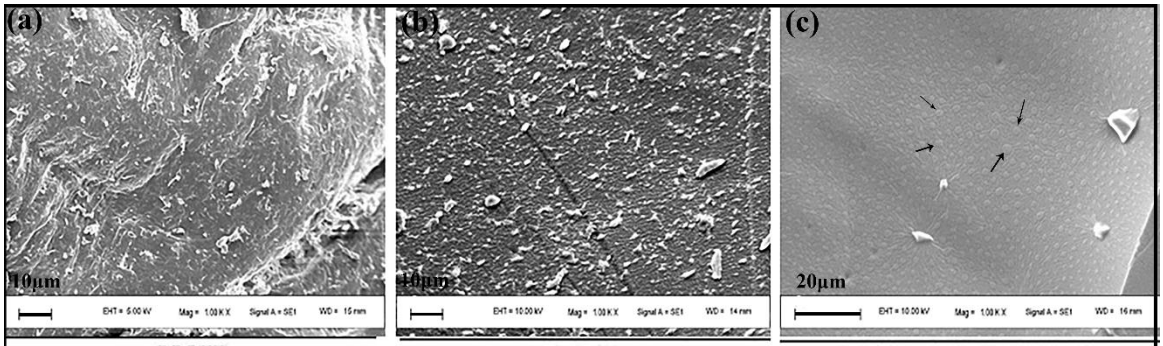

NCH		OLLA		CH-*g*-OLLA (30%)	
Element	**Weight%**	**Element**	**Weight%**	**Element**	**Weight%**
C	43.16	C	50.43	C	52.16
O	30.76	O	49.57	O	34.54
N	26.08	N	-	N	13.30

Figure 5.9. Surface topography and energy dispersive X-ray spectroscopy of (a) Neat chitosan, (b) oligo l-lactic acid and (c) CH-*g*-OLLA (30%) copolymer.

The phenomena of aggregation of polymeric micelles take place only when the filler concentration exceeds the critical micelle concentration (CMC). Above CMC, the micelles start to aggregate and form spherical structures with attached tails. In the present case, the polymeric micelles are made of hydrophilic chitosan head with hydrophobic OLLA tail. Hence, SEM analysis supports the grafting phenomena, occurred on chitosan backbone by the attachment of OLLA chains. The EDX analysis is also performed for CH, OLLA and CH-*g*-OLLA (30%) copolymer, which affirms the existence of carbon, oxygen and nitrogen in various proportions. The weight percentage of carbon, oxygen and nitrogen are detected as 43.16, 30.76 and 26.08% respectively in the case of chitosan. However, carbon and oxygen are the only available elements in OLLA with higher weight percentage such as 50.43% and 49.57% respectively. The increment in weight percentage of carbon and

oxygen is noticed in the case of CH-*g*-OLLA as compare to CH. It is due to the attachment of OLLA side chains on chitosan backbone, which increases the number of carbon and oxygen. It is noteworthy to mention that the weight percentage of nitrogen reduces and observes only 13.30% in CH-*g*-OLLA (30%) copolymer, which confirms the consumption of nitrogen during the grafting process. Hence, it can also be concluded that the OLLA chains are grafted with NH_2 group at C2 position in chitosan.

5.2.10. Transmission electron microscopy (TEM)

The TEM micrograph explored the real insight of CH-*g*-OLLA (30%) copolymer as shown in Figure 5.10(a). It is revealed that the chitosan nanoparticles are uniformly distributed and are of spherical in shape with diameter ~2-4 nm. These spherical nano-chitosan molecules are connected with OLLA chain of average length ~4-6 nm as shown in Figure 5.10(a). Hence, the overall assembly of nano-chitosan head with OLLA tail formed a nano-amphiphilic molecule, i.e. micelle kind of structure in which the head is hydrophilic and tail is hydrophobic in nature. Obviously, some agglomeration of nano-chitosan is also observed, which is indicated by arrows in Figure 5.10(a). The electron diffraction diffuse ring patterns in SAED image clearly displayed the presence of amorphous phase of nano-chitosan in CH-*g*-OLLA (30%) copolymer as shown in Figure 5.10(b) which is also observed from XRD analysis.

The material studio 7.0 software package is used to simulate single OLLA chain of ~22 repeat units of LA at room temperature (298K). OLLA chain is prepared using material studio followed by geometry optimization with the help of Forcite module in the presence of COMPASS force field. The simulated OLLA chain is used to validate the end to end chain length, calculated by ImageJ 1.45 software from TEM image (Figure 5.10(a)). Both the properties, end to end chain length and radius of gyration (R_g), are structural properties which can be calculated directly from the software after geometry optimization. The

calculated values of end to end chain length and radius of gyration are 5.7 nm and 0.97 nm (as shown in Figure 5.10(c)) respectively which are found nearby the measured values from ImageJ software. Hence, it is confirmed that the attached tail with nano-chitosan head is only low molecular weight OLLA chain.

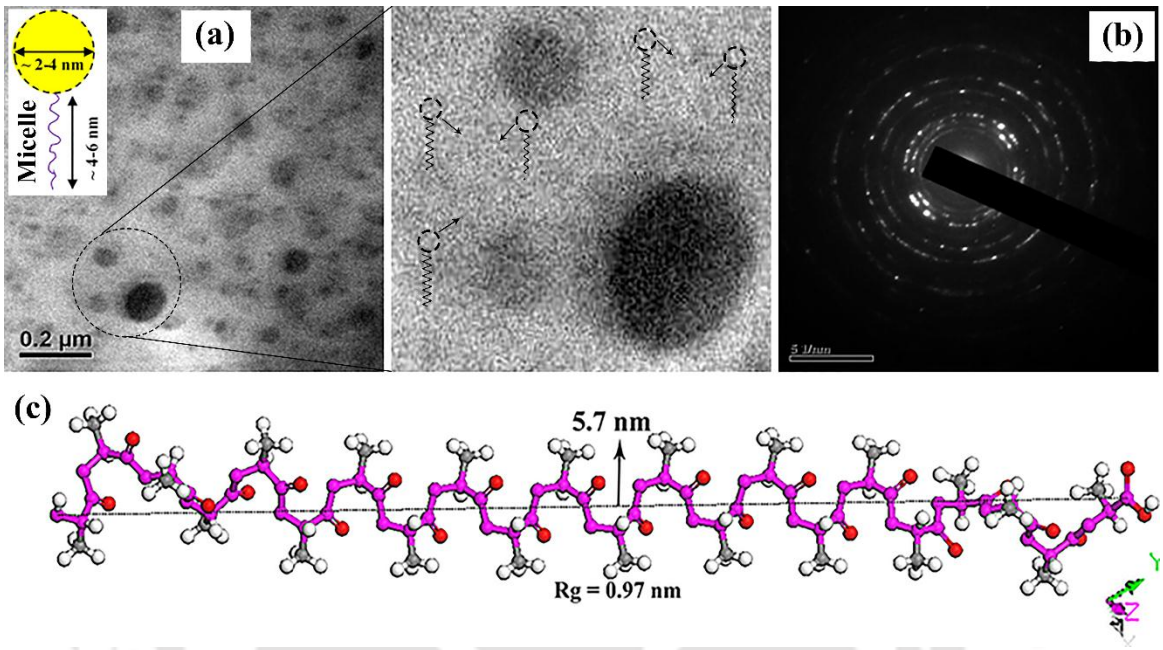

Figure 5.10. (a) TEM analysis, (b) SAED pattern of CH-*g*-OLLA (30%) and (c) end to end distance & radius of gyration of OLLA chain calculated by Material Studio 7.0 software.

5.2.11. Contact angle measurements (CA)

The optimized procedure for contact angle analysis of the prepared CH-*g*-OLLA copolymer with different concentrations, is performed as mentioned in section 2.3.17, which proves that the hydrophobicity increases with an increase in blend composition as mentioned in Figure 5.11. The value of contact angle for chitosan is observed very low i.e. ~18.2º due to its hydrophilic nature. The hydrophilic nature of chitosan is only because of free OH groups. However, the contact angle values increase approximately from 61.4º to 78.5º with

an increase in chitosan concentration from 10% to 30% in the case of CH-*g*-OLLA copolymers. This nonobvious increment in the contact angle is due to the occupancy of functional groups at chitosan backbone by OLLA side chains, which reflect the hydrophobic character.

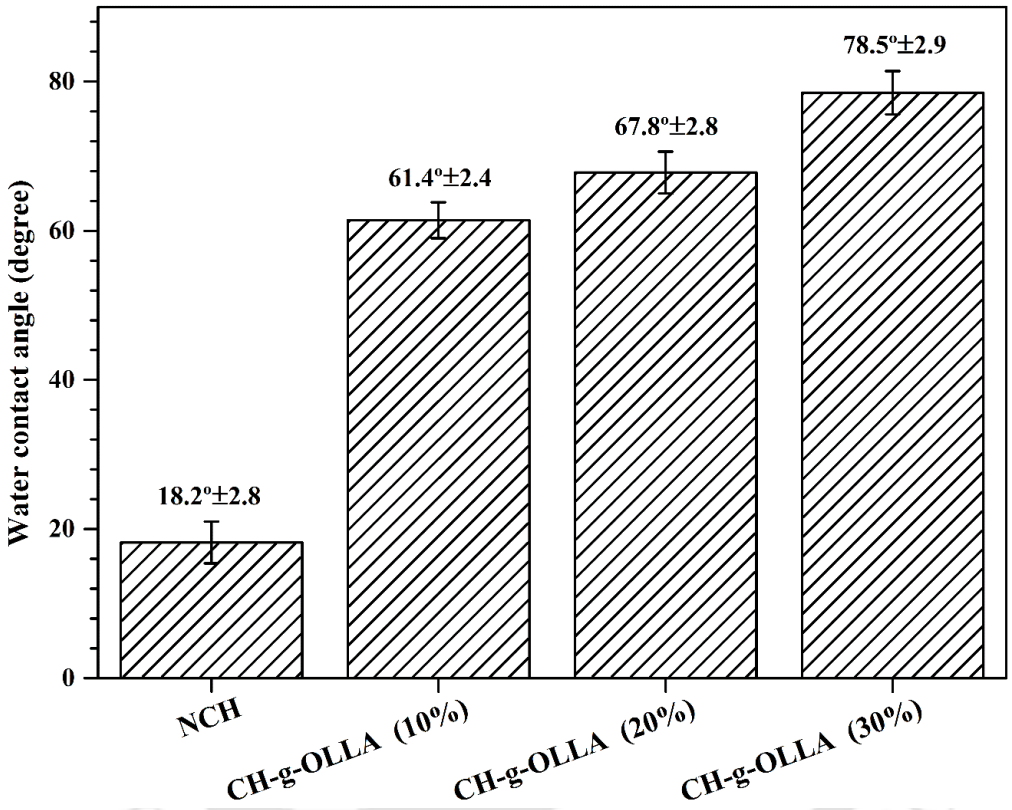

Figure 5.11. Contact angle measurements of synthesized CH-*g*-OLLA copolymer.

Hence, the functional groups at grafted chitosan backbone can't absorb the moisture as compare to that of neat chitosan. In this way, the wettability of copolymers can be tuned as per requirement in various applications. Such copolymers have potential to be utilized in biomedical applications due to have moderate wettability, which is highly required for cell adhesion. Cell adhesion and differentiation also depend on other factors such as polymer chemistry, surface topography, and cell type.

5.3. Summary

The synthesis of chitosan-*graft*-oligo(l-lactic acid) (CH-*g*-OLLA) was conducted by microwave assisted *insitu* condensation polymerization technique. The synthesis of CH-*g*-OLLA copolymers with various concentrations resulted in the conversion of hydrophilic chitosan to hydrophobic copolymer. Various parameters such as grafting efficiency, percentage grafting, percent yield and percent homopolymer were calculated using distinct equations based on weight of reactants and products. The FTIR and NMR analyses confirmed that the grafting of *oligo*-(lactic acid) on chitosan backbone occurred at -NH_2 groups. The XRD analysis revealed that the synthesized copolymer is amorphous in nature. No T_c and T_m were detected in DSC analysis suggested that well-ordered molecular chains are not present in copolymer. The thermal stability of CH-*g*-OLLA (30%) copolymer is very close to the thermal stability of chitosan. Significant change in the surface morphology was observed by SEM analysis which also supports grafting. The presence of CH nanoparticles were observed in TEM images. The surface characteristics of synthesized copolymers were observed by contact angle analysis. The improvement in hydrophobicity occurred with increase in CH concentration confirmed the reduction in polar groups due to grafting.

Chapter 6

Fabrication and Characterization of Poly (Lactic Acid)/Chitosan-*Graft*-Oligo(L-Lactic Acid) Bionanocomposite Films by Solution Casting Technique

This chapter demonstrates the utilization of synthesized chitosan-graft-oligo(l-lactic acid) (CH-g-OLLA), a nano-amphiphilic molecule, as a nano-filler for improvement in multiple properties of poly (lactic acid) (PLA) films, essential for stringent food packaging applications. Fourier Transform Infrared spectroscopy (FTIR) analysis shows the presence of amide-ester bond at 1539 cm^{-1} which confirms the structural grafting of OLLA chains with chitosan molecules. The prepared PLA/CH-g-OLLA bionanocomposite films appear with uniform dispersion of nano-amphiphilic CH-g-OLLA molecules with self-assembled micelles having size as low as ~20 nm and as high as ~150 nm with core-shell morphology in PLA matrix. This nano-filler is found very effective towards significant reduction in oxygen permeability (P) by ~10 folds due to the reduction in solubility of oxygen molecules and improvement in crystal nucleation density due to availability of nano-nucleating sites. The onset of thermal degradation of PLA/CH-g-OLLA films is also found comparable to that of PLA film. The glass transition temperature (T_g) of bionanocomposites is decreased by more than 18 °C with increase in CH-g-OLLA loading which indicates the improved plasticization characteristics of PLA matrix. The reduction in T_g of PLA with improvement in elongation at break and multi-fold reduction in oxygen permeability makes this bionanocomposite films, a promising candidate for stringent food packaging applications.

6.1. Introduction

Development of biocompatible and biodegradable films with high gas barrier properties are essential for its uses in stringent food packaging applications. Generally, packaging is essential for food products to acts as safeguard against environment and mechanical damage during tansport. Plastics are preferred for packaging applications due to their light weight, easy handling and comparable properties than other packages made of glass, metal, wood, ceramic, etc. Various existing conventional synthetic plastics such as PET, PP, PE and PPC can be either made by addition or condensation polymerization from petrochemical feedstock. These plastics are considered non-degradable at different levels in the environment, which can probably imbalance the ecological and environmental CO_2 cycle and also create health issues for humans and other living creatures **[Zembouai et al., 2013]**. To overcome such problems, the significant efforts are under way to develop new degradable polymeric products and its processes, which can possibly reduce the environment-related hazards by reducing carbon footprint. In this regard, aliphatic polyesters such as PLA, polyglycolic acid (PGA), PCL and PHA are the mostly used polymers in current scenario due to their biodegradable characteristics and are mainly derived from bio-based resources, which further helps to reduce carbon footprint. However, it has been realized that the combination of above-mentioned polymers with bio-polymers, can be an alternative of petrochemical based polymers, which are currently used for food packaging. Therefore, chemical modification of bioplastics is one of the smart techniques by which hydrophilic bio-polymers can be dispersed in hydrophobic polymers in order to tailor the required properties **[Wu et al., 2006]**. Hence, tailored bioplastics can be the most promising candidate as an additive for future bioplastic applications **[Peelman et al., 2013]**. PLA, a synthetic environment friendly bio-based polymer, can be synthesized using lactic acid (2-hydroxy propionic acid) (LA), has earned the maximum engrossment due to its

renewable natural resources like corn, sweet potato, tapioca starch, wheat, sugar feedstock and waste products from agriculture industry by fermentation **[Wu et al., 2006; Suyatma et al., 2004; Bocchini et al., 2010; Silverajah et al., 2012; Saiwaew et al., 2014]**. It has commendable thermal, mechanical and barrier properties with superior transparency in the processed materials, which increases its utility in food packaging and medical applications.

Chitosan is also an extremely recommended bio-polymer for food packaging application due to its enormous functional properties **[Suyatma et al., 2004]**. The increasing demand of chitosan is due to its film forming ability without any additives **[Rubentheren et al., 2015; Vasile et al., 2013]**. The gas barrier properties of chitosan films are observed to be better than that of PE films **[Suyatma et al., 2005; Suyatma et al., 2010; Suyatma et al., 2011]**. In addition, a highly reactive amino group presents in chitosan structure, makes it suitable to utilize in many applications such as food packaging, wound dressing, drug delivery, fuel cell, waste-water treatment, bio-medical, etc. **[Niamsa and Baimark, 2009]**. Chitosan can also be used in active food packaging due to its antimicrobial, antioxidant and anti-fungal characteristics **[Vasile et al., 2013]**. It can prevent the growth of bacteria, yeast and fungus in the packed food which can extend the food shelf life. On the other hand, the effective molecular level dispersion of chitosan in hydrophobic PLA is not possible due to its hydrophilic nature. This limitation can be eliminated by converting hydrophilic chitosan into hydrophobic in nature by grafting it with the hydrophobic polymer such as PLA **[Xiao et al., 2001]**. It is noteworthy to mention that grafted hydrophobic chitosan should have better compatibility with PLA than other conventional polymers. Grafting technique is much effective to create new polymer with improved properties by combining two or more polymers and indeed a better technique than mixing and blending **[Suyatma et al., 2010]**.

Gas barrier property is important to characterize the film's suitability for food packaging applications. It is defined as a steady-state property that describes the extent to which a gaseous permeant molecule can solubilize into polymer matrix and then the rate at which it diffuses through the film, with a driving force, difference in concentration of diffusent molecules between two sides of the film. Oxygen is an important component for oxidation of food which decreases its quality and shelf life too **[Sun et al., 2014]**. Oxygen transmission rate test (OTR) shows the ease of oxygen molecules passing across the film when a partial pressure gradient of oxygen applied on it **[Park et al., 2012]**. It is a complex phenomenon, which is based on four main stages to transport gas through a film. The first stage is gas adsorption by the film at ambient atmosphere-film interface. The second stage is dissolution of gas in polymer matrix. The third stage is gas diffusion inside and through the film. The fourth step is desorption of gas from the film interface to the ambient atmosphere. If oxygen transmission rate is controlled by diffusion phenomenon then third step will be the rate limiting among all four steps. Similarly, the second step will be the rate determining step if the permeation is controlled by miscibility of penetrant in polymer matrix. Basically, the gas permeation across the film proceeds through the amorphous phase of polymers which depends on distinct factors such as the ratio between crystalline and amorphous zones, compatibility of fillers with polymer matrix, polymeric chain mobility and hydrophilic-hydrophobic ratio. The interaction between polymer matrix and plasticizer or other additives are also an important factor in gas permeability **[Matet et al., 2015; Darie et al., 2014; Souza et al., 2009]**. Tortuosity is one of the factors which improves the oxygen permeability (P) due to the increment in diffusion path of gas molecules due to exfoliation of nano-filler in the polymer matrix.

Three types of permeability through films mainly affect the food packaging, which includes oxygen permeability, carbon dioxide permeability, and water vapor permeability. Chitosan

can prevent gases to enter into the plastic packaging film due to its inherent solubility of oxygen. Different types of additives are added into the bio-polymer films to improve food quality, minimize microbial growth and extend shelf life. The additives may be antioxidants, antimicrobial, colors, anti-fungal agents, and nutrients. The widely used chitosan can be mixed with any polymer to enhance its performance such as pulp fiber chitosan sheet **[Gallstedt and Hedenqvist, 2006]**, montmorillonite nano-clay and rosemary essential oil interaction with chitosan **[Abdollahi et al., 2012]**, chitosan coated grease proof paper **[Kjellgren et al., 2006]**, chitosan coated polyethylene **[Kurek et al., 2012]**, nano-multilayer coating of pectin and chitosan **[Medeiros et al., 2012]** and hydroxypropyl methylcellulose edible films with chitosan/tripolyphosphate nanoparticles **[Moura et al., 2009]**. On the other hand, few of the reported literatures on grafted bio-polymers have exposed a new direction of utilizing natural resources. In this line, **Suyatma et al., 2004** prepared PLA-chitosan blend for improving water vapor transmission rate (WVTR) as well as mechanical property. The results showed an improvement in WVTR whereas, tensile strength and elastic modulus were decreased due to incompatibility of PLA solution with chitosan. The incompatibility issue of chitosan with PLA was further addressed by **Luckachan and Pillai, 2006**. They prepared chitosan/oligo (L-lactide) graft polymers by polymerization of L-lactide onto chitosan via ring opening polymerization using $Ti(OBu)_4$ as catalyst and prepared PLA is appeared as increased hydrophilicity and controlled degradation rate. Interestingly, in other study, chitosan-*graft*-PLA was prepared by chemical modification of chitosan with PLA via 1-ethyl-3-(3-dimethylaminopropyl) carbodiimide (EDC) mediated coupling reaction. The thermal stability and solubility were improved by PLA introduction into the structure of chitosan and widely used in the fields of tissue engineering and drug delivery

[Li et al., 2011]. Hence, the existing problem of incompatibility between PLA and chitosan has not been solved till date.

The main aim of this study is to enhance barrier, thermal and mechanical properties of PLA films by incorporating CH-*g*-OLLA copolymer as filler. In this regard, PLA and CH-*g*-OLLA are used to prepare bionanocomposite films by solution evaporation method. PLA is used as matrix material whereas, CH-*g*-OLLA is used as a reinforcement or filler material. Various proportions of PLA and CH-*g*-OLLA are used and different properties such as structural, thermal, surface and mechanical are evaluated to know the best result of the prepared bionanocomposite films. The dispersion of CH-*g*-OLLA has been discussed in surface morphology and structural modification, which is confirmed in FTIR analysis. The detailed oxygen barrier study of bionanocomposite films has been conducted to calculate oxygen permeability, solubility coefficient, and diffusion coefficient. Moreover, the activation energy with pre-exponential factor and regression coefficient have also been calculated using Arrhenius expression as mentioned in Eq. 2.25.

6.2. Results and discussion

6.2.1. Chemical interactions in PLA/CH-*g*-OLLA bionanocomposite films

The absorption bands at 754 cm^{-1} and 1383 cm^{-1} are attributed to the $-CH-$ bending in the molecular structure of PLA and also 754 cm^{-1} referred to the crystalline phase of PLA in PLA and its bionanocomposite films. The absorption band at 870 cm^{-1} is observed in all the film samples except chitosan which denotes $-C-C-$ stretching and also attributed to the amorphous phase of PLA as shown in Figure 6.1(a). It means that PLA and bionanocomposite films are semi-crystalline in nature. The absorption bands at 1082 cm^{-1} and 1182 cm^{-1} have resembled $-C-O-$ stretching in PLA and its bionanocomposite films. The other absorption band is detected at 1452 cm^{-1} in the case of PLA and its bionanocomposite films which confirmed the $-CH_3$ bending or methyl asymmetric

deformation of PLA. A sharp and intense peak at 1751 cm^{-1} is observed for all the samples except chitosan which showed $-C=O$ (carbonyl stretching) valance vibration. All these above-explained peaks are not observed in chitosan films. Furthermore, the strong vibrations of amide I band ($-C=O$ stretching) and amide II band ($-N-H$ bending) are confirmed at 1638 cm^{-1} and 1543 cm^{-1} in chitosan and bionanocomposite films. However, these vibrations showed peaks with low intensity in bionanocomposite films because filler (CH-*g*-OLLA) comprised of less amount of chitosan, i.e. 1, 3 and 5 wt% was mixed with PLA matrix. Hence, it confirmed the presence of chitosan in bionanocomposite films. Very small and new peak at 1539 cm^{-1} is noticed only in the case of bionanocomposite films as incorporated in Figure 6.1(b**)** which is attributed to the presence of amide ester linkage (–OCONH–) **[Li et al., 2008]**. Hence, grafting of OLLA on chitosan is confirmed.

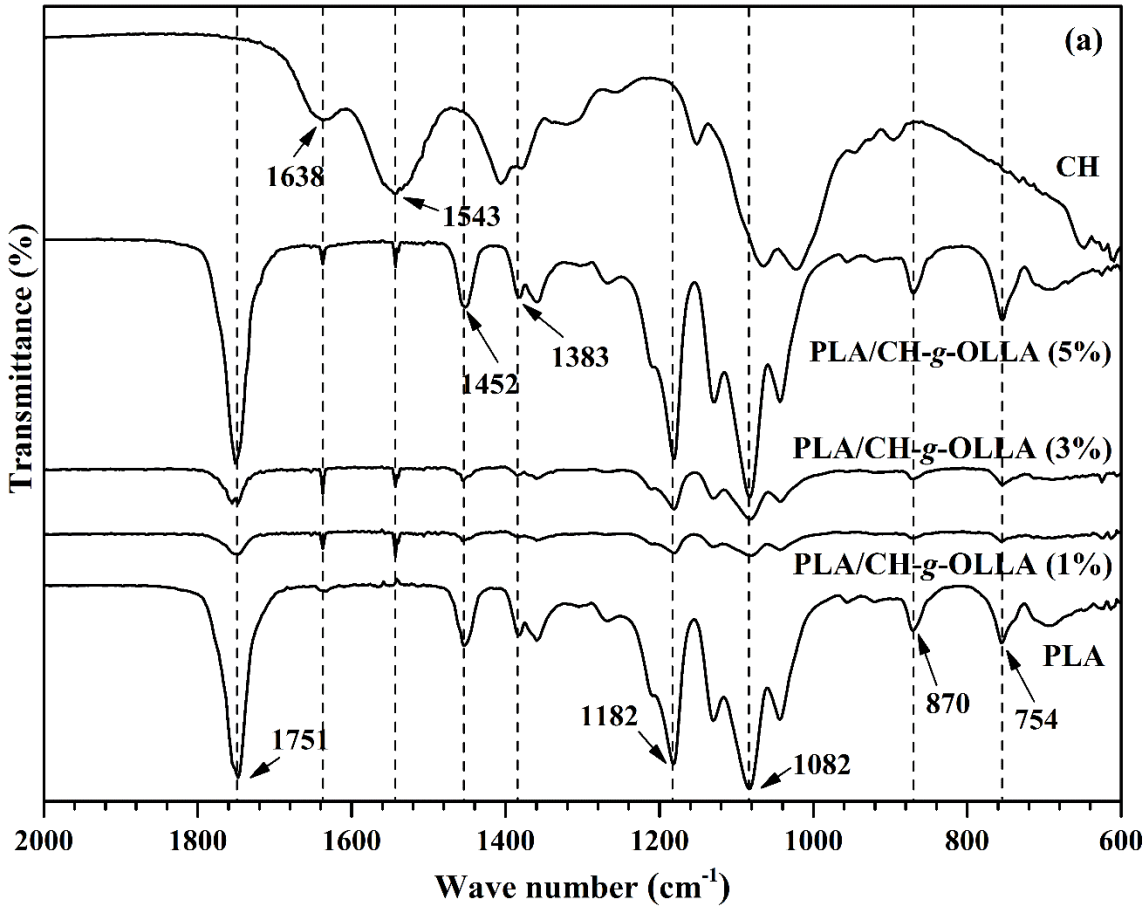

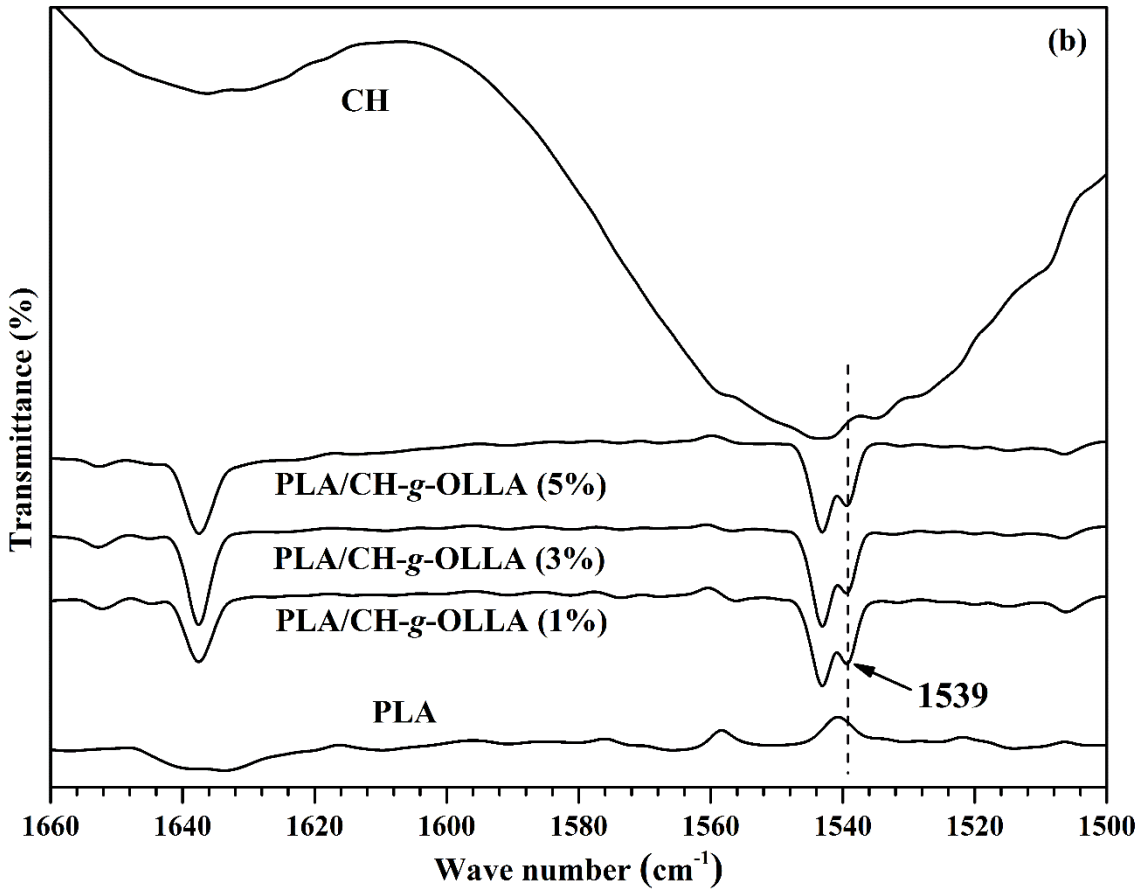

Figure 6.1. FTIR spectra of PLA, CH and its bionanocomposite films (a) in the range of 600-2000 cm^{-1} and (b) in the range of 1500-1660 cm^{-1}.

6.2.2. Crystal structure analysis

XRD patterns are evaluated for PLA, chitosan and its bionanocomposite films as shown in Figure 6.2. The absence of peaks in chitosan films shows its amorphous nature. Whereas, a sharp crystalline peak at 2θ =16.7º is observed from [2, 0, 0/1, 1, 0] reflections for PLA and its nanocomposite films. It shows the crystalline structure (α form) of PLA. The reflection pattern [2, 0, 0] shows the typical orthorhombic crystal structure of PLA. In the XRD analysis, three more reflection patterns are observed as [0, 1, 0], [2, 0, 3] and [0, 1, 5] at 14.9º, 19.1º and 22.3º respectively for PLA and its nanocomposite films. The peaks at 19.1º and 22.3º also show α form of PLA whereas, the peak at 14.9º confirms the β form of PLA. The intensity of all these three peaks decrease with increase in filler loading

weight percentage of filler in PLA matrix. It means that I_{cr} is reduced continuously from ~47% to ~36% with an increase in loading wt% as calculated by Eq. 2.11. No significant shift is observed in the diffraction peaks means that the nano-filler did not affect the ordered structure of matrix material and showed no phase separation. Hence, the XRD results illustrated that all the nanocomposite films are semi-crystalline in nature.

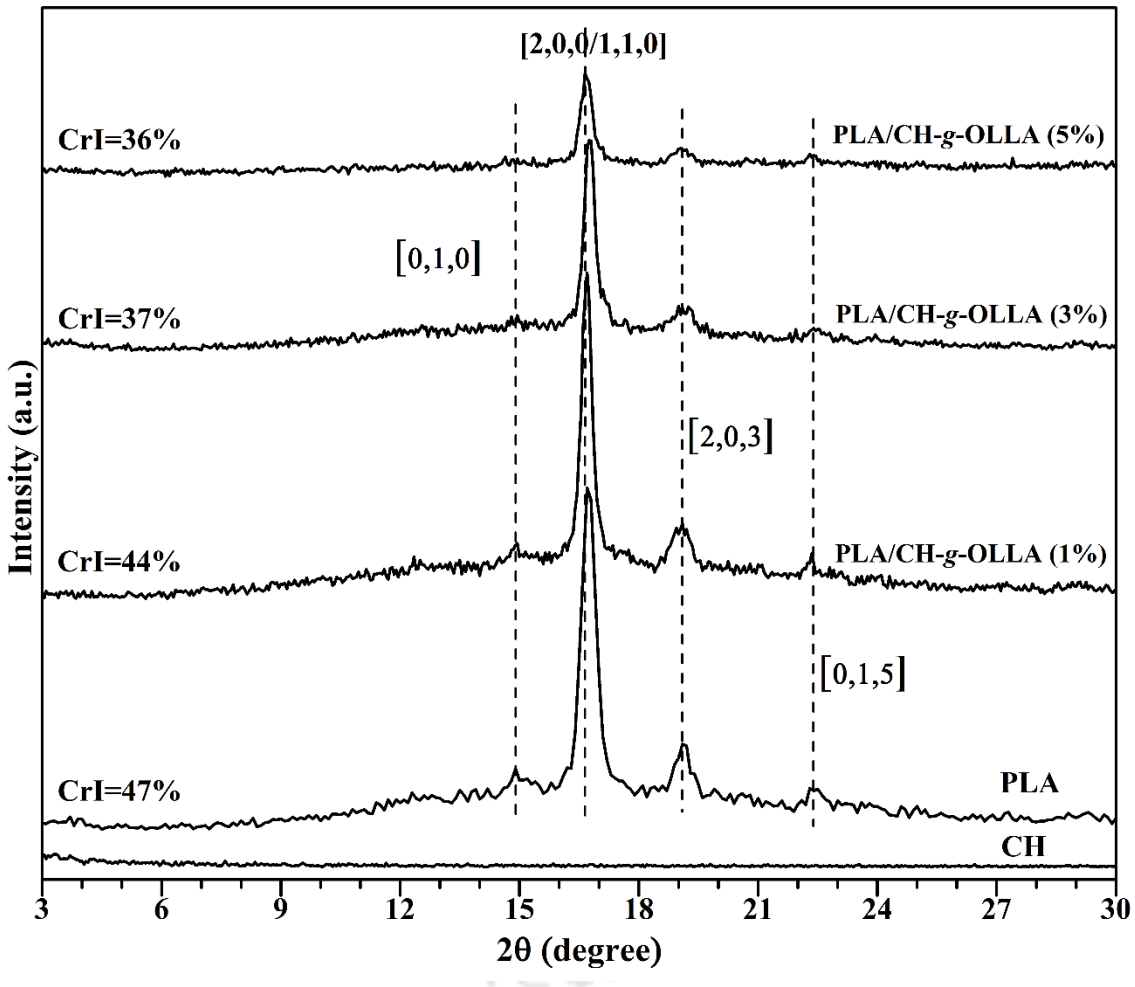

Figure 6.2. XRD patterns of PLA, CH and its bionanocomposite films with their crystallinity index.

6.2.3. Differential scanning calorimetry (DSC)

DSC analysis was conducted to figure out the crystallization and melting behavior of film samples with two heating and cooling cycles as mentioned in section 2.3.10. The purpose of first heating was to remove the physically and chemically bounded water or moisture from film samples. The glass transition temperature (T_g) of PLA films is reduced significantly up to 18 ºC with an increase in filler loading due to plasticizing effect of the low molecular weight of CH-*g*-OLLA as shown in Figure 6.3. However, the T_g value of chitosan film is detected at ~175 ºC which is close to the literature value, i.e. ~196 ºC **[Suyatma et al., 2005]**. It is noteworthy to mention that T_g value of any polymer can be tuned by changing the molecular weight of polymers. The low molecular weight polymeric chains are shorter in length and can move freely as compared to high molecular weight polymeric chains. Variation in T_g also depends on different properties such as the degree of deacetylation of chitosan, water amount, crystallinity and hydroxyl or amine groups in the macro-molecule chain **[Suyatma et al., 2005]**. The heat capacity at constant pressure is reduced up to 0.4 J/g.K with an increase in filler concentration, which means that the less amount of heat is required to raise the temperature in the case of bionanocomposites films. This is only possible when molecular movement of shorter polymer chains in composites increases due to experiencing less obstruction and entanglement from adjacent polymer chains, which results in enhancing in the amorphous region of PLA/CH-*g*-OLLA bionanocomposite films. A small reduction up to ~2 ºC is detected in T_{cc} of PLA films with increment in filler concentration due to the presence of deformed shape and size of some crystals in PLA matrix. No T_{cc} peak is observed for chitosan film in this range. The absence of crystallization peak denotes the absence of crystals or ordered structure of crystals, which confirms the amorphous nature of chitosan film. The melting behavior of PLA film showed a unimodal endothermic peak at 153.2 ºC which exhibits α crystalline form of PLA

[Valapa et al., 2015]. The slight reduction in melting temperature (T_m) up to ~2 ºC is observed in PLA films by an increase in filler concentration due to the heterogeneous distribution of crystals as well as non-uniform crystal thickness. Bimodal endothermic melting peaks, during DSC analysis also corroborate with the presence of two phases (α and β) of PLA, which is also confirmed by XRD analysis of PLA/CH-*g*-OLLA bionanocomposite films as shown in Figure 6.3.

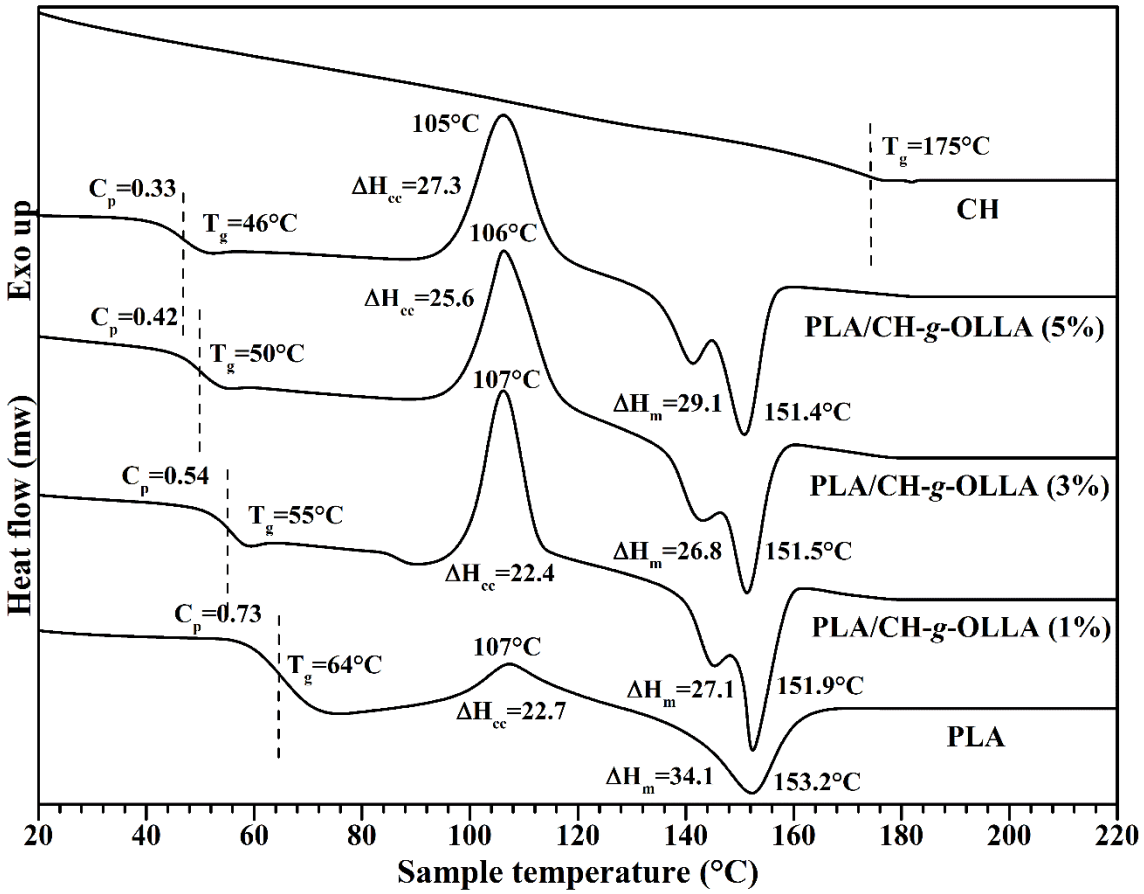

Figure 6.3. DSC thermographs of PLA, CH and PLA/CH-*g*-OLLA bionanocomposite films obtained from second heating.

The shifting of T_m towards lower value is also due to the reduction in the stability of PLA molecules with the addition of filler. The heat of fusion for melting peaks is reduced than that of PLA, which is associated with the strong chemical interaction or hydrogen bonding

between matrix and filler. No melting peak is observed for chitosan film in this range due to its amorphous nature as shown in Figure 6.3. Single T_g in the DSC thermographs confirmed the uniform dispersion of CH-*g*-OLLA in PLA matrix for each combination. Hence, no phase separation has occurred in such nanocomposite films.

6.2.4. Thermogravimetric analysis (TGA)

The TGA and DTGA curves of PLA, chitosan and its nanocomposite films are displayed in Figure 6.4(a) & (b). Figure 6.4(a) revealed that there are two distinguishable peaks in chitosan and PLA/CH-*g*-OLLA bionanocomposites, whereas single peak is detected in PLA films. The thermal degradation of chitosan and PLA/CH-*g*-OLLA bionanocomposites is characterized by two significant weight losses **[Bonilla et al., 2013]**. The first weight loss is observed in the temperature range of 75 to 155 ºC in PLA/CH-*g*-OLLA bionanocomposites films. It is attributed to the moisture vaporization and the removal of unbound and bound water from the film samples. The residue of acetic acid is also removed with bound and unbound moisture from chitosan film in the temperature range of 49 to 168 ºC. The quantity of unbound and bound moisture is higher in chitosan film due to its hydrophilic nature. The second weight loss is totally responsible for material degradation. The second weight loss in PLA and its nanocomposite films is observed in the range of 260 to 420 ºC. Maximum thermal stability is observed in PLA film which reduces with increase in filler loading weight % in PLA/CH-*g*-OLLA films. This phenomenon is attributed to the increment in the acidic sites generated during the degradation of higher loadings of CH-*g*-OLLA in the PLA matrix, which degrades the film samples at lower temperature. Hence, the degradation temperature decreases with increasing filler concentration **[Ambrosio-Martin et al., 2014]**. The increment in short polymeric chains can also deform the crystal structure and that can reduce the percentage crystallinity of the film samples which supports the XRD analysis. The onset degradation temperature (T_{on})

for PLA, 1, 3 and 5 loading wt% films are observed at 315, 291, 261 and 260 ºC respectively. On the other hand, the offset degradation temperature (T_{off}) for PLA, 1, 3 and 5 wt% loading films are observed 410, 386, 386 and 370 ºC respectively. It means that the T_{on} and T_{off} are shifted to the lower temperature values. The percentage of weight loss is observed ~93, ~94, ~93 and ~90% for PLA, 1, 3 and 5 wt% loading films, respectively. The maximum peak temperature (T_p) is found 371, 356, 356 and 327 ºC for PLA, 1, 3 and 5 wt% loading films, respectively from DTGA curve as shown in Figure 6.4(b). The percentage of weight loss at T_p is found ~67, ~64, ~70 and ~59% for PLA, 1, 3 and 5 wt% loading films, respectively. The second weight loss of chitosan film is completely different from PLA and its nanocomposite films.

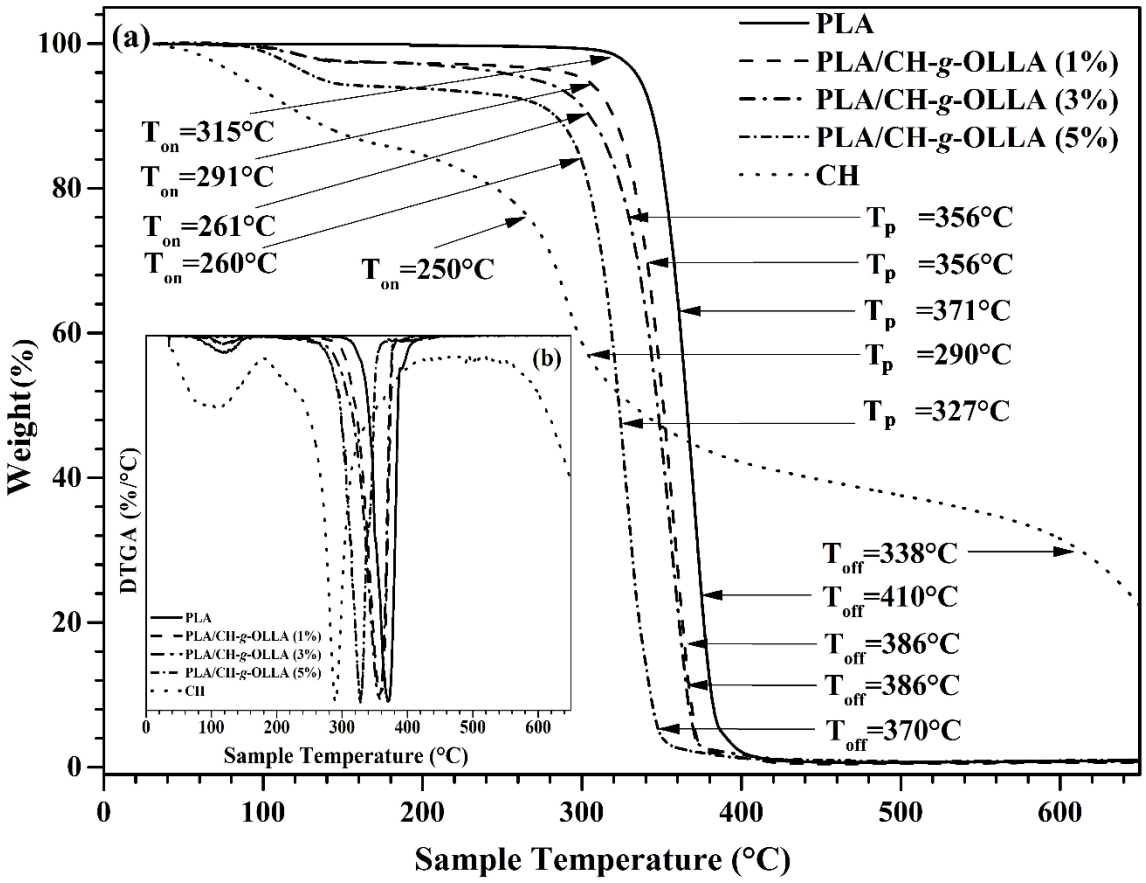

Figure 6.4. (a) TGA and (b) DTGA curves of PLA, chitosan and PLA/CH-*g*-OLLA bionanocomposite films.

The T_{on} and T_{off} during second weight loss in chitosan film are observed at 250 and 338 ºC respectively, which exhibits ~30% weight loss. The T_p is observed at 290 ºC during second weight loss in chitosan film. The percentage of weight loss at T_p is found 35%. The second weight loss in chitosan film can be explained due to the saccharide structure degradation of chitosan molecule. It also includes the dehydration of saccharide rings and the polymerization and decomposition of acetylated and deacetylated units of chitin **[Bonilla et al., 2013]**. The residual weight % is calculated 0.84, 0.68, 0.80, 1.02 and 22.23% for PLA, PLA/CH-*g*-OLLA (1%), PLA/CH-*g*-OLLA (3%), PLA/CH-*g*-OLLA (5%) and chitosan films respectively. The formation of carbonaceous char may be responsible for residual mass.

6.2.5. Scanning electron microscopy (SEM)

The flake kind of structures are detected on the surface of pristine PLA and CH films as shown in Figure 6.5(a) & (b), respectively. The unevenness and roughness due to flakes are detected on both the film surfaces, which is more on CH film surface than that on PLA film. However, the surface of bionanocomposite films becomes smoother after the addition of nanoamphiphilic CH-*g*-OLLA in PLA matrix as displayed in Figure 6.5(c), (d) & (e). The uniform dispersion of CH-*g*-OLLA is observed in the form of three dimensional spherical particles with core-shell morphology in PLA matrix. The density and size of *insitu* generated spheres increases with the addition of filler amount. The size of spheres varies in the range of ~0.6 to 2.1 μm, ~0.4 to 2.6 μm and ~1.8 to 6.6 μm with an increase in filler concentration i.e. 1, 3 and 5% respectively. Actually, the spheres are formed due to the aggregation of polymeric micelles head, which is connected with the low molecular weight, hydrophobic OLLA chain as a tail. Further, the OLLA chain is connected with the long PLA chain. The hydrophobicity of PLA/CH-*g*-OLLA bionanocomposite films should be higher than that of CH films due to the branching of OLLA chains on chitosan backbone.

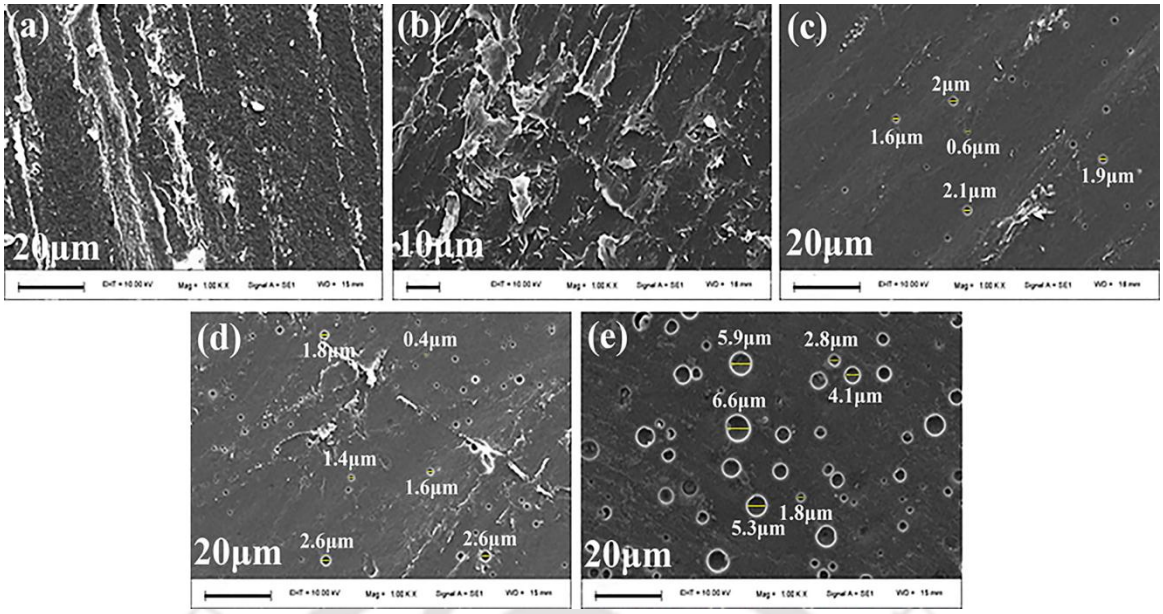

Figure 6.5. SEM images of (a) PLA film, (b) CH film, (c) PLA/CH-*g*-OLLA (1%) film, (d) PLA/CH-*g*-OLLA (3%) film and (e) PLA/CH-*g*-OLLA (5%) bionanocomposite films.

6.2.6. Field emission scanning electron microscopy (FESEM)

The surface topography of PLA/CH-*g*-OLLA (5%) bionanocomposite film showed the uniform dispersion of nano-amphiphilic CH-*g*-OLLA molecules as self-assembled micelles in the form of spheres of various diameter in PLA matrix as shown in Figure 6.6(a). The spheres are an aggregate of polymeric micelles head, which is referred as hydrophilic nano-chitosan. The micelles head are attached with low molecular weight, hydrophobic OLLA chains which are further connected to PLA Matrix. The self-assembled micelles are formed only when the concentration of these molecules in a solution is higher than the critical micelle concentration (CMC). The free energies of chitosan and OLLA molecules can be reduced by agglomerating into aggregated structures. Whereas, the entropy of mixing is the controlling factor below CMC, which restricts the molecules to aggregate. The size and shape of the aggregates depend on the characteristics of existing nano-chitosan and OLLA chains. It is noticed that the number and size of the spherical particles increased

with an increase in filler loading due to agglomeration. It is observed that some of the nano-amphiphilic CH-*g*-OLLA molecules are liberated from the surface of the three-dimensional, solid CH-*g*-OLLA spherical aggregates as shown in Figure 6.6(b). This kind of erosion happens due to the unbalancing between surface energy and repulsive energy acting on the micelle head-groups and OLLA tails. The head-groups are crowded into a smaller surface area as the repulsive energy between head-groups became increase. Hence, some of the nanoparticles of size ~50-90 nm may be eroded from the aggregates due to the application of access repulsive energy.

6.2.7. Transmission electron microscopy (TEM)

TEM analysis also revealed that nano-amphiphilic CH-*g*-OLLA molecules are three-dimensional having the uniform dispersion of chitosan nanospheres in PLA matrix as shown in Figure 6.6(c). The chitosan nanospheres are of various sizes ~10-119 nm. The presence of nanoparticles are responsible to create a tortuous path for oxygen to diffuse across the film and also enhances the oxygen solubility. Due to this, the films must show highly improved oxygen barrier properties than the control film. Such kinds of arrangement of three-dimensional array is really helpful and remarkable for improvement in food quality and shelf life of foodstuff inside the packaging. The schematic representation of the chemical interaction between PLA matrix and nano-amphiphilic CH-*g*-OLLA molecules (filler) is shown in Figure 6.6(d). The carbonyl groups of OLLA chains are chemically connected with amide groups of chitosan while the other end of OLLA chains, having hydroxyl groups, are reacted with the carbonyl groups of PLA matrix and formed a physical interaction between PLA and OLLA chains through hydrogen bonding.

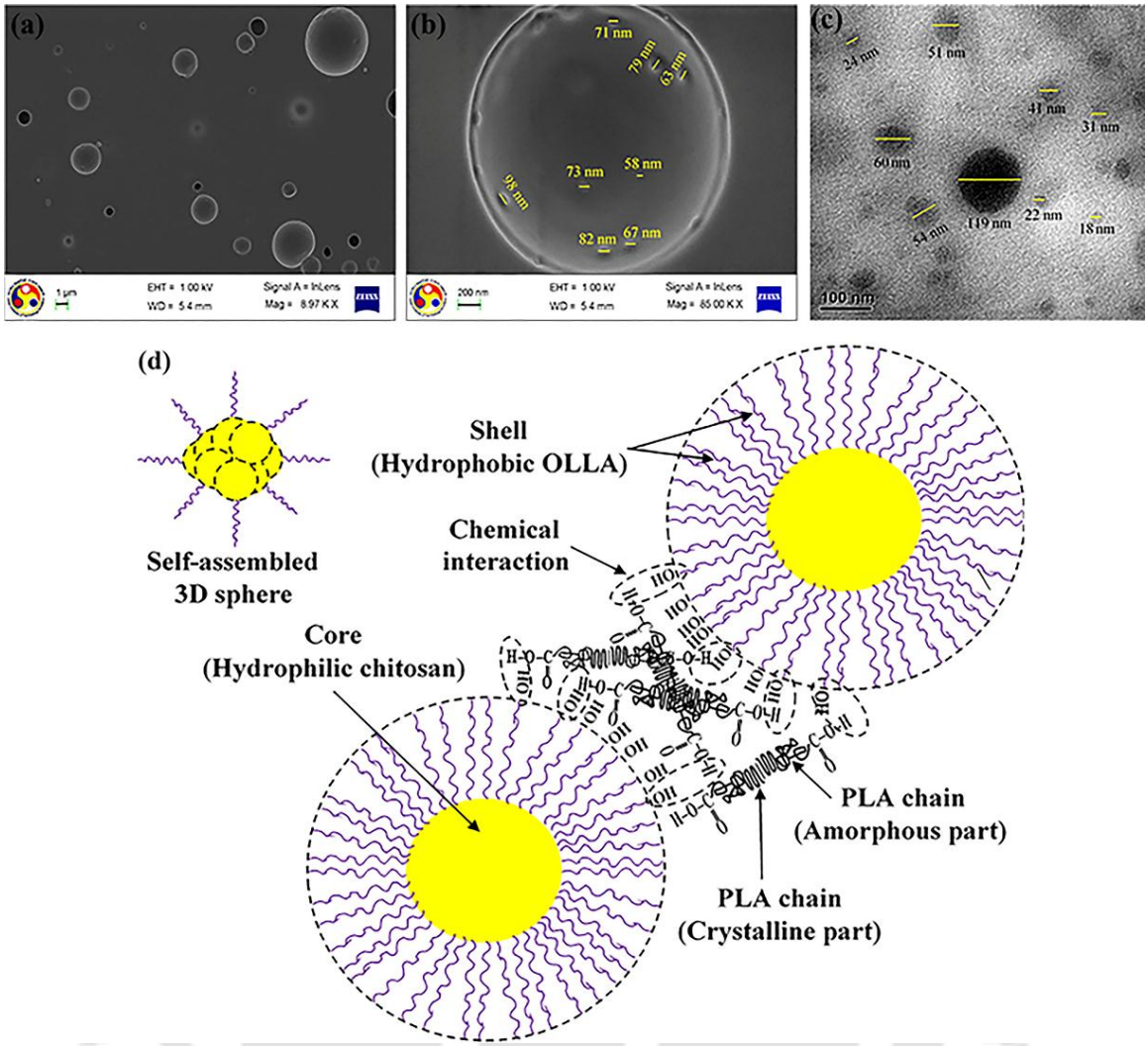

Figure 6.6. FESEM images of PLA/CH-*g*-OLLA (5%) bionanocomposite film; (a) at 8.97 KX, (b) at higher magnification ~85 KX, (c) TEM topography of PLA/CH-*g*-OLLA (5%) bionanocomposite film and (d) schematic representation of interaction between matrix and filler.

6.2.8. Mechanical properties

The mechanical property analysis was carried out for PLA, chitosan and PLA/CH-*g*-OLLA films in which UTS (MPa), %ε and Young's modulus (MPa) are calculated as presented in Figure 6.7(a), (b) & (c), respectively. The UTS of all the film samples is shown in Figure 6.7(a). It reduced from 40.85±12 MPa to 33.33±1 MPa with increase in filler loading weight percentage. The reduction (approximately 18.4%) in tensile strength for

PLA/CH-*g*-OLLA (5%) film is noticed as compared with PLA film. The associated reason is the presence of low molecular weight nano-filler (CH-*g*-OLLA) in PLA matrix. The number of shorter polymer chains of filler increases with increase in loading wt%. The shorter polymer chains tend to align faster than the longer polymer chains during the tensile test. In this way, the shorter polymer chains bring lower tensile strength and vice versa. The % E of PLA/CH-*g*-OLLA films is improved drastically from 8.88±1% to 34.3±11% which made them highly stretchable than PLA film as shown in Figure 6.7(b). It indicates that the low molecular weight nano-filler imparts plasticizing effect to the film samples. This plasticizing effect increases with increase in loading wt%. The particle volume fraction and their interactions with PLA matrix also affect the film extensibility **[Bonilla et al., 2013]**. The %E of chitosan film (21.83±12%) is higher than that of PLA film (8.88±1%). This increment in %E is highly required for food packaging application. The degree of plasticization must be higher in the case of PLA/CH-*g*-OLLA (5%) bionanocomposite film because the number of shorter polymer chains of filler will be more in this case, which increases with increase in loading wt%. It increases the randomness in the arrangement of polymer chains, which also improves the softening behaviour of bionanocomposite films. As a result, the plasticization effect increases with increase in filler loading. Young's modulus is decreased from 542±133 MPa to 298±31 MPa continuously with increase in loading up to 5 wt% as shown in Figure 6.7(c). It may contribute to the reduction in stiffness and proper distribution of filler in PLA matrix **[Chiang and Wu, 2012]**. Young's modulus of chitosan film is calculated as 324±145 MPa. It means that the stiffness of PLA films is superior to chitosan films.

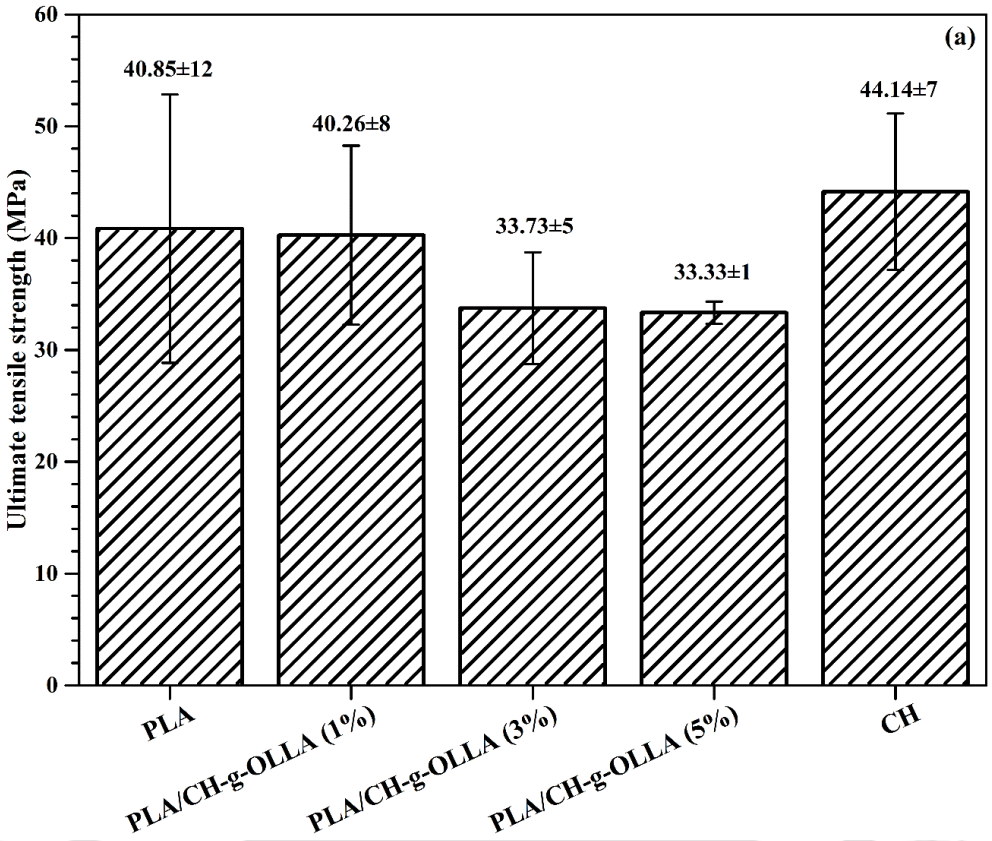

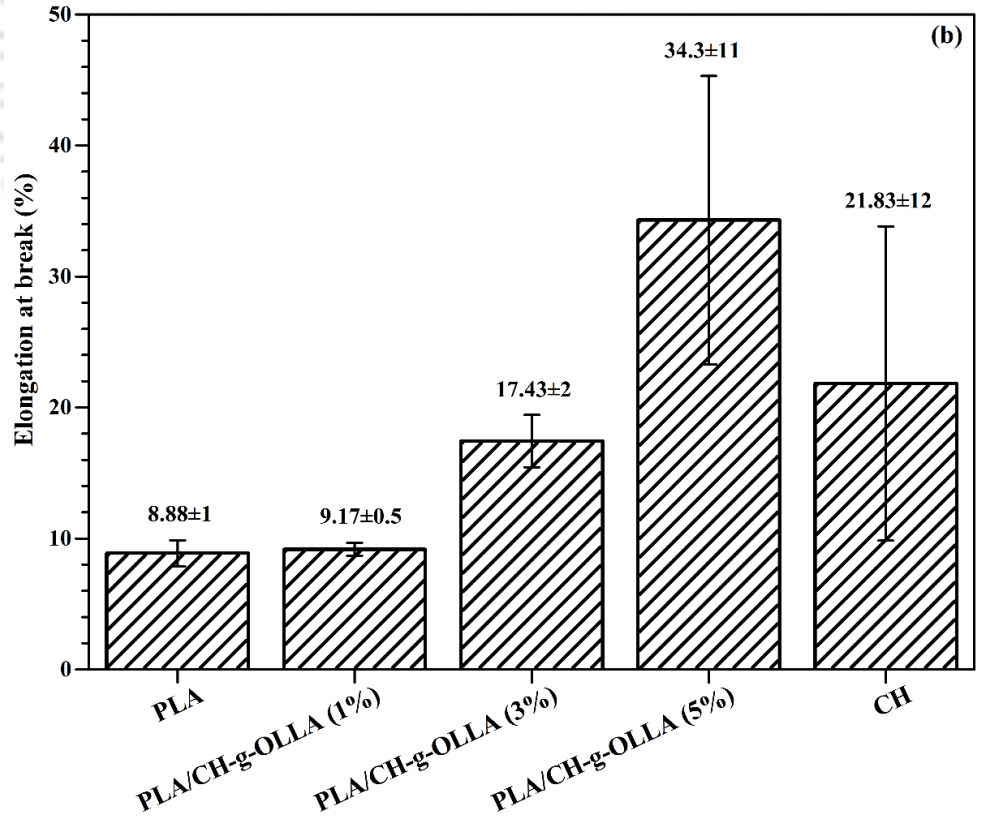

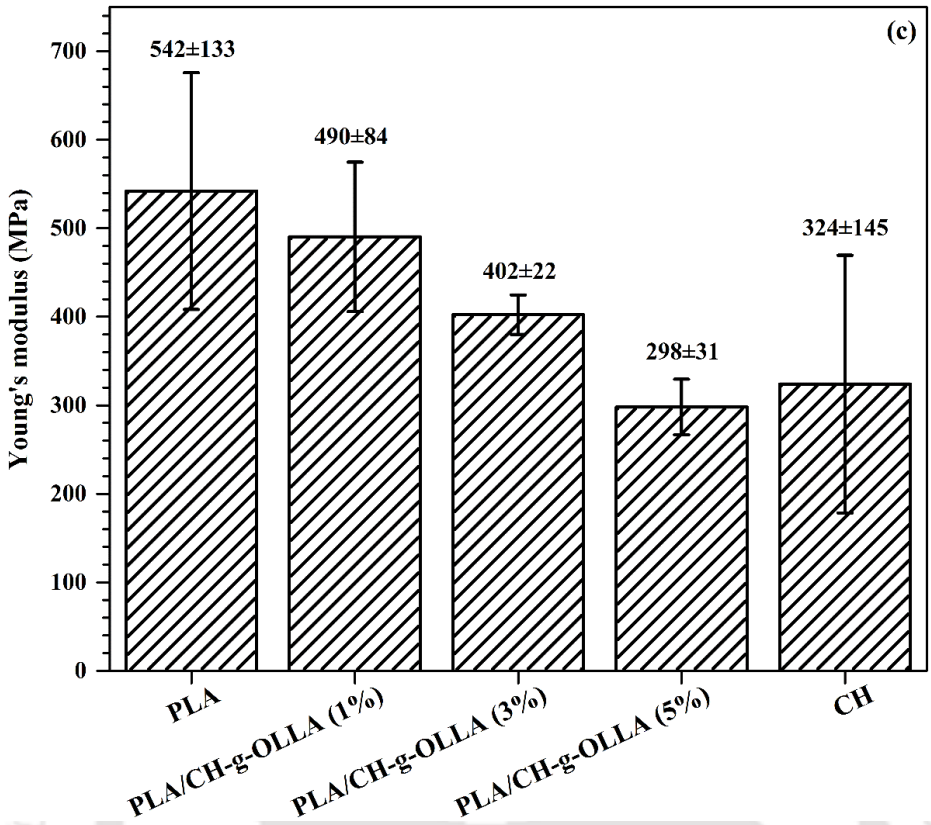

Figure 6.7. Variation in (a) Ultimate tensile strength, (b) elongation at break and (c) Young's modulus in PLA films with respect to variation in filler loading (wt%).

6.2.9. Water vapor transmission rate (WVTR)

The WVTR of PLA, PLA/CH-*g*-OLLA (1%), PLA/CH-*g*-OLLA (3%) and PLA/CH-*g*-OLLA (5%) films was studied at 37.8±0.5 ºC and 100% permeant RH as shown in Figure 6.8. It shows that WVTR×e values are increased up to 4.5, 18.6 and 62.1% with increasing filler wt% up to 1, 3 and 5%, respectively. This is due to the presence of filler material, which is low molecular weight CH-*g*-OLLA. It contains more hydroxyl and carboxyl groups than that of PLA film. These functional groups are hydrophilic in nature and absorb moisture from the atmosphere. Hence, these groups increase with an increase in filler concentration which significantly increases WVTR×e value for PLA/CH-*g*-OLLA films. The WVTR×e value for chitosan film is not observed because of its hydrophilic

nature. It is noteworthy to mention that the water vapor permeability of PLA films can be improved ~29% via layer-by-layer deposition of chitosan and cellulose nanocrystals **[Halasz et al., 2015]**.

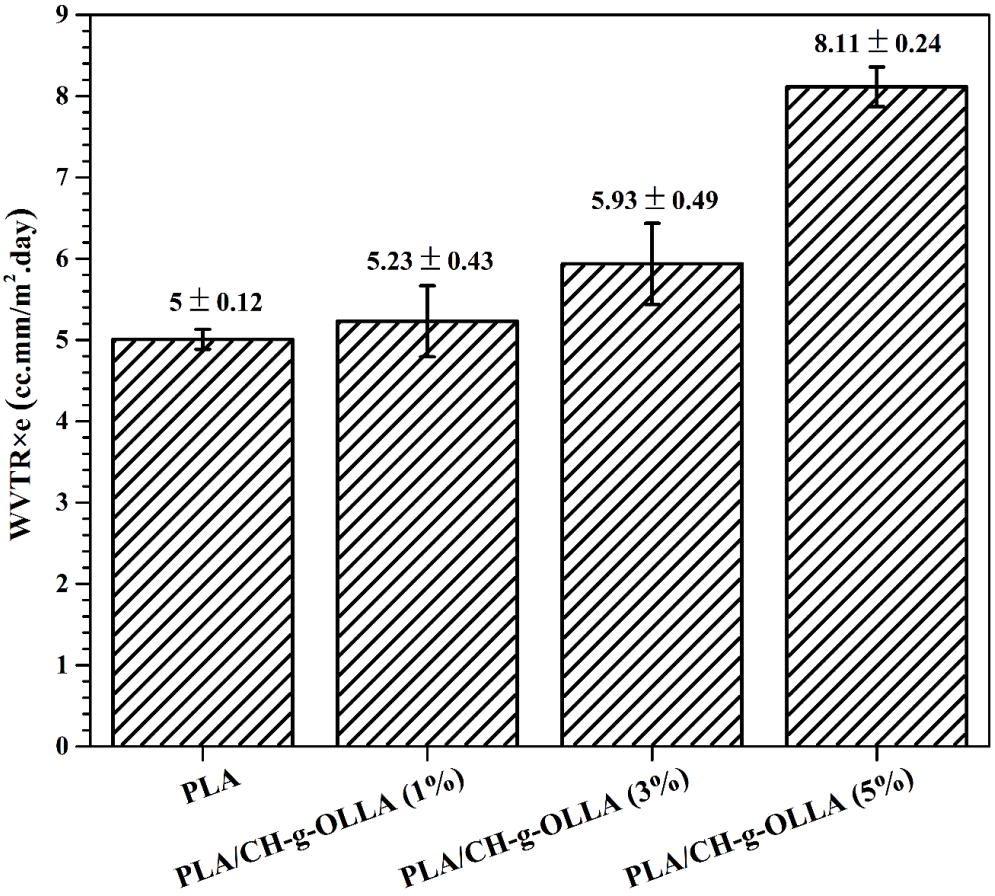

Figure 6.8. Variation in WVTR ×e values of PLA films with respect to variation in filler loading (wt%).

6.2.10. Oxygen transmission rate (OTR)

The permeability coefficient, oxygen permeability and other parameters such as diffusivity, solubility of PLA and PLA/CH-*g*-OLLA bionanocomposite films were studied to determine the effect of CH-*g*-OLLA on the gas barrier properties as shown in Table 6.1. The incorporated results brought the insight information about the diffusion mechanism of oxygen molecules through the bionanocomposite films. The solution cast

PLA/CH-*g*-OLLA bionanocomposite films showed a significant reduction in oxygen permeability by adding CH-*g*-OLLA up to 5 wt% into PLA matrix. The diffusion coefficient of PLA film is reduced with the addition of 1 wt% of filler but again increases with increase in filler loading up to 5 wt%. Whereas, the solubility coefficient reduces continuously with increasing filler percentage which clearly indicates the increase in resistance to permeation of oxygen molecules across the core and shell network formed in bionanocomposite films. A significant reduction of 39.2, 76.9 and 81.7% in oxygen permeability at 25 ºC was recorded on the addition of 1, 3 and 5 wt% CH-*g*-OLLA, respectively. The formation of unique core and shell network in the polymer matrix may be culpable for the decrement in oxygen permeability across PLA/CH-*g*-OLLA bionanocomposite films. At 25 ºC, the calculated values of diffusion and solubility coefficients are also reduced up to 26 and 83% with the addition of CH-*g*-OLLA (1%) and CH-*g*-OLLA (5%) respectively. After the addition of 3 and 5 wt% filler, the increment is observed in diffusivity as shown in Figure 6.9(d). However, the increment in diffusivity (standard deviation varies in the range of 0.05 to 0.07×10^{-12} with the variation in filler concentration) is not significant as compared to the reduction in solubility (standard deviation varies in the range of 0.04 to 0.08×10^{-5} with the variation in filler concentration). Hence, the reduction in solubility coefficient is more responsible for the decrease in gas barrier property because the occupancy of the number of active sites is increased due to nano-filler present in the polymer matrix. Hence, less availability of the number of active sites is found in PLA matrix for physical interaction with oxygen molecules. The lack of active sites in bionanocomposite films is due to the formation of amide ester linkage between PLA and chitosan which can also increase the resistance to the diffusion of oxygen molecules. The surface morphology showed the formation of spherical particles in the PLA

matrix due to the difference in polarity between chitosan backbone and PLA. The proper dispersion of solid spherical particles can further reduce the solubility coefficient.

The OTR values, obtained from the instrument, are increased with increase in temperature up to 45 ºC due to the increment in diffusion rate of oxygen in polymeric chains at higher temperatures as shown in Figure 6.9(a). The rate of change in OTR values with respect to temperature also increased with increase in operating temperature as shown in Figure 6.9(b). It clearly explained about the change in slope became higher at higher temperatures for PLA and bionanocomposite films. The chemical interaction/hydrogen bonding between PLA and CH-*g*-OLLA is responsible for the restriction in the motion of polymeric chains which also resulted in OTR values reduction with increase in filler loading. Hence, CH-*g*-OLLA is a suitable nano-filler which can create a core and shell network in the PLA matrix and increases the resistance to diffuse the oxygen across bionanocomposite films. As a result, it reduces the gas permeability over the studied range of temperatures.

Table 6.1: Oxygen barrier properties of PLA and PLA/CH-*g*-OLLA films at 25±0.1 °C and 0% RH.

Sample	Film Thickness (µm)	Permeability (cc.mm/m^2.day.kPa)	% Reduction	Diffusivity (m^2/sec)× 10^{-12}	Solubility (g/g.Pa)× 10^{-5}
PLA	118±10	9.98	-	3.25	3.56
PLA/CH-*g*-OLLA (1%)	114±15	6.07	39.2	2.42	2.91
PLA/CH-*g*-OLLA (3%)	123±10	2.31	76.9	3.39	0.79
PLA/CH-*g*-OLLA (5%)	114±8	1.83	81.7	3.47	0.61

Arrhenius expression (Eq. 2.25) was also utilized for the better understanding of the temperature effect on gas barrier properties of PLA/CH-*g*-OLLA bionanocomposite films and a plot between oxygen permeability and the inverse of temperature is made for various

filler loading as shown in Figure 6.9(c). It is noticed that the slope of the graph decreased with increasing filler concentration which confirmed the reduction in diffusivity due to the tortuous path created by nano-filler in the form of solid spherical particles. The calculated activation energies required for permeation are 33.87, 50.55, 93.04 and 87.21 kJ/mol for PLA, PLA/CH-*g*-OLLA (1%), PLA/CH-*g*-OLLA (3%) and PLA/CH-*g*-OLLA (5%) respectively. To overcome the barrier network, the amount of energy required by oxygen molecules is increased with increase in filler loading up to 3 wt%. It gives a proof of formation of stable networks that generate the highly tortuous path for gaseous molecules diffusion which results in the improvement in gas barrier properties **[Tripathi and Katiyar, 2016]**. Both, diffusivity and solubility are temperature dependent properties which increased with increase in temperature from 15 to 45 ºC individually for all the samples due to increment in the oxygen vacancy concentration as shown in Figure 6.9(d) & (e). The variation in oxygen solubility with temperature changes the oxygen vacancy concentration. The solubility is reduced continuously with increase in filler concentration for the studied range of temperature due to the decrement in the active sites. Whereas diffusivity is showing the same trend only by adding 1 wt% filler in PLA matrix, but further addition of filler is responsible for increment in diffusivity as shown in Figure 6.9(d). Finally, the conclusion of barrier property improvement is based on two factors in which the first factor is based on the constriction in movement of molecules in polymeric chains due to the chemical interaction between PLA and chitosan. The second factor is based on the formation of the tortuous path by CH-*g*-OLLA filler in PLA matrix which leads to a sufficient increment in activation energies and hence the reduction in oxygen permeability. The other most important and critical finding from barrier property analysis is that the OTR values of PLA/CH-*g*-OLLA (3%) and PLA/CH-*g*-OLLA (5%) bionanocomposite films are recorded as 9.45 and 8.79 cc/m^2.day respectively at 15 ºC. It

means that negligible oxygen molecules can pass through the bionanocomposite films at 15 ºC due to the most stable barrier network formed by CH-*g*-OLLA.

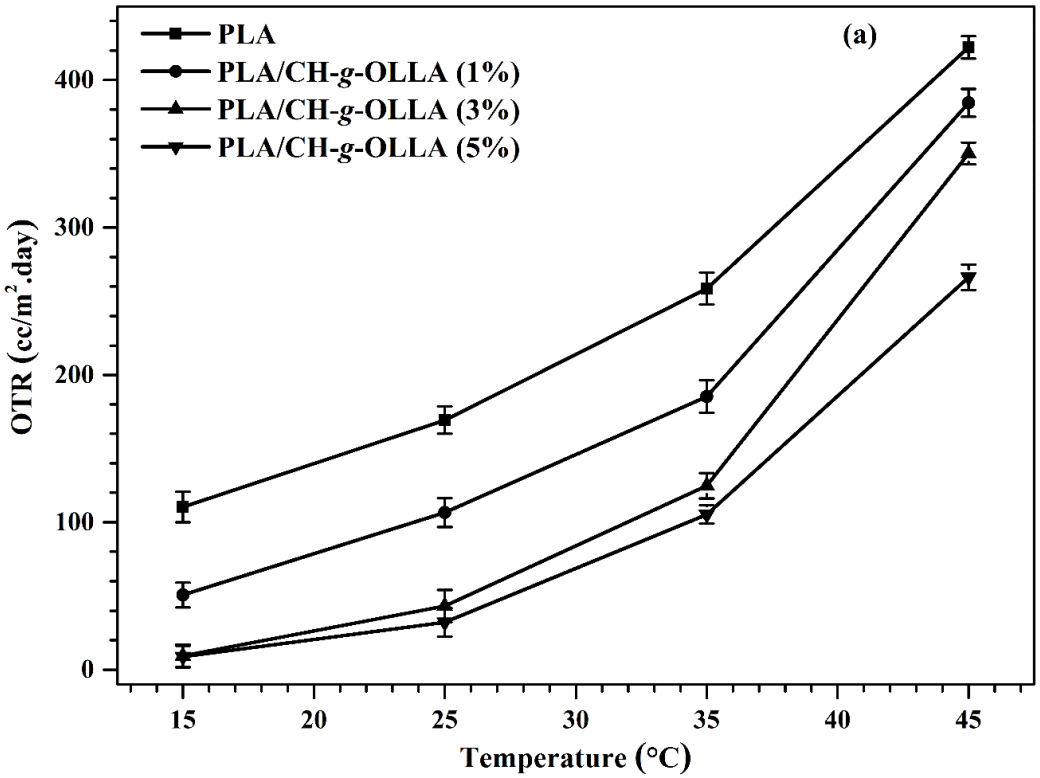

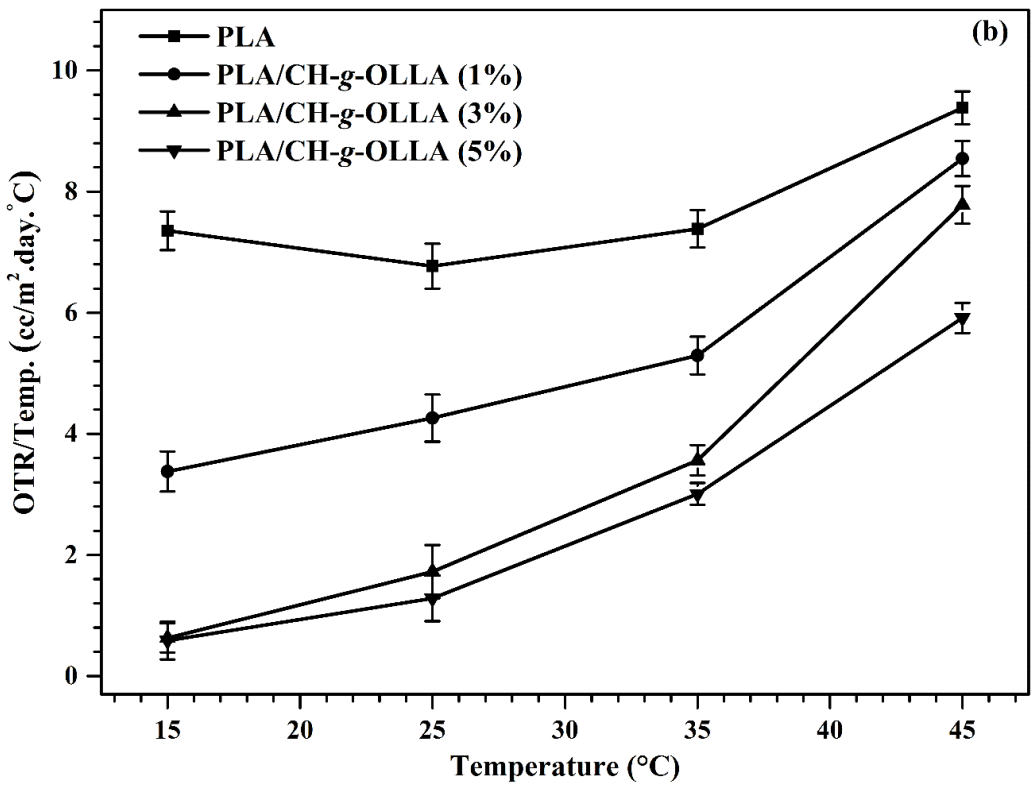

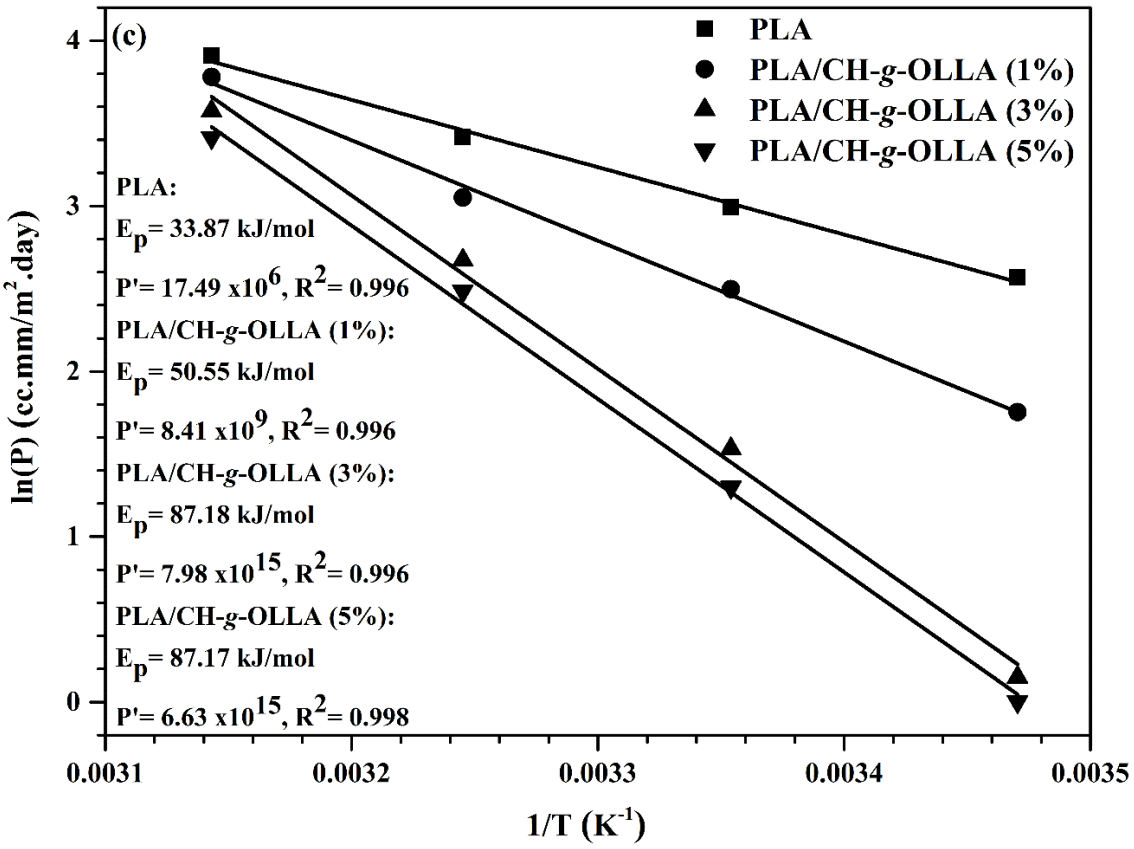

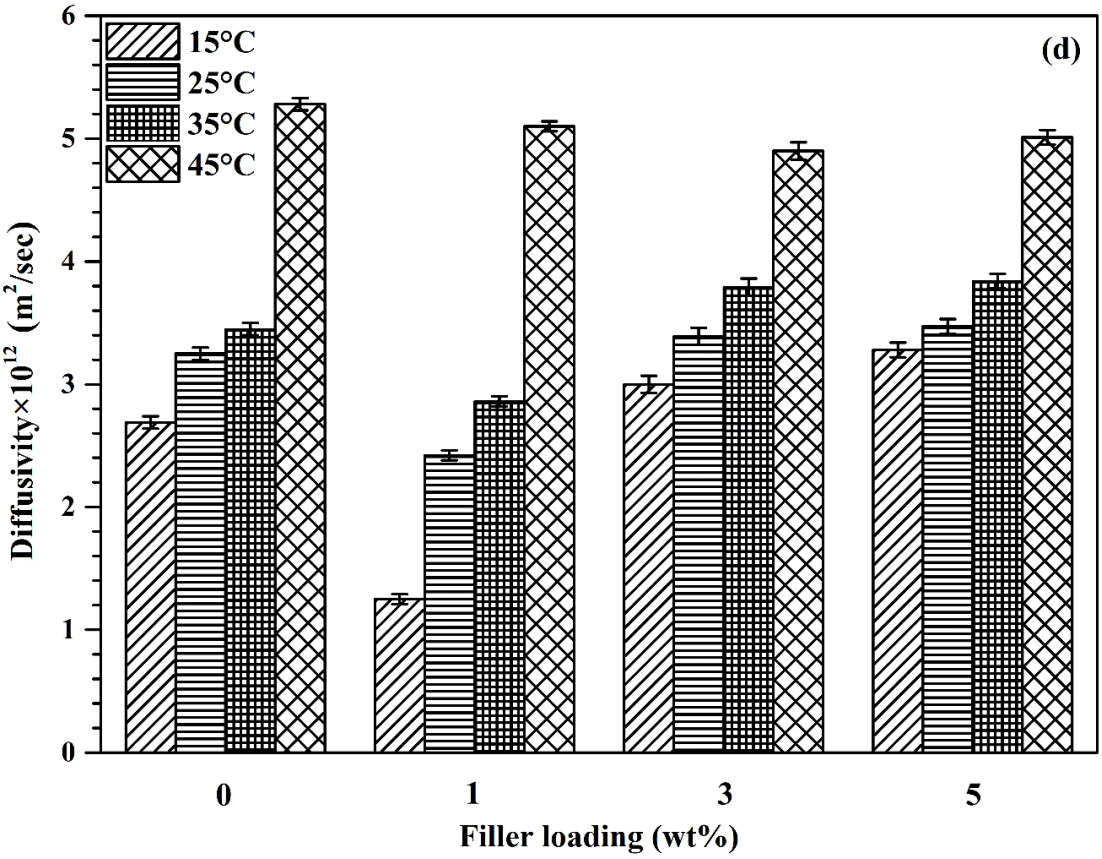

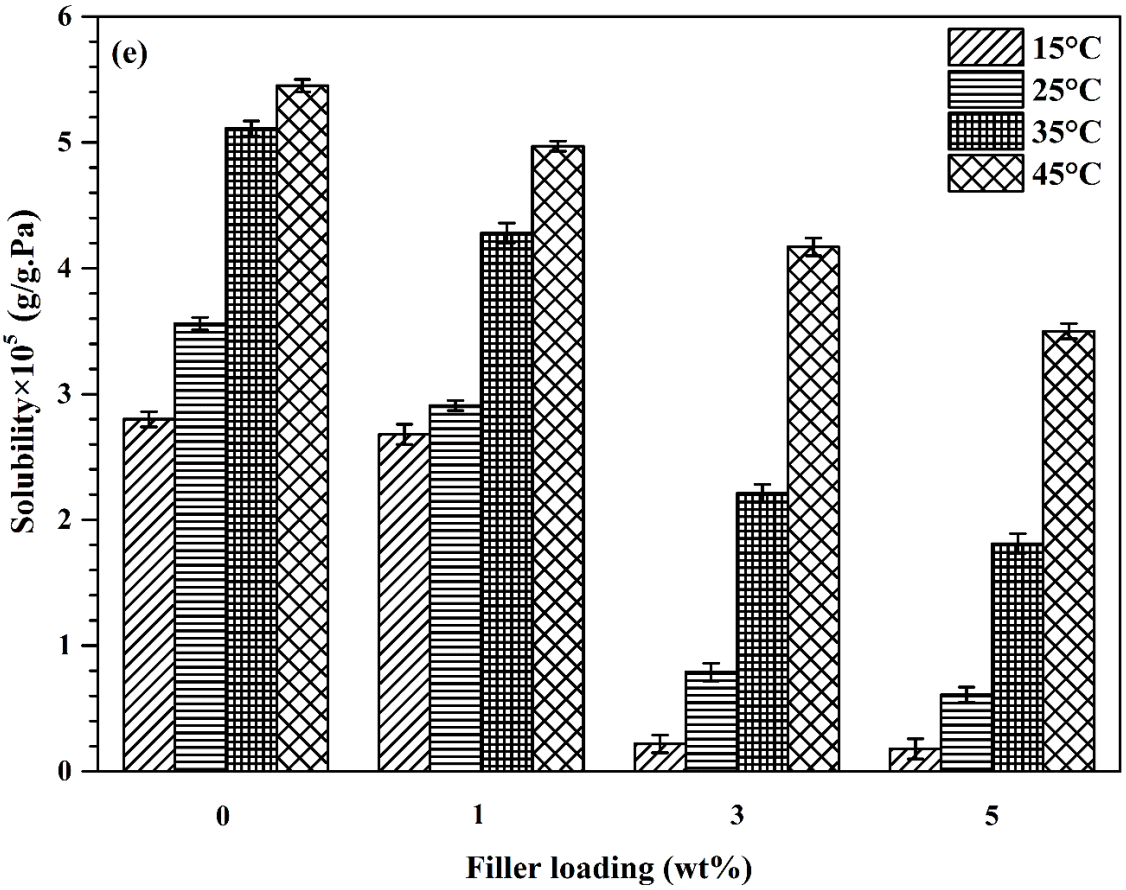

Figure 6.9. Gas barrier analysis of PLA and PLA/CH-*g*-OLLA bionanocomposite films; (a) the effect of temperature on OTR values, (b) variation in OTR/Temp with respect to temperature, (c) ln (p) vs 1/T to check the temperature dependence on permeation rate, (d) change in diffusivity at various temperatures with respect to filler loading (wt%) and (e) change in solubility at various temperatures with respect to filler loading (wt%).

6.2.11. Dynamic mechanical analysis (DMA)

Three essential properties i.e. dynamic storage modulus, loss modulus and damping factor of solution casted polymer nanocomposites at solid state are significant in mechanical testing, which are observed as a function of temperature. The storage modulus is strictly associated with the load bearing capacity of polymer nanocomposites. The E′ value of PLA film is observed as ~3042 MPa at 25 ^{o}C which is reduced upto ~42% with an increase in

filler loading of 5 wt% as shown in Figure 6.10(a). This significant reduction is due to the decrement in stiffness of the matrix imparted by CH-*g*-OLLA copolymer which inhibits the transfer of stress between matrix and filler by the reason of its spherical morphology. The storage modulus of PLA and PLA/CH-*g*-OLLA bionanocomposite films is reduced with an increase in temperature, which is significantly observed in the temperature range of 50-70 ^{o}C as displayed in the circle of Figure 6.10(a). The softening temperature of bionanocomposite films is also decreased as compare to that of PLA. The variation in loss modulus of PLA matrix by the incorporation of CH-*g*-OLLA is presented in Figure 6.10(b). The heat dissipation value of PLA is maximum at the maximum value i.e. ~243 MPa of loss modulus at particular temperature i.e. ~40 ^{o}C. The E″ values PLA/CH-*g*-OLLA (1%) and PLA/CH-*g*-OLLA (3%) bionanocomposite films are higher at reduced temperatures than that of PLA. It is possible only when the chain mobility of matrix is increased due to the incorporation of filler. The mechanical loss or damping factor is calculated by the ratio of loss modulus to storage modulus and the maximum value of tan δ represents the glass transition temperature of polymeric system. Hence, the highest tan δ value for PLA is detected at ~56 ^{o}C which is further reduced upto 42.7 ^{o}C by the addition of 5 wt% of filler as shown in Figure 6.10(c). The significant reduction of ~13.3 ^{o}C is due to the plasticization effect of CH-*g*-OLLA copolymer. It is noteworthy to mention that such an elongation property in polymer composites is highly required for food packaging applications. The tan δ peak also represents the impact resistance of polymeric system. Thus, the impact resistance of PLA/CH-*g*-OLLA bionanocomposite films is enhanced as compare to that of PLA.

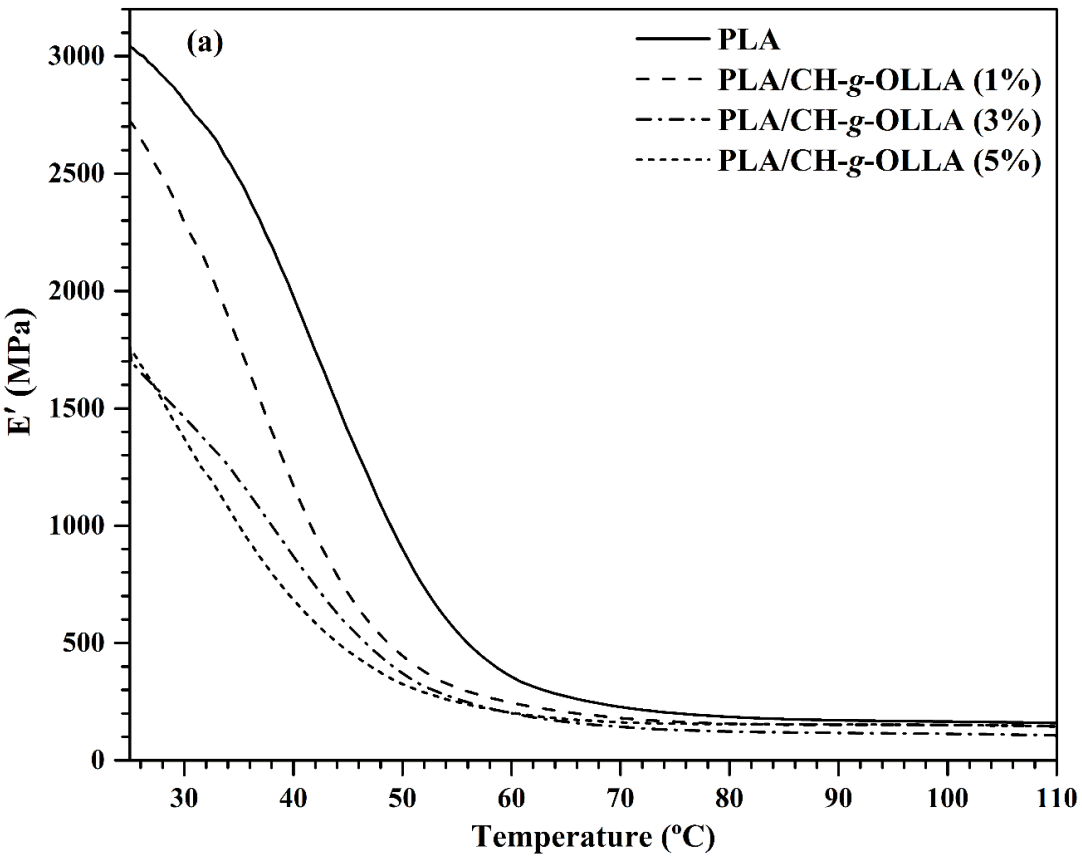

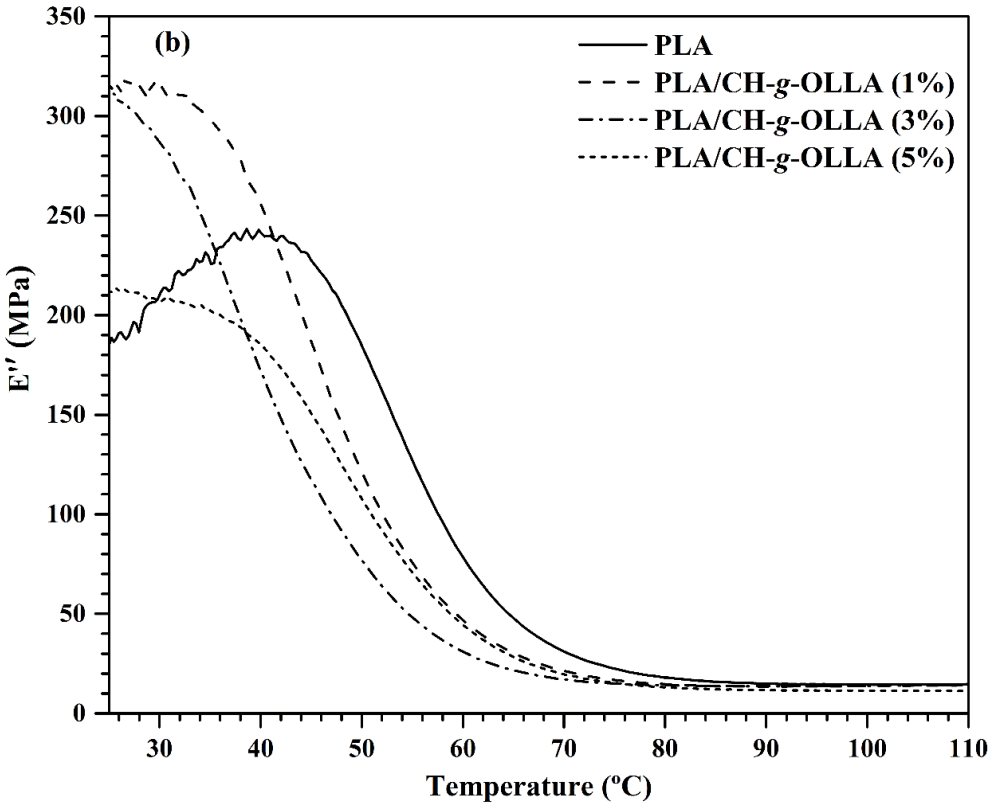

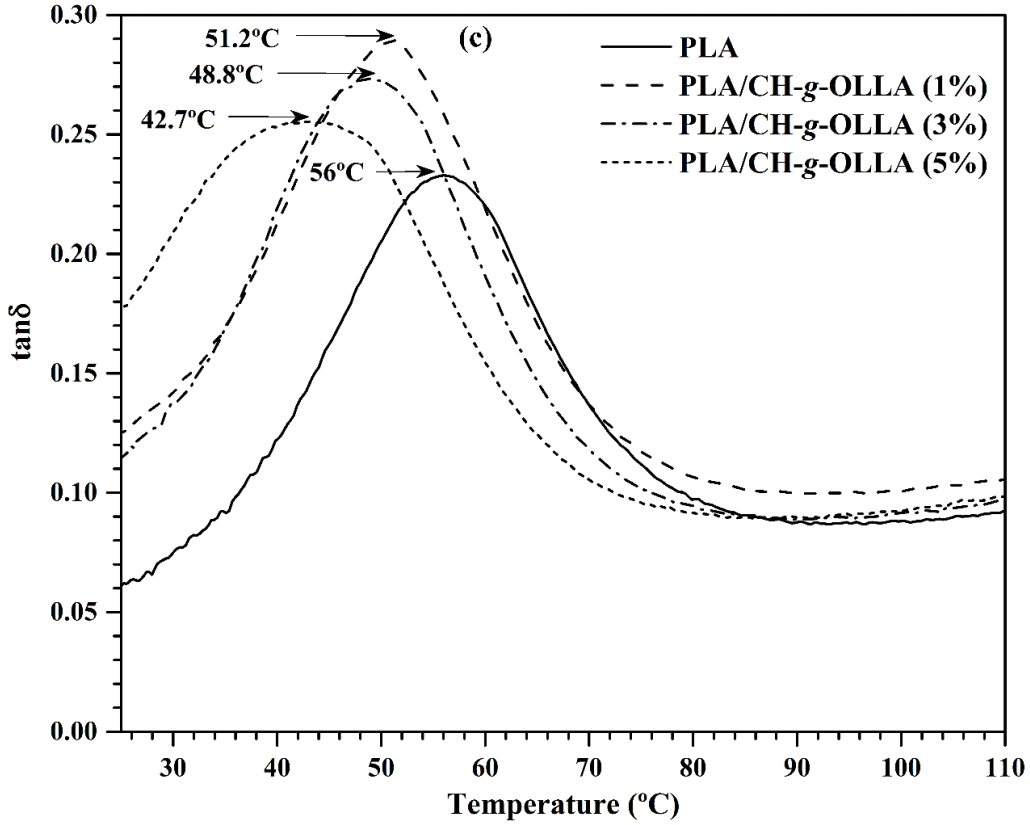

Figure 6.10. Variation in (a) storage modulus, (b) loss modulus and (c) tan δ as a function of temperature for PLA and PLA/CH-*g*-OLLA bionanocomposite films.

6.2.12. Transparency

Transparency and barrier to UV light in polymers are the, two foremost properties required in food packaging application, which helps to restrict the degradation of packed food products. PLA is extensively utilized as a packaging material due to its biodegradable nature. However, it shows poor UV barrier properties which is essential to improve for its suitability in various applications. The UV-Vis analysis has been demonstrated for PLA and its bionanocomposite films in Figure 6.11. The % transmission value of PLA film is found highest i.e. 56 and 41% in visible region and UV region respectively. At 700 nm, the transparency of PLA/CH-*g*-OLLA (1%) bionanocomposite film has been found very close to PLA, which is further reduced by increase in filler loading. Subsequently, at 400 nm, the

percent transmittance of PLA film is drastically reduced upto 27.6, 71.7 and 80.3% with the addition of 1, 3 and 5 wt% of filler as mentioned in Figure 6.11. In visible region, this significant reduction in transparency is due to the brown colour in bionanocomposite films which is imparted by CH-*g*-OLLA copolymer. The uniform dispersion of solid spherical nano-filler in PLA matrix during processing is also responsible for the reduction in transparency. In UV light region, similar kind of behaviour of PLA and its bionanocomposite films is observed as compare to that in visible region. It is meaningful to mention that at 200 nm, the percent transmittance of PLA film has been decreased upto 99% by the addition of 5 wt% of filler. This behaviour is due to the synergistic effect between PLA and CH-*g*-OLLA copolymer. In this polymeric system, PLA acts as mirror which transmits some part of UV light and rest of the part is reflected at the same time. However, the uniform dispersion of copolymer in PLA matrix behaves as blocking agent for UV light irradiation. Hence, PLA/CH-*g*-OLLA bionanocomposite films are one of the best option for UV light sensible food in packaging.

6.3. Summary

The synthesized CH-*g*-OLLA (30%) copolymer by condensation polymerization, was used as a nano-filler for the fabrication of homogeneous PLA/CH-*g*-OLLA bionanocomposite films by solution casting technique. The films were analyzed by different analytical techniques such as structural, thermal, surface, mechanical and barrier. A new acute peak at 1539 cm^{-1} was observed only in the case of CH-*g*-OLLA (30%) copolymer and PLA/CH-*g*-OLLA bionanocomposite films which confirmed the amide ester linkage ($-OCONH-$). The I_{cr} and T_g were reduced continuously from 47 to 36% and 64 to 46 ºC respectively with an increase in filler loading. A small shoulder was attached with melting peak in all PLA/CH-*g*-OLLA bionanocomposite films, which was responsible for the reduction in the crystal stability or irregular crystals. Even the thermal stability of

PLA/CH-*g*-OLLA films was reduced with an increase in filler percentage though it was found higher than the processing temperature of PLA. The filler acts as a nucleating agent in the spherulitic growth of PLA crystals. TEM analysis showed that amphiphilic CH-*g*-OLLA nanoparticles were three dimensional, spherical in shape and uniformly dispersed in the form of polymeric micelles in PLA matrix.

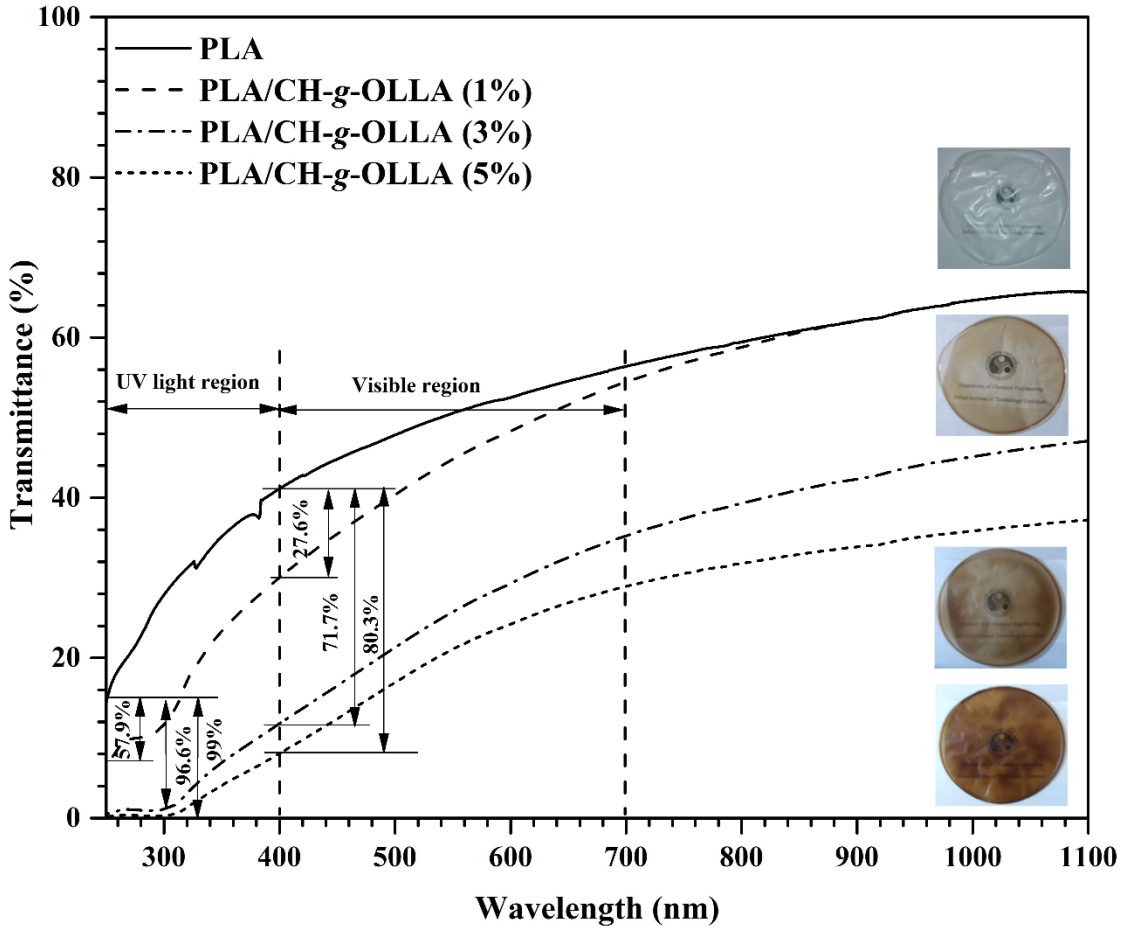

Figure 6.11. Effect of CH-*g*-OLLA copolymer on transparency of PLA films.

Such morphology supports highly tortuous path for oxygen to move across the film. UTS of PLA/CH-*g*-OLLA bionanocomposite films was found comparable to that of PLA whereas, Young's modulus was reduced with an increase in filler %. On the other hand, %E was improved drastically by incorporating filler in PLA matrix. The barrier property

results also supported the surface morphology and the % reduction in oxygen permeability were calculated up to ~81.7% at 25 °C. However, the % reduction value in oxygen permeability was increased and reached up to ~99% at 15 °C. In this way, PLA/CH-*g*-OLLA films can be one of the best substitutes to increase food shelf life in food packaging applications.

Chapter 7

Pilot Scale Processing of Poly (Lactic Acid)/Chitosan-*Graft*-Oligo(L-Lactic Acid) Bionanocomposite Films by Melt Extrusion Technique

This chapter focuses on the successful utilization of CH-g-OLLA as a nano-filler in poly (lactic acid) matrix to fabricate PLA/CH-g-OLLA bionanocomposite films by co-rotating twin screw compounder cum cast film extrusion technique (distinctly advantageous over conventional solution casting) at bench scale as well as semi-pilot scale and are demonstrated for its application in food packaging with improved oxygen barrier properties. The number average and weight average molecular weights of PLA are reduced by ~23% and ~15% respectively with an increase in filler loadings. Homogeneous dispersion of three dimensional spherical aggregates of amphiphilic nano-chitosan are observed in PLA/CH-g-OLLA bionanocomposite films using transmission electron microscopy. The best fitted theoretical models with the experimental data for mechanical modeling of extruded PLA/CH-g-OLLA samples are foam and modified foam models, Nicolais-Narkis model and modified Mitsuishi model. The permeability and solubility of oxygen across the PLA film are significantly reduced upto ~90.4 and ~95.7% with increase in filler loading upto 5 wt%. Further, the lamination technique is used to fabricate a bilayer of extruded PLA and PLA/CH-g-OLLA bionanocomposite films at ~90 ºC. The dynamic mechanical analysis of laminated PLA/CH-g-OLLA bionanocomposite films confirm a significant increment in storage modulus (~86%) and elongation (~490%) as compare to that of pristine PLA.

7.1. Introduction

The significant efforts in the development of biodegradable polymers have been performed by the researchers. Poly (lactic acid) is found as a promising bio-based synthetic polymer among all due to its comparable mechanical properties with conventional petrochemical based polymers. Though the brittle nature and higher melting point have confined its melt processability and higher oxygen transmission rate limits its application in stringent food packaging, such existing limitations can be conquered by the structural modification of PLA. The modification can be done in many ways such as copolymerization, inclusion of modifiers/additives and blending. Melt blending of PLA with other compatible polymer is an industrially viable approach, which offers the freedom to tune the properties **[Arrieta et al., 2014]**. The available literature shows that the melt blending of PLA with 25 wt % of polyhydroxybutyrate (PHB) demonstrated the improved mechanical properties as compared to PLA and also exhibited the optimum miscibility between both the polymers. The enhancement in composite properties was due to the increment in the crystallinity of PLA, which brings the nucleating effect of PHB in PLA matrix **[Arrieta et al., 2014; Zhang and Thomas, 2011]**. The other limitation of PLA is its ductility, which is less than that of conventional synthetic polymers. This limitation can be overcome by incorporation of plasticizers into PLA-based materials. The major criterion for the substances approved for food packaging are their non-toxic nature and so the plasticizers or additives used with PLA should be non-toxic and non-carcinogenic in nature. The modifiers should be hydrophobic and nonvolatile in nature so that they can be easily miscible with PLA at elevated temperatures during industrial processing. Chitosan is another biopolymer which is a product of chitin deacetylation and is one of the most examined polymers in the stream of medicals, cosmetics, food packaging and other high-tech applications for rapid advances in the construction of functional biodegradable materials. Such an efficient usage of

chitosan in countless applications is due to the presence of amine group at C2 position, which imparts the unique properties such as biocompatibility, antifungal, antimicrobial, film forming ability and so forth. Tremendous properties of chitosan have acquired the scientific and industrial attraction towards distinct areas like food science, biotechnology, biomedicine, pharmaceutics and tissue engineering **[Barata et al., 2016]**. The blending or chemical modification of chitosan with other compatible (bio) molecules can introduce various functionalities with improved properties such as thermal, mechanical performance, conductivity, barrier, luminescence among many others, which can further explore the new areas of research. The existing limitation of chitosan is its hydrophilic nature, which exhibits high susceptibility to moisture and low water barrier properties **[Bonilla et al., 2013]**. In this regard, **Suyatma et al., 2004**, have developed composite films, which were fabricated using PLA and chitosan in various proportions. The results revealed that the mechanical properties of biodegradable composite films reduced with an increase in filler concentration. Fourier transform infrared (FTIR) and thermal analysis confirmed that PLA and chitosan are incompatible with each other due to the lack of particular interaction between PLA and chitosan. In this line, **Sebastien et al., 2006** have also fabricated PLA/chitosan composite films using solution mixing and film casting approach to elaborate its antifungal and moisture barrier properties in order to make it suitable for potential food applications. The results exhibited improvement in moisture barrier and mechanical properties due to the presence of PLA and also showed significantly enriched antimicrobial properties because chitosan itself behaves as an antimicrobial agent. They also concluded that the miscibility problems between PLA and chitosan were encountered, which resulted in heterogeneous film formation. The film forming ability of chitosan can only be successfully utilized in packaging if its hydrophilic nature converts into hydrophobic by the association of this polysaccharide with a moisture-resistant

polymer using grafting, crosslinking, blending and other techniques. However, the overall biodegradability of the polymer should be maintained. In this regard, **Bonilla et al., 2013** have prepared various concentrations of PLA/chitosan biocomposite films using extrusion technique. As a result, the incorporation of various sizes of chitosan particles has decreased the rigidity, stretchability and water vapour permeability of PLA films. However, thermal properties of PLA were unaffected by the addition of chitosan particles, as the glass transition temperature of chitosan exists above 190 °C. **Aryaei et al., 2012** have also investigated the mechanical properties of solvent casted nano and micro chitosan as well as cross-linked chitosan films using sophisticated instrumentation such as nanoindentation for elastic modulus and micro-hardness. Chitosan was cross-linked with tripolyphosphate (TPP) to establish the cross-links between NH_2 and PO_4 groups of chitosan and TPP respectively. The elastic modulus, microhardness and brittleness of chitosan films were increased with the crosslinking phenomena as compared to uncross-linked films. With the objective of improving mechanical and thermal properties, **Wu and Wu, 2006** have added organically modified montmorillonite (m-MMT) in PLA matrix and prepared nanocomposite films successfully by solvent casting method. The m-MMT clay was first modified with n-cetyl trimethylammonium bromide (CTAB) cations and subsequently treated with chitosan in order to enhance the chemical similarity, thermal and mechanical properties. The degradation studies revealed that modified m-MMT has reduced the degradation rate of PLA matrix. Overall improvements in physical properties were detected as a result of the existence of various layers of inorganic silicates and improved synergy between PLA and m-MMT due to chitosan in the formulated nanocomposites. However, the properties are improved with the addition of modifier but the excess use of chemicals is always harmful for human health as it comes in contact with packed food.

The present research work is focused on the improvement in structural, thermal, mechanical and barrier properties of melt extruded PLA films by introducing CH-*g*-OLLA as filler. PLA and CH-*g*-OLLA are mixed together in various proportions to fabricate PLA/CH-*g*-OLLA bionanocomposite films at bench scale and semi-pilot scale followed by the evaluation of various physical and chemical properties. The molecular weight distribution, optical polarity and thermal properties are characterized thoroughly. The uniform dispersion of CH-*g*-OLLA in PLA matrix is examined by surface topography. The investigations on mechanical properties are performed to match the experimental values with theoretical values as calculated by various models. Further, the oxygen permeability test of PLA/CH-*g*-OLLA bionanocomposite films were carried out to evaluate its significant use in stringent food packaging application.

7.2. Results and discussion

7.2.1. Calculation of gel yield (%)

The gel yield (%) for various PLA/CH-*g*-OLLA bionanocomposite films is calculated using Eq. 2.7, which varies in the range of 98.7-93.9% as mentioned in Table 7.1. Such high values of gel yield represent that most of the nano-filler in PLA/CH-*g*-OLLA bionanocomposite films is grafted with long PLA chains with covalent bond. It also signifies that the CH-*g*-OLLA or grafted chitosan is highly soluble and compatible with PLA. Hence, the limitation of solubility of chitosan has been successfully overcome in this study. As a result, the grafted chitosan can be used efficiently in food packaging and other possible applications.

7.2.2. Attenuated total reflection-Fourier transform infrared spectroscopy (ATR-FTIR)

The miscibility of polymer blends can be investigated by FTIR spectroscopy, which can be measured by observing the difference between PLA and PLA/CH-*g*-OLLA bionanocomposite films as shown in Figure 7.1(a) and (b). Three strong peaks are observed at 1077, 1128 and 1181 cm^{-1} in the FTIR spectra of PLA and PLA/CH-*g*-OLLA bionanocomposites, which are attributed to the presence of C(O)-O-C stretching vibrations. The characteristic peak 1041 cm^{-1} is related to the -C-C- stretching and the peak at 868 cm^{-1} signifies -OH bending respectively, which are also observed in both the cases. The peak at 868 cm^{-1} represents the amorphous segments available in PLA and PLA/CH-*g*-OLLA bionanocomposite films. The small peaks of -CH- bending vibrations are positioned at 1361 and 1385 cm^{-1} in PLA and PLA/CH-*g*-OLLA bionanocomposite films, which are the results of symmetric and asymmetric deformation. A small and sharp peak at 1452 cm^{-1} corresponds to the methyl asymmetric deformation. However, a strong characteristic peak is positioned at 1747 cm^{-1}, which denotes the carbonyl stretching of PLA and is also presented in PLA/CH-*g*-OLLA bionanocomposite films. The intensity of all the above explained peaks is almost same for all the cases, which suggests that the matrix (PLA) is chemically stable even after mixing the various percentages of CH-*g*-OLLA. However, a very tiny and sharp peak is observed at 1539 cm^{-1} only in PLA/CH-*g*-OLLA bionanocomposite films as shown in Figure 7.1(b), which confirms the presence of amide ester linkage between PLA and chitosan at C2 position. It suggests that the long PLA chains are chemically grafted on chitosan backbone by a newly formed covalent bond. Similar bond formation was also observed between PLA and chitosan in our previous study. One more peak at 755 cm^{-1} resembles -CH- bending in PLA and its bionanocomposite films,

which represents the crystalline nature. Hence, the extruded PLA and PLA/CH-*g*-OLLA bionanocomposite films exhibit semicrystalline behaviour.

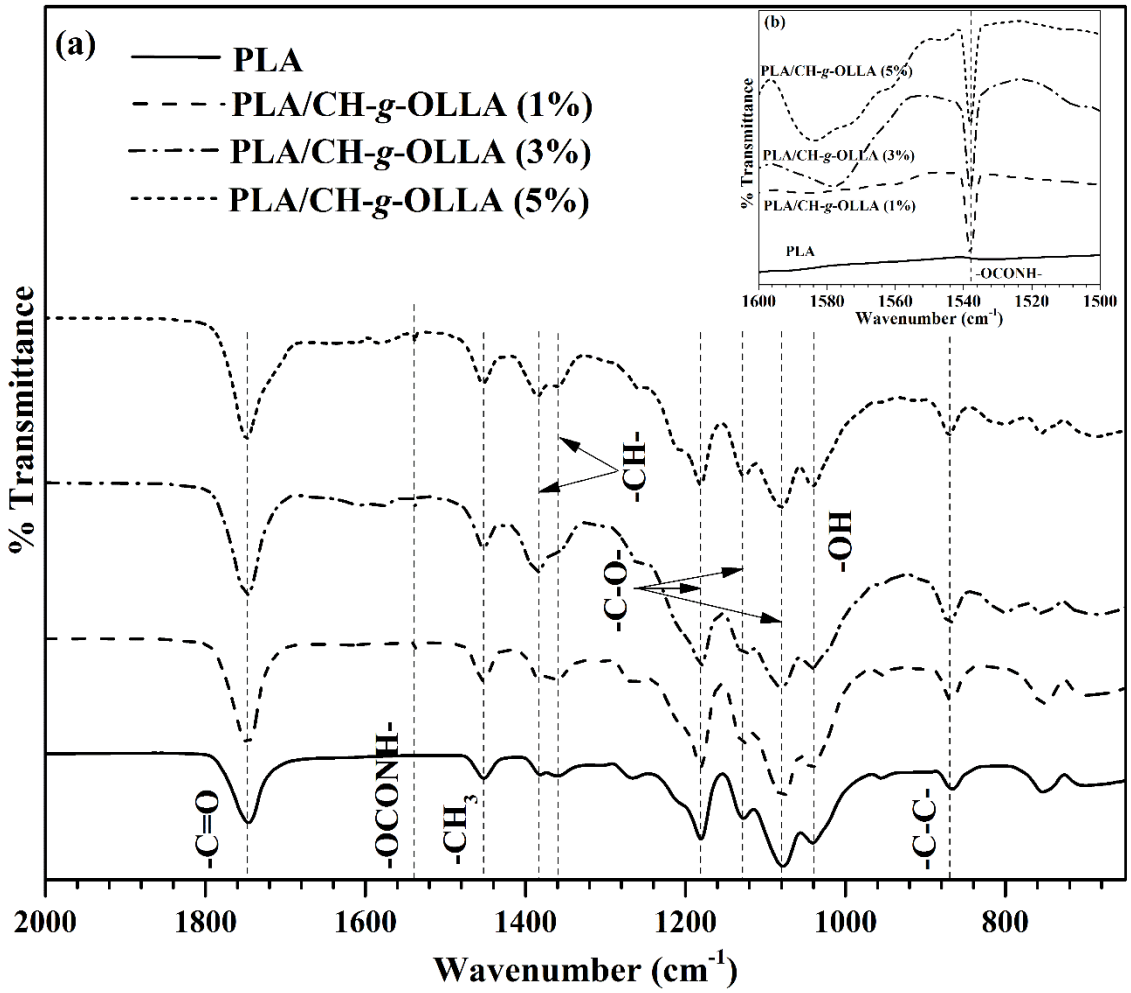

Figure 7.1. (a) FTIR spectra of PLA and PLA/CH-*g*-OLLA bionanocomposite films and (b) grafting evidence in PLA/CH-*g*-OLLA bionanocomposite films.

7.2.3. Wide angle X-ray diffraction (WXRD)

XRD diffractograms for PLA and PLA/CH-*g*-OLLA bionanocomposite films have demonstrated well resolved peaks at 14.7º, 16.4º, 18.9º and 22.1º, which corresponds to the various crystallographic planes i.e. [0, 1, 0], [2, 0, 0/1, 1, 0], [2, 0, 3] and [0, 1, 5] respectively as displayed in Figure 7.2. A sharp peak at 2θ =16.4º confirms α crystalline

structure and exhibits typical orthorhombic crystal structure of PLA matrix. A peak positioned at 22.1º in all the samples also represents the presence of α form of crystals. The existence of β crystalline form of PLA is approved by the availability of two peaks at 14.7º and 18.9º, which is less stable crystalline form than α form. It is noteworthy to mention that the sharpness and intensity of all the crystalline peaks reduce continuously with an increase in CH-*g*-OLLA loadings, which gives a clear indication about the decrement in percentage crystallinity from 37% to 27.4%. The phenomena of shifting of peaks is absent in PLA/CH-*g*-OLLA bionanocomposite films, which suggests that the ordered crystal structure is unaffected with the addition of nano-filler.

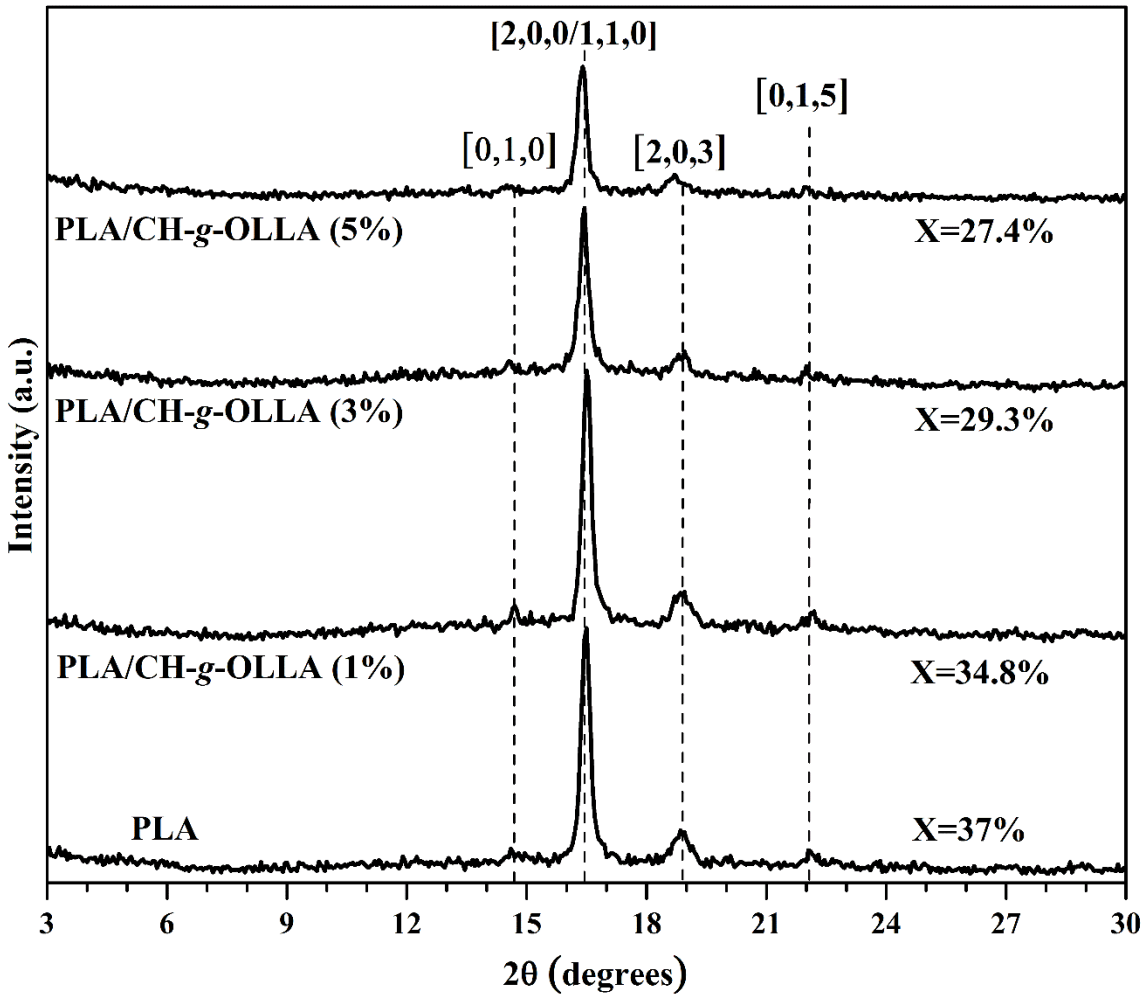

Figure 7.2. XRD analysis of PLA and PLA/CH-*g*-OLLA bionanocomposite films.

The incorporated nano-filler is responsible for strong and active interfacial interactions at the interface as well as in bulk, which clearly expresses the reinforcement effect of CH-*g*-OLLA in PLA matrix. Mostly three types of interactions are observed between PLA matrix and CH-*g*-OLLA bionanocomposites i.e. filler-filler, matrix-filler and matrix-matrix interactions as shown in Figure 7.3.

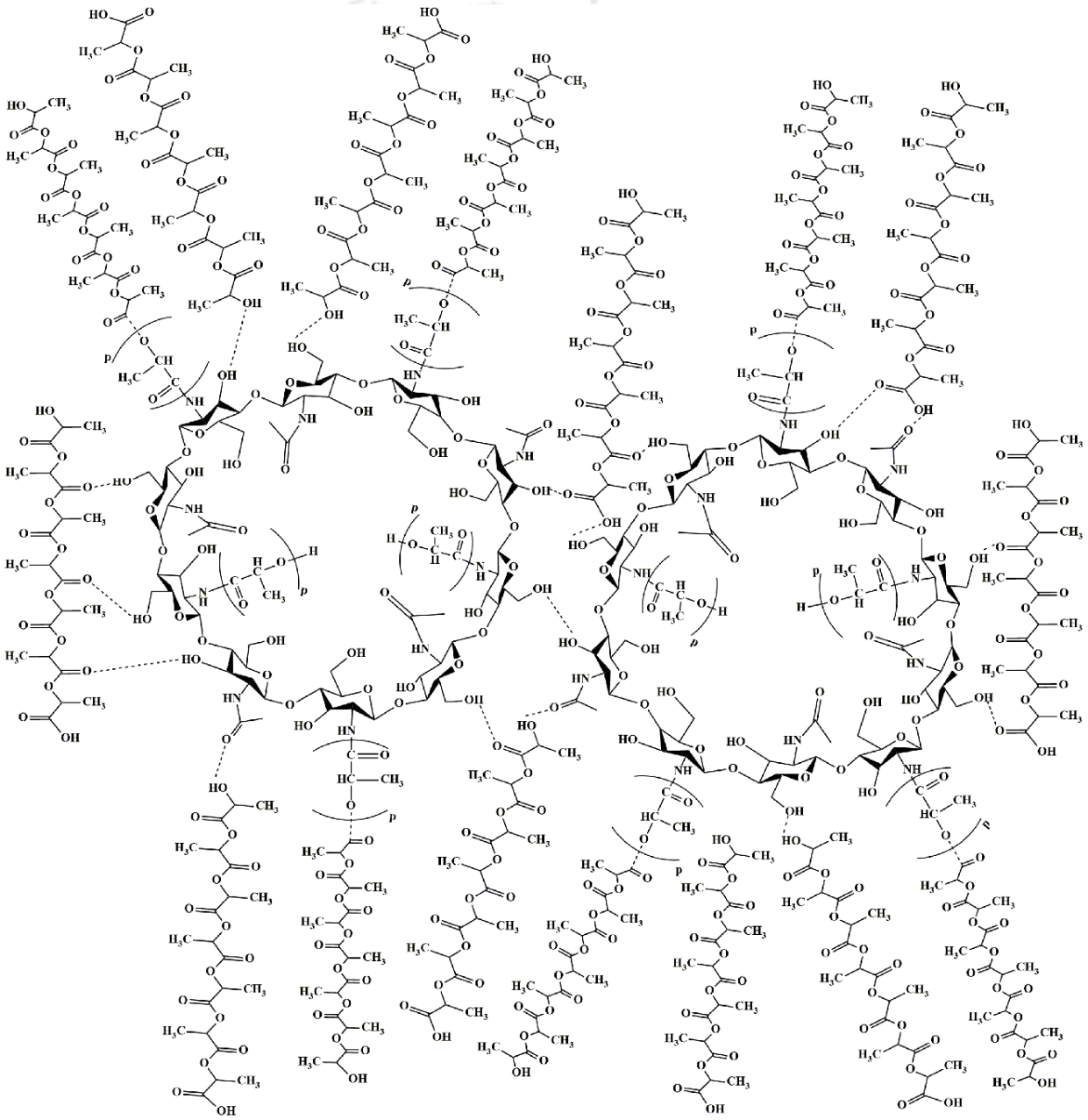

Figure 7.3. Schematic representation of interaction between PLA and CH-*g*-OLLA nano-filler.

The newly formed chemical bonds between filler-filler, matrix-filler and matrix-matrix are covalent and hydrogen bonds as displayed by dotted lines. The formation of strong covalent bonds take place between hydroxyl and carbonyl groups of CH-*g*-OLLA and PLA molecules respectively and also appears in between PLA chains. However, the formation of hydrogen bonds take place between CH-*g*-OLLA and PLA molecules and also in between CH-*g*-OLLA molecules, which enhances the network structure or tortuosity in PLA/CH-*g*-OLLA bionanocomposite films as compare to pristine PLA. This network structure may responsible for the reduction in oxygen transmission rate across bionanocomposite films. It is noticeable that the other factors such as solubility and diffusivity may also culpable for significant reduction in oxygen transmission rate.

7.2.4. Gel permeation chromatography (GPC)

The number average molecular weight (M_n) and weight average molecular weight (M_w) of pristine PLA is observed as ~155000 Da and ~264000 Da respectively. The effect of various loadings of CH-*g*-OLLA copolymer on the values of M_n, M_w and polydispersity index (PDI) of pristine PLA during melt extrusion technique is demonstrated as shown in Figure 7.4. According to Figure 7.4, the values of M_n and M_w of PLA are continuously reduced up to ~23 and ~15% respectively with an increment in the loading of CH-*g*-OLLA up to 5 wt%. This may be attributed to the alteration of long PLA chain lengths due to the increment in chitosan content. The technique 'melt extrusion' of PLA/CH-*g*-OLLA bionanocomposite films may also be one of the dominant reason for the reduction in M_n and M_w values of PLA due to applied mechanical stresses between the screws during processing. It is noteworthy to mention that the hydrolysis reactions are occurred preferentially in the amorphous phase of PLA matrix during processing, which are responsible to initiate the degradation of polyester chains. Similar results are observed by **Tenn et al., 2013** for PLA/montmorillonite based nanocomposites prepared by melt

processing. The values of PDI for PLA, PLA/CH-*g*-OLLA (1%), PLA/CH-*g*-OLLA (3%) and PLA/CH-*g*-OLLA (5%) bionanocomposite films are calculated as 1.7, 1.76, 1.76 and 1.89 respectively as shown in Figure 7.4, which suggests that the non-uniform distribution of PLA chain lengths due to the presence of CH-*g*-OLLA in various amounts.

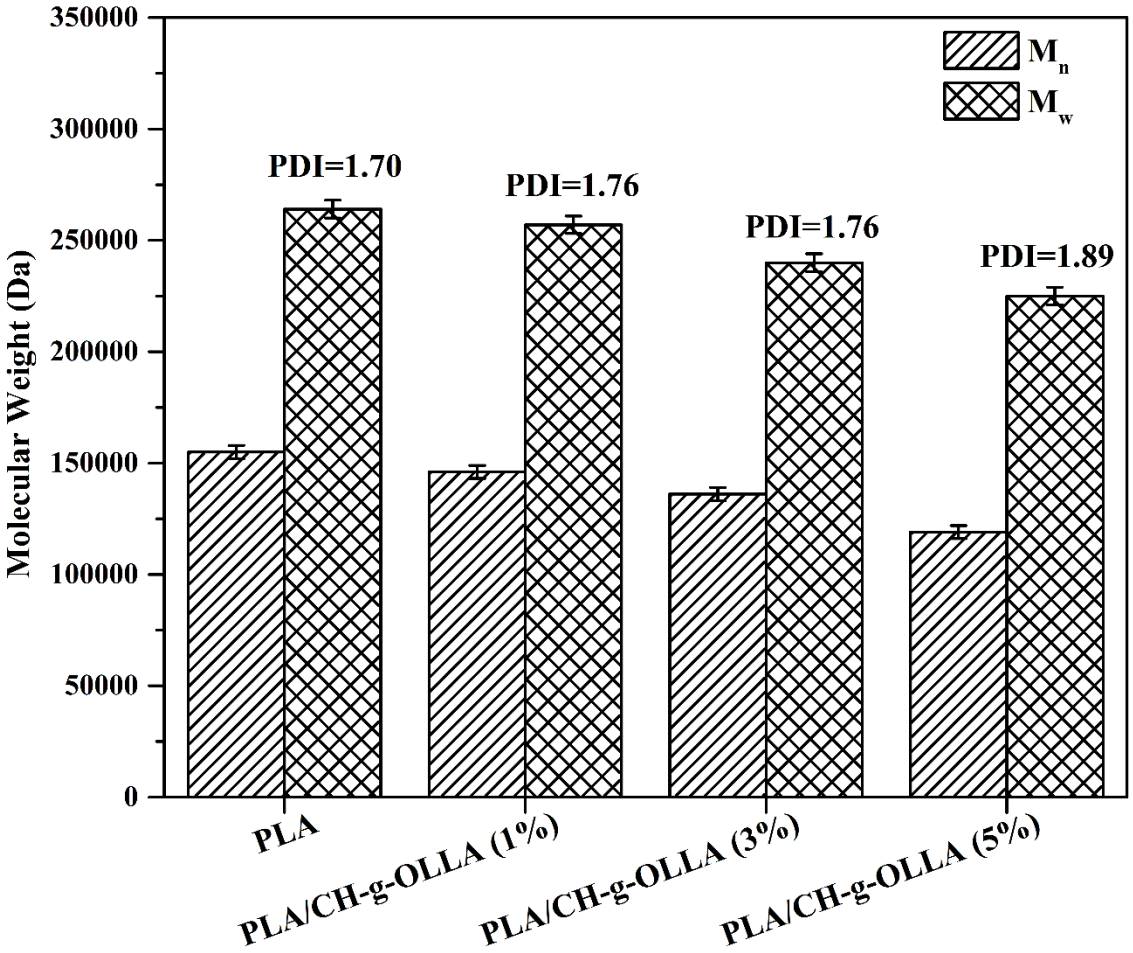

Figure 7.4. Molecular weight distribution in melt extruded PLA, PLA/CH-*g*-OLLA (1%), PLA/CH-*g*-OLLA (3%) and PLA/CH-*g*-OLLA (5%) bionanocomposite films.

7.2.5. Optical polarimetry

The specific rotation and optical rotation of PLA are observed as -155.32° and -1.55° respectively as mentioned in Table 7.1. Similar results are also observed for L-PLA by **Katiyar et al., 2011**. The specific rotation and optical rotation of PLA are reduced

continuously up to 41.8° and 0.43° respectively with an increase in CH-*g*-OLLA loadings in bionanocomposite films during solvent casting process. The possible reason for such a reduction is the grafting of OLLA chains on chitosan backbone. Chitosan is having a bulky glucosamine ring structure, which can possibly hinder the specific as well as optical rotation of PLA.

Table 7.1: Volume fraction, gel yield, specific rotation and optical rotation in PLA/CH-*g*-OLLA bionanocomposite films.

Samples	CH-*g*-OLLA (wt%)	Volume fraction of CH-*g*-OLLA (Φ_f)	Gel yield (%)	Specific rotation (º)	Optical rotation (º)
PLA	0	0	-	-155.32	-1.55
PLA/CH-*g*-OLLA (1%)	1	0.009	98.7	-127.16	-1.28
PLA/CH-*g*-OLLA (3%)	3	0.029	96.3	-126.87	-1.27
PLA/CH-*g*-OLLA (5%)	5	0.047	93.6	-113.50	-1.12

7.2.6. Differential scanning calorimetry (DSC)

The DSC thermograms and related phase transition values of PLA and PLA/CH-*g*-OLLA bionanocomposite films are embellished in Figure 7.5, which shows the variation in glass transition, cold crystallization and melting temperatures (obtained during second cycle) with an increase in CH-*g*-OLLA loading. A unimodal endothermic melting peak of neat PLA is observed at 150.3 ºC, which suggests the presence of α crystalline form with uniform crystals size. It supports the XRD data obtained for the same samples in section 7.2.3. The single melting peak in control film represents the stable crystals with uniform crystal size and its homogeneous distribution **[Valapa et al., 2016]**. In PLA/CH-*g*-OLLA (1%) bionanocomposite film, the melting temperature is shifted ~6.8 ºC towards higher value as compare to control film. This significant improvement in melting temperature concludes the negligible change in molecular weight of PLA matrix, which

shows the structure stability after the addition of 1% CH-*g*-OLLA. The increment in T_m value also signifies that the nano-filler (CH-*g*-OLLA) performs as a superior nucleating agent. The melting temperatures of PLA reduce ~3.6 and ~5.1 ºC with the addition of 3 and 5 wt% of nano-filler respectively. It happens due to the reduction in the stability of PLA crystals and in molecular weight as a result of agglomeration of nano-filler. A small shoulder is observed before the melting peak of PLA/CH-*g*-OLLA bionanocomposites due to the presence of non-uniform crystal thickness and non-homogeneous distribution of PLA crystals. The deviation in crystal thickness and its distribution depends on the variation in nano-filler content. It is noteworthy to mention that the heat of fusion is found more in the case of PLA/CH-*g*-OLLA bionanocomposite films as compare to neat PLA due to the increment in the number of nucleating sites and chemical interactions between PLA and CH-*g*-OLLA. The cold crystallization temperature of PLA reduces ~3.1, ~9.2 and ~11.8 ºC with the addition of 1, 3 and 5 wt% of CH-*g*-OLLA respectively. This significant reduction in T_{cc} value is due to the increase in diffusion rate, which enhances the migration rate of polymer chains towards the nucleus surface. The lower T_{cc} values with sharp peaks denote faster crystallization rate of PLA/CH-*g*-OLLA bionanocomposites as compare to PLA film. The improvement in crystallization rate is due to the occurrence of both the homogeneous and heterogeneous crystallizations in composites. The glass transition temperature of composites represent the softening phenomena and phase separation between filler and matrix. In the second heating cycle, the glass transition temperature of PLA/CH-*g*-OLLA bionanocomposite films reduce ~3, ~7.5 and ~11.3 ºC with the addition of 1, 3 and 5 wt% of filler respectively. A significant reduction in T_g values indicate the availability of short CH-*g*-OLLA chains, which induce the degradation of PLA and decrease the intermolecular interactions **[Peng and Li, 2014]**. The reduced T_g values of PLA/CH-*g*-OLLA bionanocomposite films represent the increment in plasticization or softening of the

polymer composites **[Suyatma et al., 2005]**. Polymer processing may be the other reason for such reduction in T_g values as the films are prepared by melt extrusion technique, which promotes the thermal degradation, if the polymer remains inside extruder for longer time. The heat capacity at constant pressure also reduces from 0.66 to 0.43 J/g.K with increasing filler loading due to less entanglement of polymer chains.

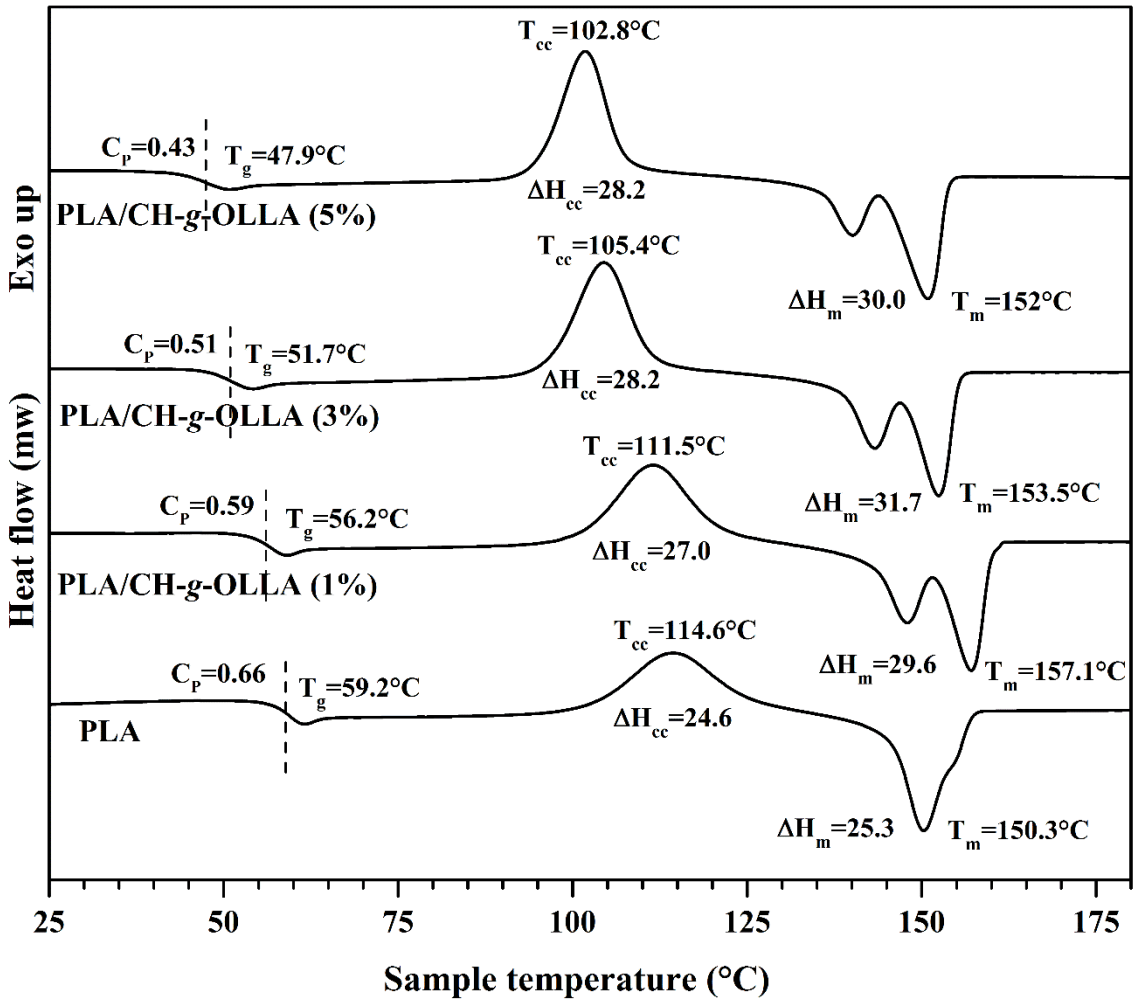

Figure 7.5. Various thermal phases of PLA and PLA/CH-*g*-OLLA bionanocomposite films during DSC analysis.

7.2.7. Thermogravimetric analysis (TGA)

A single region of weight loss percentage is detected for PLA and its bionanocomposite films at a heating rate of 5 °C/min in the graphs of temperature versus weight loss percentage and temperature versus derivative of weight loss percentage shown in Figure 7.6(a) and (b) respectively. The main region of thermal degradation of PLA is approximately 302.5-403.2 °C, which may be correlated with intramolecular trans-esterification or backbiting reaction of PLA **[Jayaramudu et al., 2013]**. The onset thermal degradation temperature of PLA/CH-*g*-OLLA bionanocomposite films reduces upto ~33 °C with an increase in filler loading. The thermal stability of bionanocomposite films can be evaluated only on the basis of the temperature value at which the maximum weight loss arises. A single peak of maximum degradation temperature is observed in PLA and PLA/CH-*g*-OLLA bionanocomposite films as displayed in Figure 7.6(b), which means that the thermal degradation of all the samples occurs in a single step process. The T_p value of PLA/CH-*g*-OLLA bionanocomposite films is continuously reduced upto ~2.7, 3 and ~7.9 °C with the addition of 1, 3, 5 wt% of nano-filler respectively. The reduction in T_{on} and T_p values of PLA/CH-*g*-OLLA bionanocomposite films is associated with the low molecular weight of CH-*g*-OLLA copolymer, which breaks the long polymer chains of PLA and fasten its thermal degradation rate **[Ambrosio-Martin et al., 2014]**. The low molecular weight chains of CH-*g*-OLLA increase with an increase in filler loading. As a result, the crystal structure and size of PLA deform which also reduce its crystallinity. The offset degradation temperature follows the similar trend as that of T_p and the allotted values for PLA and its bionanocomposite films are 403.2, 400.6, 396.2 and 389.9 °C by adding 0, 1, 3, and 5 wt% of nano-filler respectively. The weight loss percentage at maximum degradation temperature is calculated as ~96, ~95, ~89 and ~84% with continuous increase in filler loading. It is also a suitable proof for maximum polymer degradation at single

stage. At the end of the analysis, the remaining weight percent of carbonaceous char is observed as ~ 0.08, 0.14, 0.22 and 0.48% by increasing filler content as 0, 1, 3 and 5 wt% respectively.

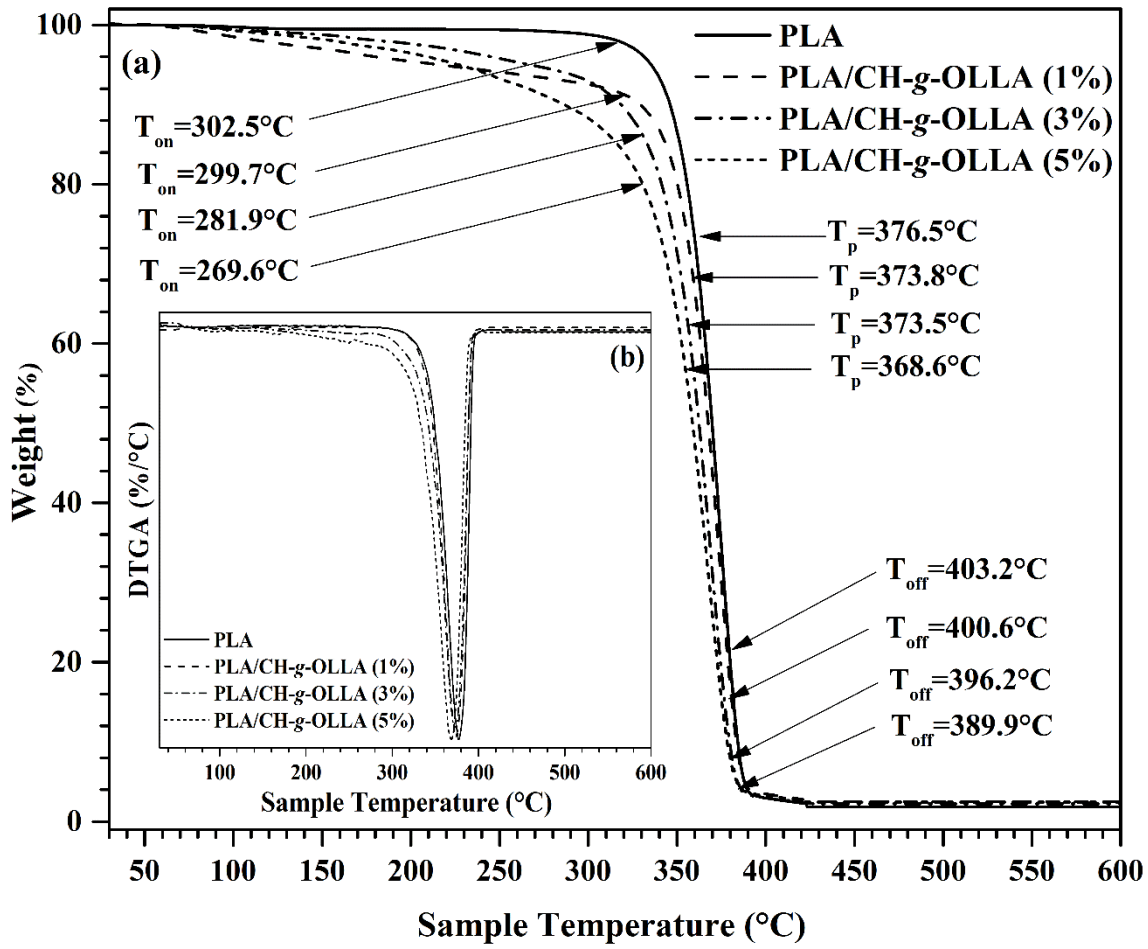

Figure 7.6. Variation in thermal degradation behaviour during (a) TGA and (b) DTG analysis of PLA and PLA/CH-*g*-OLLA bionanocomposite films.

7.2.8. Surface morphology

A clear proof of surface modification of PLA film is noticed with the addition of CH-*g*-OLLA copolymer in various proportions as shown in Figure 7.7. The control film (PLA) shows flaky rough surface, however the surface of PLA film becomes smoother after adding filler. It suggests that the filler acts as a plasticizer, which increases the elastic nature

of the film and makes it smoother. CH-*g*-OLLA copolymer forms three dimensional monodisperse spherical structures in PLA matrix, which mimics like core-shell morphology. The number of spherical structures increases with an increase in filler loadings, however the size of formed spheres lies in the range of 0.1-0.4 μm and is unaffected with the variation in filler loadings as shown in Figure 7.7(b), (c) and (d). At higher loading (5 wt%), the phenomena of agglomeration occurs in PLA/CH-*g*-OLLA bionanocomposite film. Basically, the filler behaves like a surfactant in this polymeric system in which chitosan acts as a hydrophilic head group and a short PLA chain i.e. OLLA acts as a hydrophobic tail. The dimension of chitosan head group and OLLA tail lies in the range of nano-meters, which confirms by TEM analysis as shown in Figure 7.7(e). Hence, the filler is also termed as nano-amphiphilic chitosan due to have dual characteristics (hydrophilic and hydrophobic). The spherical structures in bionanocomposite films are the aggregate of self-assembled micelles. The formation of micelles takes place only and only if the concentration of surfactant exceeds the critical micelle concentration. The value of CMC correlates with the gibbs free energy of surfactants. In this case, the formed micelles take the shape of spheres due to the applied surface tension in equal magnitude from all the sides on individual micelle. The spherical aggregates vary in the range of 25-42 nm as mentioned in Figure 7.7(e). Figure 7.7(f) shows Gaussian fit between the number of particles and particles diameter, which suggests that the diameter of most of the nano-spheres vary in the range of 4-6 nm. Nano-spheres with large diameter such as 18-21 nm also exist in the polymeric system. The spheres are interconnected with the long PLA chains and form a network structure, which can restrict the movement of polymeric chains. Hence such network can improve oxygen solubility and tortuosity in PLA matrix, which can enhance the barrier properties of bionanocomposite films as it is highly required in food packaging applications.

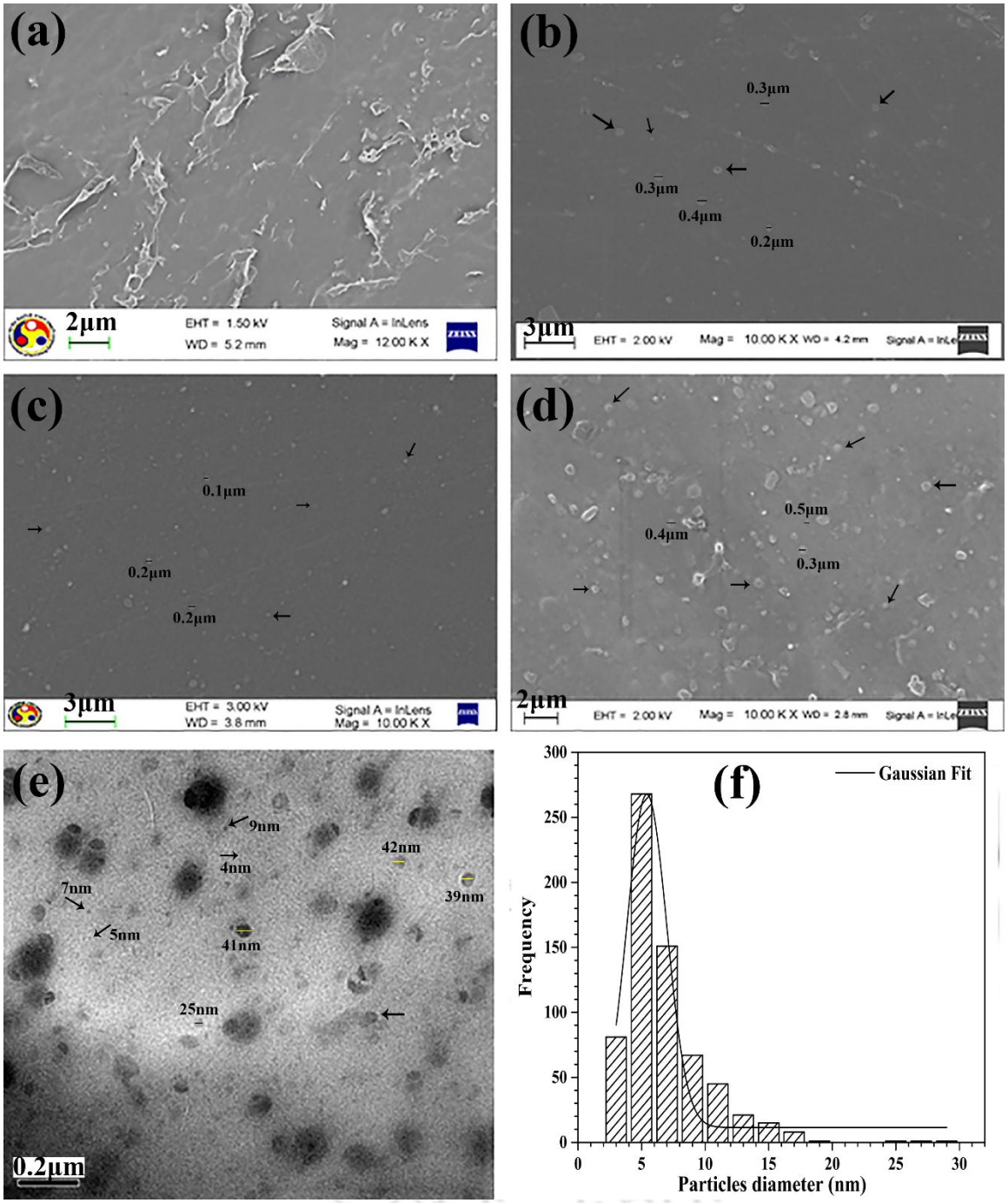

Figure 7.7. (a) FESEM images of (a) Neat PLA, (b) PLA/CH-*g*-OLLA (1%), (c) PLA/CH-*g*-OLLA (3%), (d) PLA/CH-*g*-OLLA (5%) bionanocomposite films, (e) TEM image of PLA/CH-*g*-OLLA (5%) bionanocomposite film and (f) particle size distribution in PLA/CH-*g*-OLLA (5%) bionanocomposite film.

7.2.9. Contact angle measurements

The surface characteristics such as hydrophobicity or hydrophilicity are necessary for food packaging applications, which plays an important role during handling, transport and storage of packed foodstuffs. A horizontal line is drawn parallel to x-axis at θ = 65º, which signifies the critical value between hydrophobic surface (θ > 65º) and hydrophilic surface (θ < 65º) **[Arrieta et al., 2014]**. According to the results, PLA and PLA/CH-*g*-OLLA bionanocomposite films exhibit the contact angle values more than 65º for both the probe liquids such as water and glycerol as shown in Figure 7.8. However, the contact angle value of glycerol is detected less than 65º for PLA/CH-g-OLLA (5%) bionanocomposite film. The contact angle values more than 65º represents the poor affinity of water and glycerol to the polymer surfaces, which confirms their potential utilization in packaging. After the liquid drop placed on polymeric samples, minor lowering in contact angle values is observed in first ~10 seconds due to the cohesive interaction, which helps the drop to take the shape of sphere. The spherical shape is balanced on the film surface due to the adhesive interaction, which is liable for the spreading of the liquid drop **[Sreekumar et al., 2013]**. The addition of CH-*g*-OLLA nano-filler in PLA matrix significantly increases the water resistance of PLA up to ~6.6%. The associated reason with this behaviour may be the strong interaction of hydroxyl groups of chitosan with PLA due to intramolecular hydrogen bonding as shown in Figure 7.3. Hence, chitosan hydroxyl groups can not able to do surface orientation, which may affect the surface chemical properties and leads to enhance surface hydrophobicity of PLA. The contact angle values of glycerol on PLA and PLA/CH-*g*-OLLA bionanocomposite films are observed lower than that of water. The contact angle values of glycerol on PLA film reduce continuously up to ~10% by increasing nano-filler loadings. Approximately 2.7% reduction in contact angle value of glycerol is observed for PLA/CH-*g*-OLLA (3%) bionanocomposite film. However, a drastic reduction

~7.6% is detected by increasing the filler content from 3 to 5wt% in PLA matrix. The associated reason is the presence of excess (three) hydroxyl groups in glycerol structure as compare to that of water, which may easily link with the hydroxyl groups of chitosan available at the surface of PLA/CH-*g*-OLLA bionanocomposite films by inter molecular hydrogen bonding. When glycerol is dropped on the surface of PLA/CH-*g*-OLLA, the available –OH groups in PLA/CH-*g*-OLLA form hydrogen bonds between glycerol molecules and diffusion takes place quickly as compare to that of water.

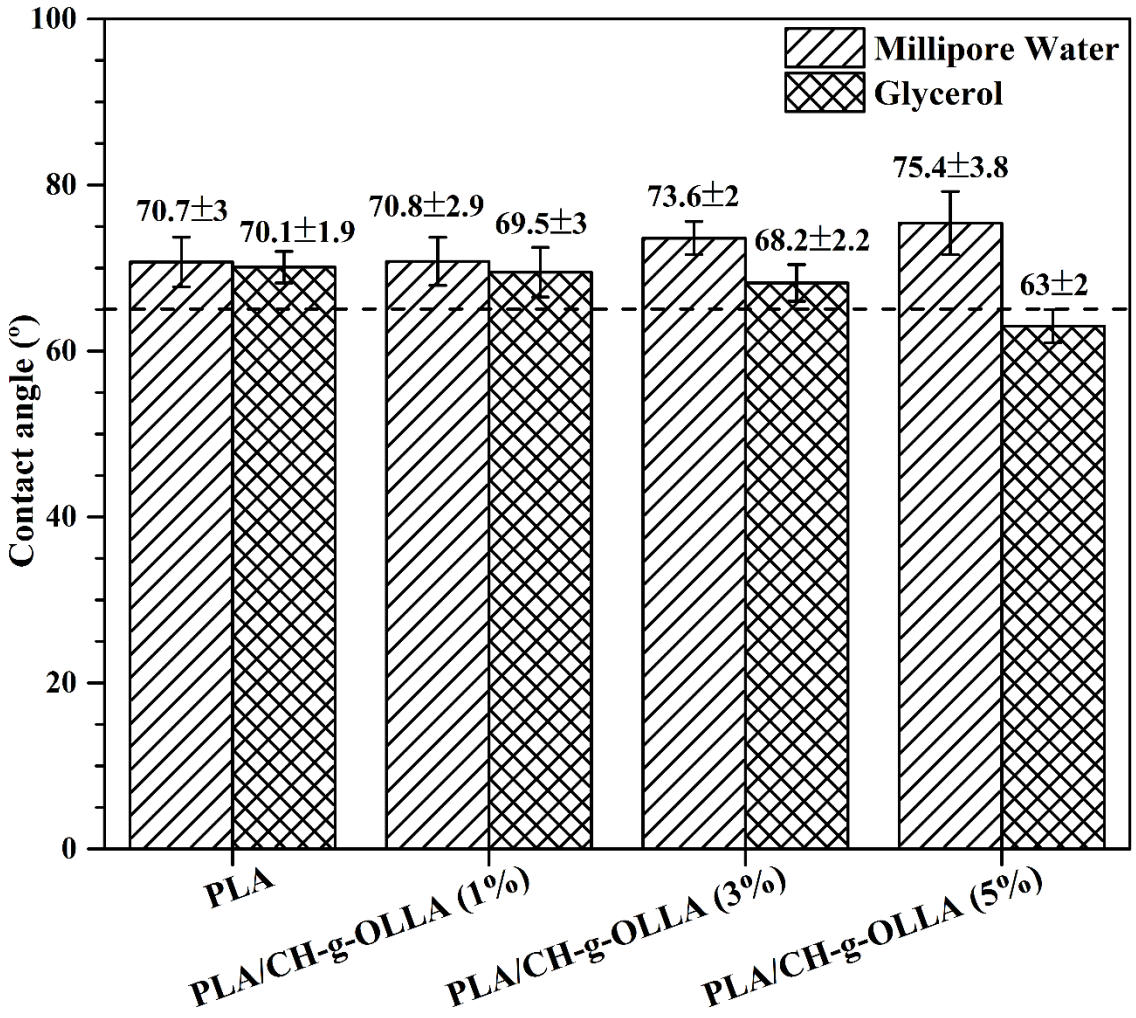

Figure 7.8. Contact angle analysis of PLA and PLA/CH-*g*-OLLA bionanocomposite films using millipore water and glycerol.

7.2.10. Mechanical properties

Theoretical modeling of mechanical behaviour

The detailed study about the behaviour of mechanical properties of PLA/CH-*g*-OLLA bionanocomposite films, a two-phase composites consist of a continuous polymer phase and particulate filler phase. The insights about the variation in mechanical behaviour (observed during experiments) with an increase in filler volume fraction can be understood very well with the help of various available models, which are able to describe Young's modulus, tensile strength and elongation at break against the variation in filler volume fraction. Nowadays, mechanical modeling and simulation of such value added polymer composites plays an important role to develop better understanding and their use in various engineering applications. Various parameters such as filler-matrix adhesion, filler size, filler shape, filler orientation, filler packing fraction and filler concentration are responsible for mechanical properties distribution in particulate filled composites. The load bearing capacity and load transfer activity from matrix to filler can produce better mechanical properties of composites than that of control. Several theories are available in literature for the modeling of Young's modulus of composite polymers with the help of various parameters. Einstein has developed two simple equations to model Young's modulus of composite polymers, which are based on "without and with adhesion" between matrix and spherical filler as mentioned in Eq. 7.1 and 7.2 **[Singla et al., 2016; Abraham et al., 2009]**. Both the equations are valid only at low filler concentrations in polymer matrix.

Einstein equation (without adhesion parameter)

$$\frac{E_c}{E_p} = (1 + \Phi_f) \tag{7.1}$$

Einstein equation (with adhesion parameter)

$$\frac{E_c}{E_p} = (1 + 2.5\Phi_f) \tag{7.2}$$

Where, E_c, E_p and $\frac{E_c}{E_p}$ are the composite modulus, polymer matrix modulus and relative modulus respectively. The value of 2.5 in Eq. 7.2 is reported for adhesion between matrix and filler. Guth and Smallwood has modified Einstein's equation (with adhesion parameter) by introducing an additional term related to inter-particle interactions at higher concentration of spherical filler as mentioned in Eq. 7.3 **[Bliznakov et al., 2000; Bigg, 1987]**.

Guth and Smallwood equation

$$\frac{E_c}{E_p} = \left(1 + 2.5\Phi_f + 14.1{\Phi_f}^2\right) \tag{7.3}$$

Further, a predictive model has been developed by Cohen and Ishai with an assumption that there is no interaction between continuous and discrete phases in polymer nanocomposites and also with an understanding about the effect of blend structure on Young's modulus, which is known as "Foam model" expressed in Eq. 7.4 **[Kakkar and Maiti, 2012; Rinawa et al., 2014]**.

Foam equation

$$\frac{E_c}{E_p} = \left(1 - {\Phi_f}^{\frac{2}{3}}\right) \tag{7.4}$$

The "Foam model" was further modified by incorporating a term called "coefficient of foamability (δ)" in to it. Hence, Eq. 7.4 can be rewritten in the form of Eq. 7.5 **[Maiti and Lopez, 1992]**.

Modified foam equation

$$\frac{E_c}{E_p} = \left(1 - \delta{\Phi_f}^{\frac{2}{3}}\right) \tag{7.5}$$

Interfacial adhesion and continuity in the structure of two phase composites are the two well-known factors which can significantly contribute in mechanical and other properties. The weakness in the structure of polymer composites can't be detected correctly by

Young's modulus data because it can be only measured at low deformations or low solid displacement, whereas tensile strength and elongation at break are the properties that can be determined at large deformations and are able to speculate the weakness in polymer structure more efficiently **[Maiti and Lopez, 1992]**. The theoretical predictions of tensile strength of a composite polymer are very difficult due to the various matrix-filler interactions and less developed as compare to Young's modulus **[Abraham et al., 2009]**. Tensile strength represents the force, which is required to stretch a composite polymer before its failure or breaking point. Some authors have developed theoretical models such as Nicolais-Narkis model and Nielsen model, which are based on relationship between volume fraction and area fraction of filler. Nicolais and Narkis have suggested a model with an assumption that there should be no adhesion between matrix and filler and failure takes place at the interphase **[Ishak and Verbeek, 2016]**. In Nicolais-Narkis model, the interaction between matrix and filler has been taken into consideration by a phase interaction parameter (K) **[Kumar et al., 2013]**. The K value is inversely proportional to phase adhesion, which means that the lower K value in Eq. 7.6 represents higher phase adhesion **[Bliznakov et al., 2000]**.

Nicolais-Narkis equation

$$\frac{\sigma_c}{\sigma_p} = \left(1 - K\Phi_f^{\frac{2}{3}}\right) \tag{7.6}$$

Where, σ_c, σ_p and $\frac{\sigma_c}{\sigma_p}$ denote composite tensile strength, matrix tensile strength and relative tensile strength respectively. The theoretical K value is typically considered as 1.21 for spherical filler with extreme poor adhesion. The theoretical tensile strength of polymer composites with poor adhesion is expressed in another form of equation, developed by Nielsen, which is termed as Nielsen model as expressed in Eq. 7.7 **[Singla et al., 2016]**. In this case, the voids in polymer matrix are occupied by filler without disturbing the

mechanical properties of polymer composites due to the presence of minimal adhesion at the interphase.

Nielsen equation

$$\frac{\sigma_c}{\sigma_p} = \exp(-\alpha\Phi_f) \quad (7.7)$$

The parameter 'α' relates with the stress concentration. If the value of α will be higher, the stress concentration effect will be more, which results the poorer adhesion between matrix and filler **[Bliznakov et al., 2000]**. The values of K and α can be calculated by comparing the experimental tensile strength of PLA/CH-*g*-OLLA bionanocomposite films with corresponding theoretical models **[Singla et al., 2016]**. In contrast with Young's modulus and tensile strength, the elongation at break is also an important parameter, which characterize the mechanical properties of polymer composites. Generally, the elongation at break of polymer matrix decreases by the inclusion of filler particulate. In rare cases, the value of elongation at break may increase by the addition of filler in polymer matrix due to the existence of good reinforcement. As a result, the fracture does not follow a direct path, rather, it goes from filler to filler. Hence, such polymer composites may have same values of elongation at break as compare to polymer matrix **[Abraham et al., 2009]**. Nielsen has developed a basic model related to elongation at break with an assumption of perfect adhesion between matrix and filler as shown in Eq. 7.8 **[Bliznakov et al., 2000]**.

Nielsen equation

$$\frac{\varepsilon_c}{\varepsilon_p} = \left(1 - \Phi_f^{\frac{1}{3}}\right) \quad (7.8)$$

Where, ε_c, ε_p and $\frac{\varepsilon_c}{\varepsilon_p}$ are termed as elongation at break of composite, polymer matrix and relative elongation at break respectively. Experimental data of Young's modulus and tensile strength indicate that the presence of filler may softening the polymer matrix, which cause the increment in elongation at break. In such cases, modified Mitsuishi model can be

effectively used to compare the experimental data with the theoretical data as per Eq. 7.9 **[Kakkar and Maiti, 2012; Rinawa et al., 2014; Mitsuishi et al., 1985; Sharma and Maiti, 2014]**.

Modified Mitsuishi equation

$$\frac{\varepsilon_c}{\varepsilon_p} = \left(1 + \beta \Phi_f^{\frac{2}{3}}\right) \tag{7.9}$$

Where, β is termed as flexibility coefficient.

The variation in mechanical properties such as Young's modulus, tensile strength and elongation at break is observed with respect to the variation in filler loadings in PLA films as shown in Figure 7.9. The experimental values of E_c are reduced continuously from 946.5 to 596.2 MPa (~37% reduction) with an increase in Φ_f values of CH-*g*-OLLA up to ~0.05 as shown in Figure 7.9(a). It is due to the existence of low molecular weight CH-*g*-OLLA in PLA matrix, which contains shorter polymer chains. The longer and entangled PLA chains are highly influenced with shorter polymer chains and break into less entangled polymer chains, which align faster at the application of load during tensile test. A graph of Young's modulus against percentage crystallinity is plotted as displayed in Figure 7.9(a′), which also exhibits the reduction in E_c values by reducing percentage crystallinity of PLA/CH-*g*-OLLA bionanocomposite films. It contributes to the increment in amorphous phase, which reduces the stiffness, uniform dispersion of nano-filler and phase interactions due to agglomeration at higher loadings. The experimental values of relative Young's modulus ($\frac{E_c}{E_p}$) fit in the range of 0.63-0.95 depending on the values of Φ_f for PLA/CH-*g*-OLLA bionanocomposite films as shown in Figure 7.9(b). Some of the theoretical models are used to understand more insights about two-phase composite system. The calculated theoretical values of $\frac{E_c}{E_p}$ using Einstein's models with and without adhesion are found higher than unity, which are also higher than the experimental values. It means

that Einstein's models show higher adhesion between matrix and filler as compare to the values calculated from experiments. Other models such as Guth and Smallwood model, Foam model and modified Foam model are also used to compare theoretical $\frac{E_c}{E_p}$ values with the experimental results. As per the results of Guth and Smallwood model, much higher theoretical values of $\frac{E_c}{E_p}$ are estimated as compare to Einstein's models with and without adhesion due to the incorporation of exponential term, which relates with inter-particle interactions at higher concentration of spherical filler. It is noteworthy to mention that the inter-particle interactions with phase adhesion exist between PLA and CH-*g*-OLLA in PLA/CH-*g*-OLLA bionanocomposite system. However, the low molecular weight of CH-*g*-OLLA imparts the adverse effect on Young's modulus and reduces its value by increasing filler content. The term for such an adverse effect is absent in above discussed theoretical models. The calculated values of $\frac{E_c}{E_p}$ using Foam model reduce with an increase in Φ_f upto 0.009, which are very close to the experimental values. Further, the theoretical values of $\frac{E_c}{E_p}$ increase with an increase in Φ_f upto 0.048. However, they remain lower as compare to neat PLA. The modified Foam model also produce theoretical $\frac{E_c}{E_p}$ values, which follow the similar trend as that of Foam model i.e. the values first decrease upto the Φ_f values of ~0.029 and then increase. All the theoretical values of $\frac{E_c}{E_p}$ are found lower than unity in the case of Foam and modified Foam models. The modified Foam model is fitted well with δ=1.871 and the value of δ at various loadings of CH-*g*-OLLA in PLA matrix and is calculated and mentioned in Table 7.2. In PLA/CH-*g*-OLLA bionanocomposite system, the chemical or physical adhesion between matrix and filler is responsible for the variation in mechanical properties. It is generated by hydrogen bonding and polar-polar interaction between carboxyl and hydroxyl groups of chitosan and PLA. However, the

effectiveness of such bonding and interactions mainly depend on filler characteristics **[Singla et al., 2016]**. Furthermore, physical interaction between matrix and filler may appear due to their differential thermal shrinkage **[Sewda and Maiti, 2007]**. PLA has higher thermally expandable and shrinkage property than that of chitosan during processing. In cooling duration after processing, PLA shrinks and anchors around chitosan spheres. Such physical anchors should always support the mechanical testing and enhance the properties because an extent of force is required to conquer the anchor points. However, anchoring between matrix and filler is very much dependent on their properties and particulate size **[Singla et al., 2016]**. The normalized Young's modulus i.e. $(E_c/X_c)/(E_p/X_p)$, is plotted against Φ_f as shown in Figure 7.9(c), which indicates that the values of normalized Young's modulus increase upto ~5.6% with an increase in Φ_f from 0-0.029 and further reduced significantly ~19.4% on increasing value of Φ_f upto 0.048. Such variation in normalized Young's modulus is observed due to the increment in rigidity of PLA/CH-*g*-OLLA bionanocomposite films as the crystallinity effect is excluded from the normalized data.

The experimental values of tensile strength decrease continuously ~30.4% with the increment in Φ_f upto 0.048 in PLA matrix as presented in Figure 7.9(d). The tensile strength versus percentage crystallinity plot also follows the similar pattern as displayed in Figure 7.9(d′). The associated reason is due to the reduction in load bearing cross-section of PLA/CH-*g*-OLLA bionanocomposite films. Similar results are observed by **Li et al., 2003** and **Sharma and Maiti, 2014** for PLA-lignin and polypropylene/SEBS-*g*-MA blends, respectively. The experimental values of relative tensile strength are plotted as a function of Φ_f, which are reduced continuously with an increase in filler volume fraction as shown in Figure 7.9(e). It indicates that the formed chemical structure of PLA/CH-*g*-OLLA bionanocomposite films is mechanically weak as

compare to that of pristine PLA. To develop the better understanding about composite structure, the experimental data of $\frac{\sigma_c}{\sigma_p}$ is correlated with the theoretical models i.e. Nicolais Narkis model and Nielsen model as mentioned in Eq. 7.6 and 7.7 respectively. The values of constants i.e. K and α used in Nicolais-Narkis model and Nielsen model respectively, are also calculated at various Φ_f values as mentioned in Table 7.2. The theoretical values of relative tensile strength are fitted well with the experimental values by using K ~1.448 in Nicolais-Narkis model and α ~5.197 in Nielsen model. It is concluded that Nielsen model has fitted much accurate than Nicolais-Narkis model as the theoretical values are very close to the experimental values at each Φ_f. The similar tests were performed for other polymeric systems such as PLA-lignin, polypropylene-talc and polypropylene-$CaCO_3$ composites in which the used α value was 1.25, 6.18 and 3.29 respectively **[Singla et al., 2016; Sharma and Maiti, 2014; Sewda and Maiti, 2007]**. The normalized tensile strength $(\sigma_c/X_c)/(\sigma_p/X_p)$ is plotted against Φ_f to distinguish between the response of phase adhesion and crystallinity as shown in Figure 7.9(f). The calculated values of normalized tensile strength are found higher than unity, which increase significantly with the increase in Φ_f values upto 0.029. The normalized tensile strength value reduces and is found below unity at Φ_f value of 0.048. It proves the strength of interphase between PLA and filler. However, the percentage crystallinity of PLA matrix reduces significantly with increase in Φ_f. The behaviour of elongation at break of PLA/CH-*g*-OLLA bionanocomposite films is completely opposite as compare to that of Young's modulus and tensile strength. The elongation at break of bionanocomposites increases ~47% with an increase in Φ_f as presented in Figure 7.10(a).

Table 7.2: Calculated values of coefficient of foamability (δ), adhesion parameter (K), stress concentration constant (α) and flexibility coefficient (β) in PLA/CH-*g*-OLLA bionanocomposite films.

Sample	Theoretical models			
	Modified Foam model (δ value)	**Nicolais-Narkis model (K value)**	**Nielsen model (α value)**	**Modified Mitsuishi model (β value)**
PLA	-	-	-	-
PLA/CH-*g*-OLLA (1%)	1.097	0.770	3.643	4.527
PLA/CH-*g*-OLLA (3%)	1.718	1.275	4.409	3.586
PLA/CH-*g*-OLLA (5%)	2.797	2.298	7.539	3.579
Mean value	1.871	1.448	5.197	3.897

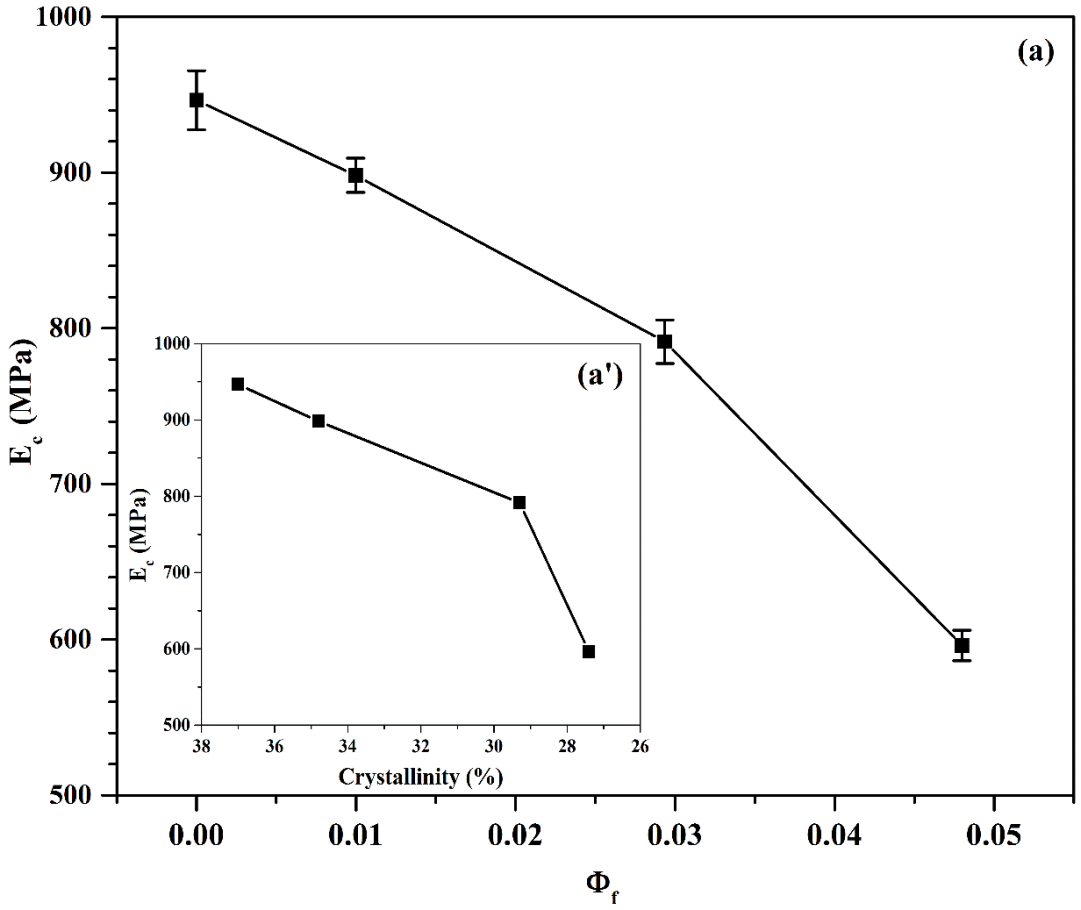

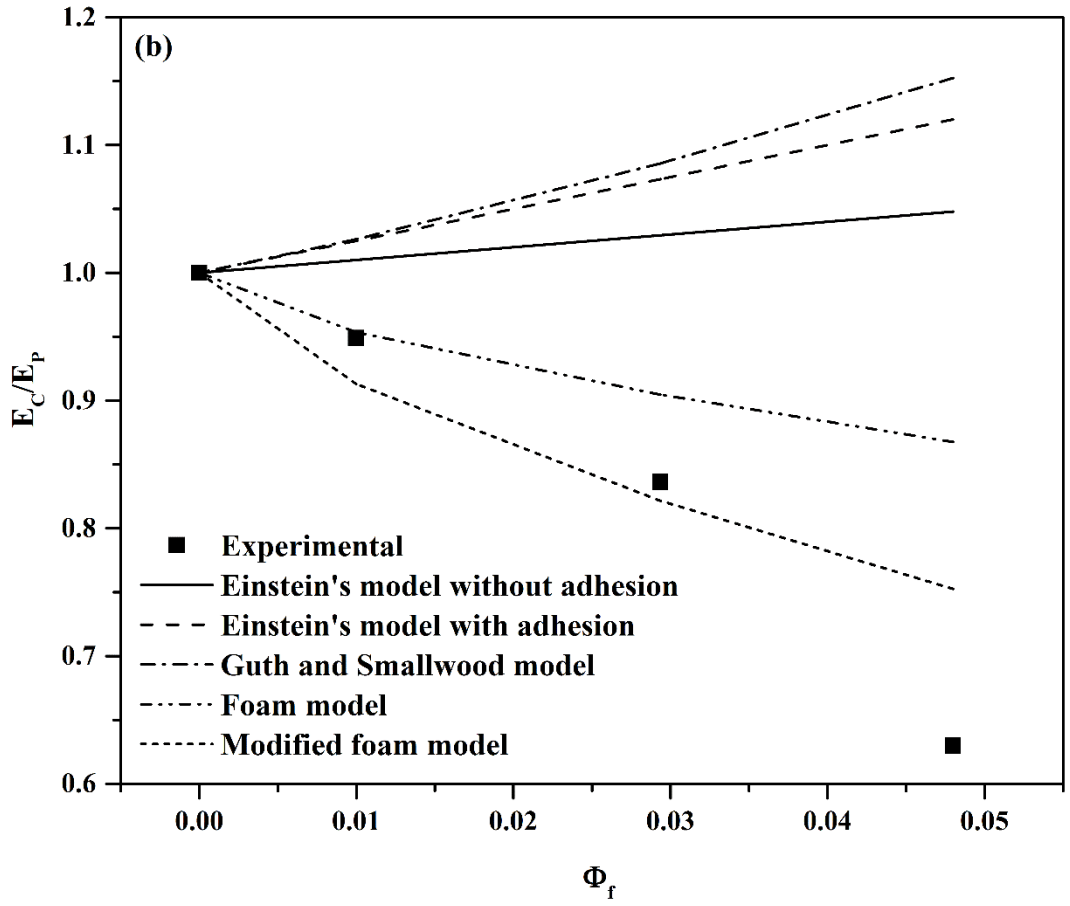

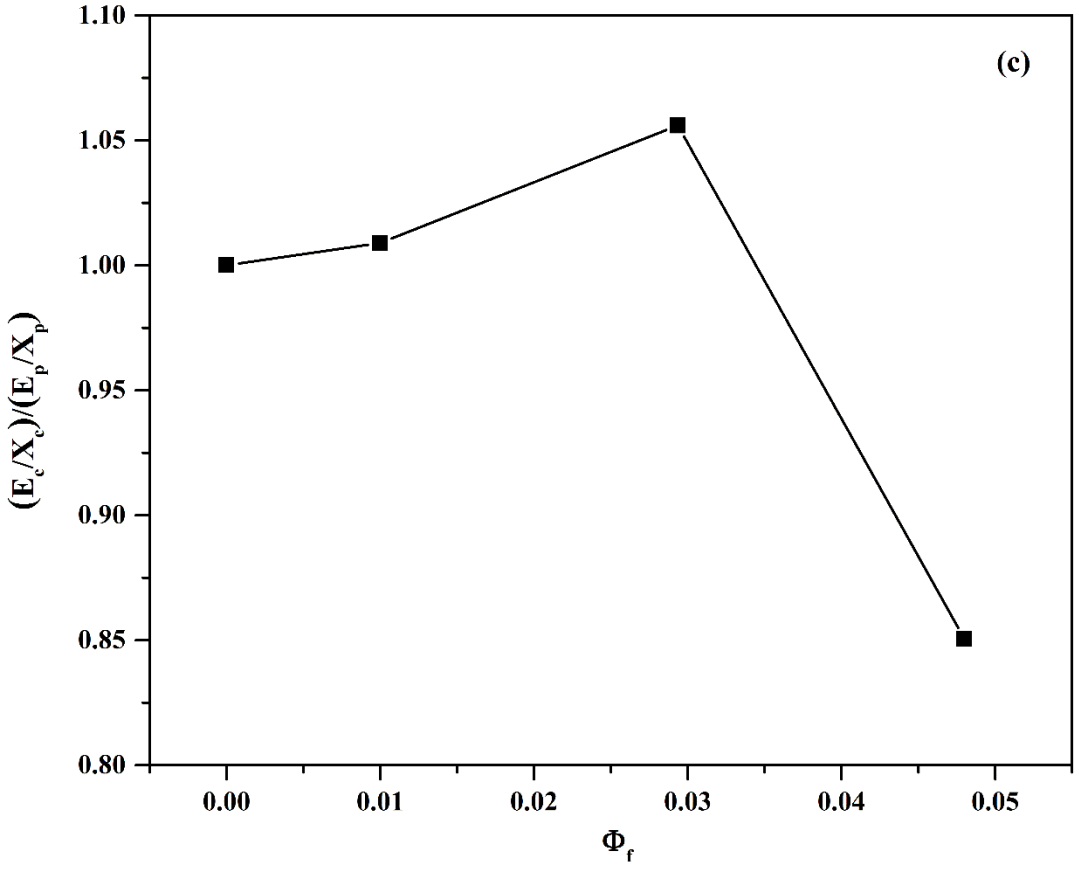

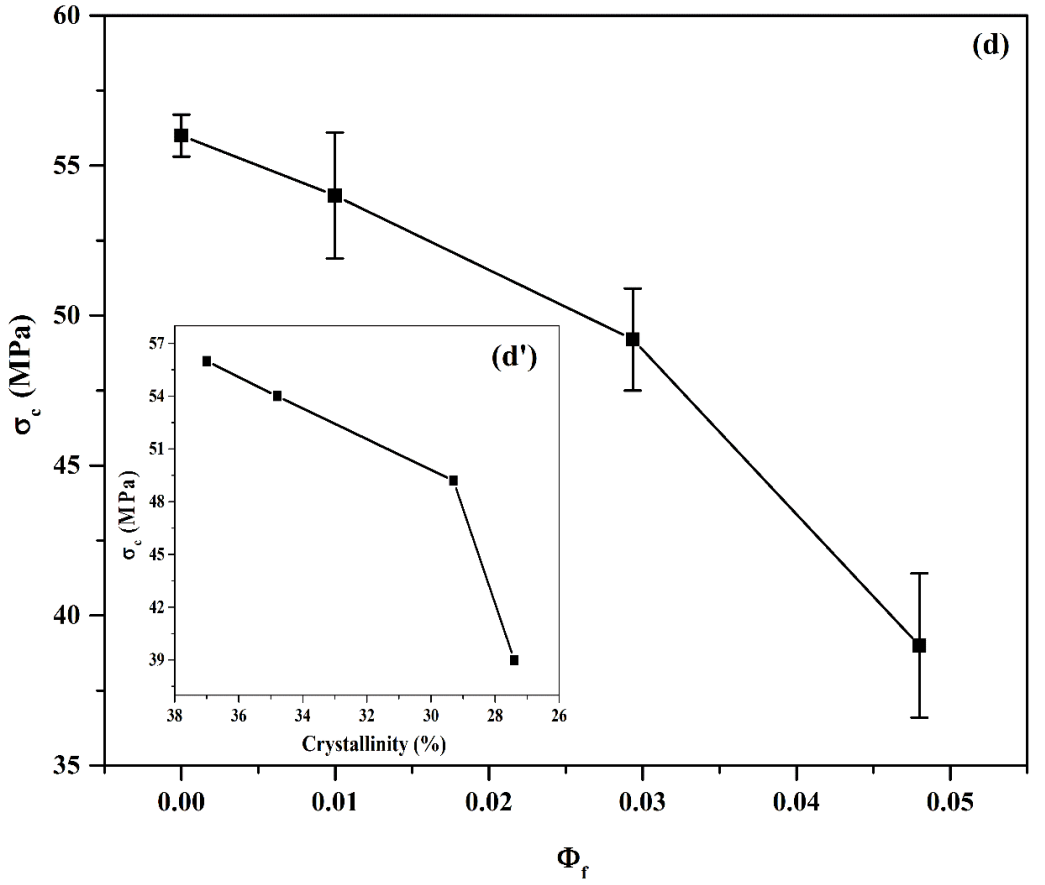

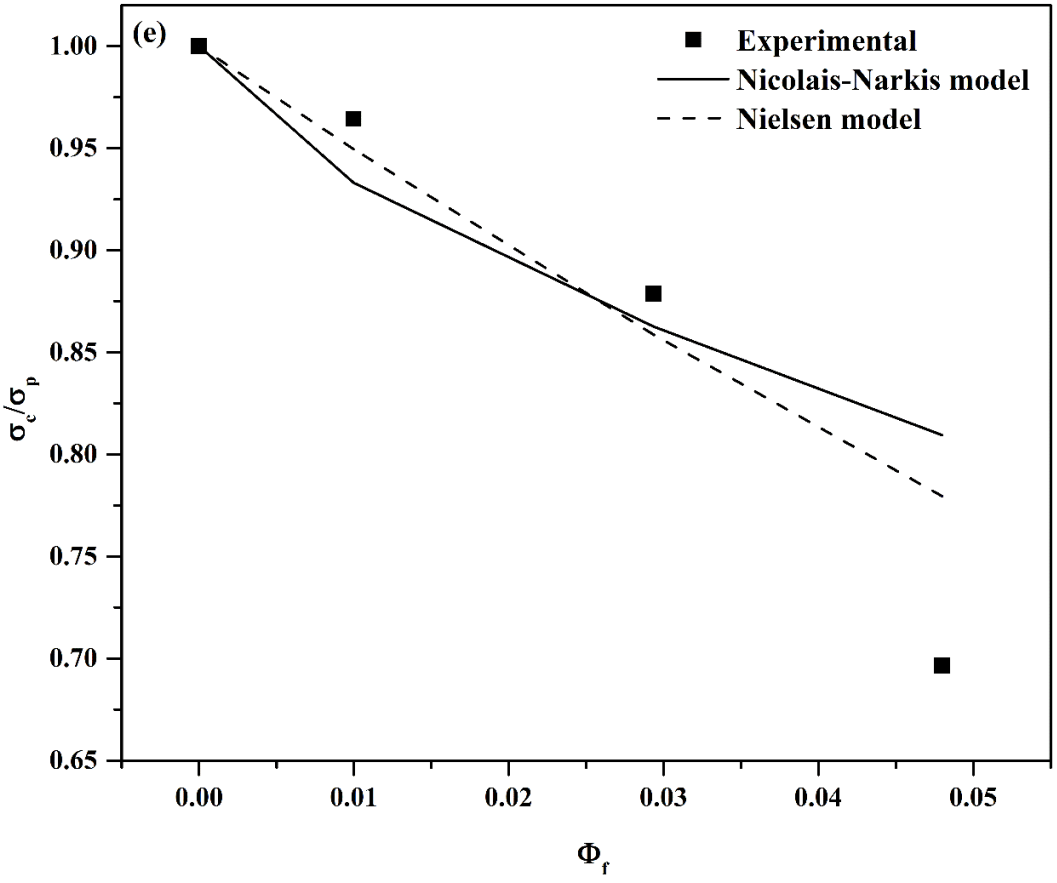

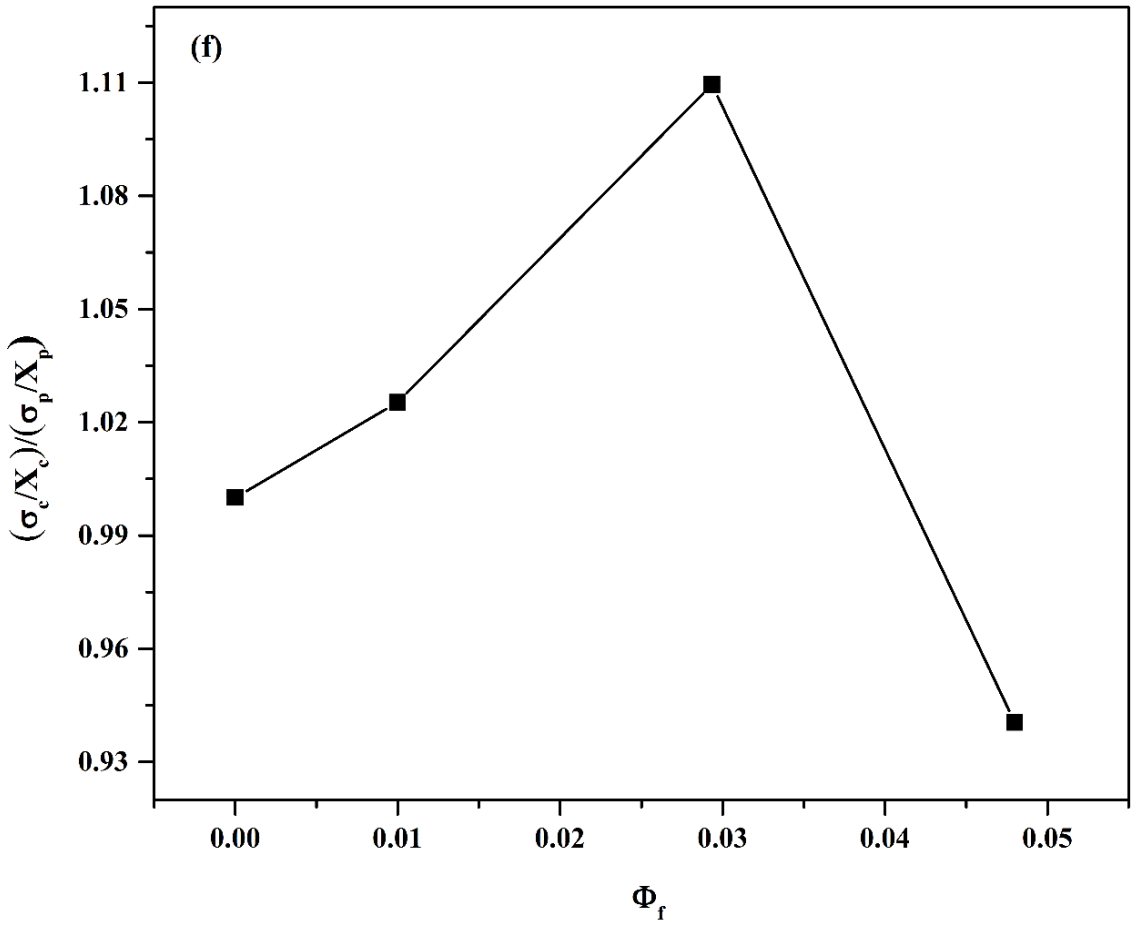

Figure 7.9. Variation in (a) Young's modulus (E_c) against volume fraction (Φ_f), (a′) Young's modulus against percentage crystallinity (X), (b) relative Young's modulus data against volume fraction using experimental values, Einstein's model without adhesion, Einstein's model with adhesion, Guth and Smallwood model and Foam model of Cohen and Ishai, (c) normalized Young's modulus against volume fraction, (d) tensile strength (σ_c) against volume fraction, (d′) tensile strength against percentage crystallinity, (e) relative tensile strength data against volume fraction using experimental values, Nicolais-Narkis model and Nielsen model, (f) normalized tensile strength against volume fraction of PLA films with respect to CH-*g*-OLLA weight percentage.

It significantly increases the stretchability of bionanocomposite films as compare to that of PLA as the plasticizing effect of CH-*g*-OLLA plays an important role. The elongation at break is plotted against percentage crystallinity of PLA/CH-*g*-OLLA bionanocomposite films as shown in Figure 7.10(a′) and found similar improvement in ε_c with decrease in X_c%, which is due to the reduction in strong adhesion between interphases and increment in free volume fraction in PLA.

The experimental values of relative elongation at break ($\frac{\varepsilon_c}{\varepsilon_p}$) increase from 1 to 1.47 (more than unity) with an increase in Φ_f as presented in Figure 7.10(b). The $\frac{\varepsilon_c}{\varepsilon_p}$ values are found more than unity, which means that a strong degree of adhesion exists between matrix and filler. The calculated data of $\frac{\varepsilon_c}{\varepsilon_p}$ is compared with well-established Nielsen's model and modified Mitsuishi model. The theoretical values of $\frac{\varepsilon_c}{\varepsilon_p}$, calculated by Nielsen's model are found much lower than that of experimental values for bionanocomposite films, which also confirms the strong adhesion between matrix and filler generated by polar interactions. However, the bionanocomposite films show higher softening effect than that of pristine PLA, which is included in modified Mitsuishi model in terms of flexibility coefficient. As a result, the theoretical data of $\frac{\varepsilon_c}{\varepsilon_p}$ shows a close agreement with the experimental values at each value of Φ_f. The calculated β values at various Φ_f are mentioned in Table 7.2 and the mean value (3.897) is used to calculate the theoretical values. The normalized elongation at break $(\varepsilon_c/X_c)/(\varepsilon_p/X_p)$ is determined as a function of Φ_f as shown in Figure 7.10(c), in which the values increase ~99% with the increment in Φ_f and the obtained values are much higher than unity. It also implies significant phase adhesion and chemical interaction between PLA and CH-*g*-OLLA **[Kakkar and Maiti, 2012]**.

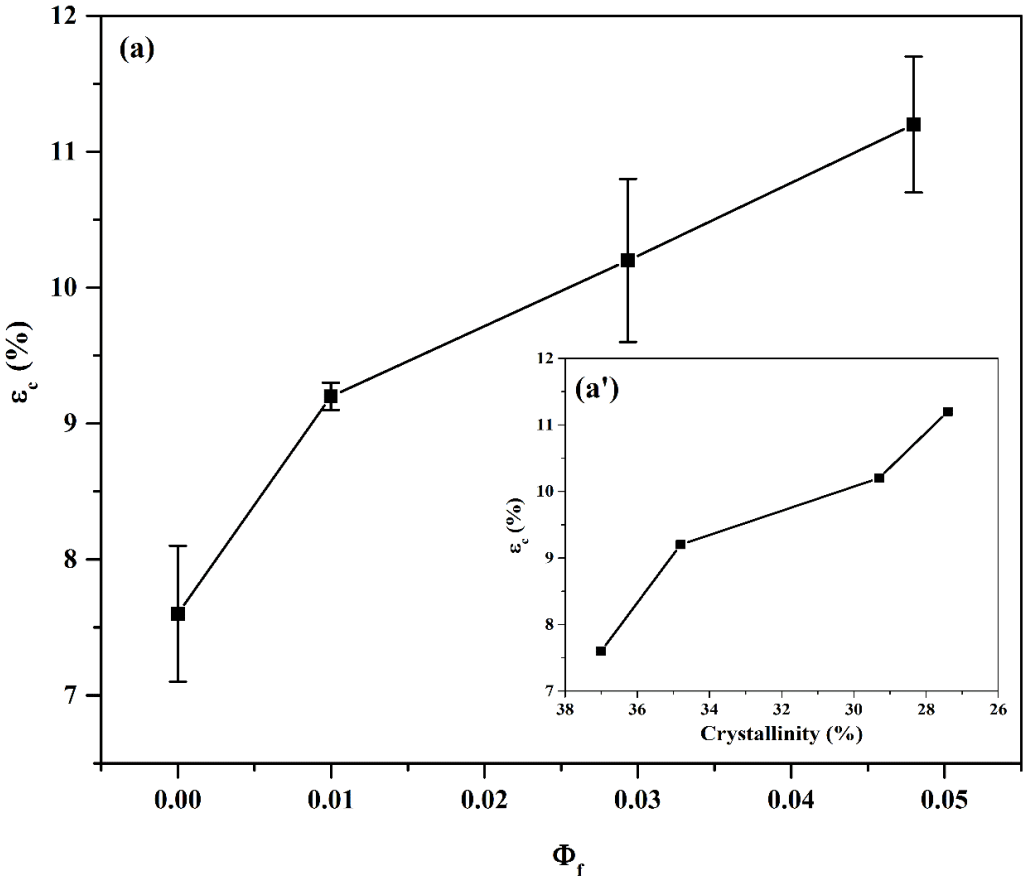

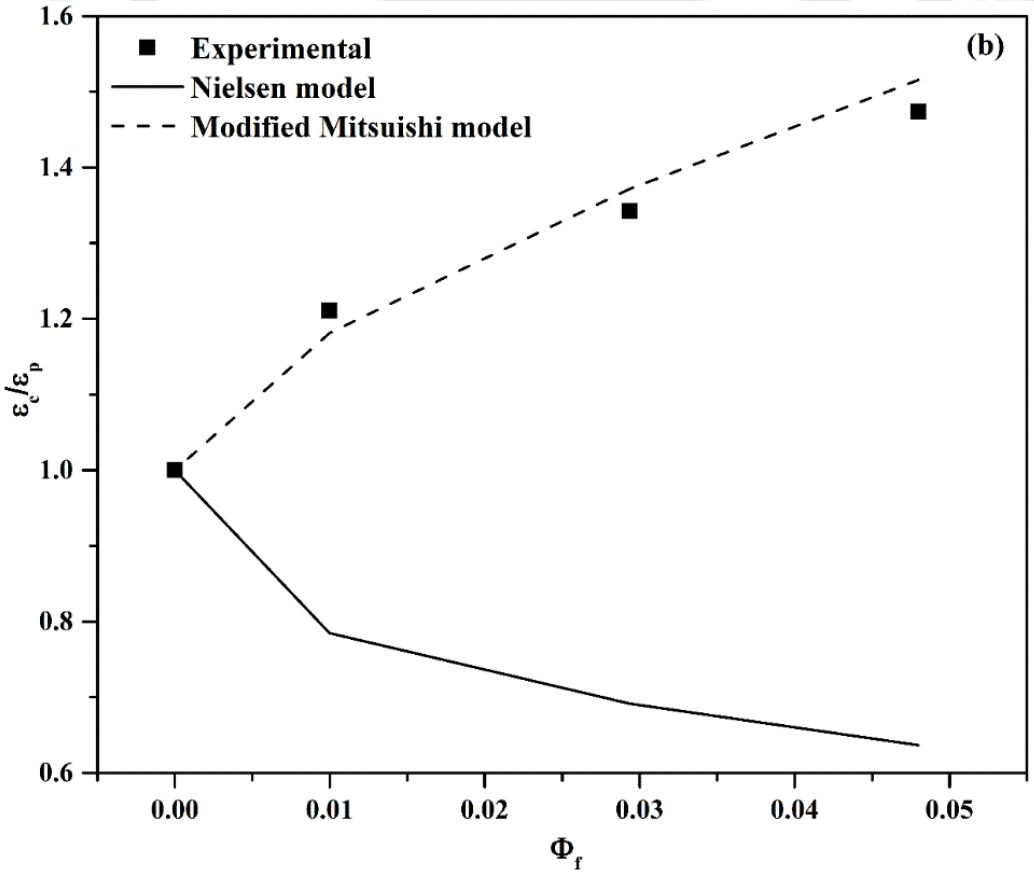

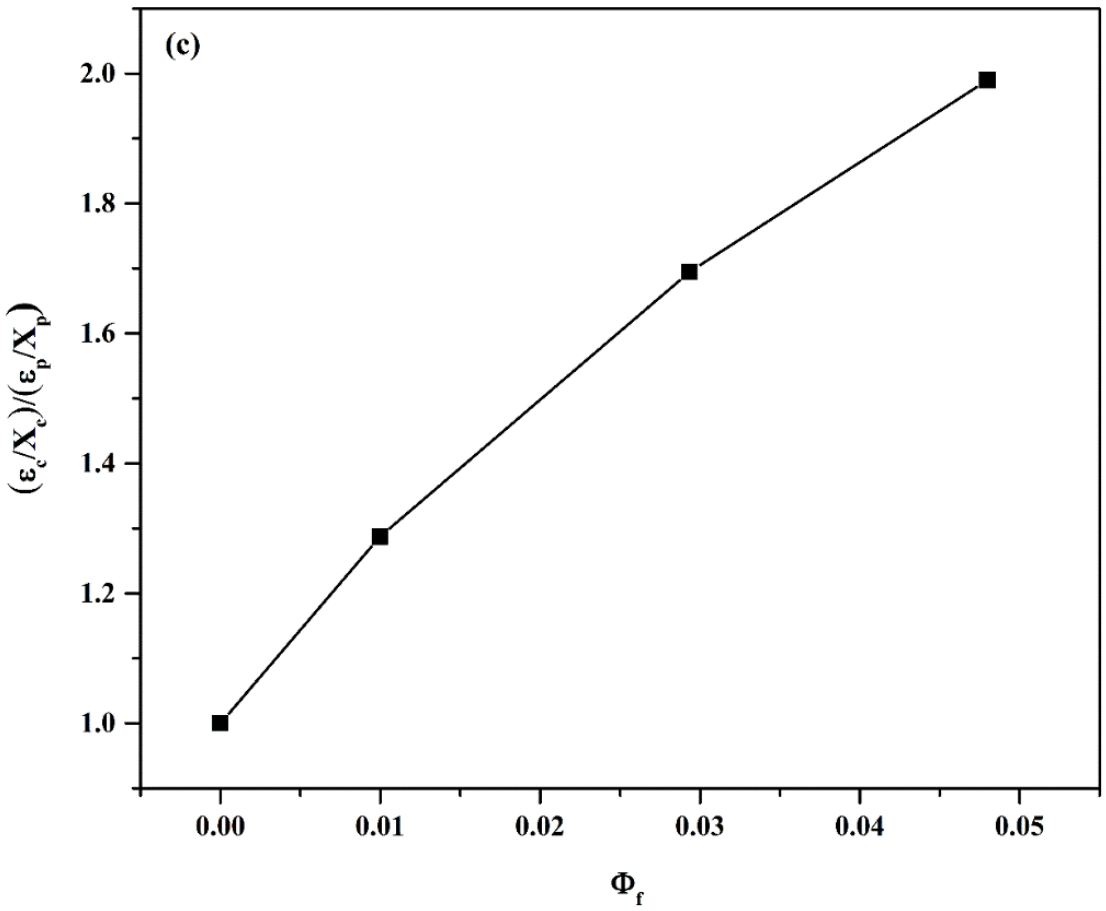

Figure 7.10. Variation in (a) elongation at break (ε) (%) against volume fraction, (a′) elongation at break against percentage crystallinity, (b) relative elongation at break data against volume fraction using experimental values, Nielsen model and modified Mitsuishi model and (c) normalized elongation at break against volume fraction of PLA/CH-*g*-OLLA bionanocomposite films.

7.2.11. Shore hardness test

The shore hardness test is performed using PLA and PLA/CH-*g*-OLLA bionanocomposite films and the variation is plotted as a function of filler wt% as shown in Figure 7.11. The mean hardness value of melt blended pristine PLA film is measured ~81.8±0.8. Other researchers such as **Hamad et al., 2015, Graupner and Mussig, 2011,**

Jamshidian et al., 2010 and Ma et al., 2012 have also measured the hardness value of PLA i.e. 86, 81.5, 88 and 86 respectively, which are very close to the value mentioned in this research work. It is observed that the shore hardness value of PLA is reduced ~0.9, 6 and 25.7% with the addition of 1, 3 and 5 wt% filler respectively. It is due to the presence of low molecular weight filler in PLA matrix, which is elastomeric in nature. Hence, PLA becomes more ductile due to CH-*g*-OLLA copolymer, which is favourable during thermoforming and extrusion **[Byrne et al., 2009]**.

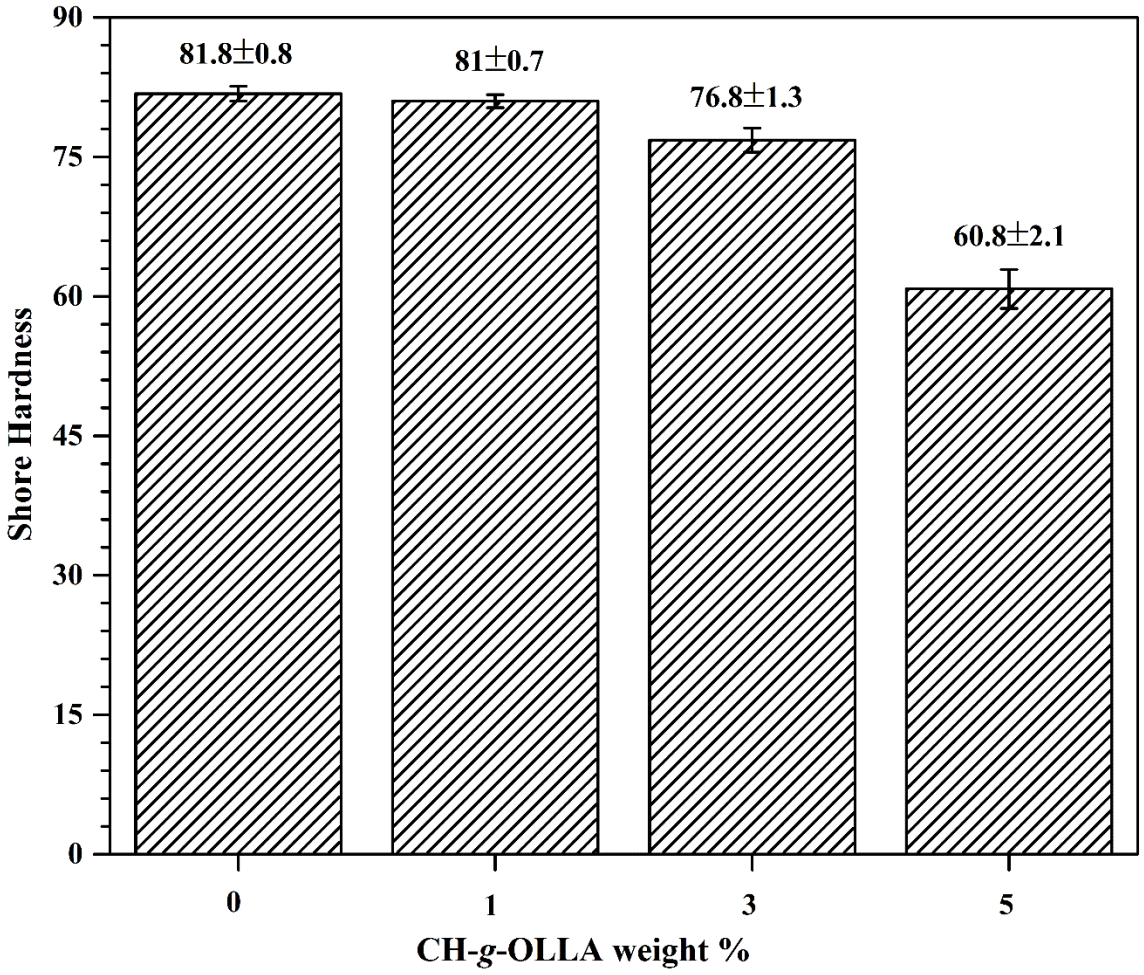

Figure 7.11. Variation in shore hardness of PLA films with respect to CH-*g*-OLLA wt %.

7.2.12. Water vapour transmission rate (WVTR)

The effect of CH-*g*-OLLA copolymer on the WVP values of PLA film is noticed at 37.8±0.5ºC and 50% RH as displayed in Figure 7.12. The WVP value of PLA is calculated ~1.33±0.02 cc.mm/m^2.day.kPa, which is very close to the WVP values published in literatures **[Dhar et al., 2015]**. The increment of ~5.3, 8.3 and 9% is estimated in WVP values of melt extruded PLA film with an increment of 1, 3 and 5 wt% in nano-filler loadings due to the reduction in percentage crystallinity of polymer nanocomposites (as mentioned in XRD analysis), which may increase the amorphous phase in PLA/CH-*g*-OLLA bionanocomposite films.

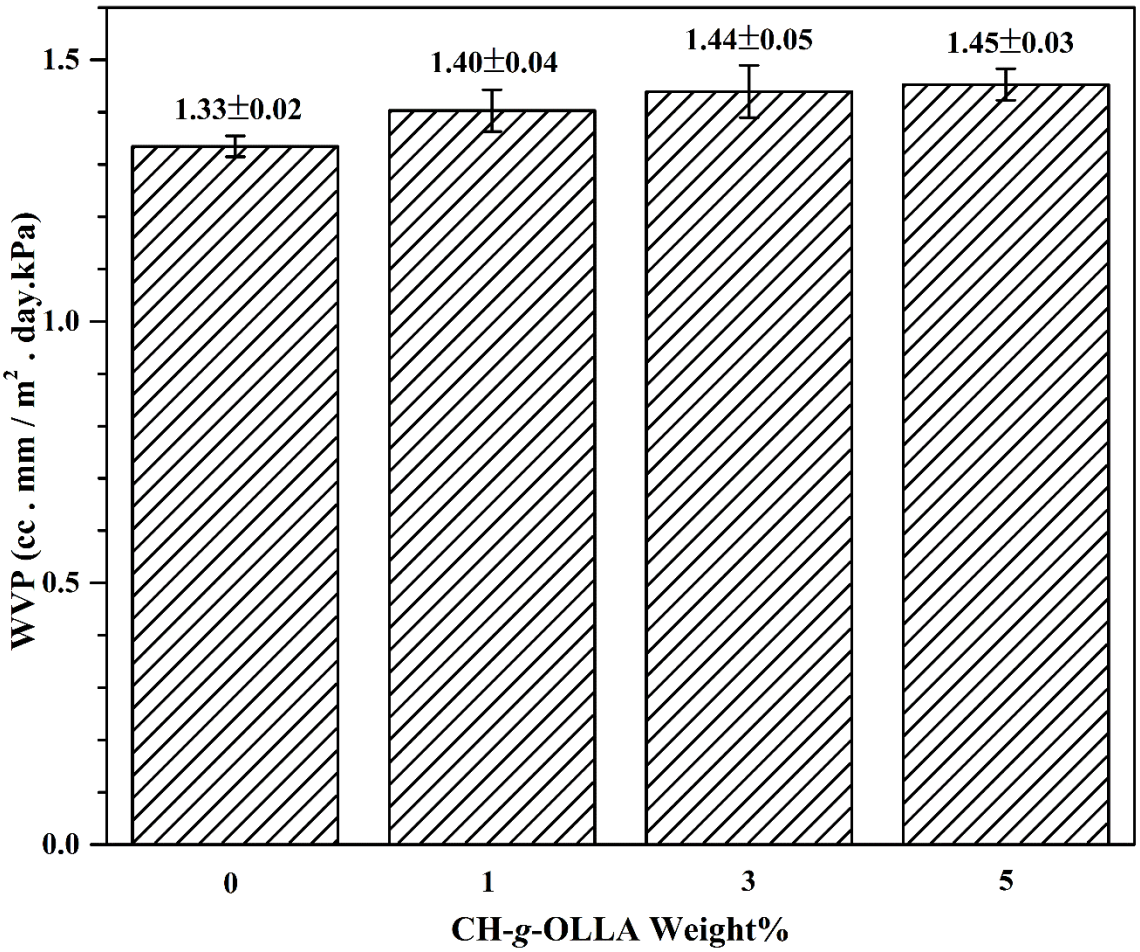

Figure 7.12. Variation in water vapour permeability in PLA and PLA/CH-*g*-OLLA bionanocomposite films.

The amorphous phase supports the transportation of water molecules across the film. The agglomeration of nano-filler at higher loadings (shown in TEM analysis) may also responsible for the increment in WVP values. The presence of free carboxyl and hydroxyl groups in PLA/CH-*g*-OLLA bionanocomposite films are hydrophilic in nature and attract more water molecules as compare to control film, which can also increase the WVP values.

7.2.13. Oxygen transmission rate (OTR)

The transportation behaviour of oxygen molecules across the melt extruded PLA film is characterized by determining the values of oxygen permeability, diffusivity, solubility and their variation with an increase in filler weight percentage is composed in Figure 7.13(a) and (b). A significant reduction of ~82.7% is observed in oxygen permeability of PLA film only by the addition of 1 wt% of nano-filler and it is further reduced upto ~90.2 and ~90.4% by adding 3 and 5 wt% of CH-*g*-OLLA respectively in PLA matrix. This huge reduction in OP is due to the formation of complex network structure between filler and matrix.

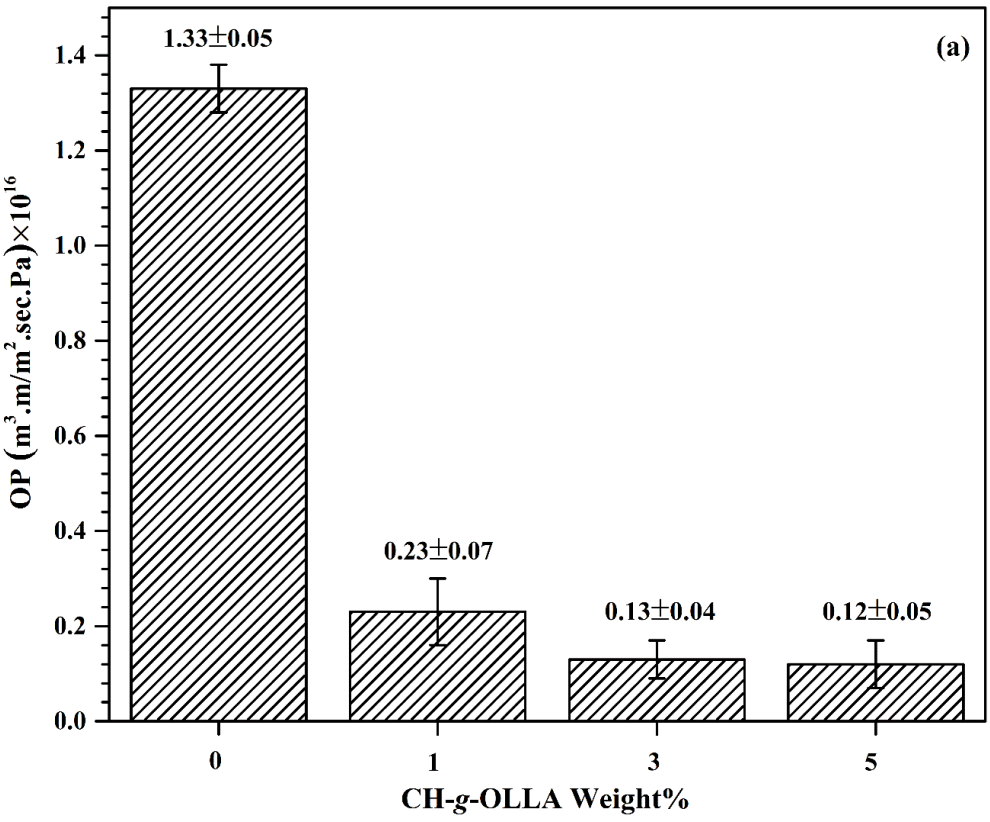

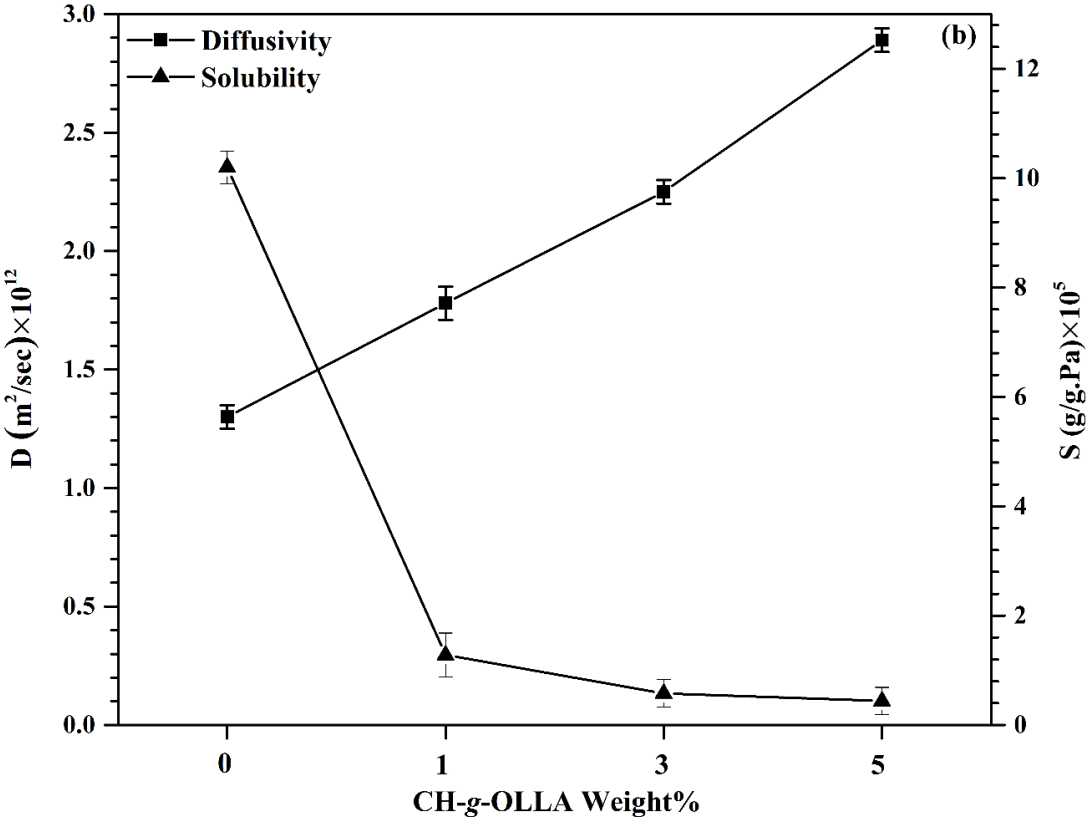

Figure 7.13. Variation in (a) oxygen permeability and (b) diffusivity and solubility with respect to filler loading in PLA and PLA/CH-*g*-OLLA bionanocomposite films.

The calculated value of diffusivity for PLA film is increased significantly upto ~37, ~73 and ~75% with the inclusion of 1, 3 and 5 wt% of nano-filler respectively due to the agglomeration of nano-particles. However, the solubility of oxygen across the PLA film is drastically reduced upto ~87.5, ~94.3 and ~95.7% by adding 1, 3 and 5 wt% of CH-*g*-OLLA respectively as shown in Figure 7.13(b). Hence, it is confirmed that the solubility of oxygen molecules through the films is the governing parameter because the difference in the values of diffusivity and solubility is of the order of 10^7, which signifies a clear increment in the resistance of oxygen permeation across PLA/CH-*g*-OLLA bionanocomposite films due to the increment in the retention of oxygen molecules as the number of the active sites increases with the addition of nano-filler. The homogeneous

dispersion of nano-filler in PLA matrix, amide ester linkage, hydrogen bonding and other chemical interactions between filler and matrix may further decrease the value of solubility coefficient.

7.2.14. Optical properties

Optical properties of PLA/CH-*g*-OLLA bionanocomposite films are important parameters in packaging applications as well as its acceptability by end users **[Dadashi et al., 2014]**. The variation in colour parameters is noticed by the addition of CH-*g*-OLLA copolymer as mentioned in Table 7.3. The value of L* for melt extruded pristine PLA film is measured as 90.83±0.11, which is found close to the values i.e. 97.26±0.02 and 92.1±0.2 obtained by **Byun et al., 2010** and **Samsudin et al., 2014** respectively. The L* value is decreased ~12.6, ~20.9 and ~41.7% with the addition of 1, 3 and 5 wt% filler in PLA matrix due to the reduction in whiteness. The dark brown colour of the nano-filler is responsible for such reduction in whiteness. The magnitude of whiteness shows the ability of light reflection, which favour to show vibrant colours. Hence, better visualization is occurred in PLA film **[Cheng et al., 2016]**. The value of a* increases significantly from -0.31±0.001 to 8.73±0.04, which denotes the drastic increment in redness and reduction in greenness of PLA/CH-*g*-OLLA bionanocomposite films. The increment in b* values i.e. from 4.67±0.02 to 27.35±0.03 is detected in PLA films due to the uniform dispersion and increment in filler loadings. Such increment in b* values reflects the enhancement in yellowness due to the effect of temperature at the time of processing, which may cause degradation in film samples **[Ahmadzadeh et al., 2016]**. The value of ΔE* is determined as 0.14±0.11 for PLA film, which increases significantly upto 45.01±0.28 with the addition of 5 wt% of filler due to observe the significant change in colour between PLA and PLA/CH-*g*-OLLA bionanocomposite films. The value of C* also increases from 4.68±0.06 to 28.71±0.03 with the increase in filler loading, which indicates the increment in the saturation of colours.

Table 7.3: Calculated various parameters of colour measurement for PLA and PLA/CH-*g*-OLLA bionanocomposite films.

Sample	L*	a*	b*	ΔE*	C*
PLA	90.83±0.11	-0.31±0.001	4.67±0.02	0.14±0.11	4.68±0.06
PLA/CH-*g*-OLLA (1%)	79.37±0.21	1.65±0.05	15.27±0.08	15.66±0.23	15.36±0.03
PLA/CH-*g*-OLLA (3%)	71.86±0.14	3.53±0.07	20.73±0.11	25.07±0.13	21.04±0.07
PLA/CH-*g*-OLLA (5%)	52.90±0.26	8.73±0.04	27.35±0.03	45.01±0.28	28.71±0.03

7.2.15. Lamination of PLA/CH-*g*-OLLA bionanocomposite films

An industrially viable 'lamination technology' is developed for the lamination of various layers of polymers and polymer composites to obtain a single sheet of laminated polymers with superior properties. The lamination is completely a thermal phenomenon in which the stacked polymeric layers pass in between the two rollers, which are heated at constant temperature and rotate on their axis at a constant speed with a degree of separation based on the thickness of polymer films. In the present research work, we successfully demonstrate the lamination of PLA with PLA/CH-*g*-OLLA bionanocomposite films at particular conditions by rotating hot press as shown in Figure 7.14(a), (b) and (d). Figure 7.14(a) and (b) display the logos of our institute in which one is laminated with the help of two PLA films and other is laminated with one PLA and one PLA/CH-*g*-OLLA bionanocomposite films respectively. It is meaningful to mention that the transparency of both laminated films are quite impressive, however, it is higher for laminated PLA films than that of laminated composite films. Figure 7.14(c) clearly demonstrates the schematic of filler's geometry i.e. three dimensional spheres with core-shell morphology (mentioned in TEM analysis), which present in PLA films. The schematic representation of lamination process of two PLA/CH-*g*-OLLA bionanocomposite films is displayed in Figure 7.14(d), which clearly shows the difference in surface morphology before and after lamination with

the help of images captured by optical microscope (Eclipse LV100N POL, Nikon Co., Japan).

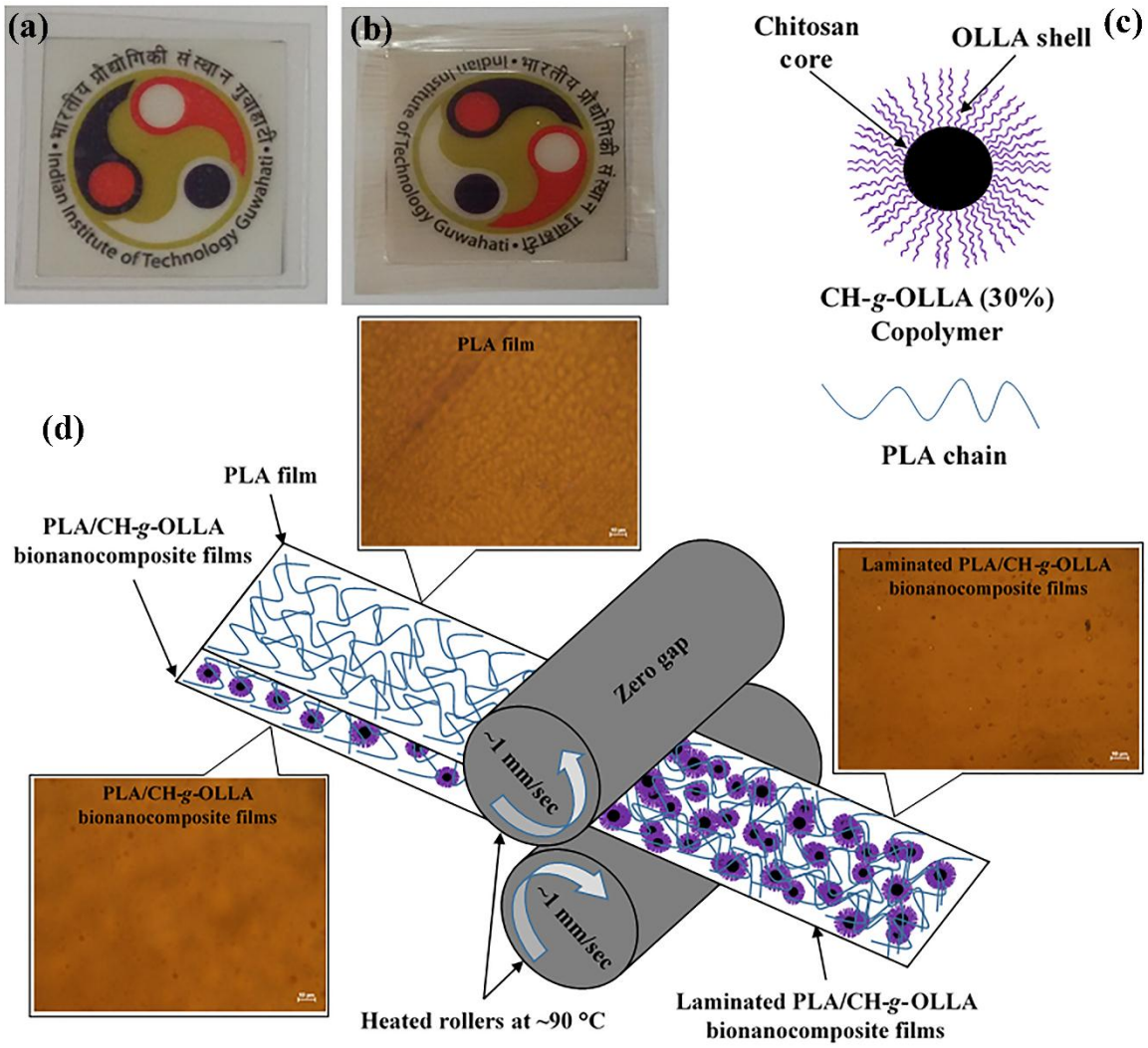

Figure 7.14. Laminated IITG logo with (a) pristine PLA films, (b) PLA/CH-*g*-OLLA bionanocomposite films; (c) the schematic representations of CH-*g*-OLLA (30%) copolymer and PLA chain and (d) lamination procedure of PLA/CH-*g*-OLLA bionanocomposite film with PLA at 90 °C.

The number of filler particles, PLA chain entanglement and their interactions in bionanocomposite film increase after lamination. The formation of such complex network

may interrupt the diffusion of oxygen and other gases across the laminated film and improves the gas barrier properties. Other physico-chemical properties can also be improved due to the evolution of an interlocking pattern among polymeric chains, interfacial bond strength, inter and intra molecular hydrogen bonding between filler-filler, matrix-matrix and filler-matrix **[Huda et al., 2008; Rhim, 2013]**.

7.2.16. Dynamic mechanical analysis of laminated PLA/CH-*g*-OLLA bionanocomposite films

The storage modulus, loss modulus, damping factor and elongation (dL) of neat PLA, PLA/CH-*g*-OLLA and laminated PLA/CH-*g*-OLLA bionanocomposite films are measured at 3 °C/min in the temperature range of 20-100 °C as shown in Figure 7.15(a) and (b). The E′ values of PLA, PLA/CH-*g*-OLLA and laminated PLA/CH-*g*-OLLA bionanocomposite films decrease continuously with an increase in temperature and become zero at 95 °C. The value of E′ represents polymer hardness and elastically stored energy at the time of deformation process. At higher temperature (~95 °C), the chains mobility in the polymers may increase and causes the reduction in hardness. However, the E′ value of PLA increases ~23% with the addition of nano-filler due to the transfer of load to both filler and matrix as shown in Figure 7.15(a). The value of E′ of laminated PLA/CH-*g*-OLLA bionanocomposite films increases drastically upto ~86% as compare to that of pristine PLA because lamination helps to improve the dispersion of nano-filler in PLA matrix and polymer-filler interface becomes proper, which restricts the molecules for their rotational and translational motions. As a result, E′ increases significantly after lamination. The loss modulus represents energy dissipation, however, it is stiffness or hardness of a polymer. The highest values of E" are detected at 43.4, 24 and 63 °C in the case of PLA, PLA/CH-*g*-OLLA and laminated PLA/CH-*g*-OLLA bionanocomposite films respectively, which represent the viscous properties of polymer used. At this temperature, the molecular segmental motions

occur with difficulty, which dissipates much of the force. The highest value of tan δ at a particular temperature corresponds to the glass transition temperature of polymer. The peaks of tan δ are observed at 55.4, 51.2 and 66.3 °C for PLA, PLA/CH-*g*-OLLA and laminated PLA/CH-*g*-OLLA bionanocomposite films respectively as shown in Figure 7.15(b). The values of temperature denote the glass transition temperature of particular polymer, which are very close to DSC analysis. The T_g value of PLA reduces ~7.6% with the addition of CH-*g*-OLLA due to the plasticization effect. However, the T_g value of laminated PLA/CH-*g*-OLLA bionanocomposite film increases significantly (upto ~19.7%) as compare to that of PLA due to the strong chain to chain interaction between matrix-matrix and filler-matrix. It is observed that the elongation takes place for all the cases, which increases with an increase in temperature after T_g. In the case of PLA film, the elongation increases slowly in the complete range of temperature. However, a rapid increase in elongation is observed for PLA/CH-*g*-OLLA bionanocomposite film as shown in Figure 7.15(b). It is also noticeable that a remarkable improvement in elongation is recognized for laminated PLA/CH-*g*-OLLA bionanocomposite film. Such an immense improvement in elongation is due to the existence of mechanical interlocking, which generates high stress bearing zones at contact locations and hence, the reinforcing effect is improved. In such a way, the mechanical properties of polymers and polymer composites can be tuned for specific applications by using lamination technique.

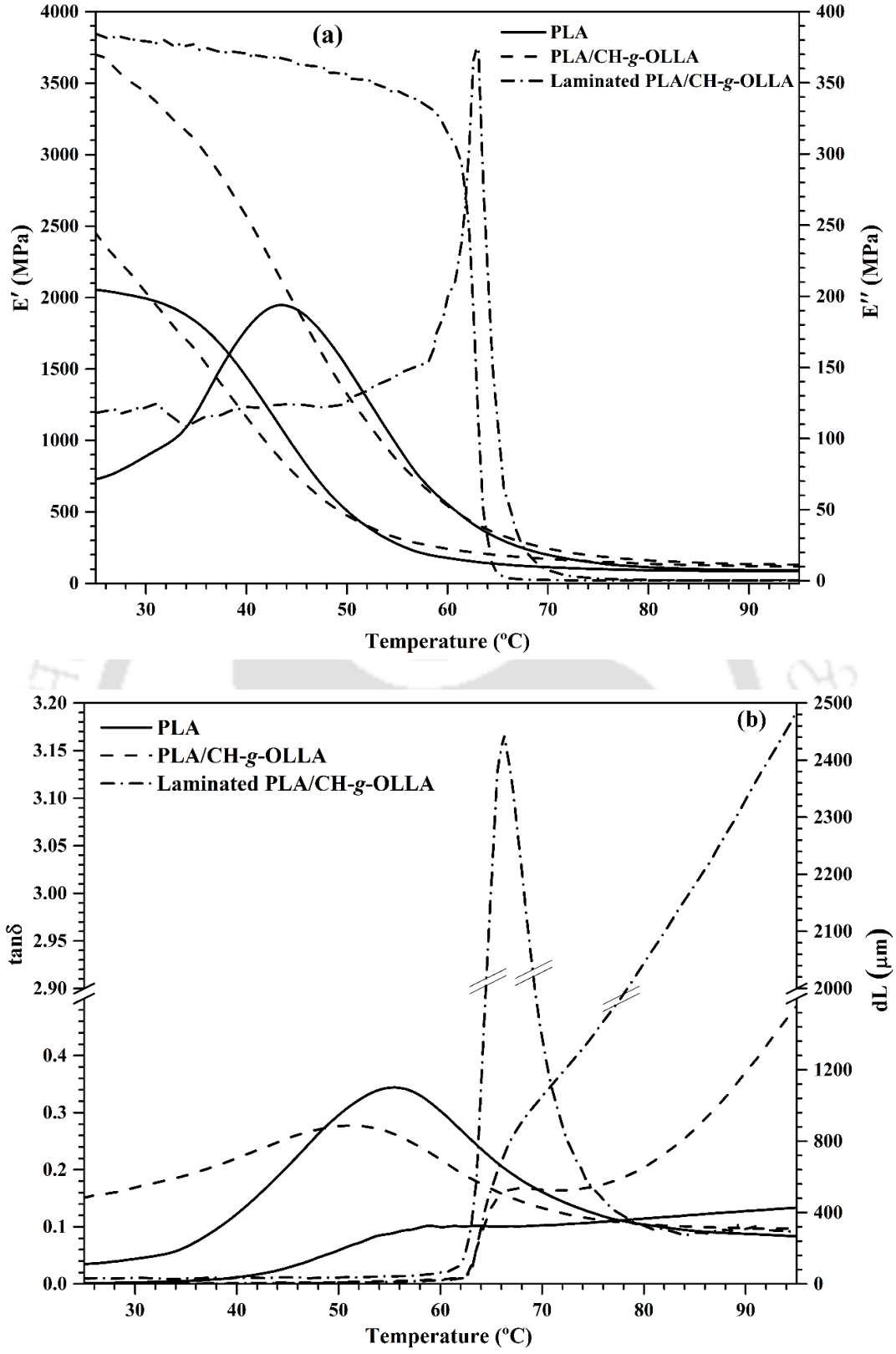

Figure 7.15. Variation in (a) storage modulus, loss modulus and (b) damping factor and change in elongation against temperature for PLA, PLA/CH-*g*-OLLA and laminated PLA/CH-*g*-OLLA bionanocomposite films.

7.3. Summary

The synthesized nano-filler was melt extruded with PLA in various proportions at lab scale as well as pilot plant scale by using co-rotating mini twin screw extruder and large twin-screw extruder having throughput of ~10 kg polymer/h respectively. The fabricated PLA/CH-*g*-OLLA bionanocomposite films were structurally characterized with the help of FTIR, WXRD and GPC analyses. FTIR confirmed the formation of new chemical bond i.e. amide ester linkage between chitosan and OLLA with the help of new peak, which was appeared only in PLA/CH-*g*-OLLA bionanocomposite films at 1539 cm^{-1}. XRD analysis showed a gradual reduction of ~26% in percentage crystallinity of extruded PLA film with an increase in CH-*g*-OLLA wt%. The GPC analysis corroborated with the reduction of ~23% and ~15% in M_n and M_w of PLA by adding a low molecular weight filler upto ~5 wt%. The lowering in molecular weight was due to the breakage of longer PLA chains. The glass transition and crystallization temperatures of PLA were decreased upto ~11.3 and ~11.8 ºC with the addition of 5 wt% of nano-filler. It was due to the reduction in molecular weight, which enhances the molecular mobility of polymer chains. The thermal stability of extruded PLA/CH-*g*-OLLA bionanocomposite films was reduced ~7.9 °C by adding 5 wt% of nano-filler in PLA matrix. During TGA analysis, the maximum weight loss percentage in PLA was observed as ~96, ~95, ~89 and ~84% at peak degradation temperature by adding 1, 3 and 5 wt% nano-filler, which confirmed the single step degradation. It is noteworthy to mention that the degradation temperature of bionanocomposite films was higher than the processing temperature of PLA. Melt extruded PLA/CH-*g*-OLLA bionanocomposite films have shown excellent oxygen barrier as compare to that of PLA. The addition of 5 wt% of nano-filler in PLA matrix reduced the values of oxygen permeability upto ~90.4%. The associated reason with such drastic reduction in OP is the formation of impermeable network structure and unavailability of

active sites for the diffusion of oxygen molecules. Solubility is also the main factor for ~10 fold reduction in OP, which was also proved by detecting a drastic reduction of ~95.7% in the solubility of oxygen across PLA/CH-*g*-OLLA bionanocomposite film. Further, the lamination of PLA with PLA/CH-*g*-OLLA bionanocomposite film was successfully performed at ~90 °C with the roller speed of ~1 mm/sec, which have shown a significant improvement in storage modulus and elongation as compare to that of PLA film. Hence, the developed PLA/CH-*g*-OLLA and laminated PLA/CH-*g*-OLLA bionanocomposite films have potential to replace fossil based conventional plastics used in packaging applications.

Chapter 8

Thermal Degradation Behaviour of Poly (Lactic Acid)/Chitosan based Films

In this chapter, the extracted chitosan from Muga silkworms and synthesized CH-g-OLLA (30%) copolymer are used as filler in PLA/CH biocomposite and PLA/CH-g-OLLA bionanocomposite films. Non-isothermal degradation kinetics, proposed by Kissinger, Kissinger-Akahira-Sunose, Flynn-Wall-Ozawa and Augis & Bennett models, are utilized to estimate the activation energies (E_a) for PLA, which are 254.1, 260.2, 257.0 and 259.1 kJ/mol respectively. The reduction in E_a values of both types of films may be elucidated by intermolecular distance and enrichment in chain mobility. The evolved gaseous products like hydrocarbons, carbon dioxide, carbon monoxide and cyclic oligomers are successfully identified with hyphenated TG-FTIR analysis in the case of PLA/CH-g-OLLA bionanocomposite films.

8.1. Introduction

Reuse and recycling is a growing area of research which enhances value to the non-degradable polymeric waste. The environmental impact of degradable conventional synthetic polymers (considering time scale) are increasing continuously due to their huge applications in daily life. Biodegradable polyesters are explored as an alternative to replace the synthetic polymers to improve the environmental balance. One of the potential candidate among biodegradable polymers i.e. poly (lactic acid) is utilized in various applications due to its origin. It has also acquired much awareness for its use in medical, pharmaceutical and other consumer goods **[Fan et al., 2004]**. The limitations of PLA are its thermal and photo-stability, which restrict the use of PLA for most engineering applications. The associated reason is that the repeat unit of aliphatic ester in PLA is sensitive to heat and easily breakdown during hydrolysis **[Fan et al., 2004]**. Hence, thermal degradation analysis is a unique part to understand the thermal behaviour of PLA with its degradation mechanism and formed products in the interest of the improvement in thermal stability of PLA. Various components such as molecular weight distribution, residual oligomers & monomers and metal catalyst influence the thermal degradation of PLA **[Tsuji and Fukui, 2003]**. According to the available literatures, the degradation products of PLA are mainly composed of cyclic oligomers with lactides having other products like acetaldehyde, carbon monoxide, carbon dioxide and ketene **[Fan et al., 2004; Li et al., 2009]**. Many researchers have performed thermal degradation kinetics study for PLA and its composites films [**Fan et al., 2004; Tsuji and Fukui, 2003; Li et al., 2009**]. **Aoyagi et al., 2002** has calculated the activation energy (E_a) value in the range of 80 to 160 kJ/mol for PLA, which increases with an increase in conversion values and finally concluded that degradation of PLA follows two mechanisms. **Wu et al., 2008** has studied the deviation in thermal stability of PLA by adding multi-walled carbon nanotubes

(MWCNTs) as a filler. They have concluded that the change in thermal stability was very less at the initial degradation stage. However, it has improved slightly at higher degradation level. Another study on thermal degradation was conducted by **Wu and Wu., 2006** by using poly lactide/clay nanocomposites (PLACNs) and found the reduction in thermal stability with increasing clay content in PLA matrix. **Li et al., 2009** has used Flynn-Wall-Ozawa and invariant kinetic parameter (IKP) methods to calculate the E_a values of PLA and PLA modified with hydroxyapatite nanoparticles (PLA/g-HA). The calculated $E_a$values from both the methods were close to each other and varied from 152 to 166 kJ/mol for PLA/g-HA and PLA films. They concluded that the thermal stability increases but E_a value decreases with an increase in g-HA. Many researchers have utilized other various methods such as oxidative degradation and photo degradation with thermal degradation to understand the degradation behaviour of polymers.

Chitosan is also one of the most promising biopolymer, which has ability to change the current scenario of consumption of conventional synthetic polymers in various applications **[Balau et al., 2004; Muraleedharan et al., 2015]**. The limitations of chitosan are its hydrophilic nature and solubility which restrict it to be used in packaging and other applications. Chitosan may be utilized in food packaging application, if its hydrophilic nature converts into hydrophobic, which can be possible by modification of chemical structure of chitosan by attaching some other hydrophobic polymer as a side chain. Such modifications are really helpful to encourage the growth of biopolymers at industrial scale and further promotes the reduction of fossil fuels based conventional polymers. It is also necessary to have the knowledge about the thermal degradation behaviour of polymers to make it viable at industrial scale. In this line, **Georgieva et al., 2012** has used non-isothermal degradation kinetics to calculate $E_a$value of chitin and chitosan from crab shells by using Coats-Redfern and Kissinger-Akahira-Sunose (KAS) methods. The two

stage decomposition was detected for both the samples. For the first stage degradation, the $E_a$values of chitin and chitosan were found ~154 and 126 kJ/mol respectively. Whereas, $E_a$values were calculated as 114.8 and 99.1 kJ/mol for the second stage degradation. **De Britto and Campana-Filho, 2007** performed thermal decomposition of chitosan under isothermal and non-isothermal conditions by using FWO and Kissinger methods. The $E_a$values for chitosan were obtained ~138.5 and 149.6 kJ/mol by Kissinger and FWO models respectively. Whereas, the $E_a$value was calculated ~153 kJ/mol under isothermal condition. A thermal degradation kinetic study of chitosan and N,N,N-trimethyl chitosan was also carried out by **De Britto and Campana-Filho, 2004**. The study suggests that the thermal stability was reduced due to the methylation of chitosan. The similar trend of $E_a$values has also been calculated by Broido's and MacCallum's methods. MacCallum's method explains that $E_a$value decreases with increase in degree of methylation. **Ou et al., 2010** developed a chitosan-cobalt complex and performed thermal degradation kinetics in inert nitrogen atmosphere. The results indicated that chitosan-cobalt complex degrades via two-step reaction in inert atmosphere. The increment in heating rates can increase the degradation temperatures and maximum reaction rate. The kinetic parameters were calculated by FWO and Friedman methods. Whereas, Coats–Redfern method was applied to figure out the degradation mechanism. The similar variation in activation energies of chitosan-cobalt complex was observed from two kinetic methods. In the first degradation stage, the solid-state decomposition was observed as non-spontaneous and follows a mechanism in which nucleation and growth are involved.

The objective of this study is to perform differential scanning calorimetry to monitor the thermal behaviour of fabricated PLA/CH-*g*-OLLA bionanocomposite films (using solution casting technique) up to a suitable temperature range. Thermogravimetric analysis is performed at various temperatures to analyse the non-isothermal degradation kinetics using

different model fitting and model free methods to calculate the kinetic parameters such as activation energy and regression coefficient for PLA with its bionanocomposite films as it has not been examined till now. The calculated kinetic parameters using different methods are compared and discussed.

8.2. Basic theoretical consideration

A general reaction has been applied to describe the thermal decomposition of polymeric materials.

$$P\left(\frac{\text{solid}}{\text{liquid}}\right) \rightarrow Q\left(\frac{\text{solid}}{\text{liquid}}\right) + R\ (\text{volatile or gases}) \tag{8.1}$$

Where, P and Q are the starting material and R is the reaction product during the consumption of P and Q.

The decomposition rate ($\frac{d\alpha}{dt}$), for isothermal reactions may be given as:

$$\frac{d\alpha}{dt} = k(T)f(\alpha) \tag{8.2}$$

Where, $\alpha = \text{Extent of conversion} = \frac{W_0 - W_t}{W_0 - W_f}$, W_0, W_t and W_f are initial weight, weight at time t and final weight of the sample respectively. k(T) is rate constant at temperature T. f(α) is a reaction model function depends on degradation mechanism. The temperature dependant rate constant may be explained by the Arrhenius equation:

$$k(T) = A\exp\left(-\frac{E_a}{RT}\right) \tag{8.3}$$

Where, A, E_a, R and T are the pre-exponential factor (1/sec), activation energy (kJ/mol), universal gas constant (8.314 J/mol.K) and Absolute temperature (K) respectively. The above Eqs. 8.2 and 8.3 can be combined such as:

$$\frac{d\alpha}{dt} = A\exp\left(-\frac{E_a}{RT}\right)f(\alpha) \tag{8.4}$$

The decomposition rate ($\frac{d\alpha}{dt}$), for non-isothermal reactions with a linear heating rate ($\beta = \frac{dT}{dt}$) may be given as:

$$\frac{d\alpha}{dT} = A\frac{1}{\beta}\exp\left(-\frac{E_a}{RT}\right)f(\alpha) \qquad (8.5)$$

Where, $\frac{d\alpha}{dT}$ is the rate of non-isothermal reactions and β is the heating rate. The activation energy and pre-exponential factor have been calculated by the rate equations if and only if the known function $f(\alpha)$ remains constant for the entire duration of the reaction which is rarely possible in the case of solid state reactions **[Salehi et al., 2012]**. The thermal degradation of polymeric samples is highly complicated so it is assumed that the degradation reaction follows a simple nth order reaction to reduce the complicacy. Hence, the reaction model function $f(\alpha)$ is shown in the form of $(1-\alpha)^n$, where, n denotes the order of reaction. In the case of gas and liquid kinetics, the collision and energy barriers theories generally associated with Arrhenius parameters can be directly represented by the kinetic parameters obtained from TGA data. But, solid state kinetics do not based on the same consideration. Hence, in this case, the activation energy has been defined as the average excess energy obtained from the vibration of an atom or molecule at a desired temperature. This activation energy is also termed as "apparent activation energy". It is also associated to the rupture of chemical bonds **[Yuzay et al., 2010]**.

The existence of different approaches has been suggested to determine the kinetic parameters obtained from isothermal and non-isothermal TGA data. Such approaches or methods have been proposed to solve the above equations by integration, differentiation and approximation. On that basis, models are majorly divided into two types i.e. Isoconversional or model free methods and model fitting methods **[Yuzay et al., 2010]**.

8.2.1. Isoconversional or model free methods

Isoconversional methods have been considered as the most appropriate methods to calculate the activation energy of thermally activated reactions. Such methods have been used to calculate the activation energy at progressive conversion values (α) without any modelistic assumptions **[Muraleedharan et al., 2015]**. Isoconversional methods do not require the knowledge of the exact thermodegradation mechanism. According to the isoconversional principle, the rate of reaction is a function of temperature at a constant extent of conversion. These methods are based on multiple heating rate values **[Diaz-Celorio et al., 2012]**.

8.2.1.1. Kissinger-Akahira-Sunose model

It is an integral isoconversional method which is also known as generalized Kissinger method. It is based on the Murray and White approximation for temperature integral and is given as:

$$\frac{d\alpha}{f(\alpha)} = \frac{A}{\beta}\exp\left(-\frac{E_a}{RT}\right)dT \tag{8.6}$$

Integrate the Eq. 8.6 with the initial condition of $\alpha = 0$ at $T = T_0$ and the following expression has been obtained:

$$g(\alpha) = \int_0^{\alpha}\frac{d\alpha}{f(\alpha)} = \frac{A}{\beta}\int_{T_0}^{T}\exp(-\frac{E_a}{RT})dT \equiv \frac{AE_a}{\beta R}p\left(\frac{E_a}{RT}\right) \tag{8.7}$$

$$p\left(\frac{E_a}{RT}\right) \cong \frac{\exp\left(-\frac{E_a}{RT}\right)}{\left(\frac{E_a}{RT}\right)^2} \tag{8.8}$$

The essential assumption of this technique is that the A, E_a and $f(\alpha)$ are independent of temperature, whereas A and E_a are also independent of α. The term $g(\alpha)$ is the integral form of kinetic model. Eq. 8.7 has been integrated followed by logarithms on both sides:

$$\ln g(\alpha) = \ln\left(\frac{AE_a}{R}\right) - \ln\beta + \ln p(\frac{E_a}{RT}) \tag{8.9}$$

The final expression has been converted into the following form:

$$\ln\frac{\beta}{T^2} = \ln\left(\frac{AR}{E_a g(\alpha)}\right) - \frac{E_a}{RT} \tag{8.10}$$

The activation energy for each degree of conversion (α) has been obtained from the slope of the linear curve of $\ln\frac{\beta}{T^2}$ versus $-\frac{1}{T}$. The value of pre-exponential factor (A) has been obtained from the intercept of the same linear curve **[Aboulkas et al., 2010]**.

8.2.1.2. Flynn-Wall-Ozawa model

Flynn-Wall-Ozawa method is also a well-established integral isoconversional model **[Yuzay et al., 2010]**. The important assumption in this model is that the conversion function $f(\alpha)$ does not change with the heating rate alteration for all values of the degree of conversion (α). It follows Arrhenius type temperature dependence without any assumptions related to the form of the kinetic equation. In this model, the temperatures measurement corresponding to fixed values of α have been observed at different rates β from experiments **[Zou et al., 2009]**. Flynn-Wall-Ozawa method is relatively a simple method to calculate the activation energy from weight loss versus temperature data obtained at different heating rates. Integrate Eq. 8.6 with the condition of $\alpha = \alpha_0$ to $\alpha = \alpha_p$ on both sides and the following expression has been obtained:

$$g(\alpha) = \int_{\alpha_0}^{\alpha_p} \frac{d\alpha}{f(\alpha)} = \frac{A}{\beta}\int_{\alpha_0}^{\alpha_p} \exp(-\frac{E_a}{RT})dT \tag{8.11}$$

It is assumed that $x = \frac{E_a}{RT}$ and now integrate the right hand side of Eq. 8.11 which converts in the following form:

$$g(\alpha) = \int_{\alpha_0}^{\alpha_p} \frac{d\alpha}{f(\alpha)} = \frac{AE_a}{\beta R}p(x) \tag{8.12}$$

Taking logarithms on both sides and re-arranging, the following expression has been obtained:

$$\log \beta = \log \frac{AE_a}{g(\alpha)R} + \log p(x) \quad (8.13)$$

The doyle's approximation has been used for simplification of Eq. 8.13. It is given as:

$$\log p(x) = -2.315 - 0.4567x \quad (8.14)$$

Substituting Eq. 8.14 to Eq. 8.13 and final form of Flynn-Wall-Ozawa model equation has been given as:

$$\log \beta = \log \frac{AE_a}{g(\alpha)R} - 2.315 - \frac{0.4567E_a}{RT} \quad (8.15)$$

The activation energy and pre-exponential factor have been obtained from the slope ($\frac{0.4567E_a}{R}$) and intercept ($\log \frac{AE_a}{g(\alpha)R} - 2.315$) respectively, by plotting a linear curve between $\log \beta$ and ($-\frac{1}{T}$) at constant value of fractional conversion **[Ou et al., 2010]**. Basically, Flynn-Wall-Ozawa model has been used only for those systems, where many reactions are occurring such that the activation energy changes with time. On the other hand, this method shows failure, when widely different type of reactions are occurring simultaneously **[Venkatesh, 2013]**.

8.2.1.3. Augis & Bennett model

Augis & Bennett has proposed an isoconversional model which shows the dependence of temperature on heating rate and has also been used to calculate the kinetics parameters. The equation is as follows:

$$\ln\left(\frac{\beta}{T_m - T_0}\right) = \ln A - \frac{E_a}{RT_m} \quad (8.16)$$

Where, T_m and T_0 are the temperature at maximum degradation and the onset temperature of the DTG curve respectively. The activation energy and pre-exponential factor have been calculated from the slope ($\frac{E_a}{R}$) and intercept ($\ln A$) respectively, by plotting a linear curve between $\ln\left(\frac{\beta}{T_m - T_0}\right)$ and ($-\frac{1}{T_m}$) **[Chrissafis, 2009]**.

8.2.2. Model fitting methods

Model fitting methods are based on the different models fitting at a particular temperature obtained from DTG curve and also calculate the activation energy and pre-exponential factor. Many non-isothermal model fitting methods are available but Kissinger model is the most popular among all **[Kahrizsangi et al., 2007]**.

8.2.2.1. Kissinger model

This model fitting method has been widely used for calculating kinetic triplets (E_a, A and R). This method is based on the degradation peak temperature, obtained from the DTG curve. The activation energy has been calculated at maximum temperature from DTG curve. It should be very well understood that Kissinger is not an isoconversional method because the fractional conversion at degradation peak and peak temperature should change with change in heating rates **[Marquez et al., 2012]**. This method can also be employed to calculate activation energy without specific knowledge of the reaction mechanism **[Zou et al., 2009; Valapa et al., 2014]**. According to the principle of maxima and minima, the conversion rate derivative should be equal to zero at peak temperature. In this way, Eq. 8.6 can be re-written as:

$$\frac{d\alpha}{dT} = A\frac{1}{\beta}\exp\left(-\frac{E_a}{RT}\right)(1-\alpha)^n \qquad (8.17)$$

One assumption has been made that the maximum reaction rate occurs at the peak temperatures (T_{max}), so the conversion rate derivative at T_{max} becomes zero and the following expression has been obtained:

$$\frac{d}{dT}\left(\frac{d\alpha}{dT}\right) = \frac{d}{dT}\left[\frac{A}{\beta}\exp\left(-\frac{E_a}{RT}\right)(1-\alpha)^n\right] \qquad (8.18)$$

By putting $\frac{d^2\alpha}{dT^2} = 0$ at $T = T_m$ and re-arranging then the above equation will be expressed as:

$$\frac{E_a \beta}{RT_m{}^2 n(1-\alpha)^{n-1}} = A \exp\left(-\frac{E_a}{RT_m}\right) \tag{8.19}$$

Where, T_m is the temperature of maximum rate of decomposition. Assume that the order of degradation is one i.e. $n = 1$ then Eq. 8.19 converts into:

$$\frac{\beta}{T_m{}^2} = \frac{AR}{E} \exp\left(-\frac{E_a}{RT_m}\right) \tag{8.20}$$

Apply logarithms on both sides:

$$\ln \frac{\beta}{T_m{}^2} = \ln \frac{AR}{E} - \frac{E_a}{RT_m} \tag{8.21}$$

This Eq. 8.21 is known as famous "Kissinger" equation. The activation energy and pre-exponential factor have been calculated from the slope ($\frac{E_a}{R}$) and intercept ($\ln \frac{AR}{E}$) respectively, by plotting a linear curve between ($\ln \frac{\beta}{T_m{}^2}$) and ($-\frac{1}{T_m}$). If the curve of rate of reaction is free from shoulders and activation energy is almost constant over the entire range of conversion, it means that the decomposition process is controlled by a single step model. But the variation in activation energy with conversion is much obvious and is controlled with many possible processes involved during thermal degradation. Normally, the activation energy increases with increase in conversion **[Mroz et al., 2013]**. Some limitations are also associated with this method, so the first limitation is based on the fact that the reaction model function ($f(\alpha)$) should be independent of the heating rate to calculate the accurate value of activation energy. The second limitation is that Kissinger method is only able to produce a single value of activation energy for any process without the knowledge of its actual kinetic complexity. So, it always denotes only a single step kinetics. But, more than a single value of activation energy is required for multi-step kinetics. Hence, the support of isoconversional methods is required to verify Kissinger's kinetic parameter values **[Vyazovkin et al., 2011]**.

8.3. Results and discussion

8.3.1. Thermal degradation behaviour of PLA/CH biocomposite films

In order to understand the effect of CH on thermal decomposition behaviour of PLA, a comprehensive study was investigated in this section including Kissinger-Akahira-Sunose and Flynn-Wall-Ozawa models to study the thermal decomposition kinetics of PLA and PLA/CH-*g*-OLLA bionanocomposite films.

8.3.1.1. Influence of CH on thermal behaviour of PLA film

Thermogravimetric analysis has been performed to check the thermal decomposition behaviour of PLA and PLA/CH biocomposite films at different heating rates under inert atmosphere. The typical temperature dependent weight loss curve with its derivative for PLA and its composite films have been shown in Figure 8.1 in which the degradation behaviour of all the film samples have been compiled only at a heating rate of 20 ºC/min. The two distinguishable peaks with significant weight losses have been observed in Figure 8.1. The first peak has been observed in the temperature range of 59 to 150 ºC for all films which has been attributed to the weight loss due to the release of unbound and bound moisture from the film samples. The second peak has been observed in the temperature range of 335.4 to 394.8 ºC, which is only responsible for material degradation. PLA film shows highest thermal stability which reduces with an increase in filler concentration in biocomposite films. This degradation phenomenon has been attributed to the hydrolysis of PLA and CH into shorter polymer chains. The degradation of PLA is due to intra-molecular trans-esterification, cis-elimination and fragmentation **[Valapa et al., 2014]**. Whereas, the degradation of CH is due to the saccharide structure degradation **[Bonilla et al., 2013]**. It has been clearly observed from Figure 8.1 that the thermal stability of PLA has been reduced by the addition of filler into it and it further reduces with increase in filler concentration. This reduction is due to the increment in

shorter polymeric chains. The values of T_{on}, T_P and T_{off} for PLA and PLA/CH films have been listed in Table 8.1.

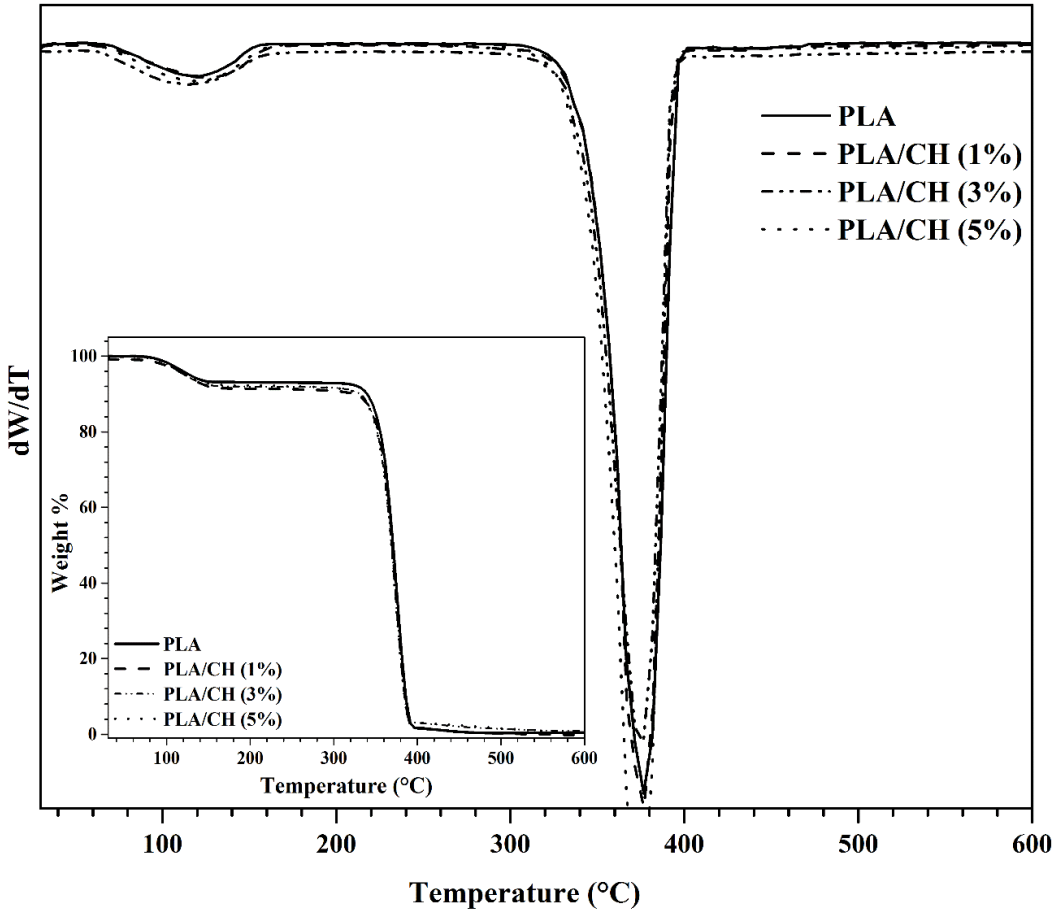

Figure 8.1. TGA and DTG curves of PLA and PLA/CH biocomposite films at the heating rate of 20 ºC/min.

Table 8.1: TGA analysis for PLA and its composite films at 20 °C/min.

Sample Name	Thickness (mm)±Std. Dev.	T_{on} (°C)	T_P (°C)	T_{off} (°C)
PLA	140±3	357.6	377.1	394.8
PLA/CH (1%)	152±9	356.9	375.7	392.3
PLA/CH (3%)	162±4	355.5	374.4	391.4
PLA/CH (5%)	147±9	345.9	370.2	391.2

8.3.1.2. Thermal degradation kinetics

The TGA and DTG curves of PLA and PLA/CH biocomposite films have been shown in Figure 8.2. All the analysis has been carried out at three different heating rates of 5, 10 and 20 ºC/min in nitrogen atmosphere. Different profiles have been observed depending on the heating rate and filler concentration. The shifting of all TGA curves to higher temperatures with increasing heating rates has been noticed as shown in Figure 8.2. This improvement is due to the less time provided for a sample to reach at a given temperature at higher heating rates. All the film samples have single degradation peak which attributes to the single stage degradation **[Valapa et al., 2014]**.

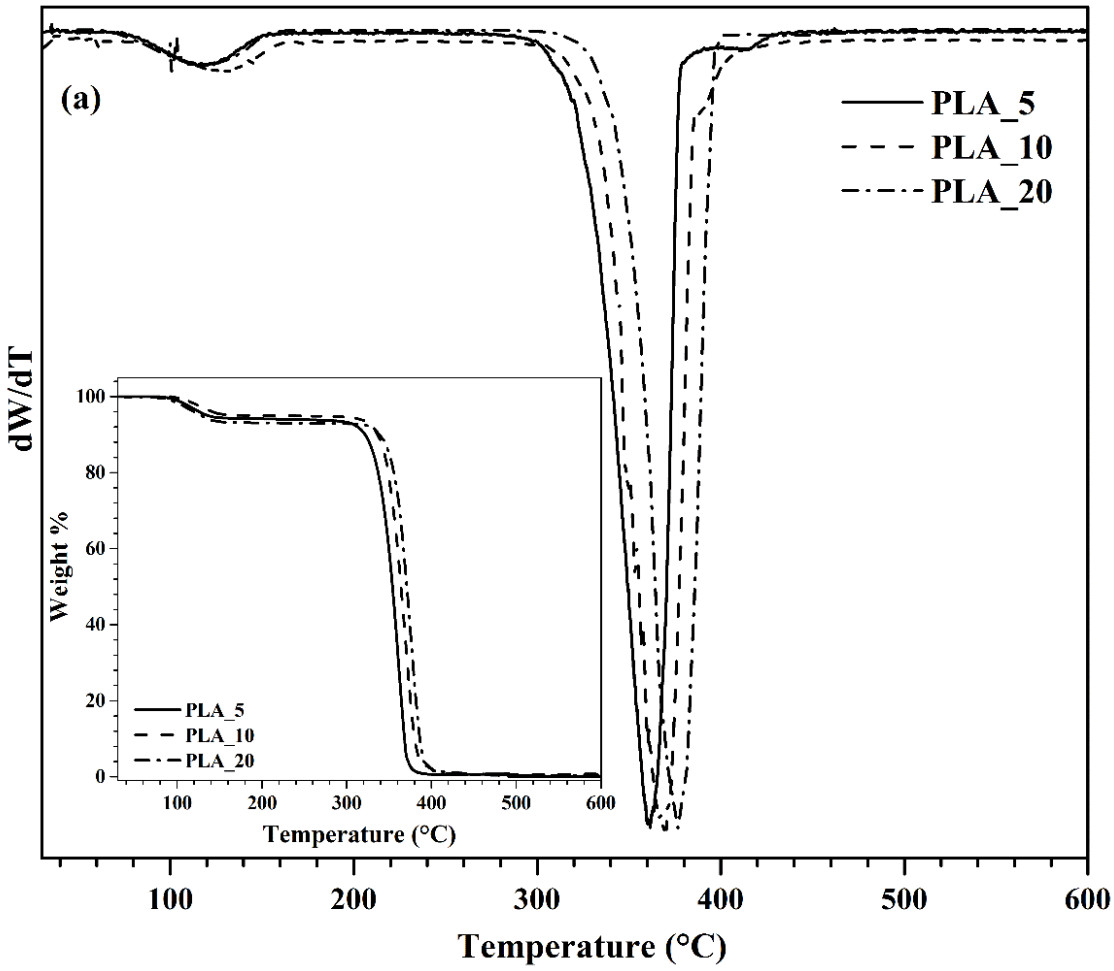

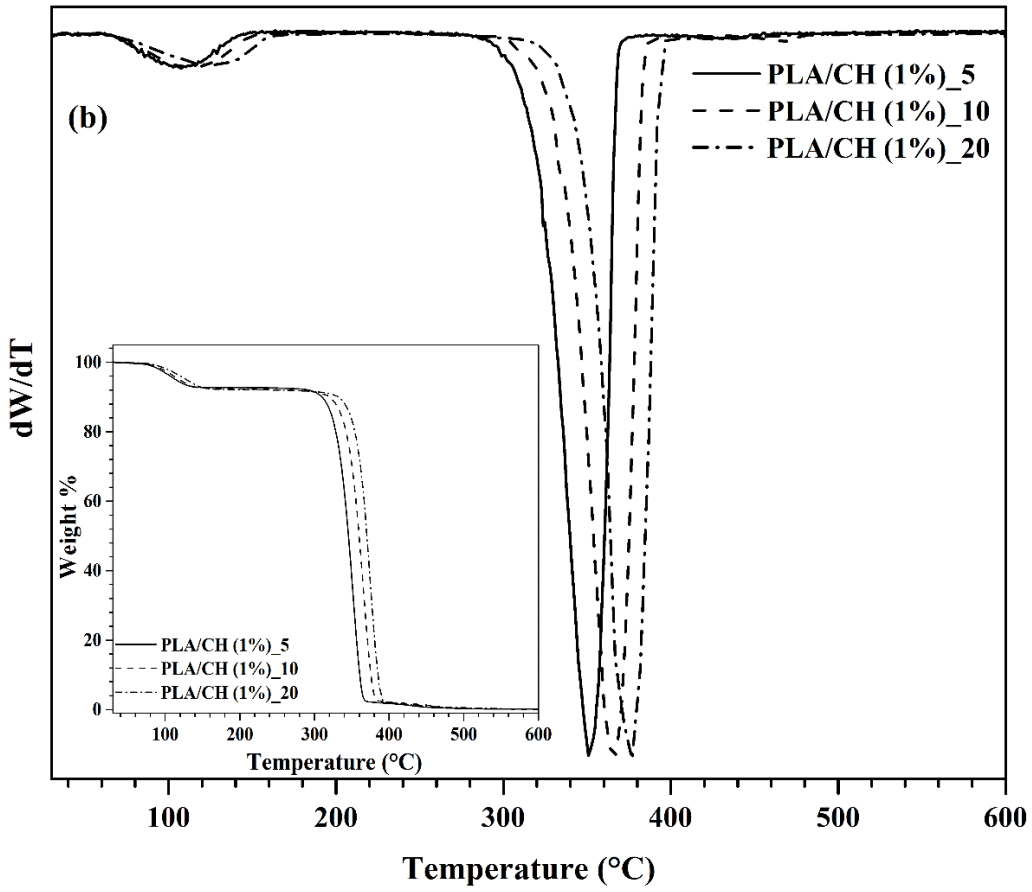

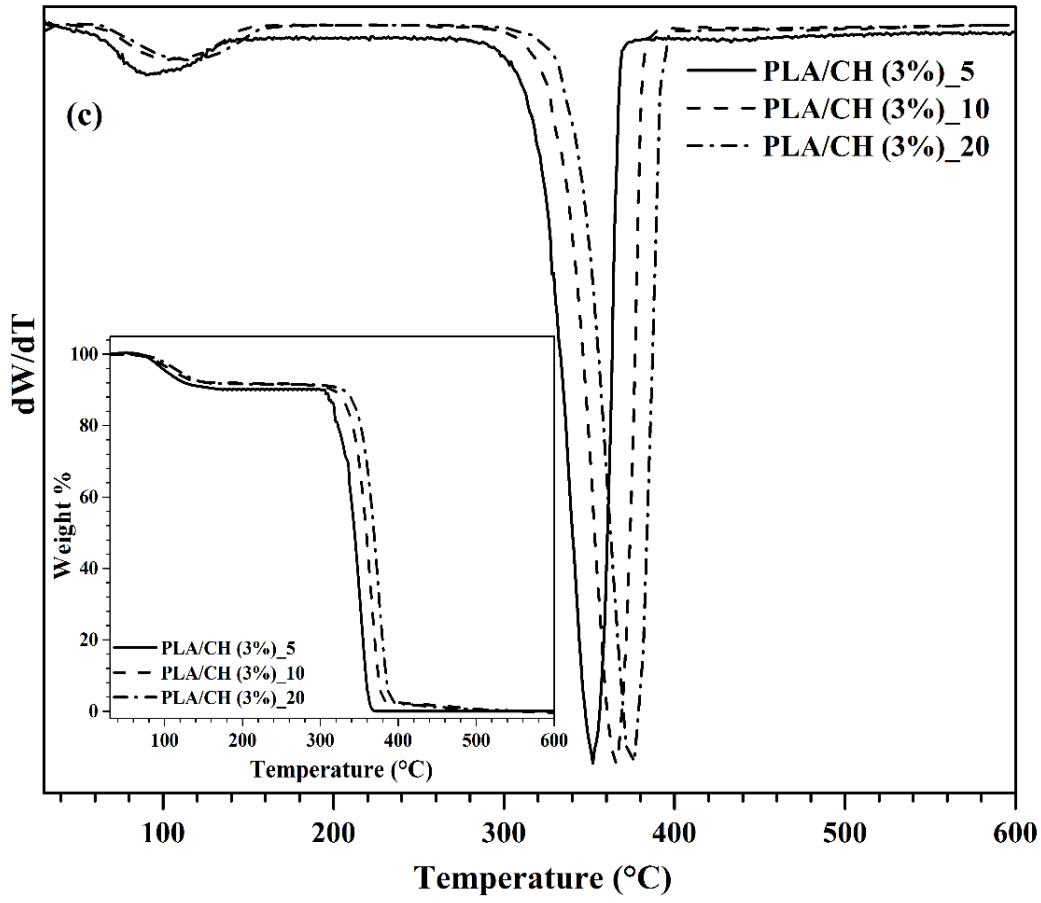

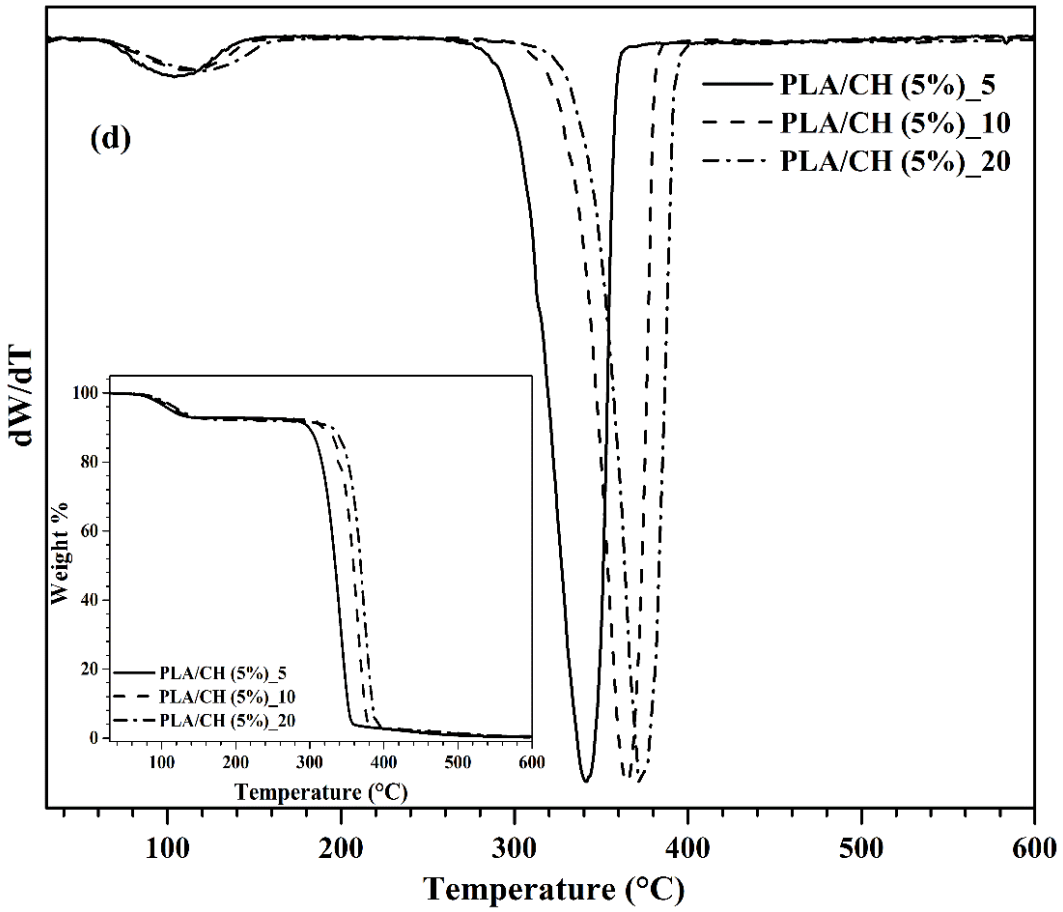

Figure 8.2. TGA and DTG curves of (a) PLA, (b) PLA/CH (1%), (c) PLA/CH (3%) and (d) PLA/CH (5%) at the heating rates of 5, 10 and 20 °C/min.

The main purpose of this analysis at different temperatures is to calculate the apparent activation energies and thermal degradation behaviour of PLA and PLA/CH biocomposite films. The apparent activation energies and regression coefficients have been calculated by using isoconversional KAS and FWO methods. These integral methods give the accurate results because the calculation of apparent activation energies and regression coefficients can be done at each conversion value.

8.3.1.3. Kissinger-Akahira-Sunose model (KAS)

This isoconversional method has been used to calculate the apparent activation energies at different conversion values by using the plot of $\ln\frac{\beta}{T^2}$ versus $-\frac{1}{T}$ for PLA and PLA/CH biocomposite films as shown in Figure 8.3. KAS is based on the assumption of first order reaction model to calculate the kinetic parameters using multiple heating rate values. The mean apparent activation energy ($\overline{E}_a$) and regression coefficient ($\overline{R}^2$) values have been shown in Table 8.2. The apparent activation energy reduces with increase in filler concentration which reveals that the thermal stability reduces continuously as discussed in Figure 8.1. The straight line at constant conversion has been drawn by using the values of $\ln\frac{\beta}{T^2}$ and $-\frac{1}{T}$ at various heating rates. All the drawn lines, at various conversions, are nearly parallel to each other for PLA and its composite films.

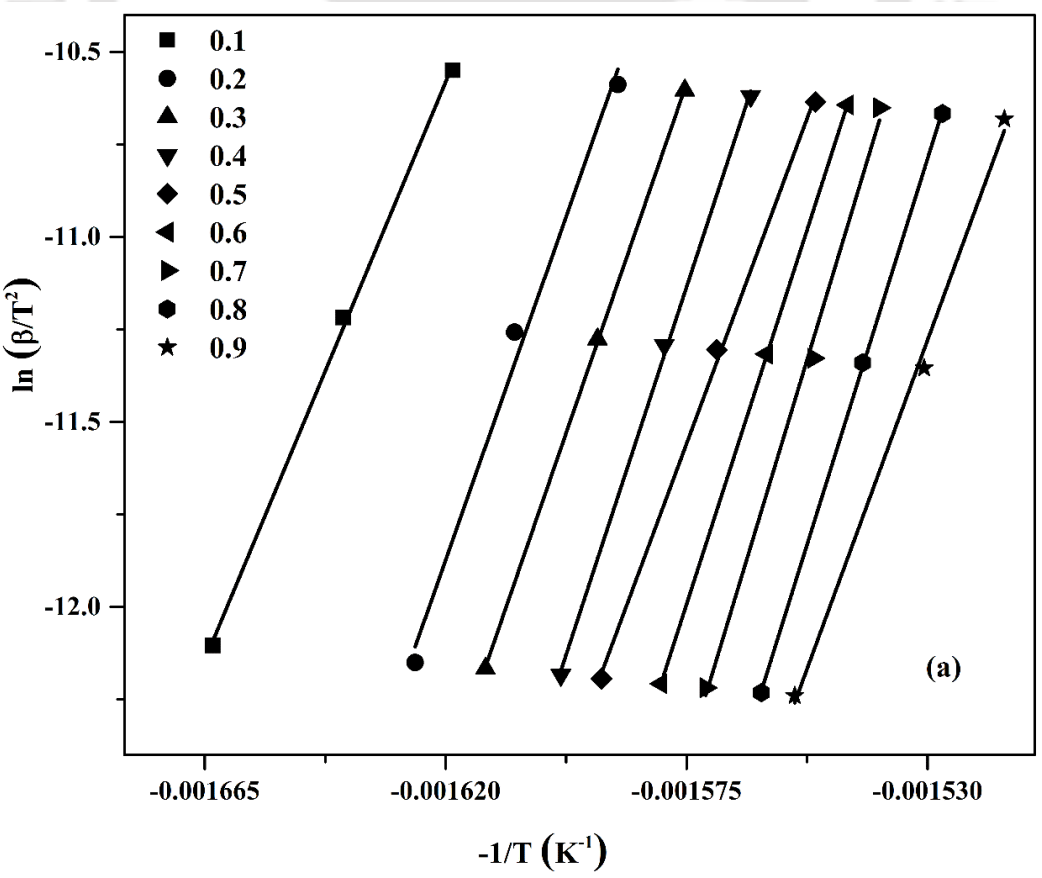

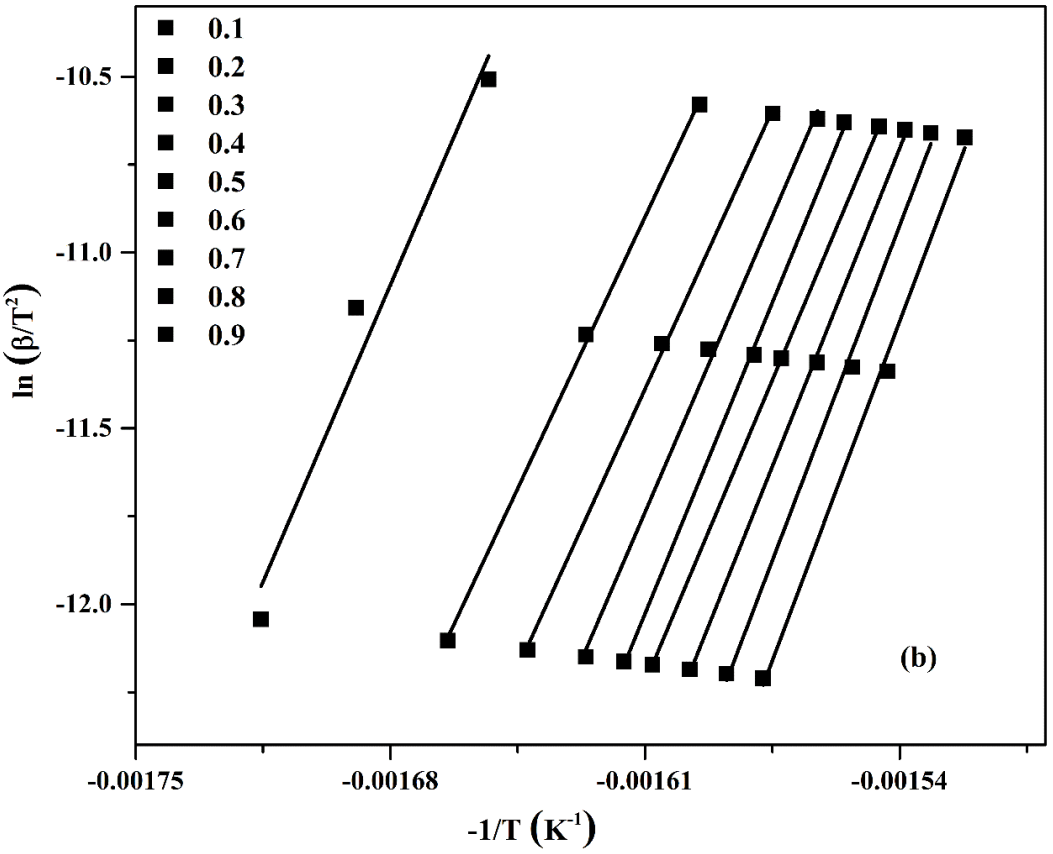

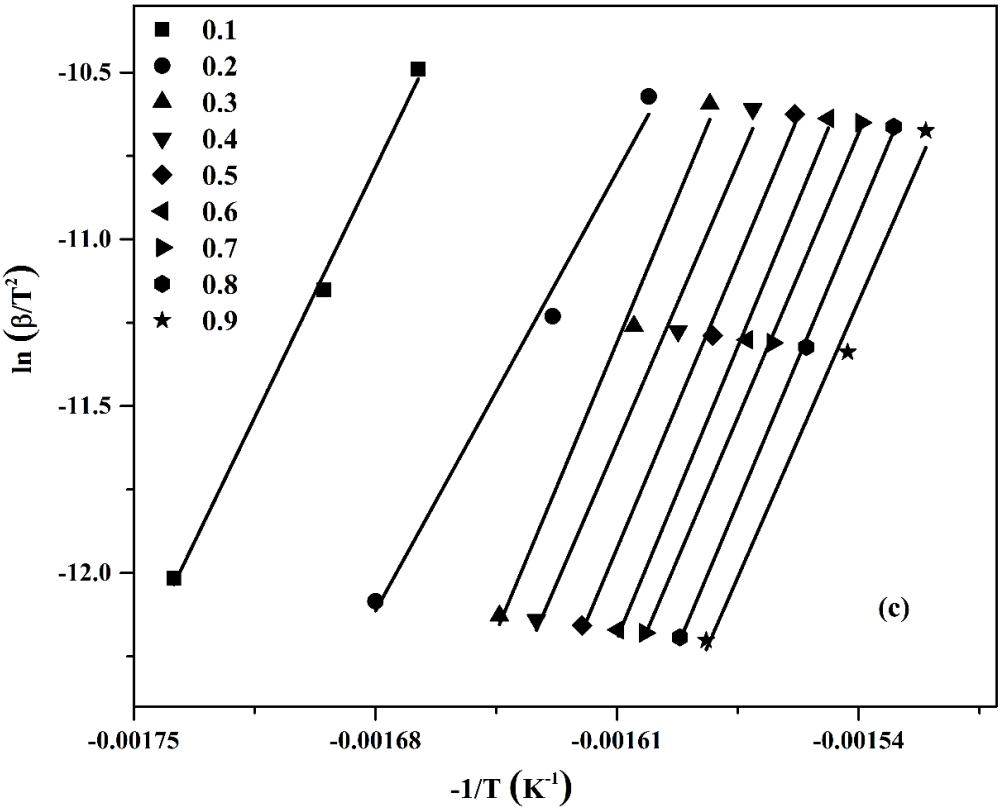

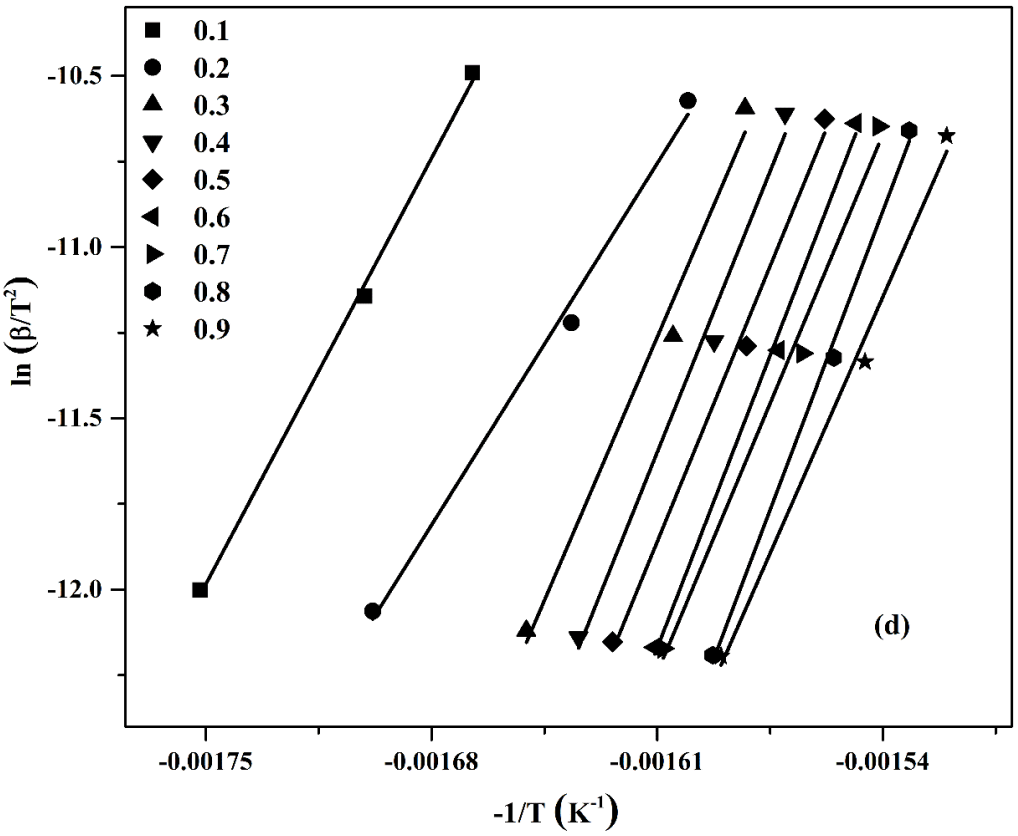

Figure 8.3. KAS plots of (a) PLA, (b) PLA/CH (1%), (c) PLA/CH (3%) and (d) PLA/CH (5%) films.

8.3.1.4. Flynn-Wall-Ozawa model (FWO)

The graphs have been plotted between $\log \beta$ and $(-\frac{1}{T})$ at different conversion values (0.1 to 0.9) for PLA and PLA/CH composite films as shown in Figure 8.4. The drawn straight lines at various conversion values are parallel for all film samples which confirms the suitability of FWO method for PLA and PLA/CH systems. It has also been observed that the straight lines are not completely parallel at lower α values such as 0.1 and 0.2 with increasing filler concentration which means that the moisture content increases with filler content. The other associated reason is that there must be some experimental or manual error during analysis **[Valapa et al., 2014; Marquez et al., 2012]**. The $\overline{E}_a$ and $\overline{R}^2$ values have been shown in Table 8.2. The calculated $\overline{E}_a$ values from KAS and FWO methods have

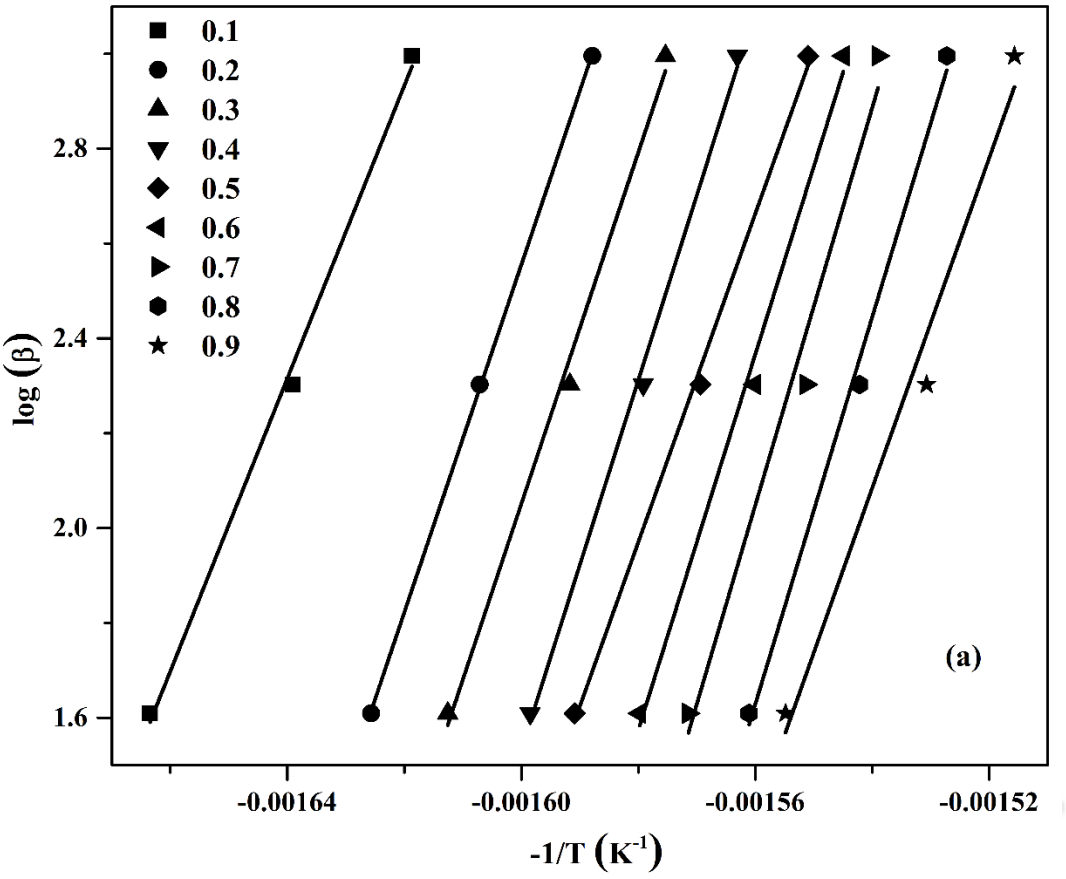

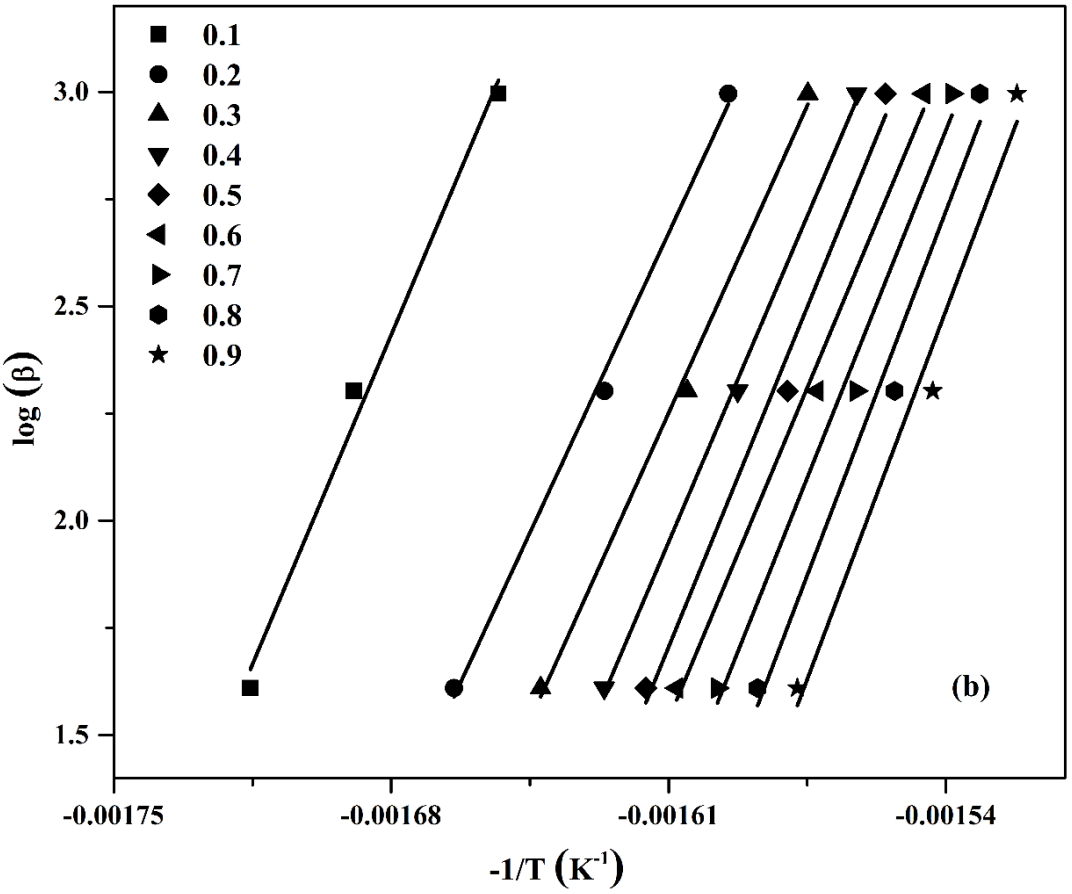

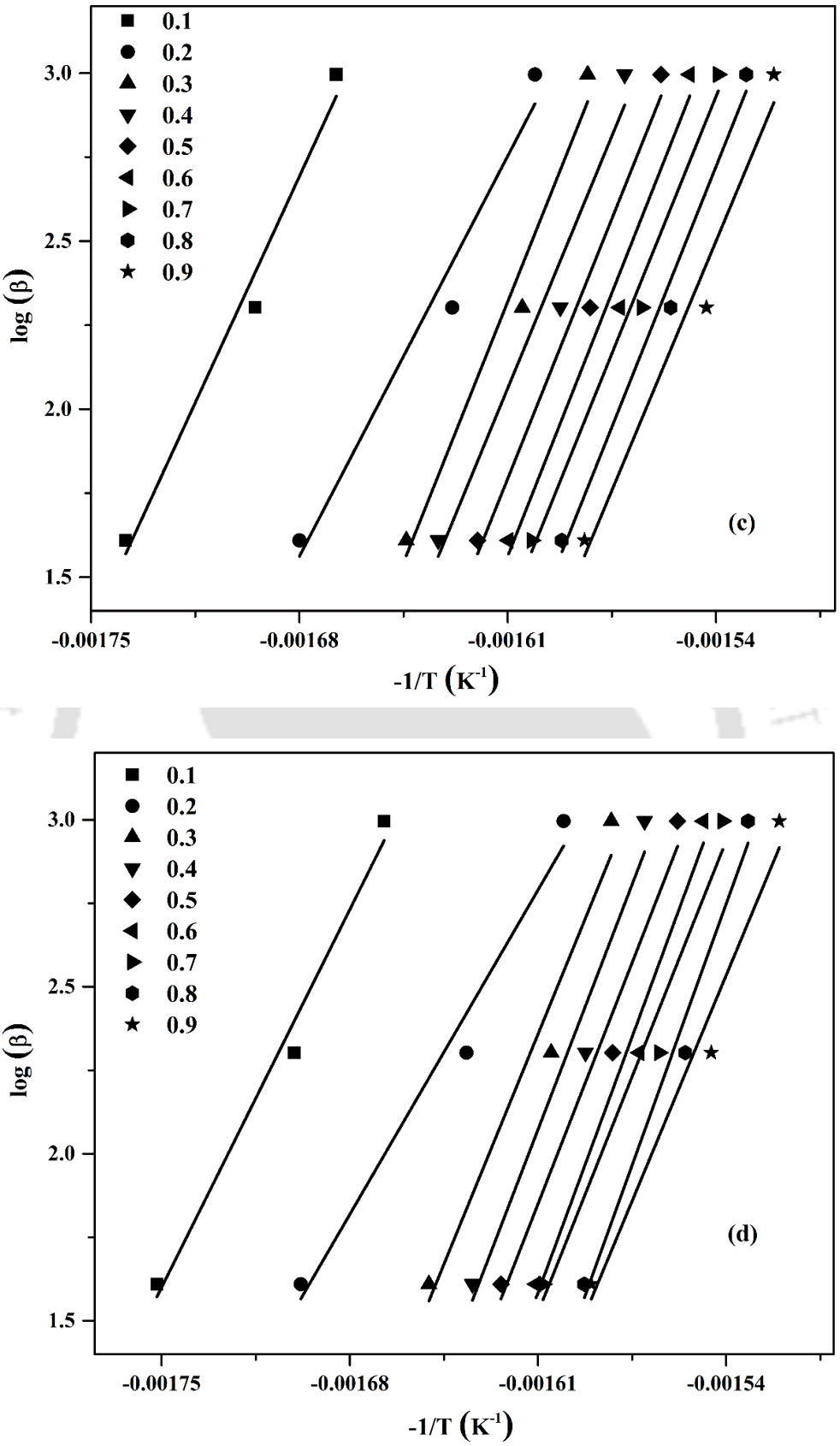

Figure 8.4. FWO plots of (a) PLA, (b) PLA/CH (1%), (c) PLA/CH (3%) and (d) PLA/CH (5%) biocomposite films.

been found close which shows that both isoconversional models are the best suited models for this polymeric system.

The apparent activation energy and regression coefficient values have been calculated and listed in Table 8.2. The table concludes that $\overline{E}_a$ values from both the models are close to each other. The $\overline{E}_a$ values reduce with an increase in filler concentration for individual model. The $\overline{R}^2$ values are in the range of 0.984 to 0.997 and 0.976 to 0.996 for KAS and FWO models respectively.

Table 8.2: The calculated $\overline{E}_a$ and $\overline{R}^2$ values from FWO and KAS models for PLA and PLA/CH biocomposite films.

Sample Name	KAS		FWO	
	$\overline{E}_a$ (kJ/mol)	$\overline{R}^2$	$\overline{E}_a$ (kJ/mol)	$\overline{R}^2$
PLA	350.99	0.997	294.35	0.993
PLA/CH (1%)	206.32	0.995	176.47	0.991
PLA/CH (3%)	195.18	0.995	167.4	0.979
PLA/CH (5%)	179.67	0.993	153.68	0.976

8.3.1.5. Apparent activation energy vs conversion

$\overline{E}_a$ vs conversion plots have been drawn with the help of calculated values of $\overline{E}_a$ at different conversions by using FWO and KAS models as shown in Figure 8.5. The $\overline{E}_a$ values vary with increase in the degree of conversion because it is purely a chemical process where no physical changes are associated with it. The variation shows a complex reaction process **[Valapa et al., 2014]**. $\overline{E}_a$ value reduces with increase in filler concentration due to the presence of higher acidic sites available during thermal degradation in PLA matrix. It accelerates the auto-catalytic effect during degradation of PLA/CH sample which always

enhances the degradation and reduces $\overline{E}_a$ value. In the case of composite films, the chitosan part gets converted into anhydrous chitosan by the removal of unbound, bound moisture during thermal degradation. It generates H^+ ions during thermal degradation of chitosan and increases with increase in filler concentration. It highly supports the degradation process. Hence, the thermal stability of PLA reduces with increase in filler concentration.

8.3.2. Thermal degradation behaviour of PLA/CH-*g*-OLLA bionanocomposite films

In order to understand the effect of CH-*g*-OLLA copolymer on thermal decomposition behaviour of PLA, a comprehensive study was investigated in this section including isoconversional and model fitting methods to study the non-isothermal thermal degradation kinetics of PLA and PLA/CH-*g*-OLLA bionanocomposite films followed by characterizing

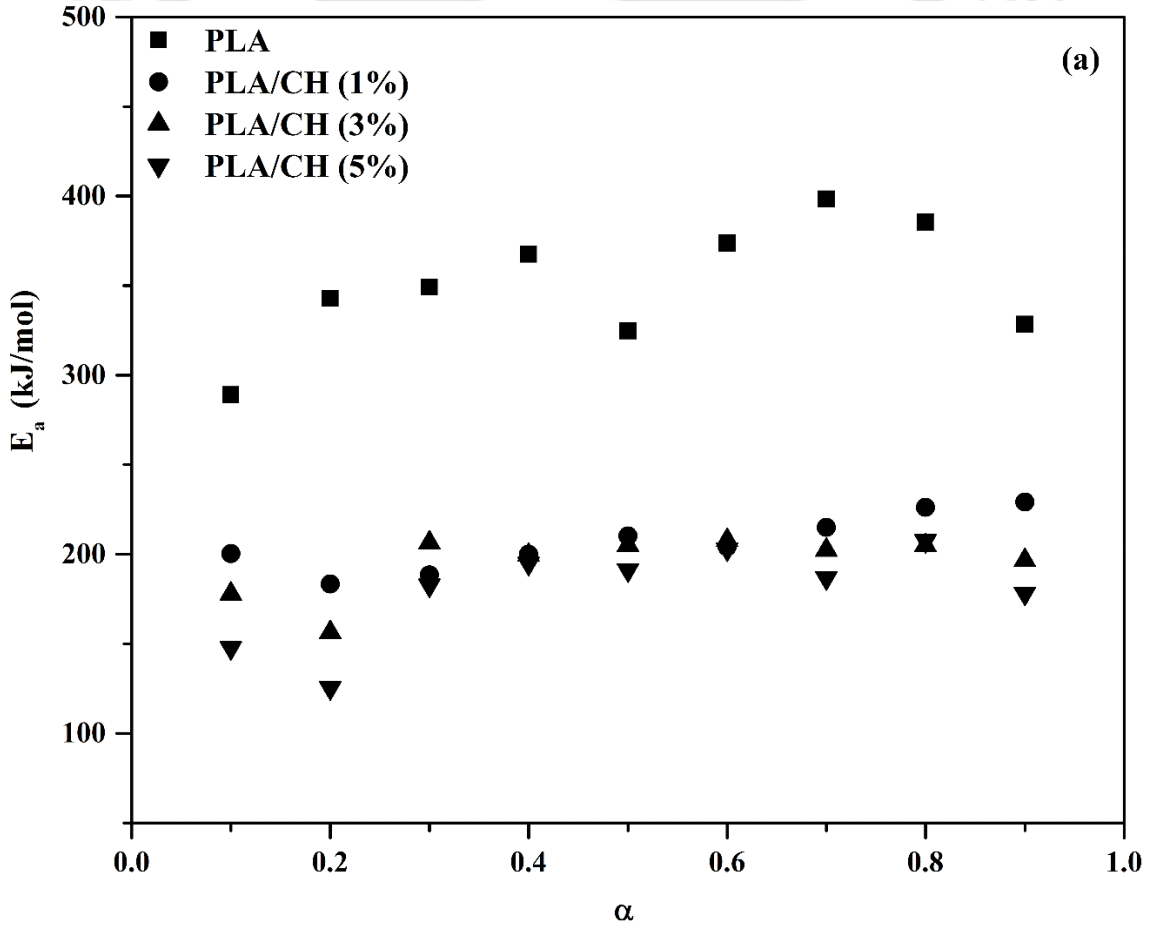

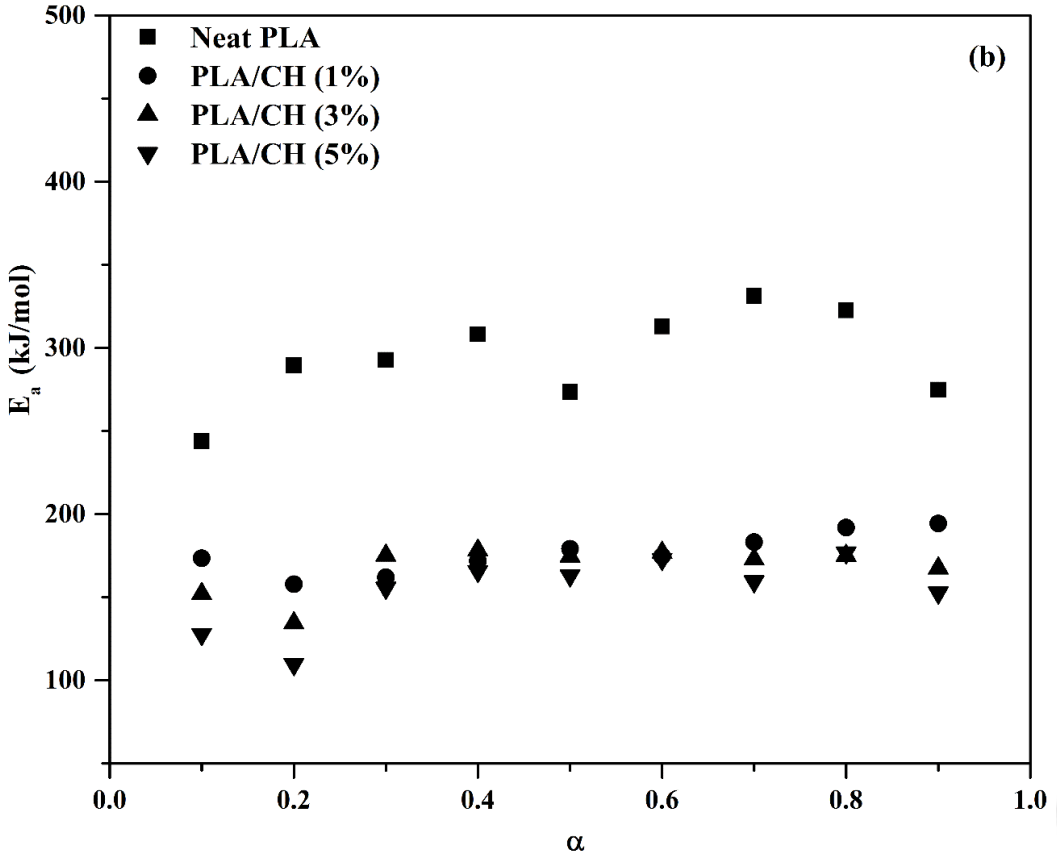

Figure 8.5. Apparent activation energy vs conversion plots of (a) KAS model and (b) FWO model for PLA and PLA/CH biocomposite films.

the evolved gaseous products and their residues in the condensed phase by TG-FTIR at variable temperatures.

8.3.2.1. Influence of CH-*g*-OLLA on thermal behaviour of PLA film

The DSC data of PLA, CH and PLA/CH-*g*-OLLA bionanocomposite films are collected for second heating cycle at 10 °C/min and plotted to observe the effect of CH-*g*-OLLA on T_g, T_{cc} and T_m as shown in Figure 8.6. The reason of first heating cycle is to eliminate the trace amount of physically and chemically enclosed moisture from samples and also to remove the previous thermal history **[Fukushima et al., 2011]**. In this research work, the second heating cycle shows that the values of T_m related to PLA and other bionanocomposite films detect almost at same temperature i.e. ~151.7 °C. It confirms that

the addition of prepared nano bio filler shows negligible effect on thermal stability of PLA films. A sharp unimodal endothermic peak at ~151.7 °C is observed for neat PLA, which confirms the presence of α-crystalline form of PLA with homogeneous distribution of α-crystals **[Valapa et al., 2014]**. However, a small shoulder is detected before the main melting peak of PLA/CH-*g*-OLLA bionanocomposite films, which clearly indicates the existence of heterogeneity in the developed crystals as well as in the distribution of crystals. It may also be possible due to the non-uniform thickness of developed PLA crystals after the reinforcement of CH-*g*-OLLA nanofiller. Although, the addition of CH-*g*-OLLA may reduce the molecular weight of PLA but can also behave as a nucleating agent **[Valapa et al., 2014]**. Melting peak for neat chitosan film is not detected in this temperature domain due to the absence of crystalline nature. The values of T_{cc} are reduced up to ~14 °C with an increase in filler loadings. The reduction in T_{cc} is because of the increment in the rate of diffusion by the addition of nanofiller, which leads to the faster migration of polymeric chains to the nuclei surface **[Liu et al., 2009]**. The peak width of cold crystallization temperature becomes sharper with an increase in filler loadings, which confirms that the rate of crystallization increases with the increment in filler loadings. Both type of crystallizations such as homogeneous and heterogeneous occur within the bionanocomposite films. Other associated reason with the reduction in T_{cc} can be the deformation of α type of crystals in PLA. In the present study, the glass transition temperature is decreased up to ~12 °C with the inflation in CH-*g*-OLLA loading as shown in Figure 8.6, which proposes that the incorporation of filler in the matrix of PLA may promote the formation of short chains due to the reduction in macromolecular interactions. The reduction in T_g values also enhances the plasticization effect, which is also required for packaging applications. The heat capacity at constant pressure also reduces from 0.57 to 0.40 J/g.K with the increment in filler loading, which indicates that the lower amount of

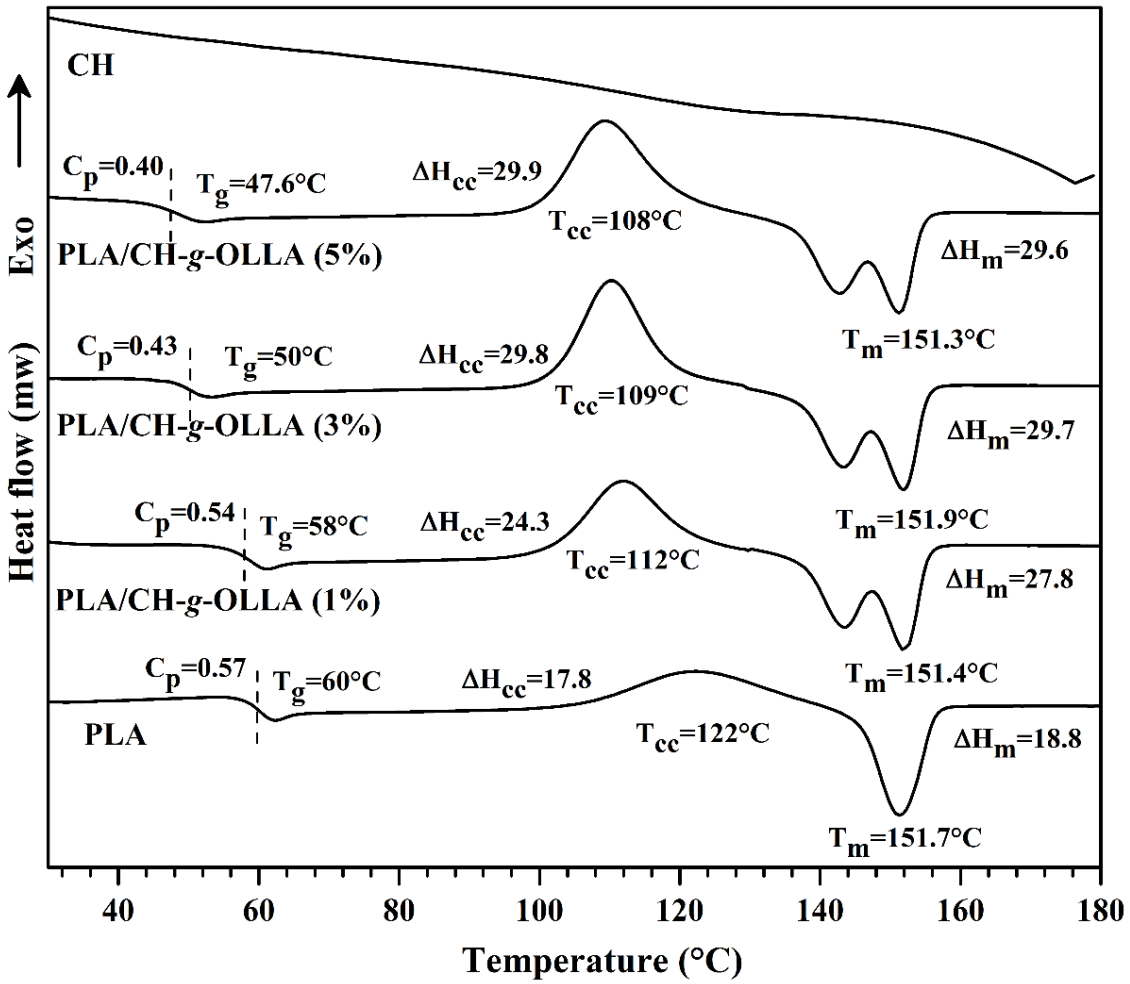

Figure 8.6. DSC thermograms for solution casted PLA, CH and PLA/CH-*g*-OLLA bionanocomposite films at 10 °C/min obtained from second heating.

heat is needed to increase the unit temperature of bionanocomposite films. It can only feasible when smaller polymeric chains experience less entanglements and obstructions from neighbour polymer chains **[De Britto and Campana-Filho, 2004]**.

8.3.2.2. Influence of CH-*g*-OLLA on degradation behaviour of PLA film

TGA analysis is utilized to observe the thermal degradation behaviour of PLA, CH and PLA/CH-*g*-OLLA bionanocomposite films under inert atmosphere at a heating rate of 10 °C/min, which removes the atmospheric air from the crucible and avoid oxidation **[Koh et al., 2008]**. Figure 8.7 reveals the presence of two distinguishable peaks for

PLA/CH-*g*-OLLA bionanocomposite films and one degradation peak for PLA, which significantly represent the percentage of weight losses **[Bonilla et al., 2013]**. In CH film, the first stage of decomposition is observed in the range of 38 to 179 °C, which is associated to the unbound and bound moisture vapourization and removal of acetic acid. The second weight loss is started from 180 °C and extended upto 422 °C, which is completely responsible for CH degradation as shown in Figure 8.7. In this temperature range, the weight loss percentage is ~44.5%. It is meaningful to mention that the degradation of CH films takes place via a complex process which includes degradation and depolymerisation of the acetylated and deacetylated units of polymers with dehydration of saccharide rings **[Balau et al., 2004; Bonilla et al., 2013]**. In PLA/CH-*g*-OLLA bionanocomposite films, the first peak attributes to the elimination of moisture, detected in the range of 75 to 165 °C. The main degradation peak is observed in the temperature range of 351 to 370 °C (compiled in Table 8.3), which is associated to the hydrolysis by trace amount of water, cis-elimination to produce acrylic acid, intramolecular transesterification leading to cyclic oligomers and fragmentation responsible for acetaldehyde and CO_2 **[Valapa et al., 2014]**. The thermal stability of PLA film is decreased with increasing nanofiller concentration due to the increment in the short chain oligomer i.e. CH-*g*-OLLA, which decomposes the films at lesser temperature as compare to that of PLA **[Ambrosio-Martin et al., 2014]**. The thermal degradation temperatures named as T [@ $\alpha = 0.1$], T [@ $\alpha = 0.5$] and T [@ $\alpha = 0.9$] correspond to 10% weight loss, 50% weight loss and 90% weight loss respectively for all the film samples are mentioned in Table 8.3. According to Figure 8.7, PLA, CH and PLA/CH-*g*-OLLA bionanocomposite films have shown only one stage of degradation. At 10% weight loss, the degradation temperature of PLA, PLA/CH-*g*-OLLA (1%), PLA/CH-*g*-OLLA (3%) and PLA/CH-*g*-OLLA (5%) films are observed as 336.8, 321.5, 306.5 and 294.0 °C respectively which means that the

decomposition temperature is reduced continuously with increasing filler amount. The associated reason is the increment in the amorphous phase of bionanocomposite films due to the presence of shorten polymer chains, which imparts plasticization to the samples.

Table 8.3: TGA analysis for PLA, CH and PLA/CH-*g*-OLLA bionanocomposite films at 10 °C/min.

Sample Name	Thickness (mm)	TGA		
		T [@ α = 0.1] (°C)	T [@ α = 0.5] (°C)	T [@ α = 0.9] (°C)
PLA	0.10±0.01	336.8	364.1	380.2
PLA/CH-*g*-OLLA (1%)	0.12±0.02	321.5	351.5	367.5
PLA/CH-*g*-OLLA (3%)	0.097±0.01	306.5	346.5	366.5
PLA/CH-*g*-OLLA (5%)	0.11±0.008	294.0	345.3	364.4
CH	0.099±0.007	122.1	330.3	-

Hence, the increment in filler concentration increases the oligomer content, which reduces the thermal stability of bionanocomposite films. CH films have shown 10% weight loss at 122.1 °C due to its hydrophilic nature which absorbs moisture from the atmosphere. At 50% weight loss, the degradation temperature of PLA, PLA/CH-*g*-OLLA (1%), PLA/CH-*g*-OLLA (3%) and PLA/CH-*g*-OLLA (5%) films are observed as 364.1, 351.5, 346.5 and 345.3 °C respectively. The thermal stability of PLA is reduced up to 18.8 °C by the addition of 1 to 5 wt% of nano-filler. This decrement in temperature is attributed to the autocatalytic cleavage of ester groups during hydrolysis of oligomer (present in the filler) with increase in PLA/CH-*g*-OLLA concentration. It is also possible that the released polar moieties during the degradation of filler can cleave the polyester segment of PLA which leads to the reduction in the degradation temperature of PLA **[Petinakis et al., 2010; Perinovic et al., 2010; Antheunis et al., 2010; Janorkar et al., 2004]**. At maximum

weight loss (at T_p) and 90% weight loss conditions, the degradation temperatures for PLA are observed as 370.3 and 380.2 °C respectively which are also decreased with an increase in filler loadings as shown in Figure 8.7. The thermal degradation behaviour at maximum and 90% weight loss conditions of PLA/CH-*g*-OLLA bionanocomposite films follows the same pattern as in 50% weight loss. The same trend in weight loss of all the film samples shows same degradation behaviour due to the existence of similar chemical bonds in their molecular structures **[Aboulkas and El Bouadili, 2010]**.

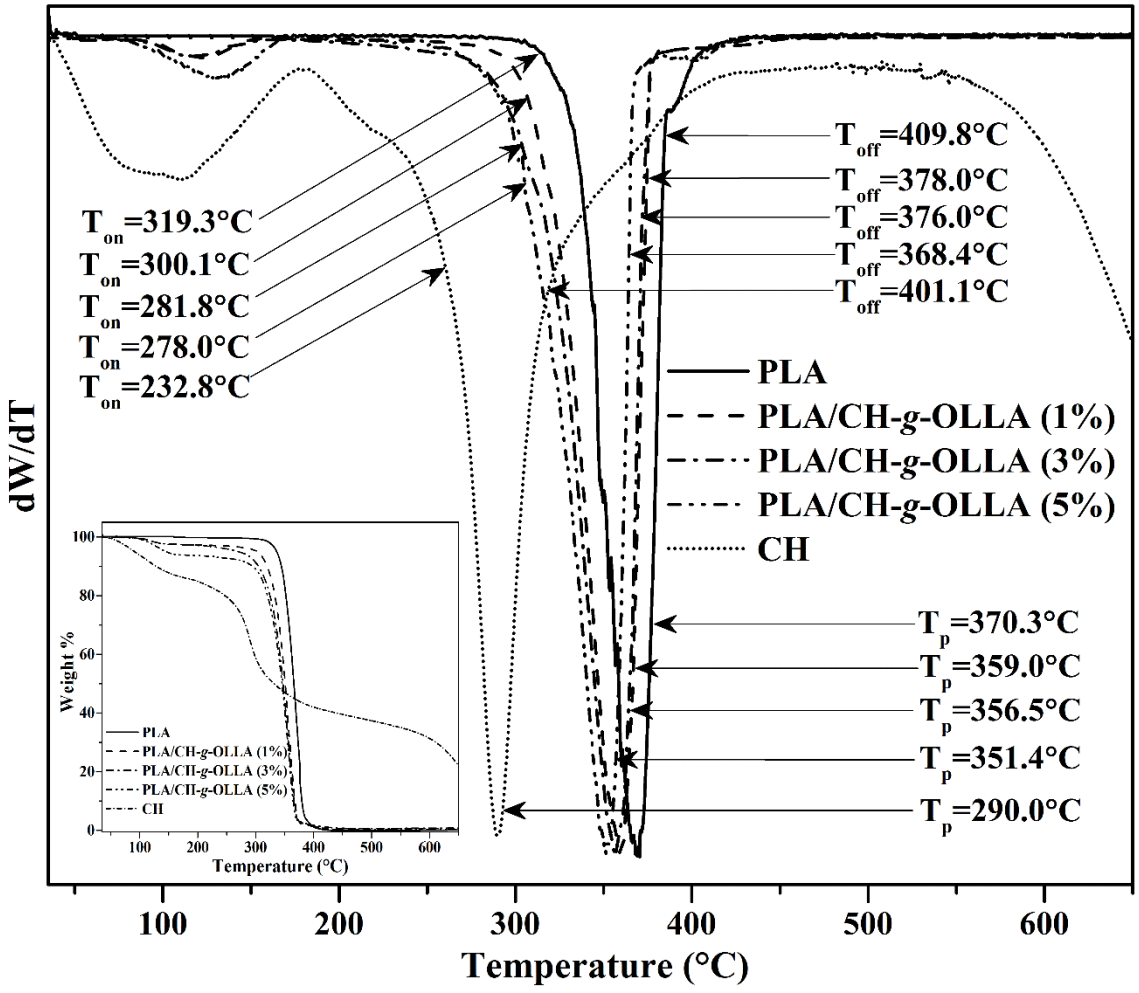

Figure 8.7. TGA and DTG curves for PLA, CH and PLA/CH-*g*-OLLA bionanocomposite films at 10 °C/min obtained from second heating.

8.3.2.3. Thermal degradation kinetics

Figure 8.8(a), (b), (c) and (d) show TGA and DTG curves for PLA and PLA/CH-*g*-OLLA bionanocomposite films at non-isothermal condition with three different heating rates i.e. 2, 5 and 10 °C/min under inert nitrogen atmosphere. It is observed that T_m improves with an increase in heating rates for all film samples due to the insufficient heat transposition from the furnace to the sample, which may generate a broad temperature difference between furnace and sample. As a result, this difference always increases with increase in heating rate. One strong consideration among various authors about such kind of temperature displacement is that a modification in the reaction mechanism can be produced with the variation in the heating rates **[Aboulkas and El Bouadili, 2010]**.

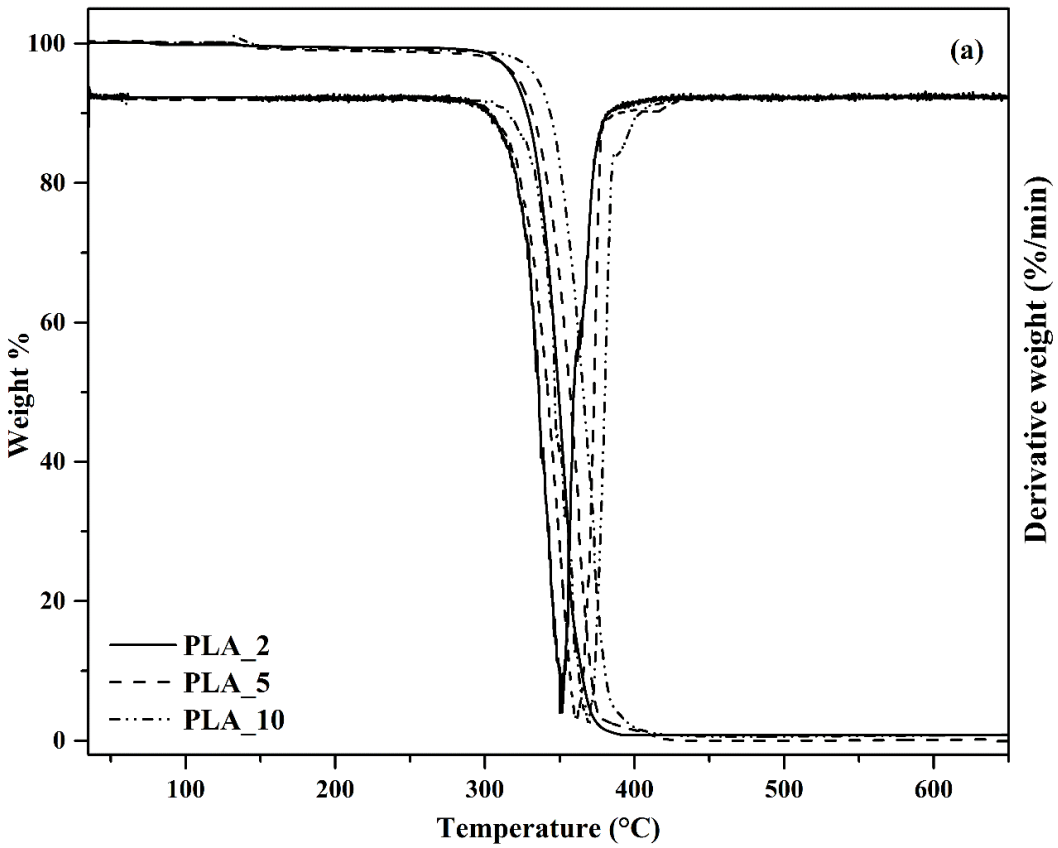

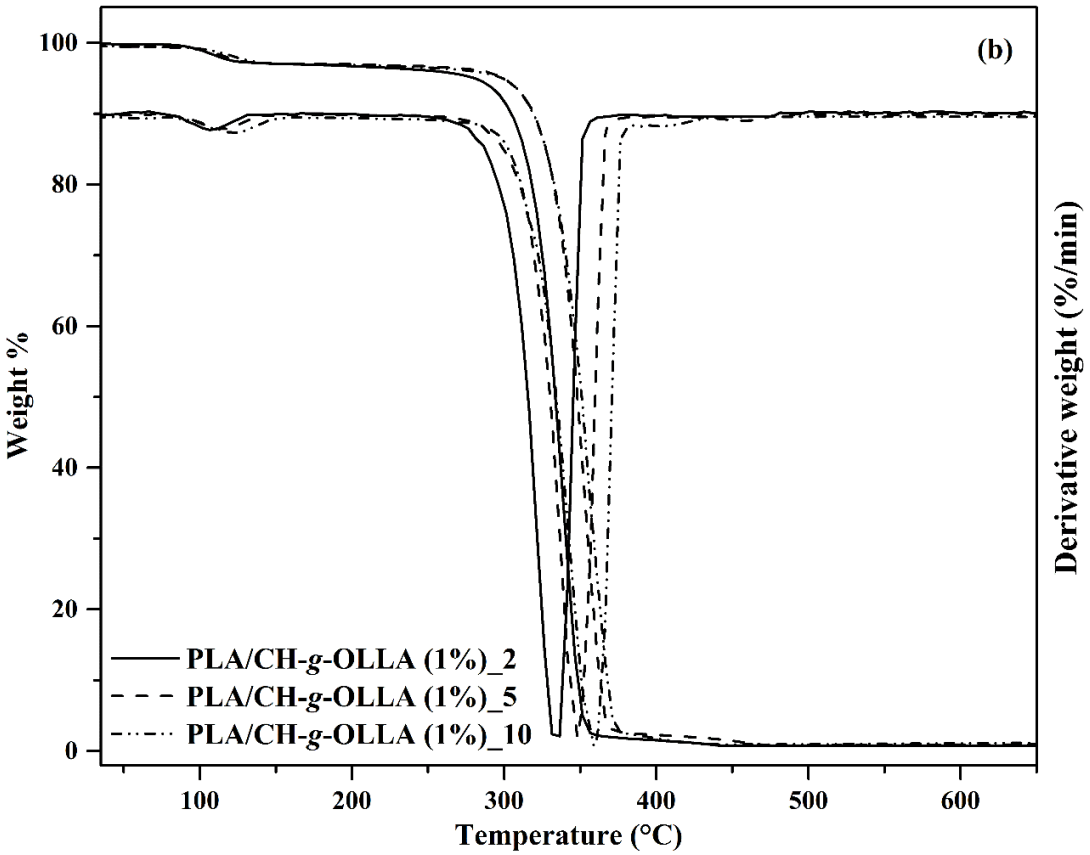

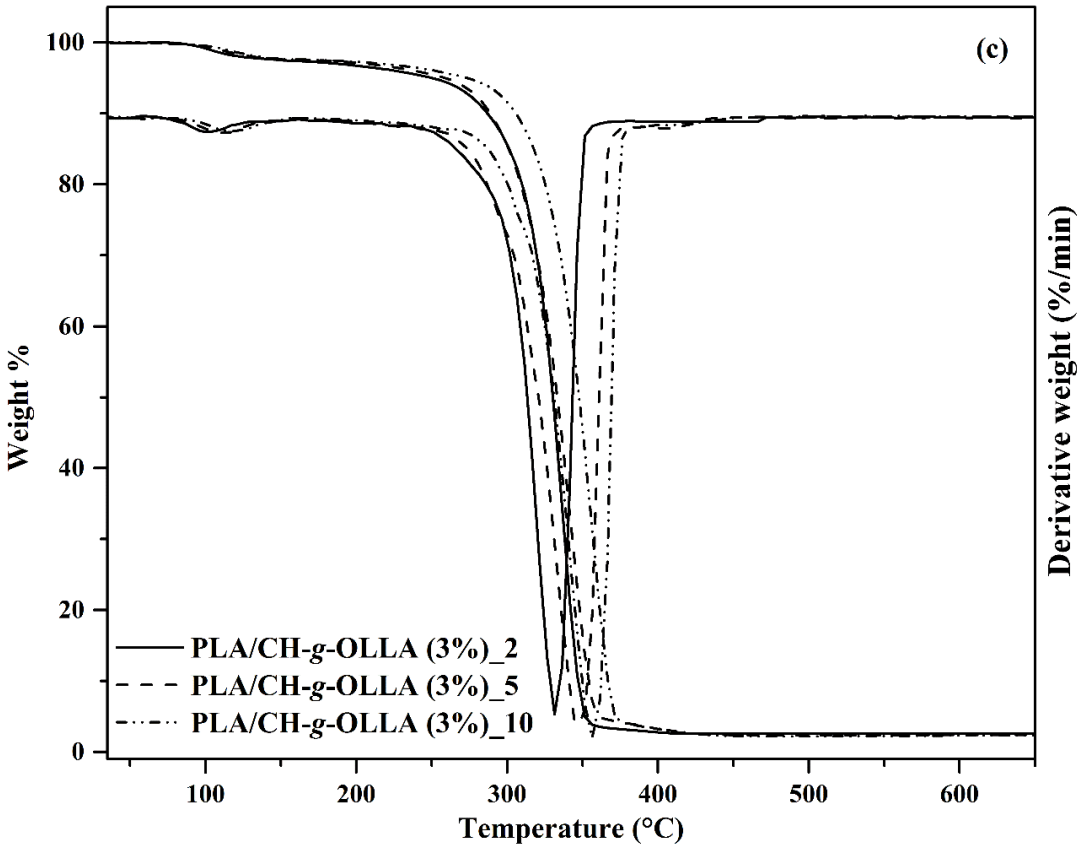

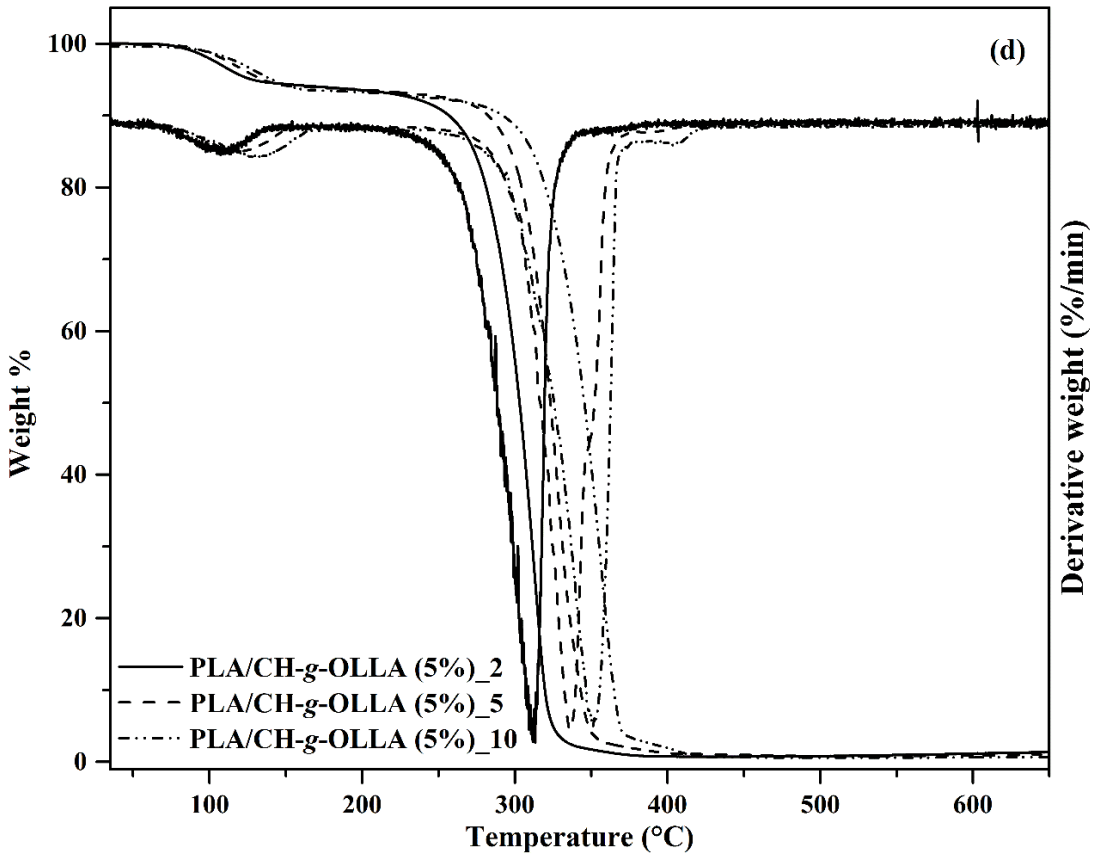

Figure 8.8. TGA and DTG curves of (a) PLA, (b) PLA/CH-*g*-OLLA (1%), (c) PLA/CH-*g*-OLLA (3%) and (d) PLA/CH-*g*-OLLA (5%) at 2, 5 and 10 °C/min.

In general, aliphatic polyesters decompose thermally via most prominent random chain scission mechanism, which is also followed by PLA and its bionanocomposite films. The kinetic parameters are calculated by using Kissinger-Akahira-Sunose, Flynn-Wall-Ozawa, Augis & Bennett and Kissinger methods at various heating rates.

8.3.2.4. Kissinger-Akahira-Sunose model

This isoconversional method is used to calculate the activation energies for PLA and PLA/CH-*g*-OLLA bionanocomposite films at different conversion values using the plot of $\ln \frac{\beta}{T^2}$ against $-\frac{1}{T}$ as mentioned in Figure 8.9(a), (b), (c) and (d) with the support of Eq. 8.10. The first order reaction model is assumed in KAS method to determine the kinetic

parameters with the help of multiple heating rate values. The slope of the fitted straight lines is increased continuously for PLA and PLA/CH-*g*-OLLA bionanocomposite films. It is observed that a random decrement/increment in E_a values with an increase in conversion from 0.1 to 0.9. However, the mean activation energy ($\overline{E}_a$) and regression coefficient ($\overline{R}^2$) values are calculated as mentioned in Table 8.4. It also reveals that the thermal stability reduces with an increase in filler loadings as presented in Figure 8.9(a), (b), (c) and (d). All the drawn lines, at various conversions (0.1 to 0.9), are parallel to each other in PLA and its bionanocomposite films, which means that the similar behaviour is followed at all conversions for all the film samples. However, the straight lines shows some deviation and are not exactly parallel at α = 0.6 and 0.7 in the case of PLA/CH-*g*-OLLA (5%) bionanocomposite film.

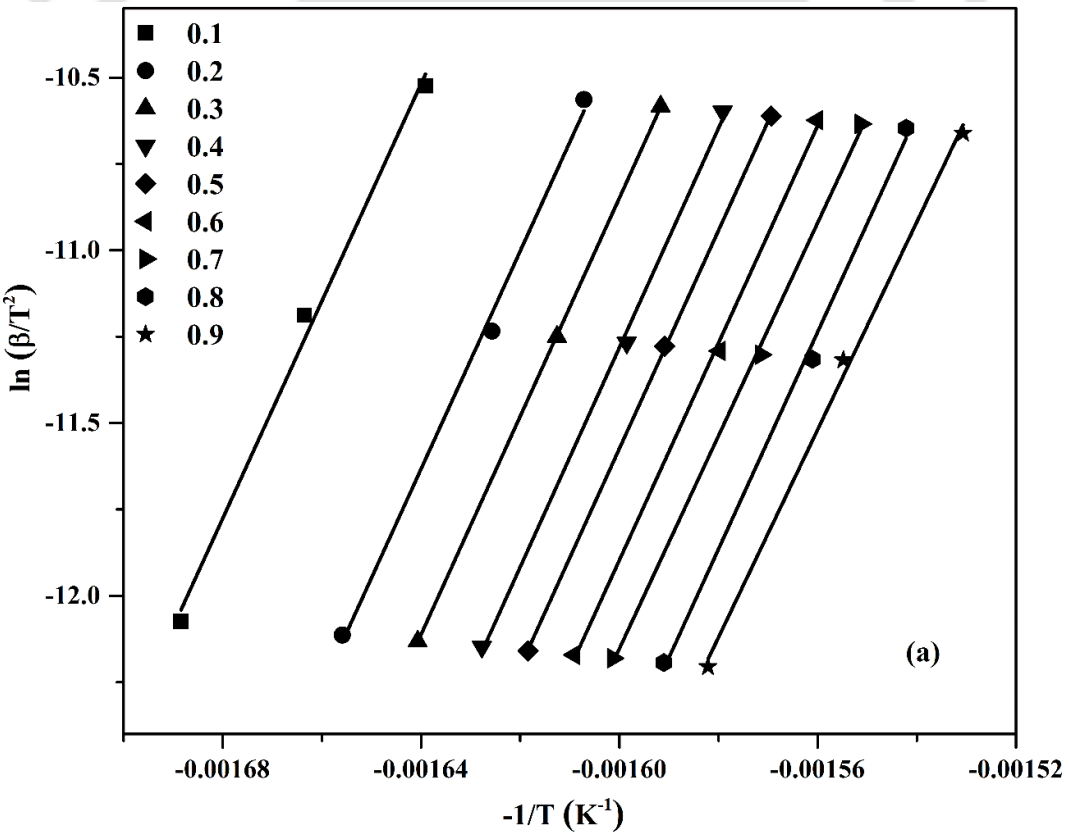

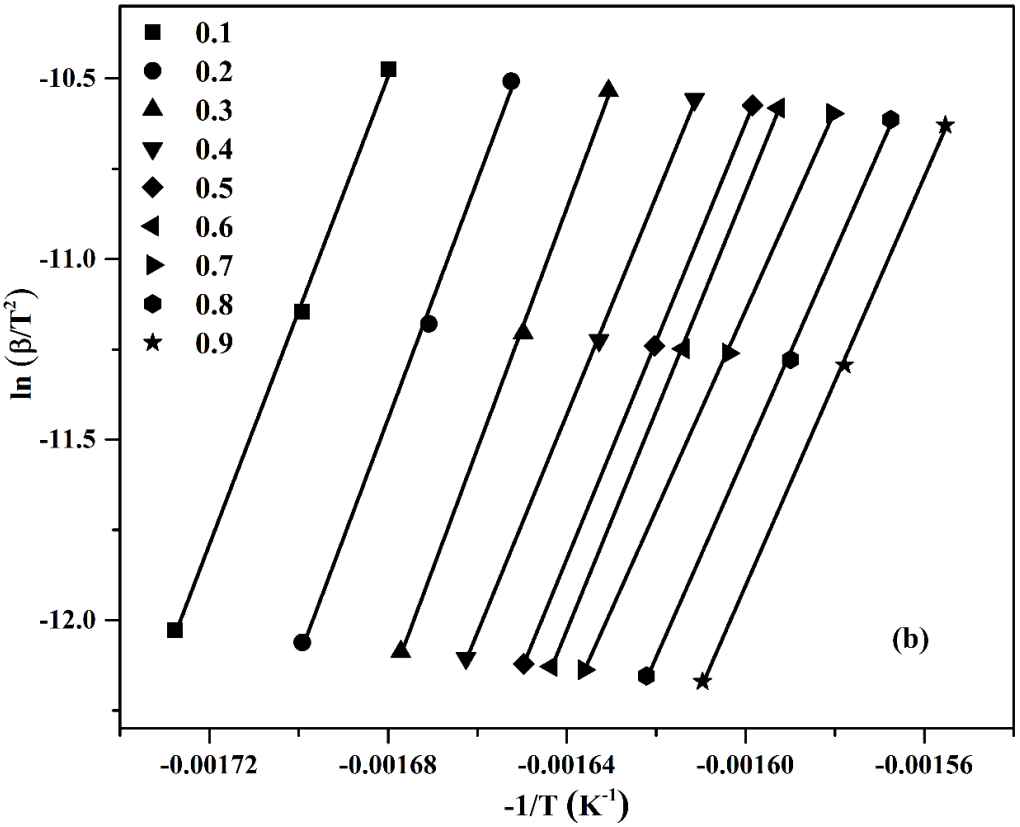

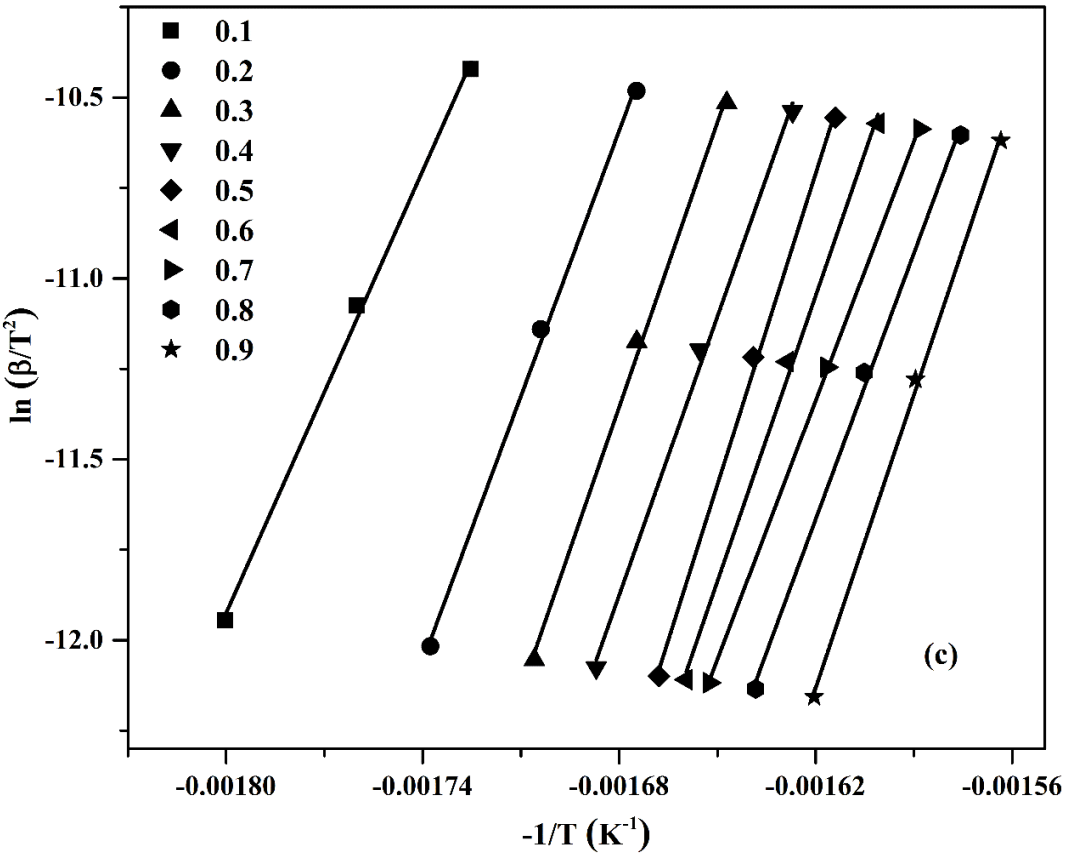

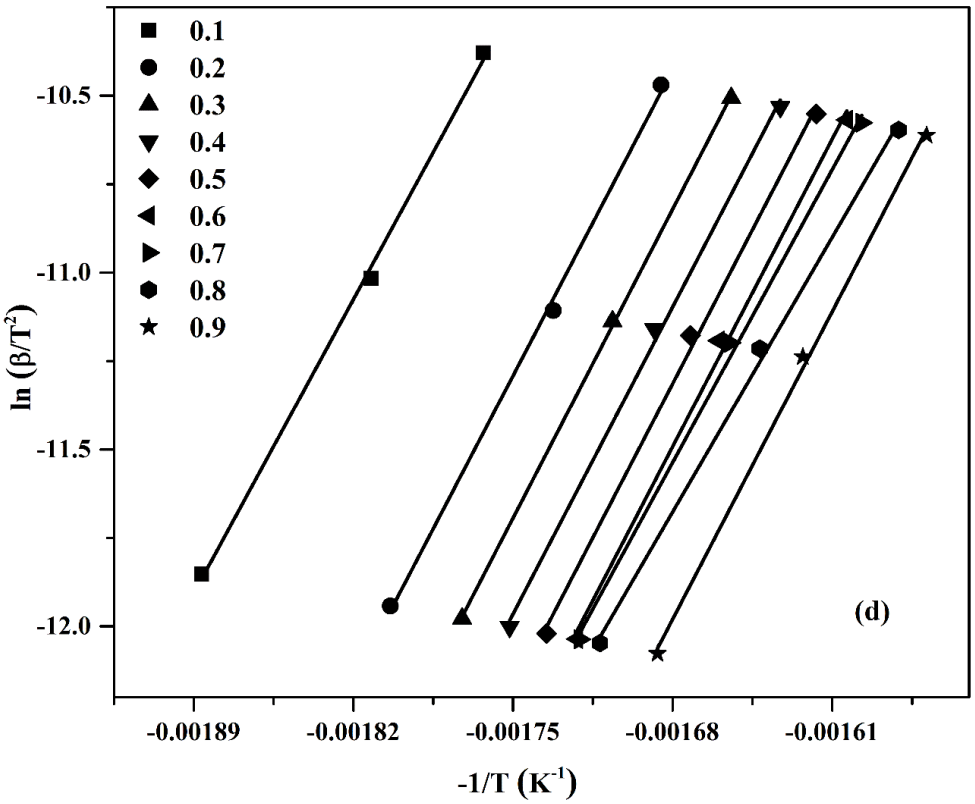

Figure 8.9. Kissinger-Akahira-Sunose plots of (a) PLA, (b) PLA/CH-*g*-OLLA (1%), (c) PLA/CH-*g*-OLLA (3%) and (d) PLA/CH-*g*-OLLA (5%) bionanocomposite films.

8.3.2.5. Flynn-Wall-Ozawa model

FWO method is used by plotting the graphs between $\log \beta$ and $(-\frac{1}{T})$ for PLA and its bionanocomposite films as displayed in Figure 8.10(a), (b), (c) and (d) with the help of Eq. 8.15. The parallel straight lines are observed at various conversion values for all film samples. Such kind of parallel lines in the conversion range (0.1-0.9) confirm the suitability of FWO method for PLA/CH-*g*-OLLA system. The slope of the drawn straight lines increases with an increase in conversion values for all the samples. A random increment/decrement in E_a values is also observed with an increase in conversion value. It is observed that the straight lines are not also parallel at α = 0.6 and 0.7 for PLA/CH-*g*-OLLA (5%) films. The deviation in the straight lines may be associated with

some manual error **[Valapa et al., 2014; Marquez et al., 2012]**. The $\overline{E}_a$ and $\overline{R}^2$ values are calculated as mentioned in Table 8.4, which also confirms the suitability of FWO model for PLA/CH-*g*-OLLA bionanocomposite films. The calculated E_a value from KAS and FWO methods are very close to each other, which shows that both isoconversional models are the prime appropriate methods for this polymeric system.

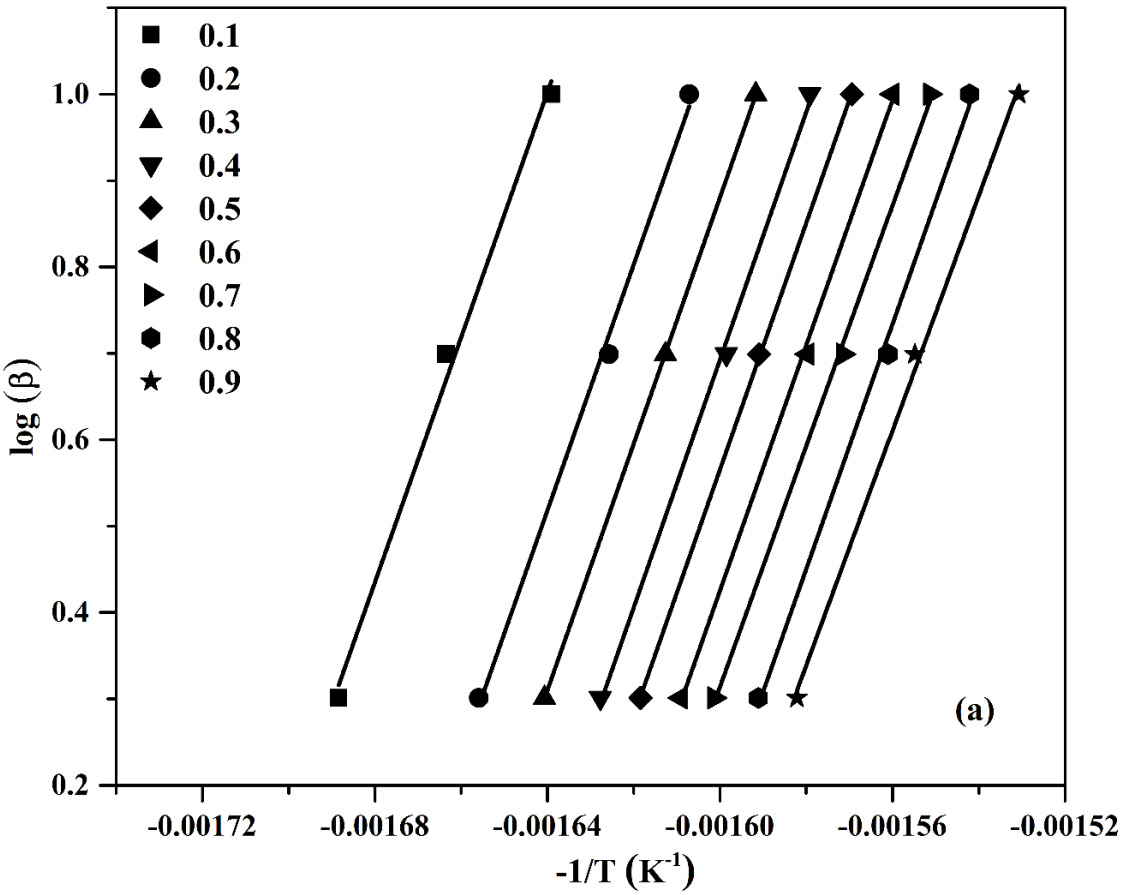

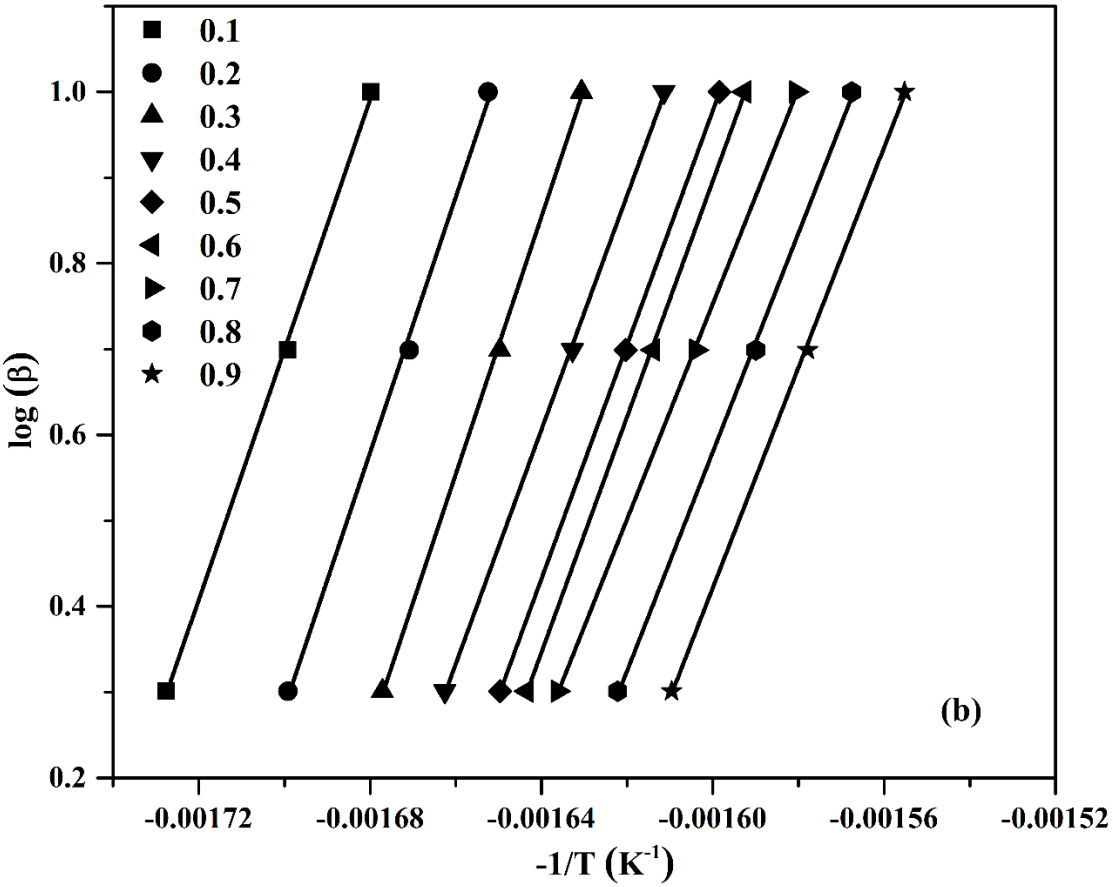

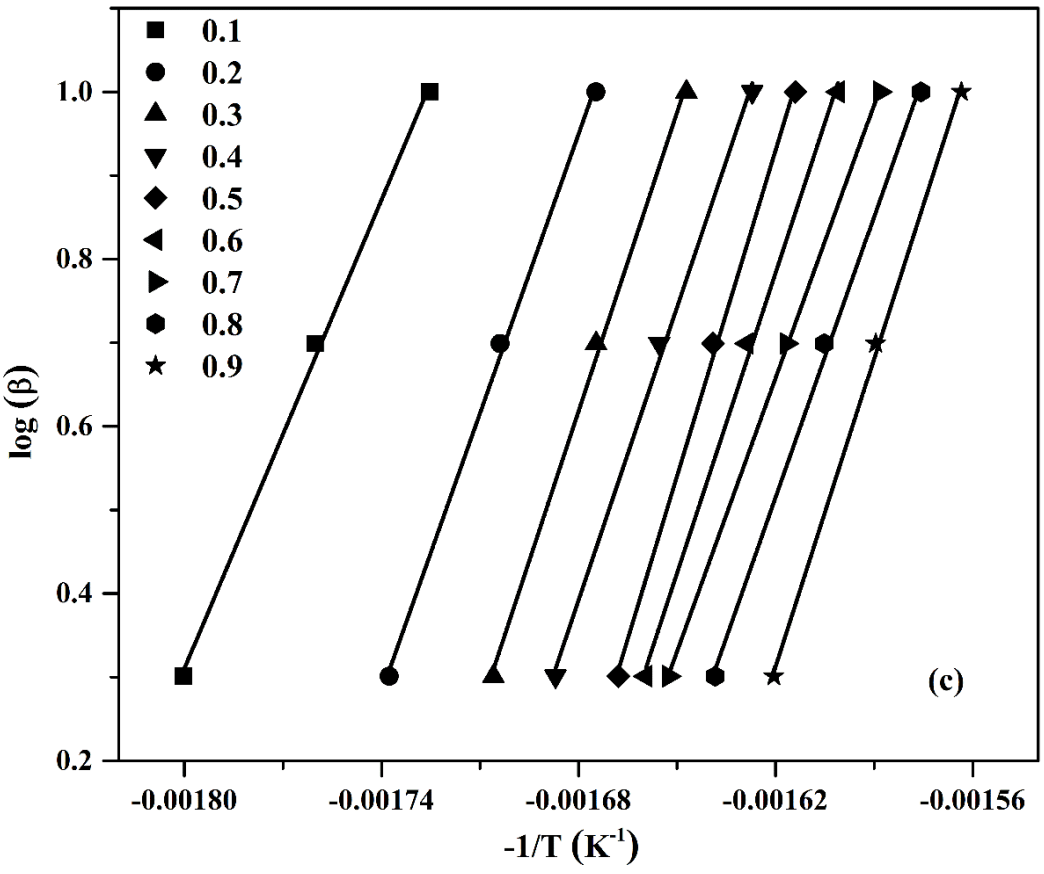

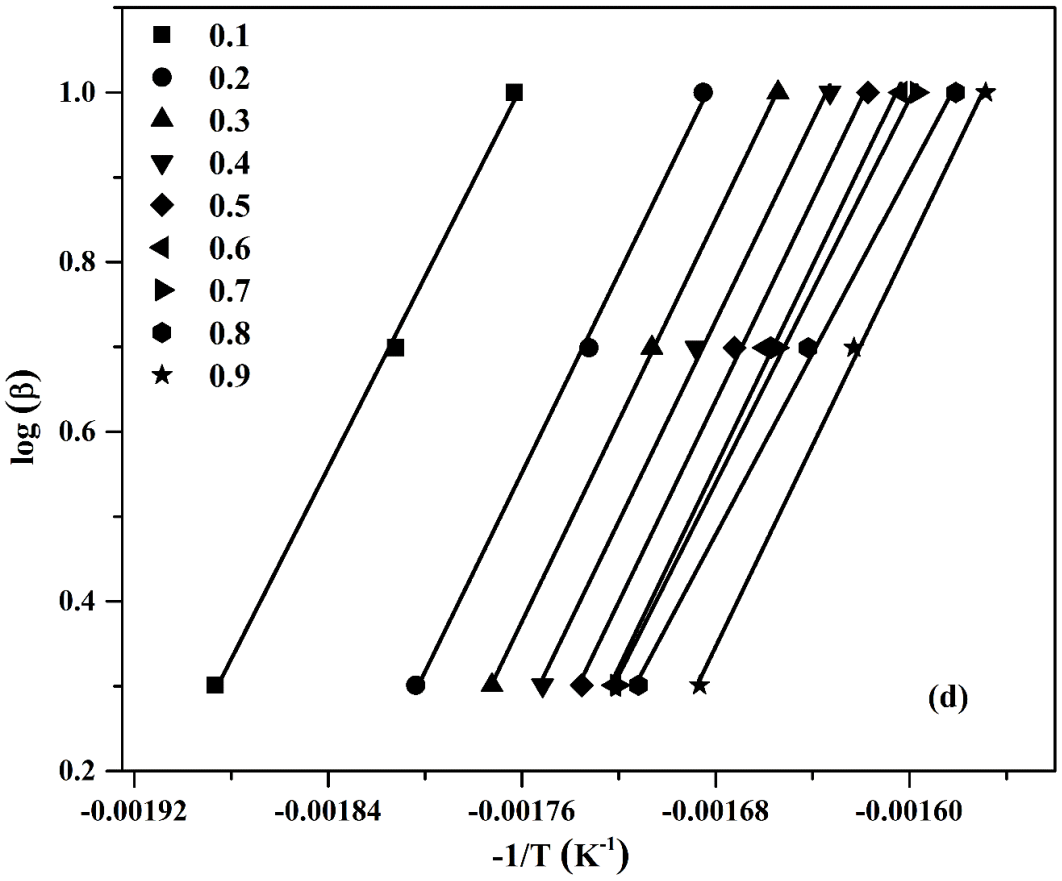

Figure 8.10. Flynn-Wall-Ozawa plots of (a) PLA, (b) PLA/CH-*g*-OLLA (1%), (c) PLA/CH-*g*-OLLA (3%) and (d) PLA/CH-*g*-OLLA (5%) bionanocomposite films.

Table 8.4: E_a and R^2 values for PLA and its bionanocomposite films calculated from FWO and KAS models.

Sample Name	FWO		KAS	
	$\bar{E}_a$ (kJ/mol)	$\bar{R}^2$	$\bar{E}_a$ (kJ/mol)	$\bar{R}^2$
PLA	257.0	0.998	260.2	0.998
PLA/CH-*g*-OLLA (1%)	250.1	0.999	252.8	0.999
PLA/CH-*g*-OLLA (3%)	209.	0.998	209.8	0.998
PLA/CH-*g*-OLLA (5%)	105.4	0.998	101.0	0.998

8.3.2.6. Augis & Bennett model

Augis and Bennett model is plotted using Eq. 8.16 to calculate the E_a values for PLA and PLA/CH-*g*-OLLA bionanocomposite films as displayed in Figure 8.11. The E_a value for each film samples is computed from the slop $(\frac{E_a}{R})$ of straight lines drawn by $\ln\left(\frac{\beta}{T_m - T_0}\right)$ against $(-\frac{1}{T_m})$ plot. Only one E_a value is obtained for each sample at maximum rate of conversion, which represents the E_a value of complete degradation process. The calculated E_a and R^2 values for PLA and its bionanocomposite are mentioned in Table 8.5.

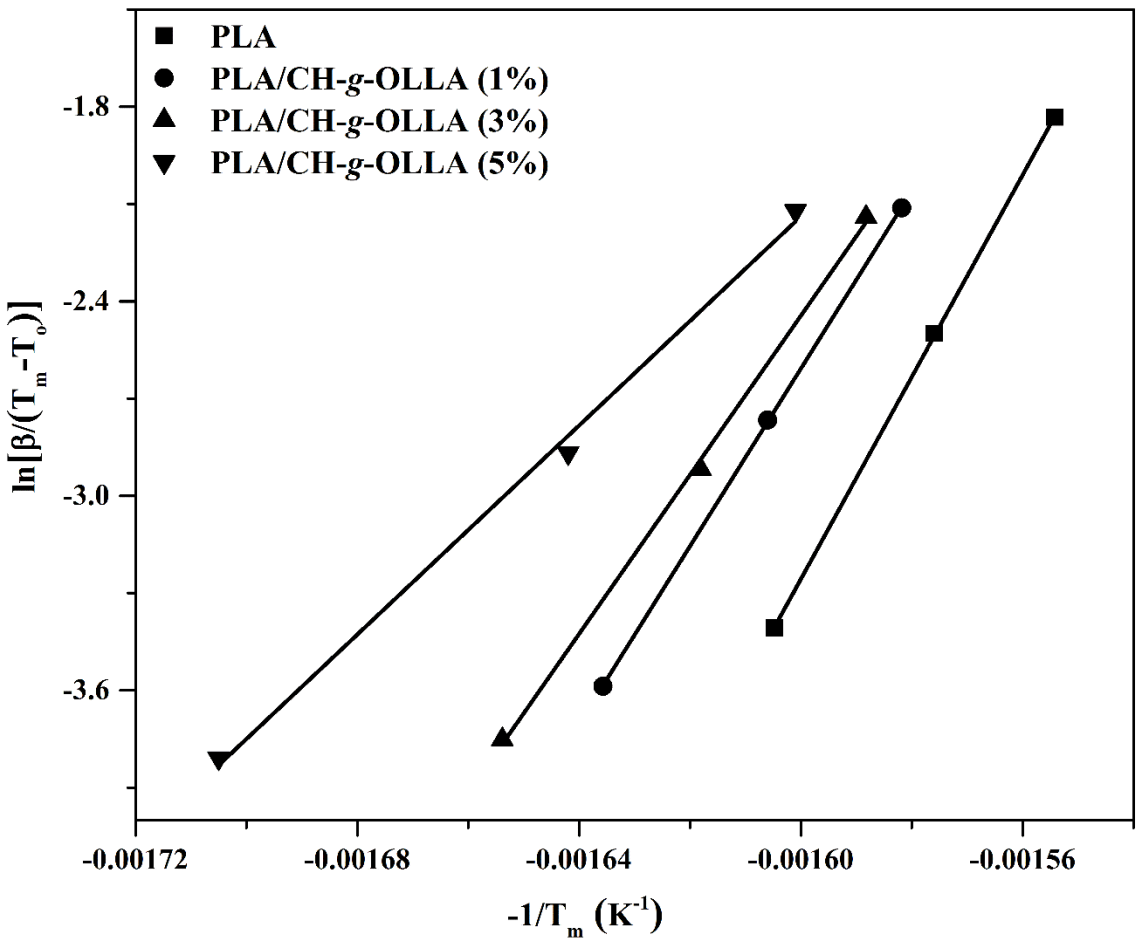

Figure 8.11. Augis & Bennett plot for PLA, PLA/CH-*g*-OLLA (1%), PLA/CH-*g*-OLLA (3%) and PLA/CH-*g*-OLLA (5%) bionanocomposite films.

The R^2 values close to 1 denotes the suitability of Augis & Benet model. The plotted straight lines at various filler loadings are not exactly parallel, which suggests the change in mechanism procedure with the addition of CH-*g*-OLLA in PLA matrix. These E_a values are also close to the values calculated by other mentioned isoconversional methods **[Chrissafis, 2008]**.

8.3.2.7. Kissinger Model

It is a model fitting method and is utilized to calculate E_a and R^2 values only at T_m with maximum weight loss rate. The straight lines are observed from the plot of $(\ln \frac{\beta}{T_m{}^2})$ against $(-\frac{1}{T_m})$ for PLA and its bionanocomposite films using Eq. 8.21 as shown in Figure 8.12. The calculated E_a and R^2 values for PLA, PLA/CH-*g*-OLLA (1%), PLA/CH-*g*-OLLA (3%) and PLA/CH-*g*-OLLA (5%) bionanocomposite films are mentioned in Table 8.5.

Table 8.5: E_a and R^2 values for PLA and its bionanocomposite films calculated from Kissinger and Augis & Bennett models.

Sample Name	Kissinger		Augis & Bennett	
	E_a (kJ/mol)	**R^2**	**E_a (kJ/mol)**	**R^2**
PLA	254.1	1	259.1	0.999
PLA/CH-*g*-OLLA (1%)	238.3	0.999	227.7	1
PLA/CH-*g*-OLLA (3%)	194.1	0.999	204.0	0.998
PLA/CH-*g*-OLLA (5%)	117.9	0.998	134.0	0.997

The drawn straight lines are not parallel to each other, which shows the different degradation mechanism followed by bionanocomposite films as compare to PLA. However, all the lines are smoothly fitted, which shows the feasibility of Kissinger model.

The same trend of calculated E_a values is observed with increase in the filler loading as observed from the other isoconversional methods. The calculated E_a values by Kissinger method are in good agreement with the KAS and FWO methods. It is noteworthy to mention that a slight variation in E_a values is observed for PLA and its bionanocomposite films as calculated by different methods. KAS and FWO methods always show the appropriate results because the E_a values are calculated at different conversion levels for each samples. However, Kissinger method can produce only one E_a value at T_m. The R^2 values also show the applicability of Kissinger and other methods to predict the thermal degradation of PLA/CH-*g*-OLLA films.

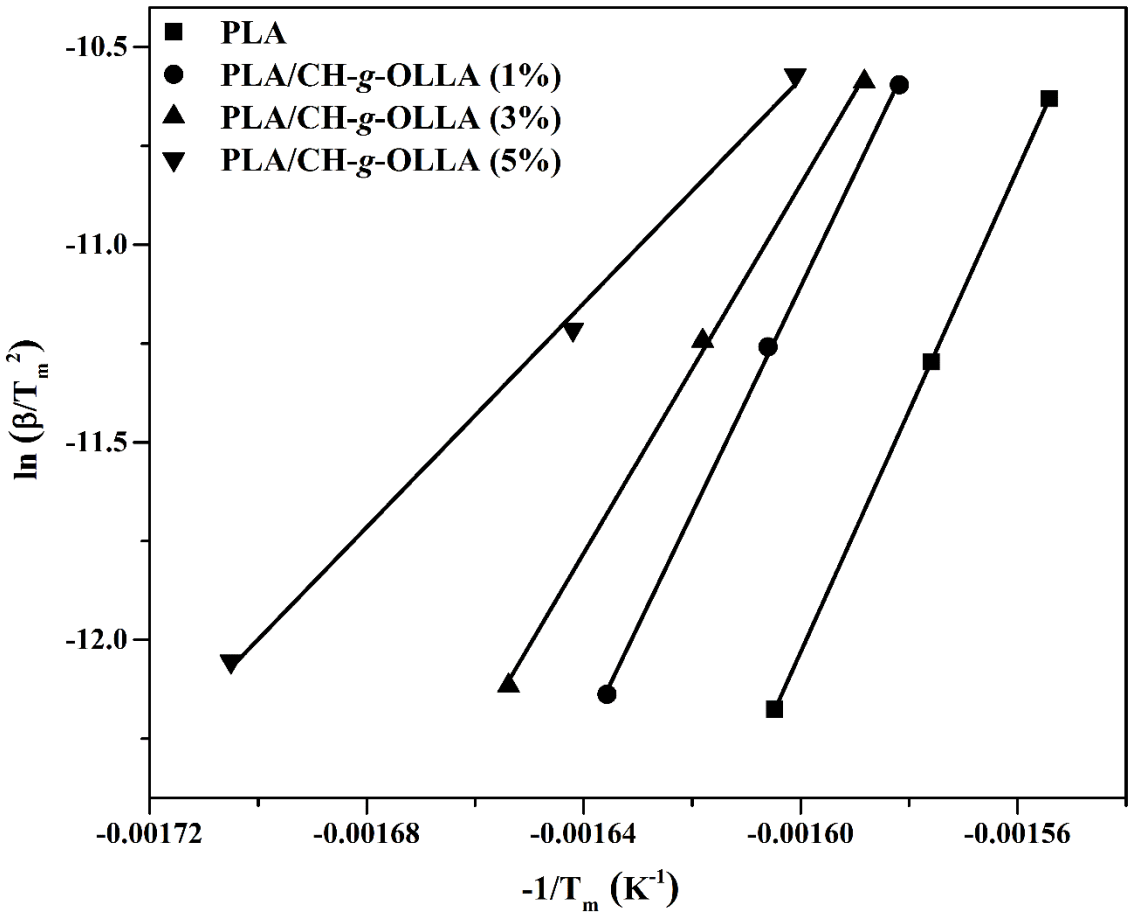

Figure 8.12. Kissinger plot for PLA, PLA/CH-*g*-OLLA (1%), PLA/CH-*g*-OLLA (3%) and PLA/CH-*g*-OLLA (5%) bionanocomposite films.

8.3.2.8. Maximum or peak temperature versus heating rate

It is concluded from the above discussion that β is directly proportional to T_m, which is increased with an increase in β for a particular sample as shown in Figure 8.13. The value of T_m is increased linearly with β for PLA and lower concentration of PLA/CH-*g*-OLLA bionanocomposite films. Straight lines are drawn by connecting all points for PLA and lower concentration of PLA/CH-*g*-OLLA films. Whereas, the linearity of the straight lines are reduced for higher concentrated PLA/CH-*g*-OLLA films.

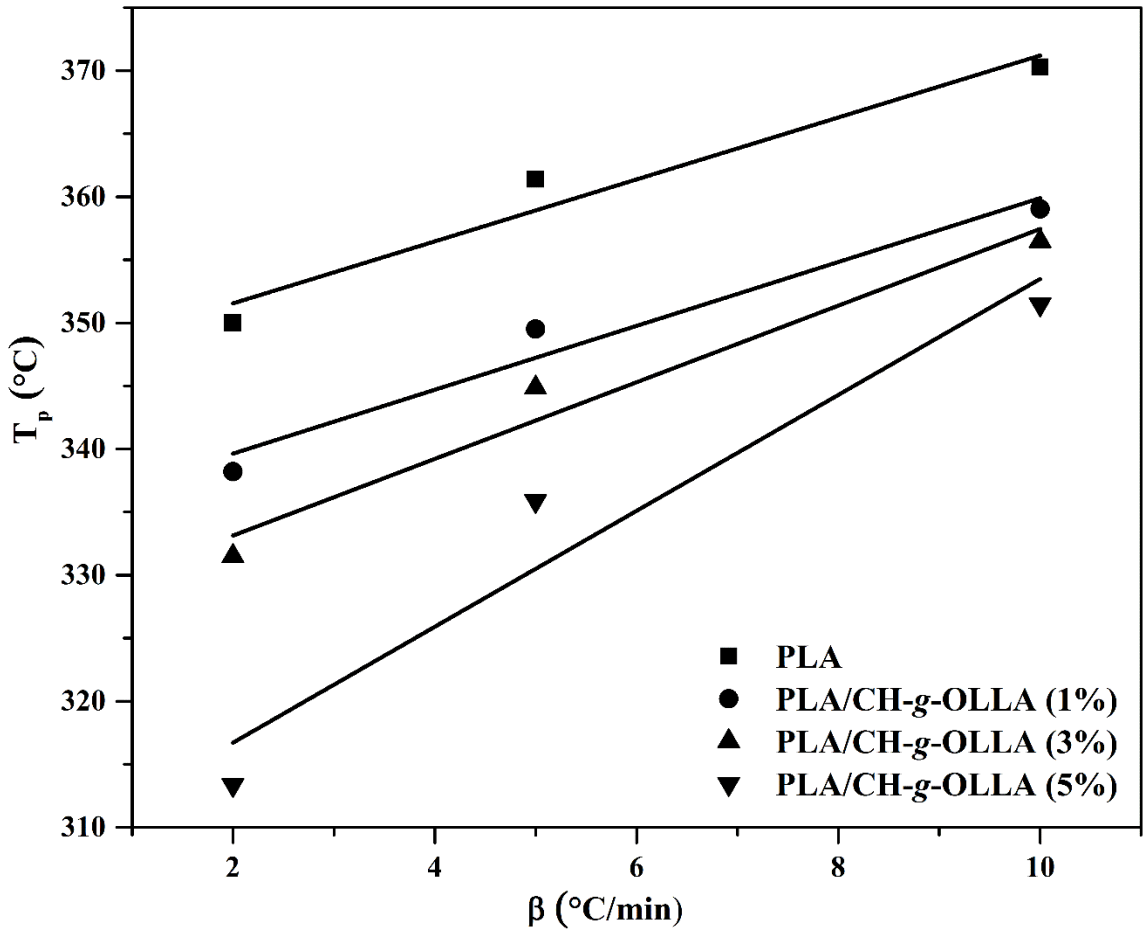

Figure 8.13. Dependence of the maximum temperature on heating rates for PLA, PLA/CH-*g*-OLLA (1%), PLA/CH-*g*-OLLA (3%) and PLA/CH-*g*-OLLA (5%) bionanocomposite films.

8.3.2.9. Activation energy versus conversion plot

The activation energy versus conversion plots are generated by using FWO and KAS models. The E_a value of degradation is a function of degree of conversion. The obtained E_a value from both the plots, varies with the degree of conversion as shown in Figure 8.14(a) and (b). The associated reason is that it is solely a chemical operation with no physical changes during degradation. Basically, the degradation of polymeric samples always reduces their molecular weights and breaks long polymer chains into smaller ones due to the bonds dissociation phenomena between the atoms. The weak sites are always present in the polymer chains. Those weak sites are always responsible to promote thermal degradation. During thermal degradation, this variation in E_a value implies the change of reaction mechanism and if the E_a value also changes with conversion then the reaction should follow a complex reaction process **[Zhang et al., 2015]**. Practically, the calculated E_a value shows less variations with the degree of conversion for PLA and PLA/CH-*g*-OLLA (5%) films for both (FWO and KAS) models as shown in Figure 8.14(a) and (b). It suggests that the overall degradation does not follow a single step mechanism. It can also be predicted that there should be the lowest experimental error. While, much deviation in activation energies are observed with different conversion values. It also shows the same behaviour with higher experimental error in PLA/CH-*g*-OLLA (1%) and PLA/CH-*g*-OLLA (3%) films for both models **[Marquez et al., 2012]**. The other reason associated with the reduction in E_a values by increase in filler loading, is the availability of higher acidic sites in the course of thermal degradation in PLA matrix, which accelerates the auto-catalytic effect during degradation of PLA/CH-*g*-OLLA samples. It always enhances the degradation and reduces the activation energy. In the case of PLA/CH-*g*-OLLA bionanocomposite films, chitosan gets transformed into anhydrous chitosan by the dismissal of unbound, bound water during thermal decomposition. It

generates H^+ ions, which increases with the addition in filler loading. The hydrolysis of ester group takes place during thermal degradation, which further converts into acids. The formation of alkyl groups also increases with this phenomena. Hence, the higher concentration of acid terminals increases the random chain scission of ester groups in PLA backbone. The produced intermediates during random chain scission process will further catalyze the autocatalytic chain-end hydrolysis of PLA oligomers. This increases rate of degradation of PLA. It is well known that the chain end hydrolysis reactions are faster than random chain scission reactions. Hence, PLA thermal consistency reduces with increase in filler loadings **[Valapa et al., 2014]**.

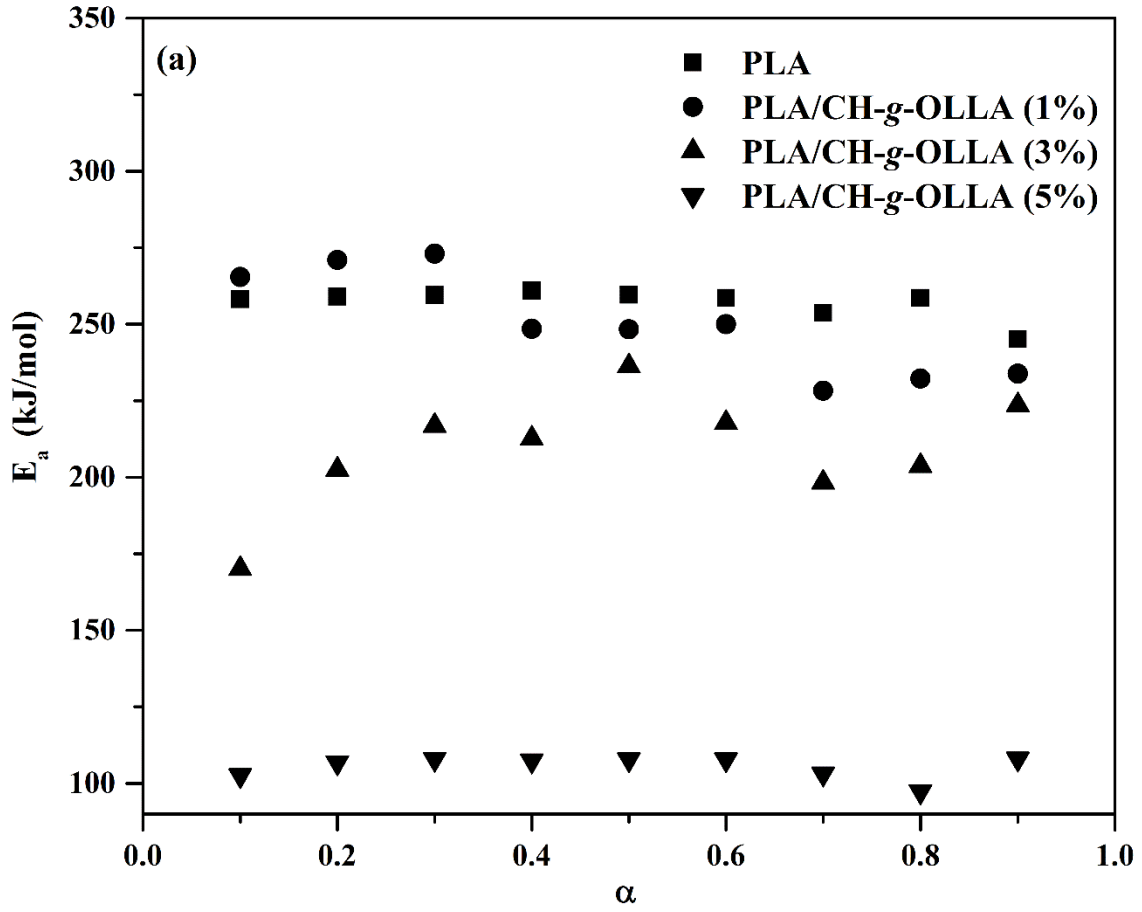

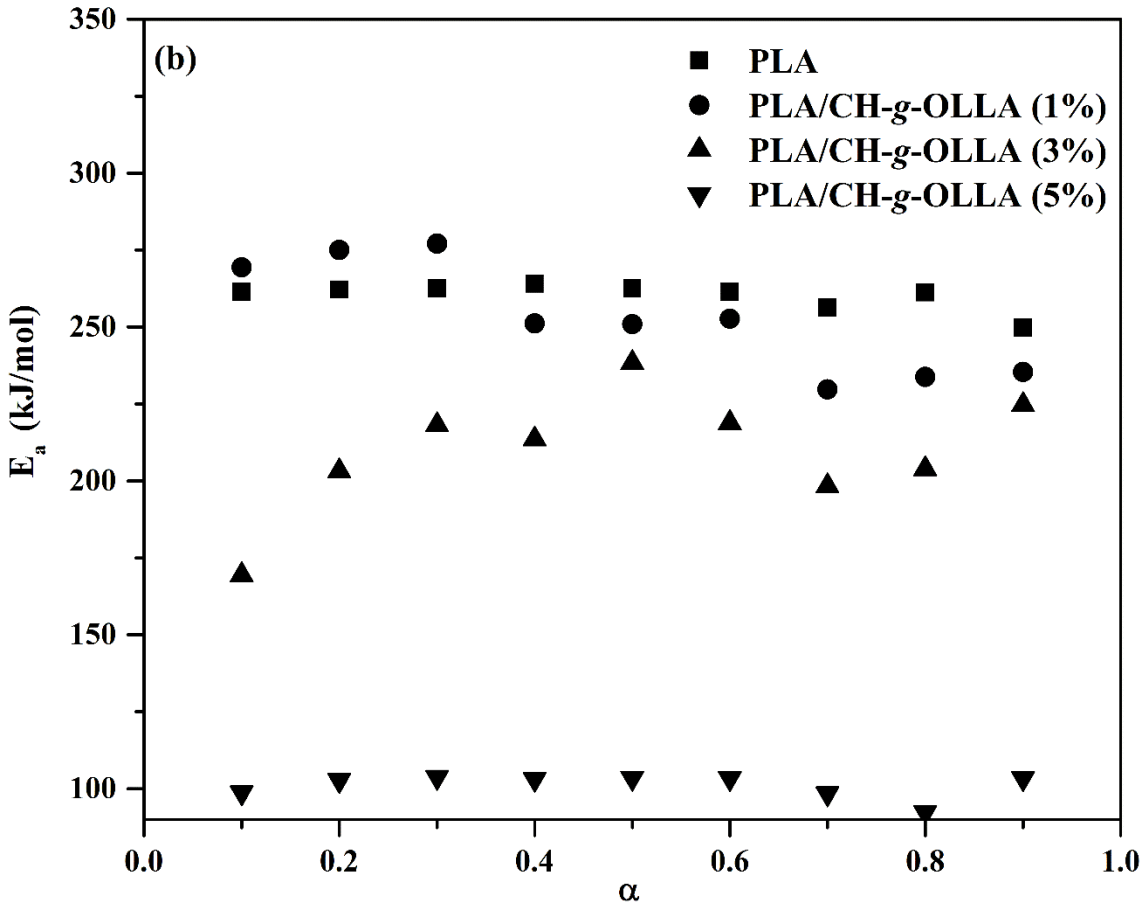

Figure 8.14. Activation energy versus conversion plots obtained from (a) FWO model and (b) KAS model for PLA, PLA/CH-*g*-OLLA (1%), PLA/CH-*g*-OLLA (3%), PLA/CH-*g*-OLLA (5%) bionanocomposite films.

8.3.3. Characterization of evolved gaseous products using TG-FTIR

The generated gases of various products from TGA furnace, are transferred to FTIR instrument to identify the specific functional groups for the purpose to identify the thermal decomposition manner of PLA, CH and PLA/CH-*g*-OLLA bionanocomposite films. The evolved gaseous products from PLA, PLA/CH-*g*-OLLA bionanocomposite films and CH are incorporated in the form of 3-D curves in a dynamic temperature range of 30 to 700 °C as displayed in Figure 8.15(a), (b) and (c) respectively. Figure 8.15(a), (b) and (c) incorporate the FTIR signals of PLA, PLA/CH-*g*-OLLA bionanocomposite films

and CH respectively, obtained at various degradation temperatures such as 250, 357, 456 and 555 °C. The main degradation products obtained from PLA are identified as water (3570 cm^{-1}), hydrocarbons (2950 and 3005 cm^{-1}), CO_2 (2352 cm^{-1}), CO (2181 and 2108 cm^{-1}) and cyclic oligomers or lactides (1791 cm^{-1}). The evolution of carbon dioxide gas is due to the chain homolysis of PLA. The current results also matches with other available literatures **[Zhao et al., 2015; Tudorachi et al., 2012]**. The other five FTIR peaks are also obtained at fingerprint region, which are identified as $-CH_3$ bending (1455 cm^{-1}), $-CH-$ stretching (1377 cm^{-1}), $-C=O$ stretching (1241 cm^{-1}), $-C-O-$ stretching (1100 cm^{-1}) and $-C-C-$ stretching (934 cm^{-1}). All the peak intensities are higher at 357 °C as compare to other mentioned temperatures, which means that the decomposition of PLA is maximum at 357 °C. The absorbance peaks of evolved gaseous products for PLA and PLA/CH-*g*-OLLA bionanocomposite films are positioned at similar wavenumbers.

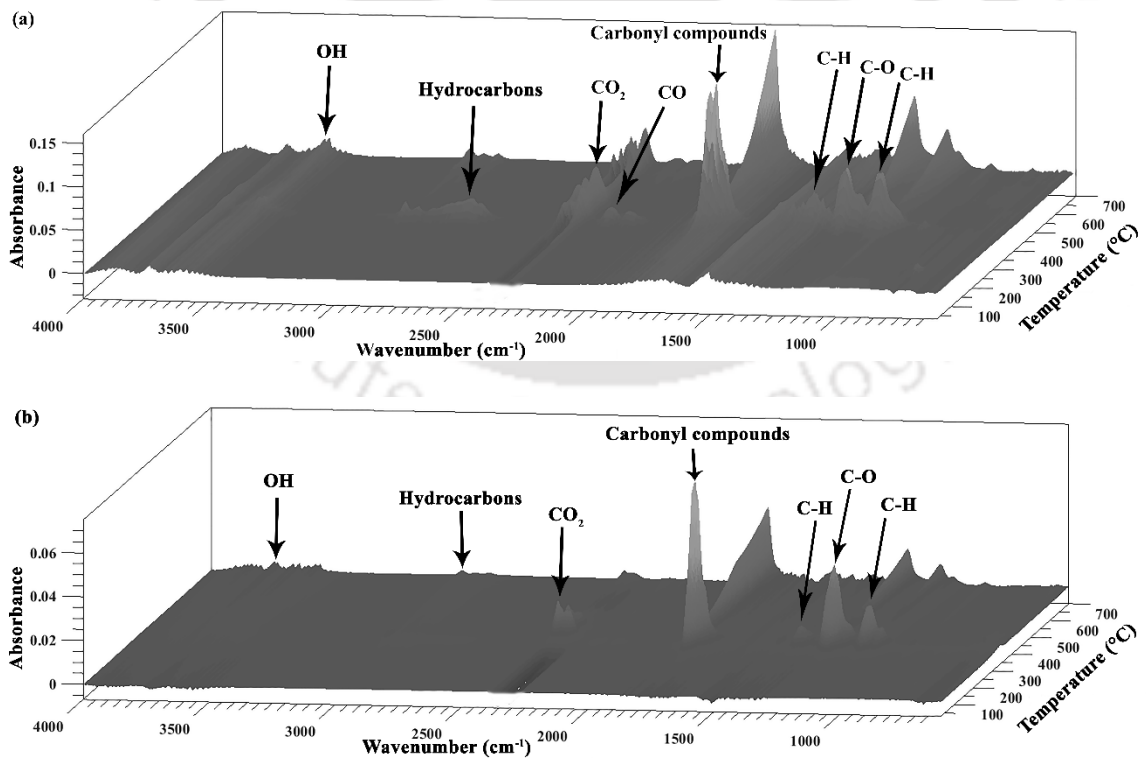

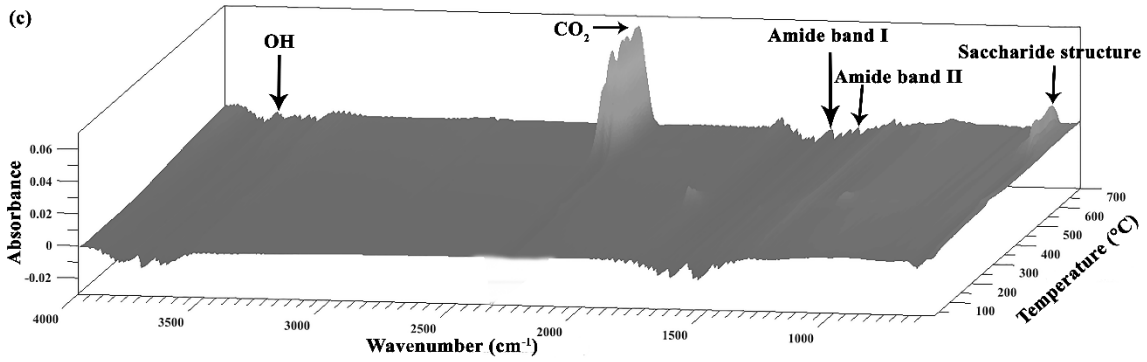

Figure 8.15. Evolved gaseous products mentioned in 3D-FTIR spectra of (a) PLA, (b) PLA/CH-*g*-OLLA (5%) bionanocomposite film and (c) chitosan film.

However, the intensity of the peaks is less in PLA/CH-*g*-OLLA as compare to PLA films. The CO peak is absent in PLA/CH-*g*-OLLA bionanocomposites, which is a valuable advantage as far as environmental health is concern. Three new peaks are monitored at 1650, 1543 and 1528 cm^{-1} in PLA/CH-*g*-OLLA bionanocomposite films, which denotes amide I band, amide II band and −NH stretching respectively as shown in Figure 8.16(b). Amide I and amide II bands represent the availability of chitin and chitosan in PLA/CH-*g*-OLLA bionanocomposites. However, −NH stretching represents the linkage between chitosan backbone and OLLA side chain, which is also a clear indication of grafting between chitosan and OLLA. The peaks intensity is very less due to the presence of polymers in trace amount. The peaks of water, $-CH_3$ bending, amide I and amide II bands are also observed at similar positions in the FTIR spectra of chitosan as shown in Figure 8.16(c). The broad peaks at 1290, 827 and 671 cm^{-1} are also observed in chitosan spectra, which represent CO − NH stretching and saccharide ring structure. The peak intensity of carbon dioxide emission at 2352 cm^{-1} is observed as highest in chitosan decomposition as compare to that of PLA and PLA/CH-*g*-OLLA bionanocomposite films.

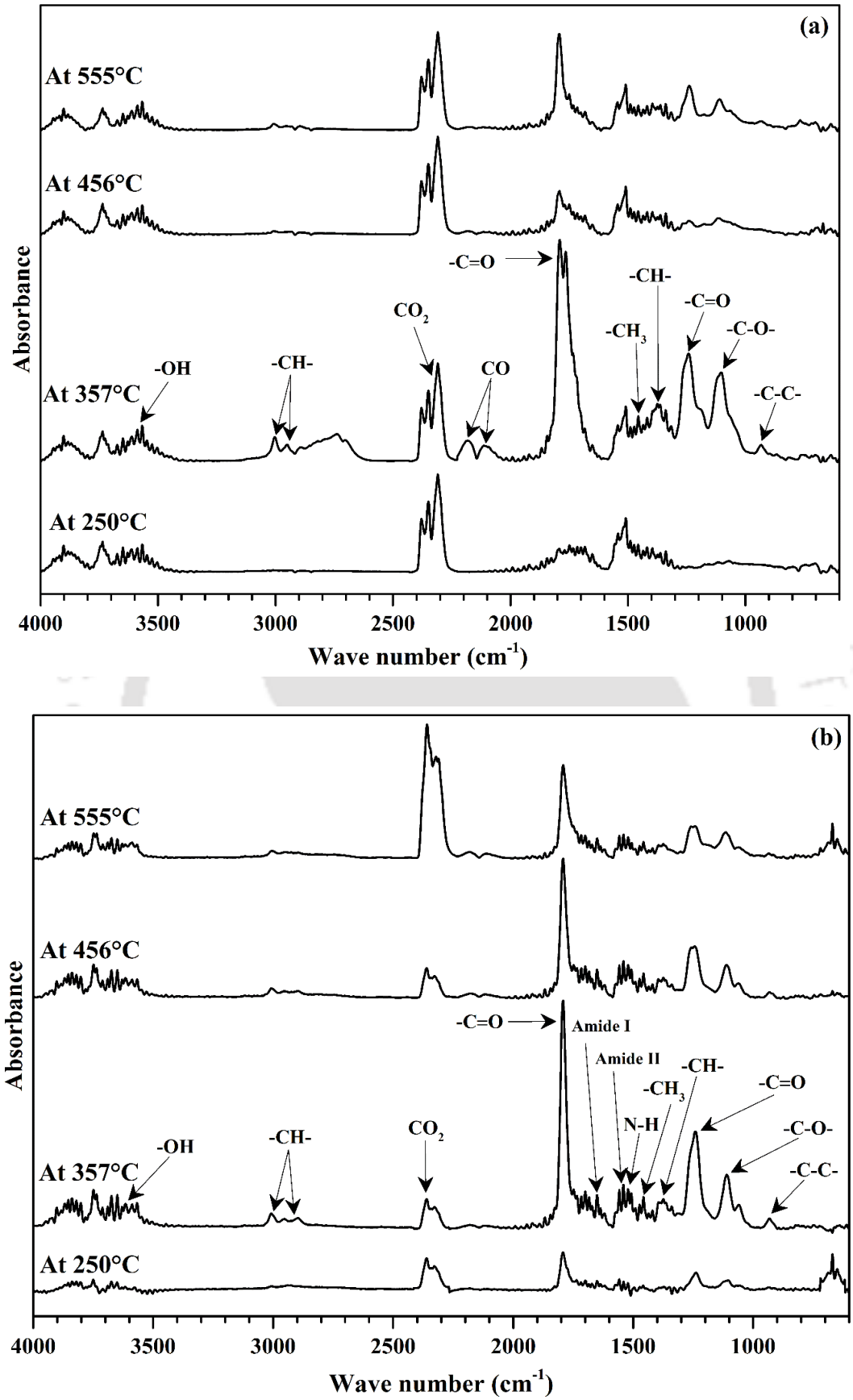

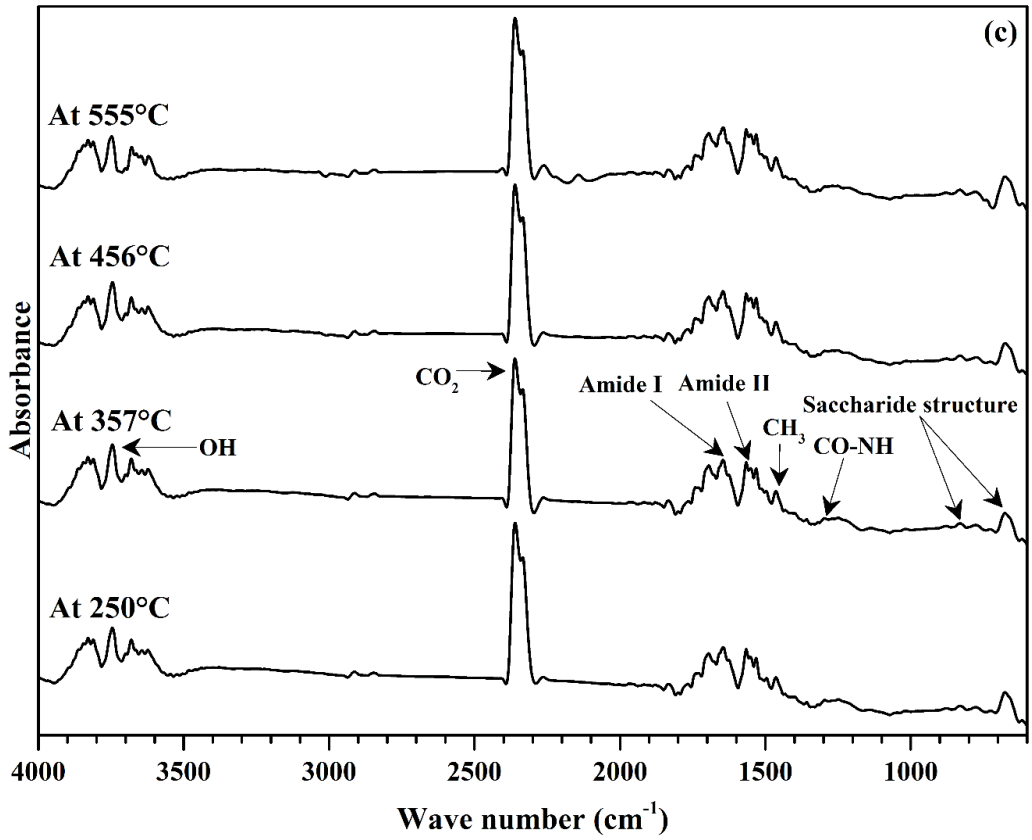

Figure 8.16. FTIR spectra of gaseous products evolved during thermal degradation of (a) PLA film, (b) PLA/CH-*g*-OLLA bionanocomposite film and (c) chitosan film at various degradation temperatures.

The peak represents to CO, is absent during chitosan degradation, which makes it biodegradable. From the above discussion, it is clear that the addition of small loadings of CH-*g*-OLLA does not alter the main degradation products of PLA. However, an obvious reduction in peak intensities is occurred in PLA/CH-*g*-OLLA bionanocomposite films as compare to 3-D images of TG-FTIR results of PLA. The reduction in peak intensities may be due to the radicals produced by the thermal degradation of amphiphilic CH-*g*-OLLA. These products may accelerate the radical reactions, which take place at higher temperatures.

8.4. Summary

The present study concludes the influence of CH on the thermal degradation behaviour of PLA films under nitrogen atmosphere at different heating rates. The TGA and DTG curves reveal that the thermal stability of PLA/CH biocomposite films reduces with increase in filler concentration. The addition of filler also reduces T_{on}, T_P and T_{off} with increase in filler concentration. All thermal stages of film samples move towards higher temperatures at higher heating rates. One main degradation peak has been observed for all the samples. The thermal degradation kinetics has also been investigated by using KAS and FWO methods for PLA and PLA/CH biocomposite films. The $\overline{E}_a$ and $\overline{R}^2$ values have been reduced continuously with increase in fillers concentration and the variations in E_a values with respect to conversion have been listed for all the samples. Similarly, the thermal stability of PLA films were decreased continuously with an increase in CH-g-OLLA wt%. Thermal degradation kinetics of PLA and PLA/CH-*g*-OLLA bionanocomposites were analyzed using isoconversional and model fitting methods. As a results, isoconversional methods were found more reliable because it calculates E_a and R^2 values at each conversion. The results suggest that PLA and PLA/CH-*g*-OLLA bionanocomposite films undergo a complex reaction mechanism during non-isothermal degradation.

Chapter 9

Crystallization Behaviour of Poly (Lactic Acid)/Chitosan based Films

This chapter demonstrates the effect of CH and CH-g-OLLA nano-filler on the crystallization behaviour of solution casted PLA films, which is also equally important for the improvement in multiple properties essential for stringent food packaging applications. In the case of CH-g-OLLA nano-filler, the improvement in crystal nucleation density of PLA films was observed after the addition of CH-g-OLLA in various proportions, which was due to the availability of newly generating nano-nucleating sites. The crystallization kinetics suggest non-three dimensional truncated spherical structures, which is controlled by the combination of thermal and athermal instantaneous nucleations. POM analysis suggested that the spherulite growth of PLA is improved significantly with the addition of CH-g-OLLA.

9.1. Introduction

A plant derived bio-based polymer i.e. poly (lactic acid) is extensively consumed as a substitute of fossil-based synthetic polymers due to its non-toxic and eco-friendliness, which encourages the researchers to explore its properties and overcome its limitations to lead upto commercial scale. PLA is mainly preferred for practical purposes and is manufactured at industrial scale in few countries such as China and USA. The utilization of PLA in various applications is limited due to high cost, low thermal stability and inferior mechanical properties as compare to fossil based polymers like PE, PET and PP. Such limitations can be eliminated by increasing the crystallinity or by enhancing the crystal nucleation density with the help of various techniques such as cross-linking, blending and stereocomplex crystallization **[Henmi et al., 2016]**. The improvement in thermal stability of PLA is a critical issue, which has widen the scope of industrial and commodity applications. The thermal stability of PLA can be enhanced by various methods. One of the most efficient method is to improve the crystallinity of PLA by incorporation of inorganic nucleating agent such as MMT, talc, nanostructured carbon and low molecular organic compounds **[Tsuji et al., 2009]**. An attempt was made to improve the crystallinity of PLA by incorporating poly(D-lactic acid) (PDLA) as a biodegradable nucleating agent **[Yamane and Sasai, 2003]**. Hence, it is observed that distinct properties, processability and production cost of PLA mainly vary with the variation in crystallization behaviour, crystallization rate and final crystallinity of the product. The production rate of PLA and heat resistance capacity increase with an increase in crystallization rate, which reduces the production cost. It is noteworthy to mention that very high crystallization rate can cause difficulty in recycling of PLA articles. Hence, it is very important to optimize the crystallization rate and its behaviour for all types of nucleating agents in the industrial production of PLA. The utilization of biodegradable crystallization-manipulating agents

such as polyesters help in the designing and fabrication of completely biodegradable polymers, which may be consumed for various biomedical and environmental applications with their improved physical properties and biodegradability. **Tsuji et al., 2009** have used very low amount (0.1 wt%) of poly(glycolic acid) (PGA) as a crystallization-accelerating agent for PLLA. However, the difference in the melting temperature of PLLA and PGA is ~50 °C. It is concluded that the crystallization-accelerating mechanism of PGA is somewhat different as compared to that of inorganic nucleating agents and PLLA/PDLA stereocomplex. It is meaningful to mention that the addition of biodegradable polyesters such as PCL and PHB in PLLA matrix may modify the mechanical and other properties. The presence of low contents (below 10 wt%) of biodegradable polyesters as additives in PLLA matrix can generate the meaningful information about the optimization of crystallization behaviour and rate of PLLA. To optimize the use of nucleating agents in PLA matrix, it is mandatory to understand the isothermal and non-isothermal crystallization kinetics theory.

The present research work is focused on the utilization of CH-*g*-OLLA copolymer in various proportions as a crystallization-accelerating agent in PLA matrix. The isothermal crystallization kinetics of PLA/CH-*g*-OLLA bionanocomposite films has been performed using Avrami equation. Polarized optical microscopy was also performed to visualize the growth of PLA crystals in the presence of CH-*g*-OLLA copolymer.

9.2. Isothermal crystallization kinetics theory

The relative crystallinity (X_t) of PLA and other bionanocomposite films reveals the influence of CH-*g*-OLLA on nucleation phenomena during isothermal crystallization. The relative crystallinity can be observed with respect to crystallization time and is calculated according to Eq. 9.1 **[Cai et al., 2011]**.

$$X_t = \frac{\Delta H_t}{\Delta H_\infty} = \frac{\int_0^t \left(\frac{dH}{dt}\right).dt}{\int_0^{t\infty} \left(\frac{dH}{dt}\right).dt} \quad (9.1)$$

Where, ΔH_t, ΔH_∞ and $\frac{dH}{dt}$ are the enthalpy of isothermal crystallization at time t, enthalpy of complete crystallization and the rate of heat evolution respectively. The relative crystallinity can also be obtained from exothermic peak area at isothermal crystallization using DSC analysis. Further, the Avrami theory is based on the assumption that the relative crystallinity always increases with crystallization time and can be applied for the determination of isothermal crystallization behavior of PLA and bionanocomposite films by using Eq. 9.2 **[Cai et al., 2011; Tsuji et al., 2009; Chen and Wu, 2014]**.

$$1 - X_t = \exp(-Kt^n) \quad (9.2)$$

The Eq. 9.2 can be modified and rewritten in the form of double logarithmic form:

$$\ln[-\ln(1 - X_t)] = \ln K + n \ln t \quad (9.3)$$

Where, X_t, t, n and K are the relative crystallinity of polymers at different time, period of crystallization process, Avrami exponent and crystallization rate constant respectively. The Avrami exponent (n) is basically correlated with the mechanism constant that depends on the kind of nucleation whereas, crystallization rate constant (K) is a growth rate constant which includes nucleation and growth rate parameters. The plot between $\ln[-\ln(1 - X_t)]$ and $\ln t$ can give the values of n and K from the slope and intercept respectively. The crystallization process can be addressed by the two crystallization stages in which the primary crystallization stage is denoted by the linear portion whereas, secondary crystallization stage represents the nonlinear portion. Another important parameter for crystallization kinetics is crystallization half time ($t_{1/2}$) which is defined as the time consumed by the sample from the start of the relative crystallinity until 50% completion. The half time can be calculated using Eq. 9.4 **[Cai et al., 2011]**.

$$t_{1/2} = (\frac{\ln 2}{K})^{\frac{1}{n}} \quad (9.4)$$

The $t_{1/2}$ value is utilized for the prediction of crystallization rate.

The spherulitic growth rate was estimated from the slope of spherulitic radius (R) plotted as a function of crystallization time (t) by using Eq. 9.5 **[Ding et al., 2013]**.

$$G = \frac{dR}{dt} \quad (9.5)$$

9.3. Results and discussion

9.3.1. Crystallization behaviour of PLA/CH biocomposite films

The crystallization behaviour of PLA/CH biocomposite films was performed at 110 ºC to observe the effect of extracted chitosan on isothermal crystallization kinetics and crystalline structure of PLA in their immiscible blends as confirmed by FESEM analysis.

9.3.1.1. DSC analysis

The first heating cycle is highly recommended for the removal of physically & chemically bonded moisture, processing defects and also to erase the polymer thermal history. In second heating cycle, the glass transition temperature of PLA is found at 60.4 ºC which is continuously reduced up to 57.5 ºC with an increase in CH loading as shown in Figure 9.1. This reduction of ~2.9 ºC is due to the formation of shorter chain segments **[Valapa et al., 2015]**. The cold crystallization temperature (T_{cc}) of PLA is observed at 121.8 ºC which is close to T_{cc} values, suggested in literature **[Tripathi and Katiyar, 2016]**. A slight reduction of up to 2.1 ºC in T_{cc} values are observed in PLA/CH biocomposite films because the addition of CH assists the diffusion rate which leads to the faster migration of polymer chains to the nucleus surface. The sharpness of the cold crystallization peaks increases with an increase in filler loading, which suggests that the rate of crystallization becomes faster to that of PLA due to the homogeneous nucleation effect **[Valapa et al., 2014]**. PLA and PLA/CH biocomposite films exhibit sharp, unimodal

endothermic melting peaks at 151, 150.4, 150 and 149.5 ºC respectively, which clearly indicates the presence of α crystalline form of PLA. A slight reduction (up to ~1.5 ºC) in T_m values of PLA/CH biocomposite films is noticed due to the reduction in thermal stability of PLA in presence of CH. It also signifies that the molecular weight of PLA reduces with the incorporation of CH as a filler.

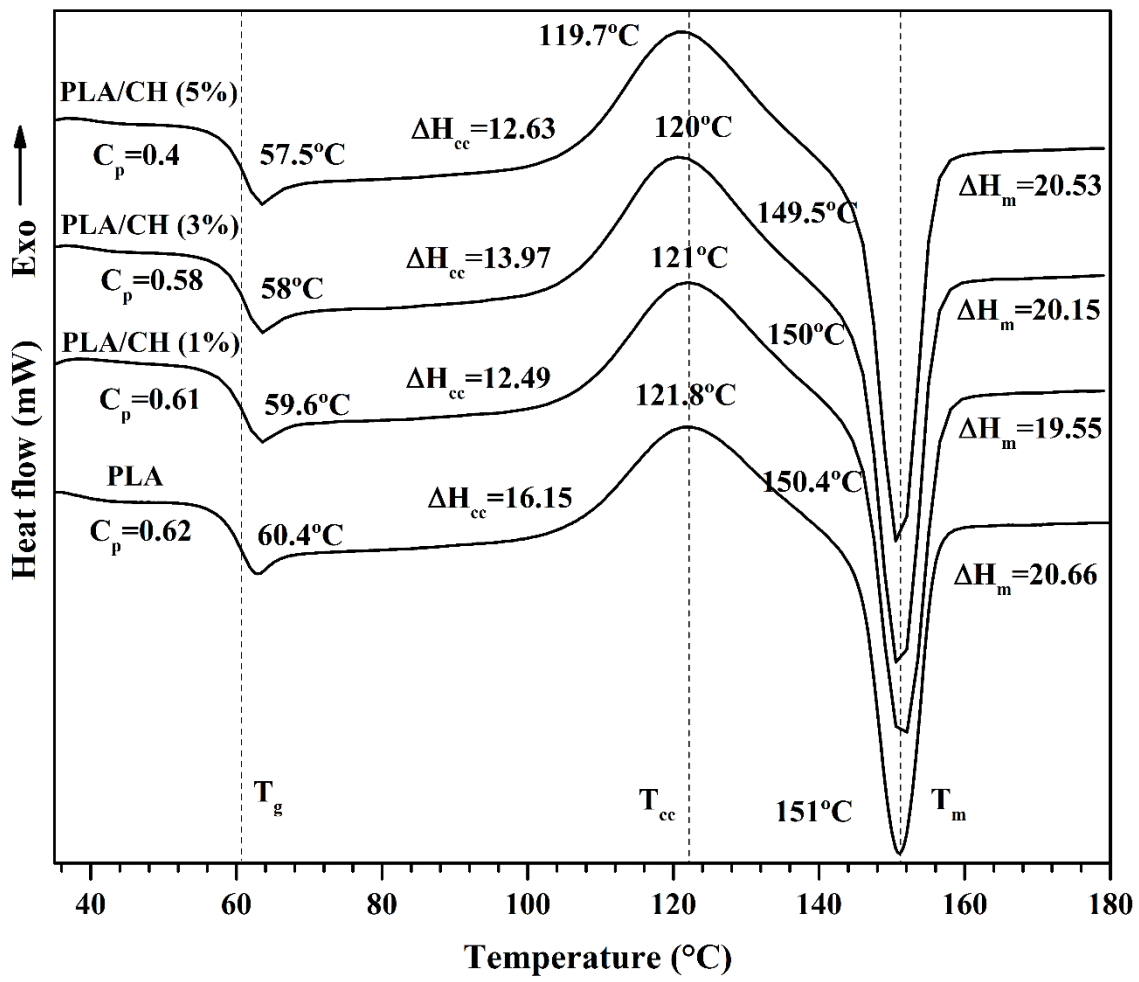

Figure 9.1. DSC thermograms of PLA and PLA/CH biocomposite films (second heating) at 10 ºC/min.

9.3.1.2. Isothermal crystallization kinetics

The crystallization behaviour at isothermal temperature and crystallization kinetics of PLA and PLA/CH biocomposite films are performed at 110 °C which is attained by cooling of polymer. At 110 °C, the heat flow is plotted as a function of crystallization time as shown in Figure 9.2(a). The time required to complete crystallization process of PLA is reduced by adding chitosan in PLA matrix. It signifies that the rate of crystallization depends on the filler loadings i.e. higher loading of filler in PLA accelerates the crystallization process. Hence, it is also concluded that the added filler i.e. chitosan acts as a nucleating agent, which is also confirmed by typical DSC analysis. The percentage crystallinity is plotted as a function of crystallization time at 110 °C to investigate insight about isothermal crystallization kinetics as shown in Figure 9.2(b). The sigmoidal isotherms are obtained for PLA and PLA/CH biocomposite films, which are shifted towards lower crystallization time with an increase in chitosan concentration. According to the Avrami equation, the graphs between $\ln[-\ln(1-X_t)]$ and $\ln t$ are plotted for PLA and PLA/CH biocomposite films as shown in Figure 9.2(c). The calculated values of n and K are mentioned in Table 9.1. A straight line pattern is followed by all the film samples, which corresponds to the primary crystallization whereas, a slight deviation is observed at the end of the crystallization process of PLA and PLA/CH biocomposite films, which signifies the secondary crystallization process. The primary crystallization is related to the clear growth of lamellar whereas, secondary crystallization belongs to the perfection of the internal spherulite crystallization along with spherulite impingement. The calculated values of 'n' lie in the range of 1 to 2 which confirms the heterogeneous nucleation in the polymer composites. The heterogeneous nucleation mechanism is a combination of thermal and athermal nucleations, which is confirmed by the non-integral values of 'n' **[Cai et al., 2011]**.

Table 9.1: Kinetics parameters of PLA and PLA/CH biocomposite films at 110 °C.

Sample	n	$K \times 10^{-2}$ (min^{-1})	$t_{1/2}$ (min)
PLA	1.89	1.67	7.2
PLA/CH (1%)	1.68	2.08	8.1
PLA/CH (3%)	1.69	1.95	8.2
PLA/CH (5%)	1.73	1.71	8.4

The K values randomly increase and then decrease for PLA/CH biocomposite films, but are still higher than that of PLA, which lie in the range of 1.67-2.08 min^{-1}. The calculated values of n and K can be used to determine another important parameter i.e. $t_{1/2}$.

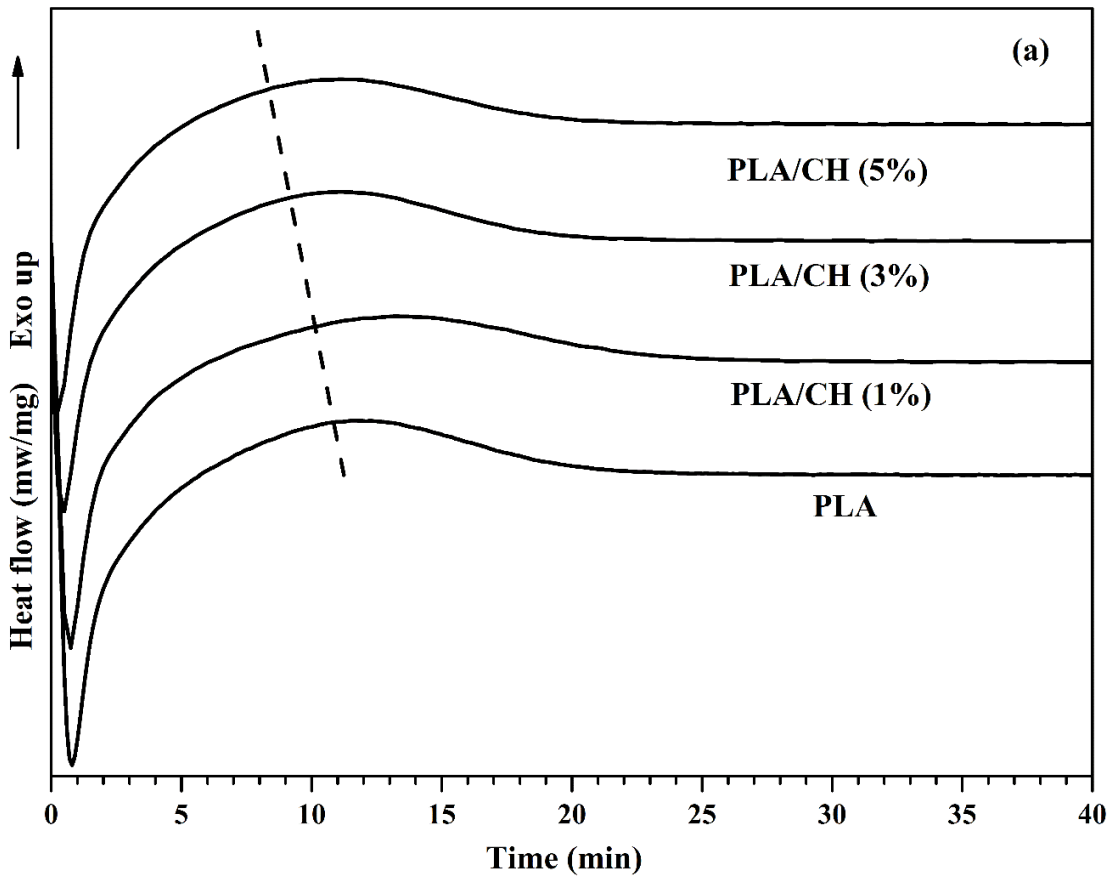

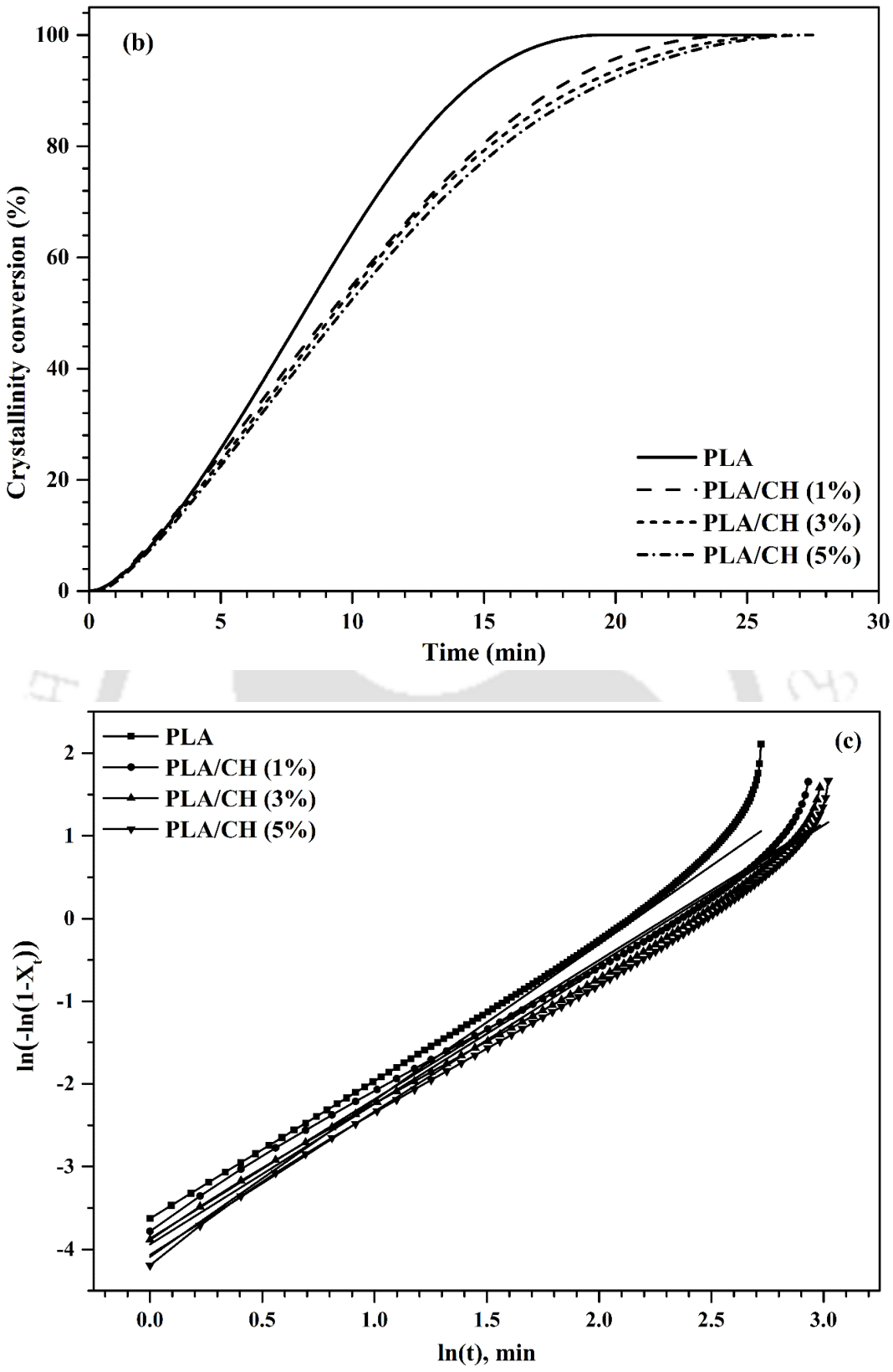

Figure 9.2. Isothermal cold crystallization at 110 °C of PLA and PLA/CH bionanocomposite films; (a) Heat flow vs. time graph, (b) percentage crystallinity as a function of crystallization time and (c) Avrami plots.

The values of $t_{1/2}$ are increased dramatically with an increase in filler loading which suggests that initially the crystallization rate was lower than that of PLA, but after half time the crystallization rate increases randomly and finally the overall crystallization rate increases with an increase in filler concentration.

9.3.2. Crystallization behaviour of PLA/CH-*g*-OLLA bionanocomposite films

The crystallization behaviour of PLA/CH-*g*-OLLA bionanocomposite films was performed at 110 ºC to observe the effect of synthesized CH-*g*-OLLA copolymer on isothermal crystallization kinetics, spherulitic morphology and their growth of PLA in their miscible blends.

9.3.2.1. DSC analysis

DSC analysis was conducted to figure out the crystallization and melting behavior of film samples with two heating and cooling cycles as prescribed in material and methods. The purpose of first heating was to remove the physically and chemically bounded water or moisture from film samples. The glass transition temperature of PLA films is reduced significantly up to 12 ºC with an increase in filler loading due to plasticizing effect of the low molecular weight of CH-*g*-OLLA as shown in Figure 9.3. It is noteworthy to mention that T_g value of any polymer can be tuned by changing the molecular weight of polymers. The low molecular weight polymeric chains are shorter in length and can move freely as compared to high molecular weight polymeric chains. Variation in T_g also depends on different properties such as the degree of deacetylation of chitosan, water amount, crystallinity and OH or amine groups in the macro-molecular chain. However, the T_g value of pure chitosan is very high i.e. ~196 ºC as compare to CH-*g*-OLLA copolymer **[Suyatma et al., 2005]**. The heat capacity at constant pressure is reduced up to 0.14 J/g.K with an increase in filler concentration, which means that less amount of heat is required to raise the temperature in case of bionanocomposites films. This is only possible when

molecular movement of shorter polymer chains in composites increases due to experiencing less obstruction and entanglement from adjacent polymer chains, which results increment in the amorphous region of PLA/CH-*g*-OLLA bionanocomposite films. The reduced value of T_g (close to room temperature) is highly required to improve toughness of bionanocomposite films used for packaging applications. A significant reduction up to ~9.4 ºC is detected in cold crystallization temperature of PLA films with increment in filler concentration (upto 5 wt%) due to the presence of deformed shape and size of some crystals in PLA matrix. The sharpness of crystalline peak in bionanocomposite films are improved due to the negligible variation in crystals size. The melting behaviour of PLA film showed a unimodal endothermic peak at 152.3 ºC, which exhibits α crystalline form of PLA **[Valapa et al., 2015]**. The significant reduction in melting temperature upto ~6 ºC is observed in PLA films by an increase in filler concentration due to the heterogeneous distribution of crystals as well as non-uniform crystal thickness. Bimodal endothermic melting peaks in bionanocomposite films corroborate with the presence of two form of crystals (α and β) of PLA as shown in Figure 9.3, which is also confirmed by XRD analysis of PLA/CH-*g*-OLLA bionanocomposite films. Both type of crystals are different in size and shape. The α form of crystals are more stable than β form. The shifting of T_m towards lower value is due to the reduction in the stability of PLA molecules with the addition of filler. Single T_g in the DSC thermographs confirmed the uniform dispersion of CH-*g*-OLLA in PLA matrix for each combination. Hence, no phase separation has occurred in such nanocomposite films.

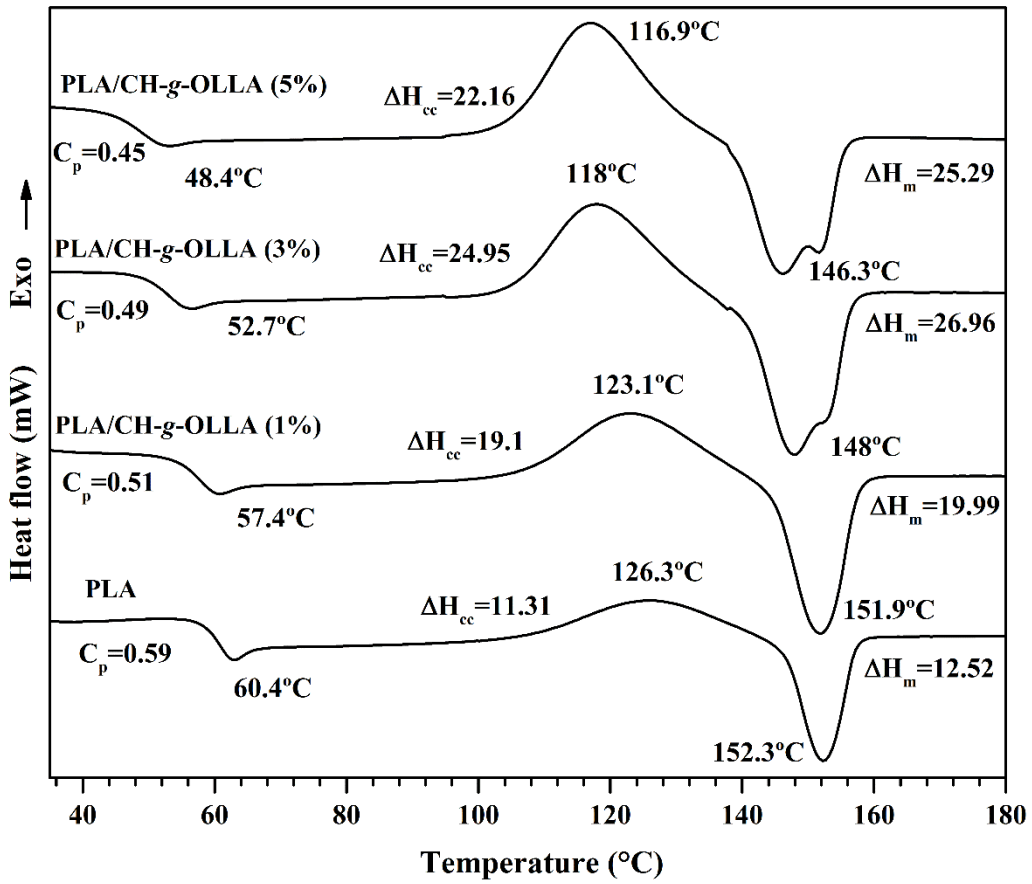

Figure 9.3. DSC thermograms of melt extruded PLA, chitosan and PLA/CH-*g*-OLLA bionanocomposite films obtained from second heating at 10 ºC/min.

9.3.2.2. Crystallization kinetics of PLA/CH-*g*-OLLA bionanocomposite films

The isothermal crystallization behavior and crystallization kinetics of PLA and PLA/CH-*g*-OLLA bionanocomposite films was conducted by DSC at an optimal temperature of 110 °C. The thermograms of PLA and PLA based composites were recorded during isothermal condition obtained by cooling the molten polymer until 110 °C and the heat released during crystallization was plotted with respect to time as mentioned in Figure 9.4(a). The crystallization behavior of PLA is strongly influenced by the addition of CH-*g*-OLLA which significantly reduced the time required for half crystallization. It suggests that the crystallization rate is faster with an increase in filler loading. The faster crystallization also indicated that the added filler acts as a nucleating agent, which is also

suggested in DSC analysis. The crystallinity conversion was plotted with respect to time at crystallization temperature to gain more knowledge about isothermal crystallization kinetics as shown in Figure 9.4(b). The obtained sigmoidal isotherms are shifted towards lower crystallization time with an increase in filler loading which means that the rate of crystallization is increased and crystals in composite films can grow faster than that of PLA. Furthermore, the Avrami equation was used to plot the graphs between $\ln[-\ln(1-X_t)]$ and $\ln t$ for PLA and composite samples as shown in Figure 9.5(a). The values of Avrami exponent and crystallization rate constant are calculated and mentioned in Table 9.2.

Table 9.2: Kinetics parameters of PLA and PLA/CH-*g*-OLLA bionanocomposite films isothermally cold-crystallized at 110 °C.

Sample	n	$K\times10^{-2}$ (min^{-n})	$t_{1/2}$ (min)
PLA	1.891	1.67	7.2
PLA/CH-*g*-OLLA (1%)	1.720	2.63	6.7
PLA/CH-*g*-OLLA (3%)	1.777	2.57	6.4
PLA/CH-*g*-OLLA (5%)	1.718	3.0	6.2

It is observed that all the samples are following a straight line pattern which signifies the primary crystallization, but some deviations are observed at the end of crystallization process which confirm the occurrence of secondary crystallization. The primary and secondary crystallizations are attributed to the outward clear growth of lamellar stacks and the perfection of the internal spherulite crystallization along with spherulite impingement respectively. The estimated 'n' values are non-integral and exist close to 2, which declare non-three dimensional truncated spherical structures. Such structures are generated due to the instantaneous nucleation controlled by diffusion process.

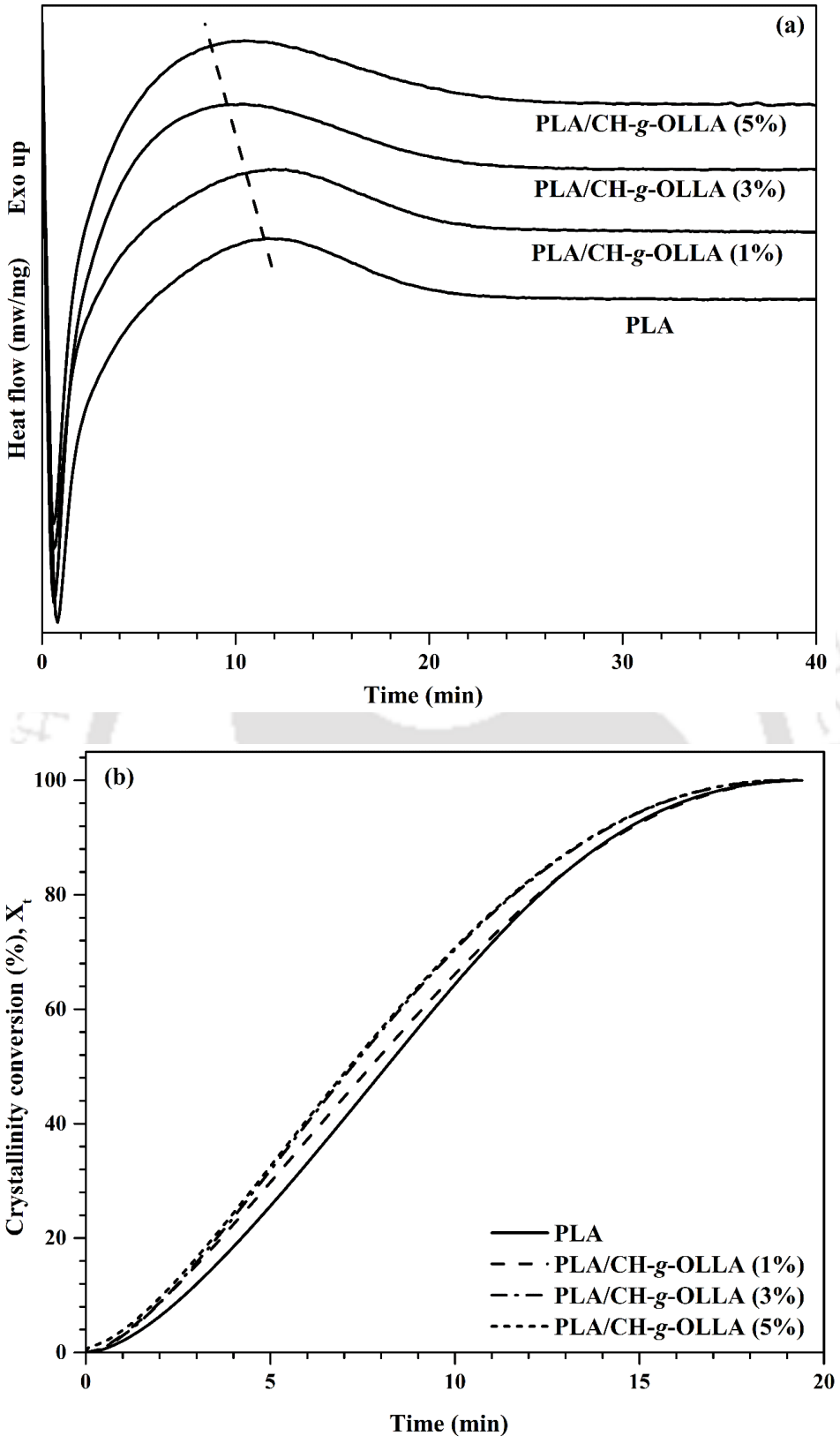

Figure 9.4. (a) Heat flow as a function of time and (b) crystallinity conversion (%) as a function of crystallization time at 110 °C for PLA and PLA/CH-*g*-OLLA bionanocomposite films.

More importantly, the non-integral values of 'n' suggest that the nucleation mechanisms are a combination of thermal and athermal nucleations **[Cai et al., 2011]**. The K values are very much sensitive to the crystallization temperature which is increased with increase in filler loading and found in the range of 1.67-3 min^{-n}. It also suggests that CH-*g*-OLLA is approved to be an effective nucleating agent which helps to boost up the crystallization rate of PLA matrix by producing more nucleating sites. It also helps reduce the melt viscosity of PLA. The another important parameter $t_{1/2}$ was calculated by using the values of n and K. The $t_{1/2}$ values are reduced with an increase in CH-*g*-OLLA concentration which implied that the incorporated filler accelerates the crystal growth. Hence, the filler used in this study acts as a nucleating agent for PLA crystallization.

9.3.2.3. Effect of CH-*g*-OLLA on spherulitic morphology and nucleation of PLA

POM analysis was performed to analyze the effect of the incorporated CH-*g*-OLLA copolymer on the spherulite growth pattern of PLA at isothermal condition (110 °C). The typical Maltese cross pattern **[Bai et al., 2016]** is recognized in PLA spherulites and the nucleation density is increased gradually with increase in crystallization time. The same kind of spherulitic pattern is also detected for PLA/CH-*g*-OLLA bionanocomposite films. It is observed that the spherulite growth rate (G) of PLA increased a little by the addition of 1 wt% filler but significantly increased with the addition of 3 and 5 wt% filler as shown in Figure 9.5(b) in which the spherulite growth rate is carefully estimated as a function of crystallization time for all the film samples. The associated reason with crystal size increment is lower molecular weight and branching of smaller polymeric chains of CH-*g*-OLLA filler which favour the folding of polymer chains. After a particular time period, the covered area by the growth of one crystal at 110 °C is higher than that of pure PLA as presented in Figure 9.6(a), (b), (c) & (d). The overall crystallization rate is accelerated in the presence of CH-*g*-OLLA which is also supported by DSC analysis.

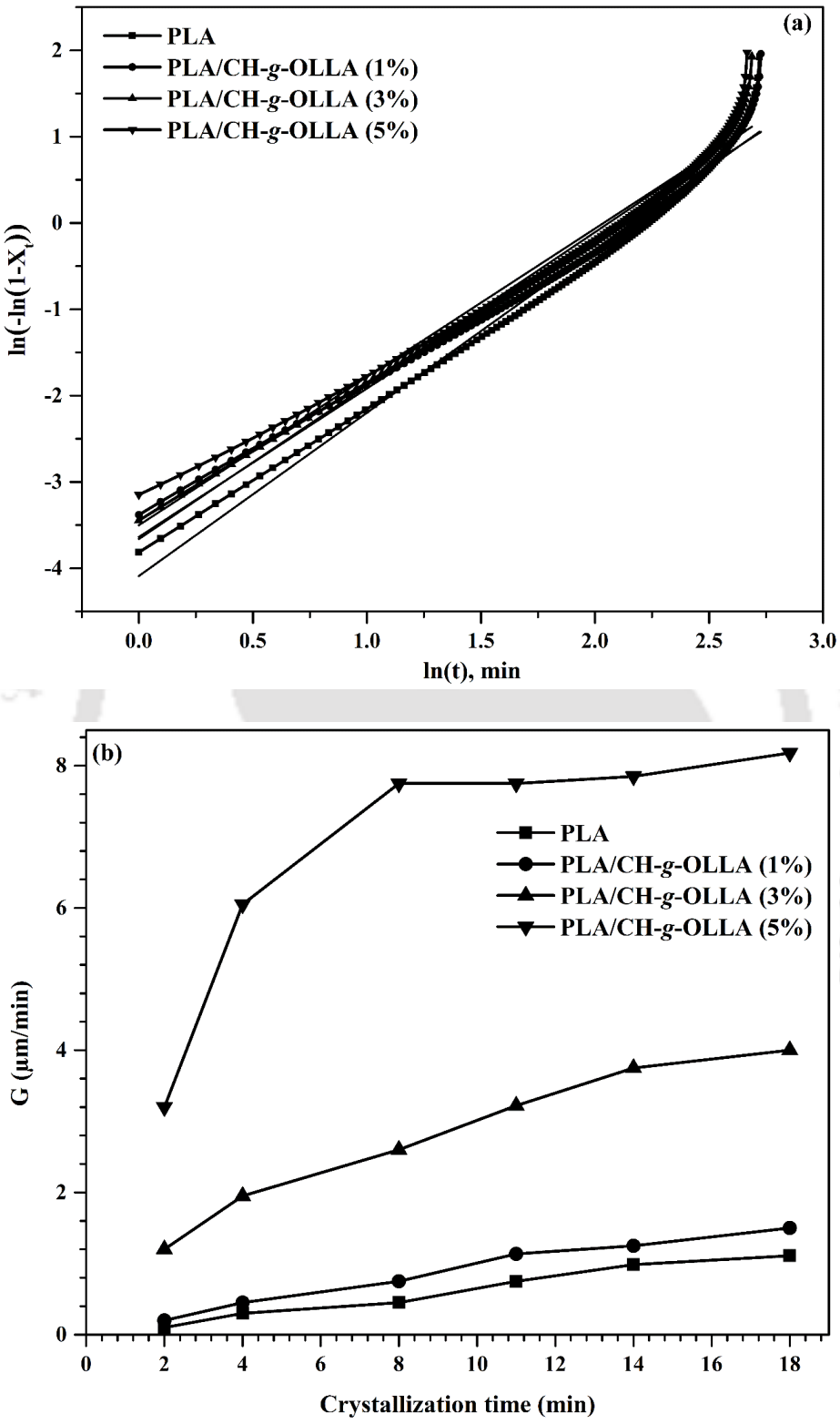

Figure 9.5. (a) Avrami plots and (b) spherulite growth rate vs crystallization time graphs at isothermal cold crystallization condition at 110 °C for PLA and PLA/CH-*g*-OLLA bionanocomposite films.

Figure 9.6(c) & (d) conclude that the fully developed spherulites only belong to pure PLA. The images also show many micron and nano sized particles through which the light is transmitted. These particles are denoted as individual nucleus of CH-*g*-OLLA, which are aligned along the radial direction of the spherulites. This alignment of nucleus is a unique phenomenon, which is governed by the difference in polarity between PLA and chitosan. The presence of nucleus is comparatively same as that of PLA. The size of the particles perfectly matched the surface morphology as shown in the inset of Figure 9.6(c). Figure 9.6(e) denotes the schematic representation of spherulite growth of PLA/CH-*g*-OLLA crystal and explains about the increment in crystal radius in a regular interval of crystallization time. The diameter of the spherulite is measured as 12, 25, 35 and 54 μm at isothermal crystallization temperature after the implementation of ~8, 11, 14 and 18 min. The spherulite diameter of bionanocomposite films is found more than that of PLA, which is due to the uniform dispersion of CH-*g*-OLLA and its nucleation effect **[Bonilla et al., 2013]**.

9.4. Summary

CH and CH-*g*-OLLA copolymer are used as nucleating agents in PLA matrix. The obtained sigmoidal isotherms are shifted towards lower crystallization time with an increase in CH-*g*-OLLA loading in PLA matrix, which signifies the fast crystallization behaviour of PLA/CH-*g*-OLLA bionanocomposite films as compared to that of pristine PLA. In case of PLA/CH-*g*-OLLA bionanocomposite films, the occurrence of primary and secondary crystallizations attributes to the outward clear growth of lamellar stacks and the perfection of the internal spherulite crystallization along with spherulite impingement respectively. POM study suggests the improvement in spherulite growth rate of PLA by the addition of 1, 3 and 5 wt% of CH-*g*-OLLA filler in PLA matrix. The alignment of individual nucleus

of CH-*g*-OLLA take place along the radial direction of PLA spherulites, which is governed by the difference in polarity between PLA and chitosan.

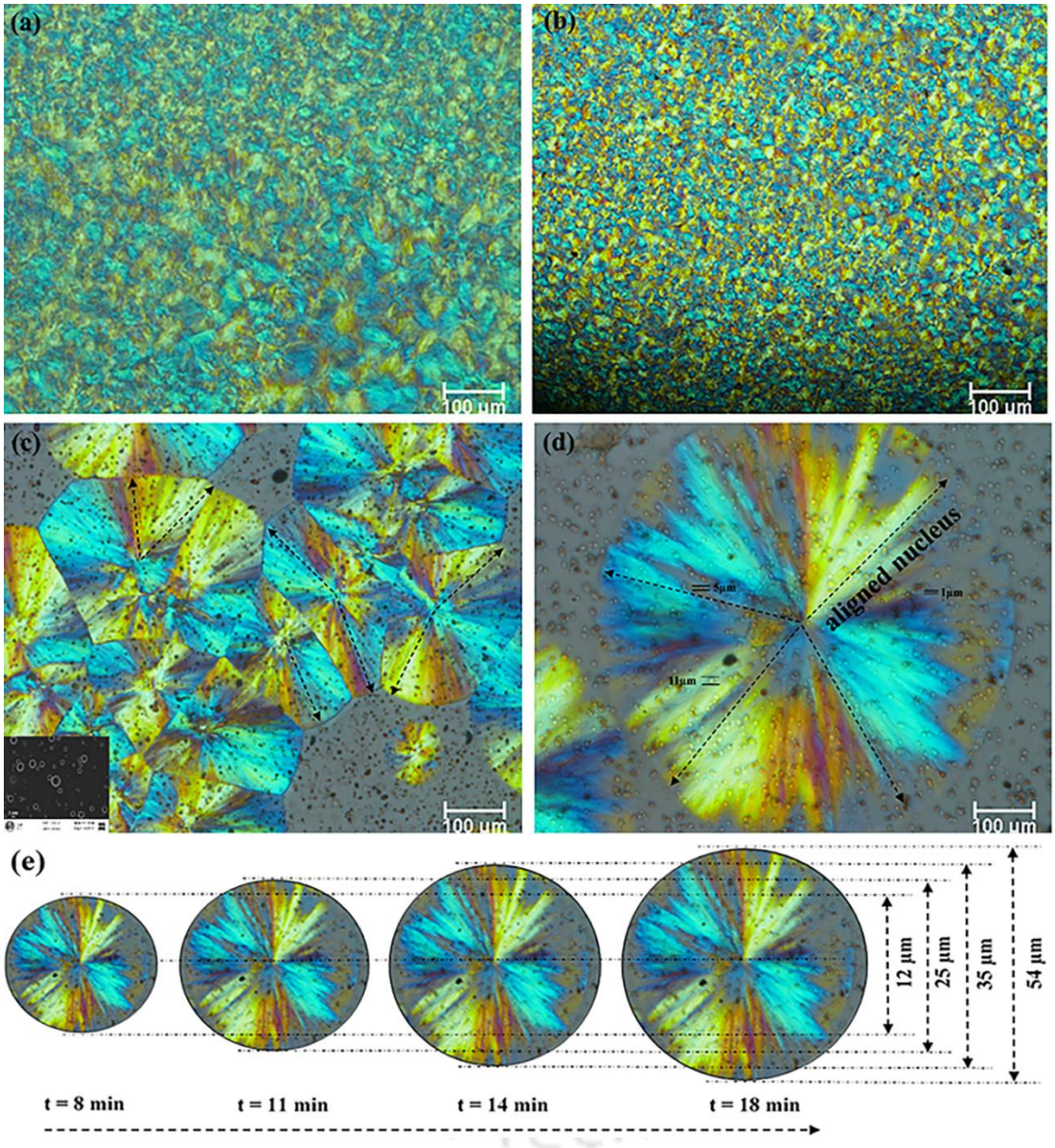

Figure 9.6: POM micrographs of (a) PLA, (b) PLA/CH-*g*-OLLA (1%), (c) PLA/CH-*g*-OLLA (3%), (d) PLA/CH-*g*-OLLA (5%) bionanocomposite films at isothermal crystallization temperature (110 °C) and (e) representation of spherulitic growth of PLA/CH-*g*-OLLA crystal.

Chapter 10
Conclusions and Future Scope

The chapter elucidates the major inferences drawn from the doctoral work and an outlook for future studies.

10.1. Conclusions

The major conclusions drawn on the basis of overall observation and major findings of the research work are as follows:

- The highly demanded chitin and chitosan biopolymers was efficiently extracted first time from Muga silkworms (*Antheraea assamensis*) by chemical treatment process. The yield of chitin and chitosan extraction from raw silkworms is 8 and 7% (dry weight basis) respectively. Deacetylation process highly depends on reaction time and temperature. DD% of extracted chitosan at various temperatures were calculated by various methods such as potentiometric titration, conductometric titration, FTIR, elemental analysis, ^{1}H-NMR and found in the range of 77 to 87%. The peaks at 1654 to 1658 cm^{-1} and 1555 to 1557 cm^{-1} in FTIR study confirmed the presence of chitin and partially deacetylated chitosan due to presence of amide I band ($C=O$ stretching) and amide II band ($N-H$ stretching) respectively. TGA analysis showed higher thermal stability of chitin than that of chitosan. Intrinsic viscosity and viscosity average molecular weight of chitosan were calculated at 25±1 ºC and found 37.5 mL/g and 44×10^{3} Da respectively.
- Poly (lactic acid) and extracted chitosan extracted from Muga silkworms were utilized as matrix and filler respectively for the preparation of various compositions of PLA/CH biocomposite films by solution casting technique. In FTIR analysis, all the regular peaks were observed at their respective positions for PLA and chitosan in PLA/CH biocomposite films. No new peaks for grafting were observed in this case. The intensity of the peaks reduced with an increase in filler concentration in XRD. FESEM analysis

proved that the present non uniform chitosan particles were of micron size, which formed agglomeration at higher concentration and resulted the reduction in mechanical and WVTR properties of PLA/CH biocomposite films.

- The synthesis of chitosan-*graft*-oligo(l-lactic acid) was conducted by microwave assisted *insitu* condensation polymerization technique, which has transformed the hydrophilic chitosan into hydrophobic copolymer. The various grafting parameters such as yield (%), percent conversion (%), grafting efficiency (%), percent grafting (%) and percent homopolymer were calculated as ~51.6, ~266.6, ~40, ~150 and ~60% respectively. The FTIR and NMR analyses confirmed that the grafting of OLLA on chitosan backbone occurred at -NH_2 groups. Significant change in the surface morphology was observed in the form of uniformly dispersed chitosan in spherical shape by SEM and TEM analyses, which also supports grafting.
- The synthesized CH-*g*-OLLA (30%) copolymer by condensation polymerization, was used as a nano-filler for the fabrication of solution casted PLA/CH-*g*-OLLA bionanocomposite films. A new acute peak at 1539 cm^{-1} was observed only in the case of PLA/CH-*g*-OLLA bionanocomposite films which confirmed the presence of amide ester linkage ($-OCONH-$) and confirmed grafting at C2 position of chitosan backbone. The I_{cr} and T_g were reduced continuously from 47 to 36% and 64 to 46 ºC respectively with an increase in filler loading. TEM analysis showed that amphiphilic CH-*g*-OLLA nanoparticles were three dimensional, spherical in shape and uniformly dispersed in the form of polymeric micelles in PLA matrix. UTS of PLA/CH-*g*-OLLA bionanocomposite films was found comparable to that of PLA whereas, %E was improved drastically by incorporating filler in PLA matrix. The barrier property results declared the % reduction (~81.7% at 25 °C and ~99% at 15 °C) in oxygen permeability.

- After successful implementation of CH-*g*-OLLA in PLA matrix by solution casting technique, it was further extended to produce by co-rotating mini twin screw extruder and large twin-screw extruder to check the industrial viability of PLA/CH-*g*-OLLA bionanocomposite films. The fabricated PLA/CH-*g*-OLLA bionanocomposite films were structurally characterized with the help of FTIR, XRD, GPC analyses and found improved results as compare to that of solution casted PLA/CH-*g*-OLLA bionanocomposite films. The GPC analysis corroborated with the reduction of ~23% and ~15% in M_n and M_w of PLA by adding a low molecular weight filler upto ~5 wt%. It is noteworthy to mention that the degradation temperature of bionanocomposite films was higher than the processing temperature of PLA. Melt extruded PLA/CH-*g*-OLLA bionanocomposite films have shown the reduction in oxygen permeability upto ~90.4%. Further, a simple and elegant lamination technique was successfully employed to laminate PLA with PLA/CH-*g*-OLLA bionanocomposite film at ~90 °C with the roller speed of ~1 mm/sec. It has produced a significant improvement in storage modulus and elongation as compare to that of PLA film.
- The TGA and DTG curves reveal that the thermal stability of PLA/CH biocomposite films and PLA/CH-*g*-OLLA bionanocomposite films reduce with an increase in filler concentration. All thermal stages of film samples move towards higher temperatures at higher heating rates. The $\overline{E}_a$ and $\overline{R^2}$ values have been reduced continuously with increase in fillers concentration as calculated by Kissinger, Augis & Bennett, KAS and FWO methods. Isoconversional methods were found more reliable because it calculates E_a and R^2 values at each conversion. The results suggest that PLA and PLA/CH-*g*-OLLA bionanocomposite films undergo a complex reaction mechanism during non-isothermal degradation.

- Isothermal crystallization kinetics suggested that CH-*g*-OLLA copolymer behaves as an efficient nucleating agent, which is able to enhance the crystals growth of PLA films. The crystallization kinetics suggests non-three dimensional truncated spherical structures, which is controlled by the combination of thermal and athermal instantaneous nucleations. POM analysis suggested that the spherulite growth of PLA is improved significantly with the addition of CH-*g*-OLLA.

10.2. Scope for future work

Recommendations for future research are as follows:

- The detailed study can be done on insight of structural modification in chitosan-*graft*-lactic acid and its computational validation using Material studio software.
- Molecular dynamic evaluation of barrier, thermal and mechanical properties behaviour of PLA and PLA/CH-*g*-OLLA bionanocomposites and its experimental validation.
- The detailed study of CH-*g*-OLLA as an antibacterial and antimicrobial agent with its toxicity, migration, biodegradation and recycling.
- Detailed study on bonding and debonding mechanism between laminated PLA and PLA/CH-*g*-OLLA bionanocomposite films.
- Fabrication of chitin and chitosan nanocrystals using extracted chitin from Muga silkworms, its dispersion in PLA matrix and various properties comparison with the existing work.
- Detailed study on fixation devices and scaffolds based on PLA/CH-*g*-OLLA bionanocomposites with the kinetics of cell proliferation, cell adhesion and growth capability.

10.3. Implications of current research work

The available plant and animal based biodegradable polymers have tremendous properties. However, they are used in limited applications due to compatibility issues, low gas barrier and low mechanical properties as compared to the conventional used plastics. Hence, the current invention solves all above limitations by formulating biobased, non-toxic, compostable and dispersible additive, which is capable to disperse uniformly in commercially available biodegradable polyesters and helps to reduce the oxygen transmission rate upto the level of PET. As a result, the shelf life of packed food in biodegradable films will be increased and will also reduce the polymer wastes as all the components used in the fabrication of polyester based films are biodegradable. Hence, the food packaging industries as well as the consumers may be benefited from the current research work due to the enhancement in shelf life of packed foodstuffs.

References

- Abdollahi, M.; Rezaei, M.; Farzi, G. *J. Food Eng.*, **2012**, 111, 343-350.
- Abdou, E. S.; Nagy, K. S. A.; Elsabee, M. Z. *Bioresour. Technol.*, **2008**, 99, 1359-1367.
- Aboulkas, A.; El harfi, K.; El bouadili, A. *Energy Convers. Manage.*, **2010**, 51, 1363-1369.
- Abraham, R.; Thomas, S. P.; Kuryan, S.; Isac, J.; Varughese, K. T.; Thomas, S. *eXPRESS Polym. Lett.*, **2009**, 3, 177-189.
- Adlim, M.; Bakar, M. A.; Liew, K. Y.; Ismail, J. *J. Mol. Catal. A: Chem.*, **2004**, 212, 141-149.
- Ahmadzadeh, S.; Keramat, J.; Nasirpour, A.; Hamdami, N.; Behzad, T.; Aranda, L.; Vilasi, M.; Desobry, S. *J. Appl. Polym. Sci.*, **2016**, 133, 42079-42089.
- Ali, S. W., Rajendran, S. and Joshi, M. *Carbohydr. Polym.*, **2011**, 83, 438-446.
- Alvarenga, E. S. D.; Pereira de Oliveira, C.; Bellato, C. R. *Carbohydr. Polym.*, **2010**, 80, 1155-1160.
- Ambrosio-Martin, J.; Fabra, M. J.; Lopez-Rubio, V.; Lagaron, J. M. *J. Mater Sci.*, **2014**, 49, 2975-2986.
- Antheunis, H.; Van der Meer, J. C.; De Geus, M.; Heise, A.; Koning, C. E. *Biomacromolecules*, **2010**, 11, 1118-1124.
- Aoyagi, Y.; Yamashita, K.; Doi, Y.; *Polym. Degrad. Stab.*, **2002**, 76, 53-59.
- Armentano, I.; Bitinis, N.; Fortunati, E.; Mattioli, S.; Rescignano, N.; Verdejo, R.; Lopez-Manchado, M. A; Kenny, J. M. *Prog. Polym. Sci.*, **2013**, 38, 1720-1747.
- Arnon, H.; Zaitsev, Y.; Porat, R; Poverenov, E. *Postharvest Biol. Technol.*, **2014**, 87, 21-26.
- Arrieta, M. P.; Lopez, J.; Hernandez, A.; Rayon, E. *Eur. Polym. J.*, **2014**, 50, 255-270.

- Aryaei, A.; Jayatissa, A. H.; Jayasuriya, A. C. *J. Mech. Behav. Biomed. Mater.*, **2012**, 5, 82-89.
- Bai, J.; Wang, J.; Wang, W.; Fang, H.; Xu, Z.; Chen, X. *ACS Sustainable Chem. Eng.*, **2016**, 4, 273-283.
- Balau, L.; Lisa, G.; Popa, M. I.; Tura, V. *Cent. Eur. J. Chem.*, **2004**, 2, 638-647.
- Balazs, N.; Sipos, P. *Carbohydr. Res.*, **2007**, 342, 124-130.
- Barata, J. F. B.; Pinto, R. J. B.; Vaz Serra, V. I. R. C.; Silvestre, A. J. D.; Trindade, T.; Neves, M. G. P. M. S.; Cavaleiro, J. A. S.; Daina, S.; Sadocco, P.; Freire, C. S. R. *Biomacromolecules*, **2016**, 17, 1395-1403.
- Baskar, D.; Kumar, T. S. S. *Carbohydr. Polym.*, **2009**, 78, 767-772.
- Bhattacharya, A.; Misra, B. N.; *Prog. Polym. Sci.*, **2004**, 29, 767-814.
- Bhattarai, N.; Ramay, H. R.; Chou, S. H.; Zhang, M. *Int. J. Nanomed.*, **2006**, 1, 181-187.
- Bie, P.; Liu, P.; Yu, L.; Li, X.; Chen, L.; Xie, F. *Carbohydr. Polym.*, **2013**, 98, 959-966.
- Bigg, D. M. *Polym. Compos.*, **1987**, 8, 115-122.
- Bliznakov, E. D.; White, C. C.; Shaw, M. T. *J. Appl. Polym. Sci.*, **2000**, 77, 3220-3227.
- Bocchini, S.; Fukushima, K.; Blasio, A. D.; Fina, A.; Frache, A.; Geobaldo, F. *Biomacromolecules*, **2010**, 11, 2919-2926.
- Bonilla, J.; Fortunati, E.; Vargas, M.; Chiralt, A.; Kenny, J. M. *J. Food Eng.*, **2013**, 119, 236-243.
- Boonfaung, P.; Wasutchanon, P.; Somwangthanaroj, A. *Pure Appl. Chem. Intern. Conf.*, **2011**, 621-624.
- Bourtoom, T.; Chinnan, M. S. *LWT-Food Sci. Technol.*, **2008**, 41, 1633-1641.

- Bujang, A.; Adila, S. N.; Suyatma, N. E. *4th International Conference on Biology, Environment and Chemistry*, **2013**, 58, DOI: 10.7763/IPCBEE.
- Burgos, N.; Martino, V. P.; Jimenez, A. *Polym. Degrad. Stabil.*, **2013**, 98, 651-658.
- Byrne, F.; Ward, P. G.; Kennedy, J.; Imaz, N.; Hughes, D.; Dowling, D. P. *J. Polym. Environ.*, **2009**, 17, 28-33.
- Byun, Y.; Kim, Y. T.; Whiteside, S. *J. Food Eng.*, **2010**, 100, 239-244.
- Cai, J.; Liu, M.; Wang, L.; Yao, K.; Li, S.; Xiong, H. *Carbohydr. Polym.*, **2011**, 86, 941-947.
- Carrasco, F.; Pages, P.; Perez, J. G.; Santana, O. O.; Maspoch, M. L. *Polym. Degrad. Stab.*, **2010**, 95, 116-125.
- Chang, J. H.; An, Y. U.; Cho, D.; Giannelis, E. P. *Polymer*, **2003**, 44, 3715.
- Cheng, D.; Zan, Y.; Du, J.; Luo, Y. *J. Appl. Polym. Sci.*, **2016**, 133, 44159-44166.
- Chen, R. H.; Hwa, H. D. *Carbohydr. Polym.*, **1996**, 29, 353-358.
- Chen, T.; Kumar, G.; Harris, M. T.; Smith, P. J.; Payne, G. F. *Biotechnol. Bioeng.*, **2000**, 70, 564-573.
- Chen, Y.; Wu, T. *Ind. Eng. Chem. Res.*, **2014**, 53, 16689-16695.
- Chiang, M. F.; Wu, T. M. *Composites: Part B*, **2012**, 43, 2789-2794.
- Choi, K. M.; Choi, M. C.; Han, D. H.; Park, T. S.; Ha, C. S. *Eur. Polym. J.*, **2013**, 49, 2356-2364.
- Chrissafis, K. *J. Therm. Anal. Calorim.*, **2008**, 95, 273-283.
- Croisier, F.; Jerome, C. *Eur. Polym. J.*, **2013**, 49, 780-792.
- Czechowska-Biskup, R.; Jarosinska, D.; Rokita, B.; Ulanski, P.; Rosiak, J. M. *Prog. Chem. Appl. Chitin Its Deriv.*, **2012**, XVII, 5-20.
- Dadashi, S.; Mousavi, S. M.; Emam-Djomeh, Z.; Oromiehie, A. *Int. J. Nanosci. Nanotechnol.*, **2014**, 10, 245-256.

- Darie, R. N.; Paslaru, E.; Sdrobis, A.; Pricope, G. M.; Hitruc, G. E.; Poiata, A.; Baklavaridis, A.; Vasile, C. *Ind. Eng. Chem. Res.*, **2014**, 53, 7877-7890.
- Dash, M.; Chiellini, F.; Fernandez, E. G.; Piras, A. M; Chiellini, E. *Carbohydr. Polym.*, **2011**, 86, 65-71.
- Dash, M.; Chiellini, F.; Ottenbrite, R. M; Chiellini, E. *Prog. Polym. Sci.*, **2011**, 36, 981-1014.
- Datta, R.; Tsai, S.; Bonsignore, P.; Moon, S.; Frank, J. *FEMS Micro-biology Reviews*, **1995**, *16*, 221.
- Debeaufort, F.; Quezada-Gallo, J. A.; Voilley, A. *Crit. Rev. Food. Sci. Nutr.*, **1998**, 38, 299-313.
- De Britto, D.; Campana-Filho, S. P. *Polym. Degrad. Stab.*, **2004**, 84, 353-361.
- De Britto, D.; Campana-Filho, S. P. *Thermochim. Acta*., **2007**, 465, 73-82.
- Dhar, P.; Tarafder, D.; Kumar, A.; Katiyar, V. *Polymer*, **2016**, 87, 268-282.
- Dhar, P.; Tarafder, D.; Kumar, A.; Katiyar, V. *R. S. C. Adv.*, **2015**, 5, 60426-60440.
- Diaz-Celorio, E.; Franco, L.; Marquez, Y.; Rodriguez-Galan, A.; Puiggali, J. *Thermochim. Acta.*, **2012**, 528, 23-31.
- Ding, N.; Shentu, B.; Pan, P.; Shan, G.; Bao, Y.; Weng, Z. *Ind. Eng. Chem. Res.*, **2013**, 52, 12897-12905.
- Drumright, R. E.; Gruber, P. R.; Henton, D. E. *Adv. Mat.*, **2000**, 12, 1841-1846.
- Duan, Z.; Thomas, N. L.; Huang, W. *J. Membr. Sci.*, **2013**, 445, 112-118.
- Dutta, P. K.; Dutta, J.; Tripathi, V. S. *J. Sci. Ind. Res.*, **2004**, 63, 20-31.
- Erdohan, Z. O.; Cam, B.; Turhan, K. N. *J. Food Eng.*, **2013**, 119, 308-315.
- Espadin, A.; Vazquez, N.; Tecante, A.; De Dios, L. T.; Gimeno, M.; Velasquillo, C.; Shirai, K. *J. Appl. Polym. Sci.*, **2014**, 131, 40252-40258.

- Fan, Y.; Nishida, H.; Shirai, Y.; Tokiwa, Y.; Endo, T. *Polym. Degrad. Stab.*, **2004**, 86, 197-208.
- Fattah, W. I. A.; Jiang, T.; El-Bassyouni, G. E. T.; Laurencin, C. T. *Acta Biomater.*, **2007**, 3, 503-514.
- Feng, F.; Liu, Y.; Zhao, B.; Hu, K. *Procedia Eng.*, **2012**, 27, 718-732.
- Ferreira, C. S.; Caridade, S. G.; Mano, J. F.; Alves, N. M. *Polym. Adv. Technol.*, **2014**, 25, 1492-1500.
- Findenig, G.; Leimgruber, S.; Kargl, R.; Spirk, S.; Stana-Kleinschek, K.; Ribitsch, V. *ACS Appl. Mater. Interfaces*, **2012**, 4, 3199-3206.
- Fomin V. A.; Guzeev V. V. *Prog. Rubb. Plastics Tech.*, **2001** 17, 186-204.
- Fortunati, E.; Peltzer, M.; Armentano, I.; Jimenez, A.; Kenny, J. M. *J. Food Eng.*, **2013**, 118, 117-124.
- Fukushima, K.; Tabuani, D.; Dottori, M.; Armentano, I.; Kenny, J. M.; Camino, G. *Polym. Degrad. Stab.*, **2011**, 96, 2120-2129.
- Gallstedt, M.; Hedenqvist, M. S. *Carbohydr. Polym.*, **2006**, 63, 46-53.
- Ganji, F.; Abdekhodaie, M. J. *Carbohydr. Polym.*, **2010**, 80, 740-746.
- Garcia, M. A.; Pinotti, A.; Zaritzky, N. E.; *Starch-Stärke*, **2006**, 58, 453-463.
- Garlotta, D. *J. Polym. Environt.*, **2002**, 9, 63-84.
- George, T. S.; Guru, K. S. S.; Vasanthi, N. S.; Kannan, K. P. *World J. Sci. Technol.*, **2011**, 1, 43-48.
- Goncalves, C. M. B.; Tome, L. C.; Garcia, H.; Brandao, L.; Mendes, A. M.; Marrucho, I. M. *J. Food Eng.*, **2013**, 116, 562-571.
- Gonzalez, A.; Igarzabal, C. I. A. *Food Hydrocolloids*, **2013**, 33, 289-296.
- Graupner, N.; Mussig, J. *Compos Part A-APPL S.*, **2011**, 42, 2010-2019.

- Gu, C. H.; wang, J. J.; Yu, Y.; Sun, H.; Shuai, N.; Wei, B. *Carbohydr. Polym.,* **2013**, 92, 1579-1585.
- Hafsa, J.; Ali Smach, M.; Khedher, M. R. B.; Charfeddine, B.; Limem, K.; Majdoub, H.; Rouatbi, S. *LWT-Food Sci. Technol.,* **2016**, 68, 356-364.
- Halasz, K.; Hosakun, Y.; Csoka, L. *Int. J. Polym. Sci.*, **2015**, 2015, Article ID 954290.
- Hamad, K.; Kaseem, M.; Yang, H. W.; Deri, F.; Ko, Y. G. *eXPRESS Polym. Lett.,* **2015**, 9, 435-455.
- Haugaard V. K.; Danielsen B.; Bertelsen G. Eur. *Food Res. Technol.,* 2003, 216, 233-240.
- Henmi, K.; Sato, H.; Matsuba, G.; Tsuji, H.; Nishida, K.; Kanaya, T.; Toyohara, K.; Oda, A.; Endou, K. *ACS Omega*, 2016, 1, 476-482.
- Hirvicorpi, T.; Nissi, M. V.; Harlin, A.; Salomaki, M.; Areva, S.; Korhonen, J. T.; Karppinen, M. *Appl. Surf. Sci.,* **2011**, 257, 9451-9454.
- http://www.plastemart.com/Plastic-Technical-Article.asp?LiteratureID=1958&Paper=biodegradable-plastics-demand-to-grow-15-percent-annually-to-2015.
- Huda, M. S.; Drzal, L. T.; Mohanty, A. K.; Misra, M. *Compos. Sci. Technol.*, **2008**, 68, 424-432.
- Inkinen, S.; Hakkarainen, M.; Albertsson, A. C.; Sodergard, A. *Biomacromolecules,* **2011**, 12, 523-532.
- Ishak, K. M. K.; Verbeek, C. J. *J. Eng. Sci.*, **2016**, 12, 77-86.
- Jamshidian, M.; Tehrany, E. A.; Imran, M.; Jacquot, M.; Desobry, S. *Compr. Rev. Food Sci. Food Saf.,* **2010**, 9, 552-571.
- Janorkar, A. V.; Metters, A. T.; Hirt, D. E. *Macromolecules,* **2004**, 37, 9151-9159.

- Jayaramudu, J.; Reddy, G. S. M.; Varaprasad, K.; Sadiku, E. R.; Ray, S. S.; Rajulu, A. V. *Carbohydr. Polym.*, **2013**, 94, 822-828.
- Jiang, T.; Deng, M.; James, R.; Nair, L. S.; Laurencin, C. T. *Acta Biomater.*, **2014**, 10, 1632-1645.
- Jiang, X.; Chen, L.; Zhong, W. *Carbohydr. Polym.*, **2003**, 54, 457-463.
- Kabiri, K.; Mirzadeh, H.; Zohuriaan-Mehr, M. *J. Iranian Polymer Journal.*, **2007**, 16, 147-151.
- Kahrizsangi, E.; Reza; Abbasi, M. H.; Saidi, A. *Iran. J. Chem. Chem. Eng.*, 2007, 26, 119-123.
- Kakkar, D.; Maiti, S. N. *J. Appl. Polym. Sci.*, **2012**, 123, 1905-1912.
- Kannan, M.; Nesakumari, M.; Rajarathinam, K.; Ranjit Singh, A. J. A. *Advances in Biological Research*., **2010**, 4, 10-13.
- Kasaai, M. R.; Arul, J.; Charlet, G. N. *J. Polym. Sci. B Polym. Phys.*, **2000**, 38, 2501-2508.
- Kasaai, M. R. *Carbohydr. Polym.*, **2010**, 79, 801-810.
- Katiyar V.; Nanavati H.; *Polym. Eng. Sci.*, 2011, 51, 2067-2077.
- Kaur, H.; Banipal, T. S.; Thakur, S.; Bakshi, M. S.; Kaur, G.; Singh, N. *ACS Sustainable Chem. Eng.*, **2013**, 1, 127-136.
- Khan, A.; Khan, R. A.; Salmieri, S.; Le Tien, C.; Riedl, B.; Bouchard, J.; Chauve, G.; Tan, V.; Kamal, M. R.; Lacroix, M. *Carbohydr. Polym.*, 2012, 90, 1601-1608.
- Khwaldia, K.; Basta, A. H.; Aloui, H.; El-Saied, H. *Carbohydr. Polym.*, **2014**, 99, 508-516.
- Kjellgren, H.; Gallstedt, M.; Engstrom, G.; Jarnstrom, L. *Carbohydr. Polym.*, **2006**, 65, 453-460.

- Koh, H. C.; Park, J. S.; Jeong, M. A.; Hwang, H. Y.; Hong, Y. T.; Ha, S. Y.; Nam, S. Y. *Desalination*, **2008**, 233, 201-209.
- Kubota, H.; Suka, I. G.; Kuroda, S.; Kondo, T. *Eur. Polym. J.*, **2001**, 37, 1367-1372.
- Kumar, S.; Satapathy, B. K.; Maiti, S. N. *Polym. Adv. Technol.*, **2013**, 24, 511-519.
- Kurek, M.; Scetar, M.; Voilley, A.; Galic, K.; Debeaufort, F. *J. Membr. Sci.*, **2012**, 403-404, 162-168.
- Lan, P.; Lv, J. *Journal of Fiber Bioengineering and Informatics*, **2008**, 1, 41-46.
- Laufer, G.; Kirkland, C.; Cain, A. A.; Grunlan, J. C. *ACS Appl. Mater. Interfaces*, **2012**, 4, 1643-1649.
- Laufer, G.; Kirkland, C.; Cain, A. A.; Grunlan, J. C. *Carbohydr. Polym.*, **2013**, 95, 299-302.
- Leceta, I.; Guerrero, P.; Cabezudo, S.; Caba, K. D. L. *J. Cleaner Prod.*, **2013**, 41, 312-318.
- Li, F.; Biagioni, P.; Finazzi, M.; Tavazzi, S.; Piergiovanni, L. *Carbohydr. Polym.*, **2013**, 92, 2128-2134.
- Li, G.; Zhuang, Y.; Mu, Q.; Wang, M.; Fang, Y. *Carbohydr. Polym.*, **2008**, 72, 60-66.
- Li, J.; He, Y.; Inoue, Y. *Polym. Int.*, **2003**, 52, 949-955.
- Li, J.; Kong, M.; Cheng, X. J.; Dang, Q. F.; Zhou, X.; Wei, Y. N.; Chen, X.G. *Int. J. Biol. Macromol.*, **2012**, 51, 221-227.
- Li, J.; Kong, M.; Cheng, X. J.; Li, J. J.; Liu, W. F.; Chen, X. G. *Int. J. Biol. Macromol.*, **2011**, 49, 1016-1021.
- Li, J.; Zheng, W.; Li, L.; Zheng, Y.; Lou, X.; *Thermochim. Acta*, **2009**, 493, 90-95.
- Lin, Y.; Jing, W.; Kang, P.; Xizoming, Z.; Zhouping, W.; Wenshui, X. *Bulletin of Korean Chemical Society*, **2011**, 32, 1277-2181.

- Liu, G. Y.; Zhai, Y. L.; Wang, X. L.; Wang, W. T.; Pan, Y. B.; Dong, X. T.; Wang, Y. Z. *Carbohydr. Polym.*, **2008**, 74, 862-867.
- Liu, S.; Sun, J.; Yu, L.; Zhang, C.; Bi, J.; Zhu, F.; Qu, M.; Jiang, C.; Yang, Q. *Molecules*, **2012**, 17, 4604-4611.
- Liu, T. G.; Li, B.; Huang, W.; Lv, B.; Chen, J.; Zhang, J. X.; Zhu, L. P. *Carbohydr. Polym.*, **2009**, 77, 110-117.
- Luckachan, G. E.; Pillai, C. K. S. *Carbohydr. Polym.*, **2006**, 64, 254-266.
- Lunt, J. *Polym. Degrad. Stab.*, **1998**, 59, 145-152.
- Ma, P.; Hristova-Bogaerds, D. G.; Goossens, J. G. P.; Spoelstra, A. B.; Zhang, Y.; Lemstra, P. J. *Eur. Polym. J.*, **2012**, 48, 146-154.
- Maiti, S. N.; Lopez, B. H. *J. Appl. Polym. Sci.*, **1992**, 44, 353-360.
- Marquez, Y.; Franco, L.; Puiggali, J. *Thermochimica Acta*., **2012**, 550, 65-75.
- Martelli, M. R.; Barros, T. T.; Moura, M. R. D.; Mattoso, L. H. C; Assis, O. B. G. *J. Food Sci.*, **2013**, 78, N98-N104.
- Matet, M.; Heuzey, M. C.; Ajji, A.; Sarazin, P. *Carbohydr. Polym.*, **2015**, 117, 177-184.
- Medeiros, B. G. D. S.; Pinheiro, A. C.; Carneiro-da-Cunha, M. G.; Vicente, A. A. *J. Food Eng.*, **2012**, 110, 457-464.
- Mitsuishi, K.; Kodama, S.; Kawasaki, H. *Polym. Eng. Sci.*, **1985**, 25, 1069-1073.
- Miyata, T.; Masuko, T. *Polymer*, **1998**, 39, 5515-5521.
- Mohammed, M. H.; Williams, P. A.; Tverezovskaya, O. *Food Hydrocolloids*, **2013**, 31, 166-171.
- Moura, C. M. D.; Moura, J. M. D.; Soares, N. M.; De Almeida Pinto, L. A. *Chem. Eng. Process.: Process Intensification*, **2011**, 50, 351-355.

- Moura, M. R. D.; Aouada, F. A.; Avena-Bustillos, R. J.; McHugh, T. H.; Krochta, J. M.; Mattoso, L. H. C. *J. Food Eng.*, **2009**, 92, 448-453.
- Mroz, P.; Bialas, S.; Mucha, M.; Kaczmarek, H. *Thermochimica Acta*., **2013**, 573, 186-192.
- Adsul, M. G.; Varma, A. J.; Gokhale, D. V. *Green Chem.*, **2007**, 9, 58-62.
- Muraleedharan, K.; Alikutty, P.; Mujeeb, V. A.; Sarada, K. *J. Environ. Polym. Degrad.*, **2015**, 23, 1-10.
- Nair, L. S.; Laurencin, C. T. *Prog. Polym. Sci.*, **2007**, 32, 762-798.
- Nakagawa, T.; Nakiri, T.; Hosoya, R.; Tajitsu, Y. *Proceedings of the 7th International Conference on Properties and Applications of Dielectric Materials*, **2003**, 499-502.
- Nemtsev, S. V.; Zueva, O. Y.; Khismatullin, M. R.; Albulov, A. I.; Varlamov, V. P. *Appl. Biochem. Microbiol.*, **2004**, 40, 39-43.
- Niamsa, N.; Baimark, Y. *Am. J. Food Technol.*, **2009**, 4, 162-169.
- Ocloo, F. C. K.; Quayson, E. T.; Adu-Gyamfi, A.; Quarcoo, E. A.; Asare, D.; Serfor-Armah, Y.; Woode, B. K. *Radiation Physics and Chemistry*., **2011**, 80, 837-841.
- Oguzlu, H.; Tihminlioglu, F. *Macromol. Symp.*, **2010**, 298, 91-98.
- Ohara, H.; Ito, M.; Sawa, S. *US Patent 6569989B2*, **May 27, 2003**.
- Olabarrieta, I.; Forsstrom, D.; Gedde, U. W.; Hedenqvist, M. S. *Polymer*, **2001**, 42, 4401-4408.
- Ou, C. Y.; Zhang, C. H.; Li, S. D.; Yang, L.; Dong, J. J.; Mo, X. L.; Zeng, M. T. *Carbohydr. Polym.*, **2010**, 82, 1284-1289.
- Ozkoc, G.; Kemaloglu, S. *J. Appl. Polym. Sci.*, **2009**, 114, 2481-2487.
- Pandey, S.; Mishra, S. B. *Carbohydr. Polym.*, **2012**, 90, 370-379.
- Pantani, R.; Gorrasi, G.; Vigliotta, G.; Murariu, M.; Dubois, P. *Eur. Polym. J.*, **2013**, 49, 3471-3482.

- Park, S. H.; Lee, H. S.; Choi, J. H.; Jeong, C. M.; Sung, M. H.; Park, H. J. *J. Appl. Polym. Sci.*, **2012**, 125, E675-E680.
- Paulino, A. T.; Simionato, J. I.; Garcia, J. C.; Nozaki, J. *Carbohydr. Polym.*, **2006**, 64, 98-103.
- Peelman, N.; Ragaert, P.; Meulenaer, B. D.; Adons, D.; Peeters, R.; Cardon, L.; Impe, F. V.; Devlieghere, F. *Trends Food Sci. Tech.*, **2013**, 32, 128-141.
- Peng, Y.; Li, Y. *Food Hydrocolloids*, **2014**, 36, 287-293.
- Peng, Y.; Wu, Y; Li, Y. *Int. J. Biol. Macromol.*, **2013**, 59, 282-289.
- Perinovic, S.; Andricic, B.; Erceg, M.; *Thermochim. Acta*, **2010**, 510, 97-102.
- Petinakis, E.; Liu, X.; Yu, L.; Way, C.; Sangwan, P.; Dean, K.; Bateman, S.; Edward, G. *Polym. Degrad. Stab.*, **2010**, 95, 1704-1707.
- Rasal, R. M.; Janorkar, A. V.; Hirt, D. E. *Prog. Polym. Sci.*, **2010**, 35, 338-356.
- Re, G. L.; Benali, S.; Habibi, Y.; Raquez, J. M.; Dubois, P. *Eur. Polym. J.*, **2014**, 54, 138-150.
- Rinawa, K.; Maiti, S. N.; Sonnier, R.; Cuesta, J. M. L. *Polym. Bull.*, **2014**, 71, 1131-1152.
- Rhim, J. W. *Food Res. Int.*, **2013**, 51, 714-722.
- Rhim, J.; Hong, S. L.; Ha, C.; *LWT- Food Sci. Technol.*, **2009**, 42, 612-617.
- Rhim, J. W.; Hong, S. I.; Park, H. M.; Ng, P. K. W. *J. Agric. Food Chem.*, **2006**, 54, 5814-5822.
- Rinaudo, M. *Prog. Polym. Sci.*, **2006**, 31, 603-632.
- Rotabakk, B. T.; Birkeland, S.; Jeksrud, W. K.; Sivertsvik, M. *J. Food Sci.*, **2006**, 71, S124-S131.
- Rubentheren, V.; Ward, T. A.; Chee, C. Y.; Tang, C. K. *Carbohydr. Polym.*, **2015**, 115, 379-387.

- Sagheer, F. A. A.; Al-Sughayer, M. A.; Muslim, S.; Elsabee, M. Z. *Carbohydr. Polym.*, **2009**, 77, 410-419.
- Saiwaew, R.; Suppakul, P.; Boonsupthip, W.; Pechyen, C. *Energy Procedia*, **2014**, 56, 280-288.
- Salehi, M.; Clemens, F.; Graule, T.; Grobety, B. *Appl. Energy*, **2012**, 95, 147-155.
- Samsudin, H.; Soto-Valdez, H.; Auras, R. *Food Control.*, **2014**, 46, 55-66.
- Sashiwa, H.; Aiba, S. I. *Prog. Polym. Sci.*, **2004**, 29, 887-908.
- Schreiber, S. B.; Bozell, J. J.; Hayes, D. G.; Zivanovic, S. *Food Hydrocolloids*, **2013**, 33, 207-214.
- Sebastien, F.; Stephane, G.; Copinet, A.; Coma, V. *Carbohydr. Polym.*, **2006**, 65, 185-193.
- Sewda, K.; Maiti, S. N. *J. Appl. Polym. Sci.*, **2007**, 105, 2598-2604.
- Sharma, R.; Maiti, S. N. *Polym.-Plast. Technol. Eng.*, **2014**, 53, 229-238.
- Silverajah, V. S. G.; Ibrahim, N. A.; Zainuddin, N.; Yunus, W. M. Z. W.; Hassan, H. A. *Molecules*, **2012**, 17, 11729-11747.
- Singh, V.; Tripathi, D. N.; Tiwari, A.; Sanghi, R. *Carbohydr. Polym.*, **2006**, 65, 35-41.
- Singla, R. K.; Maiti, S. N.; Ghosh, A. K. *Polym.-Plast. Technol. Eng.*, **2016**, 55, 475-485.
- Soares, F. C.; Yamashita, F.; Muller, C. M. O.; Pires, A. T. N. *Polym. Test.*, **2013**, 32, 94-98.
- Souza, B. W. S.; Cerqueira, M. A.; Casariego, A.; Lima, A. M. P.; Teixeira, J. A.; Vicente, A. A. *Food Hydrocolloids*, **2009**, 23, 2110-2115.
- Sreekumar, P. A.; Leblanc, N.; Saiter, J. M. *J. Polym. Environ.*, **2013**, 21, 388-394.
- Svagan, A. J.; Akesson, A.; Cardenas, M.; Bulut, S.; Knudsen, J. C.; Risbo, J.; Plackett, D. *Biomacromolecules*, **2012,** 13, 397-405.

- Sun, X.; Wang, Z.; Kadouh, H.; Zhou, K. *LWT-Food Sci. Technol.,* **2014**, 57, 83-89.
- Suyatma, N. E.; Copinet, A.; Coma, V.; Fricoteaux, F. *J. Appl. Polym. Sci.,* **2010**, 117, 3083-3091.
- Suyatma, N. E.; Copinet, A.; Legin-Copinet, E.; Fricoteaux, F., Coma, V. *J. Polym. Environ.,* **2011,** 19, 166-171.
- Suyatma, N. E.; Copinet, A.; Tighzert, L.; Coma, V. *J. Polym. Environ.,* **2004**, 12, 1-6.
- Suyatma, N. E.; Tighzert, L.; Copinet, A. *J. Agric. Food Chem.,* **2005**, 53, 3950-3957.
- Synowiecki, J.; Al-Khateeb, N. A. *Crit. Rev. Food Sci. Nutr.,* **2003**, 43, 145-171.
- Tang, C.; Xiang, L.; Su, J.; Wang, K.; Yang, C.; Zhang, Q.; Fu, Q. *J. Phys. Chem. B,* **2008**, 112, 3876-3881.
- Tang, X. Z.; Kumar, P.; Alavi, S.; Sandeep, K. P. *Crit. Rev. Food Sci. Nutr.,* **2012**, 52, 426-442.
- Tang, Z. X.; Qian, J. Q.; Shi, L. E. *Appl. Biochem. Biotechnol.,* **2007**, 136, 77-96.
- Tenn, N.; Follain, N.; Soulestin, J.; Cretois, R.; Bourbigot, S.; Marais, S. *J. Phys. Chem. C,* **2013**, 117, 12117-12135.
- Tolaimate, A.; Desbrieres, J.; Rhazi, M.; Alagui, A.; Vincendon, M.; Vottero, P. *Polymer*, **2000**, 41, 2463-2469.
- Tripathi, N.; Katiyar, V. *J. Appl. Polym. Sci.,* **2016**, 133, 43458-43466.
- Tsai, C. C.; Wu, R. J.; Cheng, H. Y.; Li, S. C.; Siao, Y. Y.; Kong, D. C.; Jang, G. W. *Polym. Degrad. Stabil.,* **2010**, 95, 1292-1298.
- Tsuji, H.; Fukui, I. *Polymer,* **2003**, 44, 2891-2896.
- Tsuji, H.; Sawada, M.; Bouapao, L. *ACS Appl. Mater. Interfaces,* **2009**, 1, 1719-1730.
- Tudorachi, N.; Lipsa, R.; Mustata, F. R. *Ind. Eng. Chem. Res.,* **2012**, 51, 15537-15545.
- Valapa, R.; Hussain, S.; Iyer, P. K.; Pugazhenthi, G.; Katiyar, V. *Polym. Bull.,* **2016**, 73, 21-38.

- Valapa, R.; Pugazhenthi, G.; Katiyar, V. *J. Appl. Polym. Sci.*, **2015**, 132, DOI: 10.1002/APP.41320.
- Valapa, R.; Pugazhenthi, G.; Katiyar, V. *Int. J. Biol. Macromol.*, **2014**, 65, 275-283.
- Vasile, C.; Darie, R. N.; Cheaburu-Yilmaz, C. N.; Pricope, G. M.; Bracic, M.; Pamfil, D.; Hitruc, G. E.; Duraccio, D. *Composites: Part B,* **2013**, 55, 314-323.
- Venkatesh, M.; Ravi, P.; Tewari, S. P.; *J. Phys. Chem. A,* **2013**, 117, 10162-10169.
- Vyazovkin, S.; Burnham, A. K.; Criado, J. M.; Perez-Maqueda, L. A.; Popescu, C.; Sbirrazzuoli, N. *Thermochim. Acta,* **2011**, 520, 1-19.
- Wang, T.; Ji, X.; Jin, L.; Feng, Z.; Wu, J.; Zheng, J.; Wang, H.; Xu, Z. W.; Guo, L.; He, N. *ACS Appl. Mater. Interfaces,* **2013**, 5, 3757-3763.
- Wang, X.; Du, Y.; Yang, J.; Tang, Y.; Luo, J. *J. Biomed. Mater. Res. A*, 2008, 84, 384-390.
- Wu, D.; Wu, L.; Zhang, M.; Zhao, Y. *Polym. Degrad. Stab.*, **2008**, 93, 577-1584.
- Wu, T. M.; Wu, C. Y. *Polym. Degrad. Stabil.*, **2006**, 91, 2198-2204.
- Wu, Y.; Yang, W.; Wang, C.; Hu, J.; Fu, S. *Int. J. Pharm.*, **2005**, 295, 235-245.
- Xiao, C.; Weng, L.; Lu, Y.; Zhang, L. *J. Macromol. Sci.-Pure Appl. Chem.*, **2001**, A38, 761-771.
- Yaghobi, N.; Hormozi, F. *Carbohydr. Polym.*, **2010**, 81, 892-896.
- Yamane, H.; Sasai, K. *Polymer*, **2003**, 44, 2569-2575.
- Yao, F.; Liu, C.; Chen, W.; Bai, Y.; Tang, Z.; Yao, K. *Macromol. Biosci.*, **2003**, 3, 653-656.
- Yoksan, R.; Chirachanchai, S. *Mater. Sci. Eng. C.*, **2010**, 30, 891–897.
- Yuan, H.; Qiao, X.; Ren, J. *J. Macromol. Sci., Part A: Pure Appl. Chem.*, **2008**, 45, 754-760.

- Yuan, Y.; Chesnutt, B. M.; Haggard, W. O.; Bumgardner, J. D. *Materials,* **2011**, 4, 1399-1416.
- Yuzay, I. E.; Auras, R.; Soto-Valdez, H.; Selke, S. *Polym. Degrad. Stab.,* **2010**, 95, 1769-1777.
- Zembouai, I.; Kaci, M.; Bruzaud, S.; Benhamida, A.; Corre, Y. M.; Grohens, Y. *Polym. Test.*, **2013**, 32, 842-851.
- Zhang, G.; Zhang, J.; Wang, F.; Li, H.; *J. Therm. Anal. Calorim.*, **2015**, 122, 419-426.
- Zhang, M.; Haga, A.; Sekiguchi, H.; Hirano, S. *Biol. Macromol.*, **2000**, 27, 99-105.
- Zhang, M.; Thomas, N. L. *Adv. Polym. Technol.,* **2011**, 30, 67-79.
- Zhao, L. M.; Shi, L. E.; Zhang, Z. L.; Chen, J. M.; Shi, D. D.; Yang, J.; Tang, Z. X. *Braz. J. Chem. Eng.*, **2011**, 28, 353-362.
- Zhao, X.; Guerrero, F. R.; Llorca, J.; Wang, D. Y. *ACS Sustainable Chem. Eng.,* **2015**, 4, 202-209.
- Zou, H.; Yi, C.; Wang, L.; Liu, H.; Xu, W. *J. Therm. Anal. Calorim.,* **2009**, 97, 929-935.
- Zhou, W.; Wang, Y.; Jian, J.; Song, S. *Int. J. Nanomed.*, **2013**, 8, 3715-3728.

Research Output

Patent application

- Dispersible Biobased Additive Formulation for Biodegradable Polymer Packaging, Vimal Katiyar, **Akhilesh Kumar Pal** and Neelima Tripathi, *Indian Patent Application,* 981/KOL/2015.

Peer reviewed articles

- **Pal, A. K.**; Katiyar, V., "Non-isothermal degradation kinetics of PLA-chitosan films Prepared by solution casting method" ***Asian Chitin J.***, 2015, 11, 37-44.
- **Pal, A. K.**, Das, A., Katiyar, V., "Chitosan from Muga silkworms (*Antheraea assamensis*) and its influence on thermal degradation behavior of poly (lactic acid) based biocomposite films" ***J. Appl. Polym. Sci.***, 2016, 133, 43710-43724.
- **Pal, A. K.**; Katiyar, V., "Nanoamphiphilic Chitosan Dispersed Poly (lactic acid) Bionanocomposite Films with Improved Thermal, Mechanical, and Gas Barrier Properties" ***Biomacromolecules***, 2016, 17, 2603-2618.
- **Pal, A. K.**; Katiyar, V., "Isothermal crystallization kinetics of poly (lactic acid)/chitosan based biocomposite films" ***Asian Chitin J.***, 2016, 12, 5-18.
- **Pal, A. K.**; Katiyar, V., "Thermal degradation behaviour of nanoamphiphilic chitosan dispersed poly (lactic acid) bionanocomposite films" ***Int. J. Biol. Macromol.***, 2017, 95, 1267-1279.
- **Pal, A. K.**; Katiyar, V., "Theoretical and analyzed data related to thermal degradation kinetics of poly (L-lactic acid)/chitosan-*grafted*-oligo L-lactic acid (PLA/CH-*g*-OLLA) bionanocomposite films" ***Data Brief***, 2017, 10, 304-311.

- **Pal, A. K.**; Katiyar, V., "Chemo-mechanical, morphological and rheological studies on chitosan-*graft*-lactic acid oligomer reinforced poly (lactic acid) bionanocomposite films" ***J. Appl. Polym. Sci.***, 2017, (Accepted).
- **Pal, A. K.**; Katiyar, V., "Melt processing of biodegradable poly(lactic acid)/functionalized chitosan nanocomposite films: mechanical modeling with improved oxygen barrier and thermal properties" *J. Polym. Res.*, **2017** (Accepted).

Articles under preparation

- **Pal, A. K.**; Katiyar, V., "Bonding and debonding mechanism between poly (lactic acid) and poly (lactic acid)/functionalized chitosan bionanocomposite laminates".
- **Pal, A. K.**; Katiyar, V., "Isothermal and non-isothermal crystallization behaviour of melt extruded nano-amphiphilic chitosan *grafted* poly (lactic acid) bionanocomposite films".

Book Chapters published

- Vimal Katiyar, Surendra S. Gaur, **Akhilesh K. Pal** and Amit Kumar, book chapter titled as 'Properties of Plastics for Packaging Applications' in book 'Polymers for Packaging Applications'. (CRC Press, Taylor & Francis Group, ISBN: 9781926895772), 2013.
- **Akhilesh Kumar Pal**, Neelima Tripathi, Rahul Patwa, Tabli Ghosh, Prodyut Dhar, Medha Mili and Vimal Katiyar, book chapter titled as 'Biobased sustainable polymers for food packaging applications' in book 'Bio-based Plastics for Food Packaging Applications'. (Smithers Rapra, ISBN: 978-1-91024-258-2), 2017.

Book Chapters under review

- Arvind Gupta, **Akhilesh Kumar Pal**, Rahul Patwa, Prodyut Dhar and Vimal Katiyar, book chapter titled as 'Green Composites with Excellent Barrier Properties' in book 'Advanced Green Composites' John Wiley and Sons.

Awards

- Received a **National Award** on "Industrial Production of Degradable Packaging Films for Stringent Food Packaging" under "Innovation in Polymeric Material" category in 6th National Award for Technology Innovation in Petrochemicals and Downstream Plastics Processing Industry organized by Government of India on 20-02-2016 at Federation of Indian Chambers of Commerce and Industry (FICCI), New Delhi.
- **Marshall Award** for best student contribution to Chitin and Chitosan Research in 2015-16 under the discipline: Application of Chitin and Chitosan in Chemistry & Environmental Application in 11th Asia Pacific Chitin and Chitosan Symposium & 5th Indian Chitin and Chitosan Society Symposium on 28-30th September, 2016 at Kochi, Kerala, India.
- Received a **Gandhian Young Technological Innovation Award** on "Processing of Biodegradable Films for Food Packaging Application with High Oxygen Barrier Properties." under "Materials Engineering" category in 6th Gandhian Young Technological Innovation (GYTI) Awards 2017 organized by Society for Research and Initiatives for Sustainable Technologies and Institutions on 05-03-2017 at Rashtrapati Bhawan, New Delhi.
- Received a **Best Poster Award** on "Poly (Lactic Acid)/Amphiphilic Chitosan Bionanocomposite Films with Improved Crystallization, Mechanical and Gas Barrier Properties" under "Departmental Best Poster" category in Research Conclave 2017

organized by Student's Academic Board, Indian Institute of Technology Guwahati on 16-19th March, 2017 at Indian Institute of Technology Guwahati.

Papers and posters in International conferences/seminars/symposia

- Research paper presented on 'PLA/Chitosan Nanobiocomposite for Food Packaging Applications' an international conference, organized by Society of Plastics Engineers, ANTEC Mumbai, during 06-07 Dec. 2012 at Mumbai, India.
- Research paper presented on 'Preparation & Characterization of PLA/Chitosan thin films' an Asia/Australia Conference (PPS-2013), organized by Polymer processing Society, during 04-07 Dec. 2013 at Mumbai, India.
- Poster presented on 'Extraction and Characterization of Chitin and Chitosan from Muga Silkworm (*Antheraea assamensis*)' an Asia/Australia Conference (PPS-2013), organized by Polymer processing Society, during 04-07 Dec. 2013 at Mumbai, India.
- Poster presented on 'Melt Extruded Poly (Lactic Acid) & Functionalized Chitosan based Bionanocomposite Films for High Gas Barrier Applications' a 4th International Conference on Advanced nanomaterials and Nanotechnology (ICANN-15), organized by Centre for Nanotechnology, Indian Institute of Technology Guwahati, during 08-11 Dec. 2015 at Guwahati, India.
- Research paper presented on 'Non-isothermal Degradation Kinetics of Lactic Acid Oligomer-*g*-Chitosan Dispersed Poly (lactic acid) Films Prepared by Solution Casting Method' 11th Asia Pacific Chitin and Chitosan Symposium & 5th Indian Chitin and Chitosan Society Symposium, organized by Chitin and Chitosan Society, during 28-30 Sep. 2016 at Kochi, Kerala, India.
- Poster presented on 'Chitosan Extraction from Muga Silkworms and its Effect on Thermal Degradation of Poly (lactic acid) Films' 11th Asia Pacific Chitin and Chitosan

Symposium & 5th Indian Chitin and Chitosan Society Symposium, organized by Chitin and Chitosan Society, during 28-30 Sep. 2016 at Kochi, Kerala, India.

- Accepted a research paper on 'Melt Extrusion of Poly (Lactic Acid)/Nano-Amphiphilic Chitosan Films for Packaging Application: The Effect of Filler on Thermal, Mechanical and Gas Barrier Properties' ICP 2017:19th International Conference on Polymer, organized by World Academy of Science, Engineering and Technology, during 25-26 June 2017 at Paris, France.

Papers and posters in National conferences/seminars/symposia

- Research paper presented on 'PLA/Chitosan Bionanocomposite films for Packaging Applications' a First symposium on Advances in Sustainable Polymers (ASP-14), organized by Department of Chemical Engineering, Indian Institute of Technology Guwahati, during 10-11 Jan. 2014 at Guwahati, India.
- Research paper presented on 'Comparative Studies on Estimation of Degree of Deacetylation of Chitosan' a First symposium on Advances in Sustainable Polymers (ASP-14), organized by Department of Chemical Engineering, Indian Institute of Technology Guwahati, during 10-11 Jan. 2014 at Guwahati, India.
- Poster presented on 'Fabrication and Characterization of Chitosan Dispersed PLA Films for High Gas Barrier Properties' a Second symposium on Advances in Sustainable Polymers (ASP-15), organized by Department of Chemical Engineering, Indian Institute of Technology Guwahati, during 21-22 Jan. 2015 at Guwahati, India.
- Poster presented on 'Extraction, Characterization and Multistage Deacetylation Kinetics of Chitosan Extracted from Muga Silkworm (*Antheraea assamensis*)' a Second symposium on Advances in Sustainable Polymers (ASP-15), organized by

Department of Chemical Engineering, Indian Institute of Technology Guwahati, during 21-22 Jan. 2015 at Guwahati, India.

- Research paper presented on 'Poly (Lactic Acid)/Chitosan Biocomposite Films: Fabrication, Characterization & Non-isothermal degradation kinetics' 68th Annual Session of Indian Institute of Chemical Engineers (CHEMCON-15), organized by Department of Chemical Engineering, Indian Institute of Technology Guwahati, during 27-30 Dec. 2015 at Guwahati, India.
- Poster presented on "Poly (Lactic Acid)/Amphiphilic Chitosan Bionanocomposite Films with Improved Crystallization, Mechanical and Gas Barrier Properties" in Research Conclave 2017, organized by Student's Academic Board, Indian Institute of Technology Guwahati on 16-19th March, 2017 at Indian Institute of Technology Guwahati.

Papers and posters in International/National conferences/seminars/symposia (presented by co-authors)

- Poster presented on 'Chitosan Dispersed PLA Films for High Gas Barrier Applications: An Industrially Viable Approach' an International Conference and Exhibition on Biopolymers & Bioplastics, organized by OMICS International, during 10-12 Aug. 2015 at San Francisco, USA.
- Poster presented on 'Isothermal Crystallization Kinetics of Poly (Lactic Acid)/OLLA-*g*-Chitosan Bionanocomposite Films' a Third International Symposium on Advances in Sustainable Polymers (ASP-16), organized by Kyoto Institute of Technology, during 4-6th Aug. 2016 at Kyoto, Japan.
- Research paper presented on 'Nanoamphiphilic Chitosan Dispersed Poly (lactic acid) Bionanocomposite Cast Films with Improved Thermal, Mechanical, and Gas Barrier

Properties' International Conference on Functional Materials, organized by Indian Institute of Technology Kharagpur, during 12-14 Dec. 2016 at Kharagpur, West Bengal, India.

- Poster presented on 'Melt Extruded Poly (Lactic Acid)/Chitosan-*grafted*-Oligo L-Lactic Acid Bionanocomposite Films for High Gas Barrier Applications' MACRO 2017 International Conference on Polymer Science and Technology, organized by The Society for Polymer Science India, during 08-11 Jan. 2017 at Thiruvananthapuram, Kerala, India.

PATENT OFFICE
INTELLECTUAL PROPERTY BUILDING
Cp-2, Sector V, Salt Lake City, Kolkata-700091
Te No. (091)(033) 23671945-46, 87 FAX No. 033 23671988
E-mail : kolkata-patent@nic.in
Web Site : www.ipindia.gov.in

सत्यमेव जयते
GOVERNMENT OF INDIA

INTELLECTUAL PROPERTY INDIA
PATENTS | DESIGNS | TRADE MARKS | GEOGRAPHICAL INDICATIONS

Docket NO : 11977
To
INDIAN INSTITUTE OF TECHNOLOGY GUWAHATI
GUWAHATI, ASSAM

Date/Time : 15/09/2015 12:09:54
Agent Number:

Sr. No.	CBR Number	Reference Number /Application Type	Application Number	Title/Remarks	Amount Paid	Amount Computed
1	11123	ORDINARY APPLICATION Pages:-20 , Claims:-10	981/KOL/2015	DISPERSIBLE BIOBASED ADDITIVE FORMULATION FOR BIODEGRADABLE POLYMER PACKAGING	8800	8800
2		E-2/1711/2015-KOL	981/KOL/2015	Form2	0	0
Total Amount					8800	8800

Received a sum of Rs. 8800 (Rupees Eight Thousand Eight Hundred only) as under

Payment Mode	Bank Name	Cheque/Draft Number	Cheque/Draft Date	Amount in Rs
Draft	Canara Bank	520478	08/09/2015	8800

Note: This is electronically generated receipt hence no signature required.

TH-1795_11610723

Non-isothermal degradation kinetics of PLA-chitosan films Prepared by Solution Casting Method

AKHILESH KUMAR PAL AND VIMAL KATIYAR*

Department of Chemical Engineering, Indian Institute of Technology Guwahati, Assam 781039, India.

ABSTRACT

Thermal stability and thermal degradation kinetics of poly lactic acid (PLA), PLA-commercial chitosan blend (PLA/NCH) films and PLA-lab made muga silkworm's chitosan blend (PLA/MCH) films has been performed by using thermogravimetric analyser (TGA)in nitrogen atmosphere under non-isothermal conditions in order to access the degradation process. TGA analysis has been performed in the temperature range between 30°C and 600°C at three different heating rates (5, 10 and 20°C/min). Two isoconversional models (Flynn-Wall-Ozawa and Kissinger-Akahira-Sunose) have been used to calculate the apparent activation energies(E_a) and regression coefficients(R^2) at different conversion values for all film samples.The results show that the calculated average apparent activation energies ($\bar{E}_a$) and average regression coefficients ($\bar{R}^2$) by Flynn-Wall-Ozawa (FWO) and Kissinger-Akahira-Sunose (KAS) models are close for all the film samples.

Key Words: *Thermal degradation; commercial chitosan; muga silkworm's chitosan; apparent activation energy; Flynn-Wall-Ozawa; Kissinger-Akahira-Sunose*

INTRODUCTION

The ecological balance has been disturbed due to the continuous increment of plastic waste in the environment. A key challenge for the researchers, is to find out an eco-friendly root for the management of the disposal of synthetic plastics. The primary solution of this problem is to replace the synthetic plastics with biodegradable plastics which can be used for packaging, medical, waste water treatment and many other applications[1]. One of the most promising candidates for such improvement is poly lactic acid (PLA) which has been already produced at industrial scale. It is a linear aliphatic thermoplastic polyester obtained from renewable resources such as sugar cane, corn and sweet potato. It is eco-friendly, bio-based, biodegradable and nontoxic material with better thermal processability. It requires 25-55% less energy to produce than that of petroleum based polymers[2].It dissolves only in chlorinated organic solvents due to its hydrophobic nature[3]. The other biopolymers such as cellulose, chitosan, gums and lignins also have potential to replace synthetic polymers. Here we used chitosan as a biolpolymer[4].

Thermal stability and recycling of biopolymers are essential for its industrial viability.So, a better understanding on thermal degradation kinetics of biopolymers is required to explore further new applicationsin different areas. Thermal degradation kinetics of PLA, chitosan and its derivatives has been widely explored by various researchers[5-8]. The kinetics is based on three kinetic parameters such as apparent activation energy (E_a), pre-exponential factor (A) and the kinetic model ($f(\alpha)$).$E_a$is the most important parameter among them to discuss the thermal stability of any polymer.$E_a$of thermal degradation of any polymer, in the form of films or powder, can be calculated at isothermal and non-isothermal conditions by using isoconversional and model fitting methods. The calculated $E_a$values from these methods should always be different due to their individual conditions and limitations. It is very difficult to compare the values obtained from different methods due to their critical applicable conditions.

The degree of deacetylation (DD%) is the critical parameter of chitosan on which all the properties such as solubility, crystallinity, biodegradability, viscosity, biocompatibility, antimicrobial, antibacterial, antioxidant and thermal stability depend[4,9-10]. The E_a value also varies with acyl/amine substituent. The degree of substitution of these functional groups is also important in the case of chitosan derivatives but it's very difficult to check such influence on thermal degradation kinetics. The E_a value depends on the chemical nature of side chains and average degree of substitution. In this way, thermal degradation techniques have been established to be more convenient and dependable approach to guide and manage the significance of numerous degradation phenomena on biodegradable polymers such as swelling, photo oxidation and hydrolysis. The properties like mechanical and morphology of film samples can be changed due to chain cleavage process.Mostly, the thermal degradation of PLA depends on intramolecular transesterification reactions leading to cyclic oligomers of lactic acid and lactide. Meanwhile, these cyclic oligomers again combine with linear polyesters via insertion reactions. The different gases have been generated during degradation process in inert atmosphere. The major released gases may contain carbon monoxide, carbon dioxide, acetaldehyde and methylketene.

In the present study, PLA, commercial chitosan (NCH) and lab made silkworm's chitosan (MCH) have been utilized to prepare NPLA, PLA/NCH and PLA/MCH films with different concentration of NCH and MCH by solvent casting method. The non-isothermal degradation kinetics of these film samples have been performed to calculate E_a and R^2 values by using isoconversional models such as FWO and KAS. A comparison between these two methods has been done to check the applicability, variation in E_a and the best suited kinetic model.

Asian Chitin J., 11(1), 37-44 (2015)

*Corresponding author: E-mail: vkatiyar@iitg.ernet.in

Isothermal crystallization kinetics of poly(lactic acid)/chitosan based biocomposite films

AKHILESH KUMAR PAL AND VIMAL KATIYAR*

Department of Chemical Engineering, Indian Institute of Technology Guwahati, Guwahati, Assam-781039, India

ABSTRACT

This study reveals the fabrication of poly(lactic acid) (PLA)/ chitosan (MCH) based biocomposite films (PLA/MCH) by solution blending of PLA with MCH followed by detailed investigations on isothermal crystallization kinetics. Chitosan is extracted successfully from Muga silkworms via chemical treatments. All the regular peaks of PLA and MCH are observed in biocomposite films by FTIR analysis. XRD analysis confirms the regular lattice arrangement of PLA chains in PLA/MCH films. These peak intensities were reduced with chitosan loading which suggests the increment in amorphous nature of biocomposite films. DSC analysis reveals that the Glass transition temperature (T_g), cold crystallization temperature (T_{cc}) and melting temperature (T_m) are reduced up to 1.9°C, 4.6°C and 3.2°C respectively with the increase in MCH concentration due to the plasticizing effect of short polymer chains of PLA. At isothermal conditions, the crystallization phenomenon in PLA/MCH biocomposite films occurs faster to that of PLA films. Isothermal crystallization kinetics of PLA/MCH biocomposite films suggests that the values of Avrami exponent show heterogeneous nucleation, which is a combination of thermal and athermal nucleations. Further, observed reduction in water vapour permeability of PLA/MCH biocomposite films is preferable for cell proliferation and cell attachment in biomedical applications.

Key Words: *Muga silkworms, chitosan, poly(lactic acid), water vapour permeability, isothermal crystallization kinetics*

INTRODUCTION

Recently, the use of bio-polymers and its modification with tailored and controlled properties have attracted more attention to overcome the existing limitations of conventional polymers in various applications. In the recent time, the development of new, greener and sustainable products from abundant natural resources are increased in order to reduce the environmental hazards and to provide substitutes of fossil based polymers. In the biobased category, Chitosan (*β*-(1,4)-2-amino-2-deoxy-D-glucose), a cationic polysaccharide, is the second most available renewable bio-polymer, found in the form of chitin, which is also termed as N-acetyl glucosamine. In general, chitin is available in the exoskeleton of marine creatures such as crabs, shrimps, lobsters and insects such as worms, cockroaches, fungi etc. It is non-toxic, hydrophilic and biodegradable in nature. Chitosan can be transformed from chitin by chemical as well as biological methods. Chemical method is favorable in terms of product yield and reaction time. The uniqueness of chitosan is its amine group at C-2 position, which increases its versatility and potential in various fields such as packaging, drug delivery, pharmaceuticals, tissue engineering, textiles, cosmetics industries etc. The restricted solubility of chitosan may limit its applications. However significant interest has been generated among the researchers to minimize such limitations and explore more insight of its characteristics such as non-toxic, biocompatible and easily acceptable in biomedical areas. Chitosan can be available in many forms such as flakes, micro-particles, whiskers, nano-particles, gels etc. It is a promising candidate of the twenty-first century with some of the unique material properties such as chemical reactivity, solubility, film forming ability, antimicrobial, antioxidant, anti-fungal, interesting optical properties and biodegradability.[1] Chitosan is widely used as an edible packaging or coating due to its existing film forming ability without any additives. The chitosan films exhibit good gas barrier and mechanical properties which are comparable with those of many commercial polymers.[2] It cannot be used as packaging material due to its hydrophilicity. Hence, chitosan can be promoted as a filler with biodegradable, non-toxic, hydrophobic polymers such as poly(lactic acid) (PLA).

Asian Chitin J., **12 (1)**, 5-18 (2016)

*Corresponding author: E-mail: vkatiyar@iitg.ernet.in

JOURNAL OF Applied Polymer SCIENCE

Chitosan from Muga silkworms (*Antheraea assamensis*) and its influence on thermal degradation behavior of poly(lactic acid) based biocomposite films

Akhilesh Kumar Pal, Ananya Das, Vimal Katiyar
Department of Chemical Engineering, Indian Institute of Technology Guwahati, Guwahati, Assam, 781039, India
Correspondence to: V. Katiyar (E-mail: vkatiyar@iitg.ernet.in)

ABSTRACT: The research work is focused on extraction of chitin from Muga silkworms (MS) and its conversion into chitosan by chemical treatment process. The extracted amount of chitin and chitosan from MS were obtained ~8 wt % and ~7 wt %, respectively. Potentiometric titrations, conductometric titrations, elemental analysis, ^{1}H-NMR and FTIR analyses were employed to calculate the degree of deacetylation of chitosan (extracted at 80 °C after 10 h) and found as 77% ± 2, 81% ± 1.8, 82% ± 2.4, 97.77% ± 0.3, and 82% ± 1.8, respectively. The deacetylation process of chitin showed pseudo-first order reaction kinetics and activation energy was estimated as ~15.5 kJ/mole. The extracted chitosan (at 80 °C after 10 h) showed higher crystallinity and improved thermal stability with respect to chitosan extracted from other marine sources. Subsequently, poly(lactic acid) (PLA) and extracted chitosan dispersed biocomposite films were prepared by solution casting method. Significant dispersion of chitosan (extracted at 80 °C after 10 h) micro-particles were observed in biocomposite films using FESEM analysis. Due to chitosan interaction with PLA, significant reduction in thermal degradation and activation energy was observed during nonisothermal degradation scan of such films using Flynn-Wall-Ozawa and Kissinger-Akahira-Sunose models. © 2016 Wiley Periodicals, Inc. J. Appl. Polym. Sci. **2016**, *133*, 43710.

KEYWORDS: biodegradable; composites; degradation; films; polysaccharides

Received 18 December 2015; accepted 28 March 2016
DOI: 10.1002/app.43710

INTRODUCTION

Chitin is a natural, inflexible and nitrogenous polysaccharide with long-chain polymer of N-acetyl glucosamine (GlcNac), which is a derivative of glucose.[1–6] Chitin is found in the exoskeletons of insects and marine creatures such as crabs, lobsters, shrimps, fungi, etc.[7–9] The arrangement of polar functional groups such as acetyl and hydroxyl groups may allow the intermolecular hydrogen bonding among adjacent polymeric chains which can further enhance the miscibility of chitin with polar polymer matrix. The preferred extraction technique of chitin can be chemical method over biological method due to cost effectiveness, lesser time consumption and higher yield. Before chemical treatment, it is necessary to remove impurities like dust, dry flesh, soluble and insoluble components. So far, the highest yield of chitin ~46 wt % was obtained from squid pens and the lowest yield ~2.3 wt % was reported from *Saccharomyces gutulata* among various other microbial sources.[3,7–9]

Deacetylation is a direct conversion step from chitin into chitosan and degree of deacetylation (DD %) suggests the possible fraction of both acetylated as well as deacetylated pendent groups on its repeat unit. Due to this, chitosan is also known as copolymer of glucosamine and acetylated glucosamine units which exhibit versatile properties like biodegradability, biocompatibility and low toxicity on the basis of its origin.[2,5,8,10–15] If the DD % of this copolymer is less than 50%, it is termed as chitin which is insoluble in most of the organic and inorganic solvents, otherwise it is entitled as chitosan which is hydrophilic in nature and soluble in weak acidic aqueous solutions such as acetic, nitric and phosphoric acids. The expansion, aggregation and stiffness of the macromolecular chains strongly depend on the DD %, whereas DD % can be regulated by tuning deacetylation reaction parameters such as temperature, reaction time, and solvent concentration.

The amine group at C-2 position in chitosan has unique properties which have raised its consumption in many applications such as packaging, agriculture, food, cosmetics, textiles, pharmaceutical, biomedical and refinement of industrial effluents.[7,16] Due to its biocompatible and biodegradable properties, it is used in cotton membranes for wound dressing which gradually wear off with time as it heals.[17] Chitin and chitosan are fungistatic in nature and hence, are compatible with lots of biologically active components used in cosmetic products. Chitosan can be used preferentially in sunscreen lotions due to covalently

Article

pubs.acs.org/Biomac

Nanoamphiphilic Chitosan Dispersed Poly(lactic acid) Bionanocomposite Films with Improved Thermal, Mechanical, and Gas Barrier Properties

Akhilesh Kumar Pal and Vimal Katiyar*

Department of Chemical Engineering, Indian Institute of Technology Guwahati, Assam, India

ABSTRACT: This article demonstrates the synthesis of lactic acid oligomer-grafted-chitosan (OLLA-*g*-CH), a nanoamphiphilic molecule, by in situ condensation polymerization and its effective use as a nanofiller for improvement in multiple properties of poly(lactic acid) (PLA) films, essential for stringent food packaging applications. Fourier transform infrared spectroscopy (FTIR) analysis shows the presence of amide-ester bond at 1539 cm^{-1}, which confirms the structural grafting of OLLA chains with chitosan molecules. This nanoamphiphilic OLLA-*g*-CH molecule act as surfactant containing hydrophilic chitosan head and hydrophobic OLLA tails with average size in the range of ~2−4 nm. Prepared PLA/OLLA-*g*-CH bionanocomposite films appear with uniform dispersion of nanoamphiphilic OLLA-*g*-CH molecules with self-assembled micelles having size as low as ~20 nm and as high as ~150 nm with core−shell morphology in PLA matrix. This nanofiller is found very effective toward significant reduction in oxygen permeability (OP) by ~10-fold due to the reduction in solubility of oxygen molecules and improvement in crystal nucleation density due to availability of nanonucleating sites. Ultimate tensile strength (UTS) of PLA/OLLA-*g*-CH bionanocomposite films are relatively comparable to that of PLA, however, elongation at break is improved significantly. The onset of thermal degradation of PLA/(OLLA-*g*-CH) films is also found comparable to that of PLA film. The glass transition temperature (T_g) of bionanocomposites is decreased by more than 18 °C with increase in OLLA-*g*-CH loading, which indicates the improved plasticization characteristics of PLA matrix. The crystallization kinetics suggest nonthree dimensional truncated spherical structures, which is controlled by the combination of thermal and athermal instantaneous nucleations. POM analysis suggested that the spherulite growth of PLA is improved significantly with the addition of OLLA-*g*-CH. The reduction in T_g of PLA with improvement in elongation at break and multifold reduction in oxygen permeability offers this bionanocomposite films, a promising candidate for stringent food packaging applications.

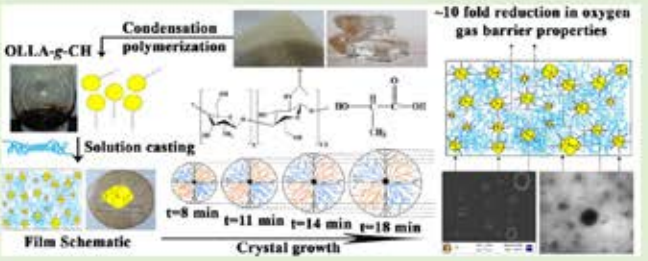

1. INTRODUCTION

Development of biocompatible and biodegradable films with high gas barrier properties are essential for its uses in stringent food packaging applications. Generally, packaging is essential to protect food from the environmental damage. Plastics are preferred for packaging applications due to their lightweight and comparable properties than other packages made of glass, metal, wood, ceramic, etc. Various existing conventional synthetic plastics such as polyethylene terephthalate (PET), polypropylene (PP), polyethylene (PE), polybutylene succinate (PBS), and polypropylene carbonate (PPC) can be either made by addition polymerization or condensation polymerization from petrochemical feedstock. These plastics are considered nondegradable at different levels in the environment which can probably imbalance the ecological and environmental CO_2 cycle and also create health issues for humans and other living creatures.[1] To overcome such problems, the significant efforts are under way to develop new degradable polymeric products and its processes, which can possibly reduce the environment-related hazards. In this regard, aliphatic polyesters such as poly(lactic acid) (PLA), polyglycolic acid (PGA), polycaprolactone (PCL), and polyhydroxyalkanoates (PHA) are the most popular polymers in current scenario due to their biodegradable characteristics and origin from biobased resources which further help to reduce carbon footprint. However, it has been realized that the combination of above-mentioned polymers with biopolymers, can be an alternative of petrochemical based polymers which are currently used for food packaging. Therefore, chemical modification of bioplastics is one of the smart techniques by which hydrophilic biopolymers can be dispersed in hydrophobic polymers in order to tailor the required properties.[2] Hence, tailored bioplastics can be the most promising candidate as an additive for future Bioplastic applications.[3]

PLA, a synthetic environment friendly biobased polymer, can be synthesized using lactic acid (2-hydroxy propionic acid) (LA), has earned the maximum engrossment due to its renewable natural resources like corn, sweet potato, wheat,

Received: May 1, 2016
Revised: June 22, 2016
Published: June 22, 2016

DOI: 10.1021/acs.biomac.6b00619
Biomacromolecules 2016, 17, 2603−2618

International Journal of Biological Macromolecules 95 (2017) 1267–1279

Contents lists available at ScienceDirect

International Journal of Biological Macromolecules

journal homepage: www.elsevier.com/locate/ijbiomac

Thermal degradation behaviour of nanoamphiphilic chitosan dispersed poly (lactic acid) bionanocomposite films

Akhilesh Kumar Pal, Vimal Katiyar*

Department of Chemical Engineering, Indian Institute of Technology Guwahati, Assam, 781039, India

ARTICLE INFO

Article history:
Received 28 August 2016
Received in revised form 5 October 2016
Accepted 1 November 2016
Available online 11 November 2016

Keywords:
Poly (lactic acid)
Nanoamphiphilic chitosan
Thermal degradation kinetics

ABSTRACT

In the present study, nano-amphiphilic chitosan termed as chitosan-*grafted*-oligo L-lactic acid (CH-*g*-OLLA), is synthesized by microwave initiated insitu condensation polymerization. The synthesized CH-*g*-OLLA becomes hydrophobic in nature due to chemical bond formation between chitosan backbone and OLLA chains. Further, CH-*g*-OLLA (30%) bionanocomposite is used as a nanofiller in poly (lactic acid)/chitosan-*grafted*-oligo L-lactic acid (PLA/CH-*g*-OLLA) bionanocomposite films. Surface morphology shows a homogeneous dispersion of CH-*g*-OLLA in the form of spherical aggregates, which vary in the range of ~20 to 150 nm. Non-isothermal degradation kinetics, proposed by Kissinger, Kissinger-Akahira-Sunose, Flynn-Wall-Ozawa and Augis & Bennett models, are utilized to estimate the activation energies (E_a) for PLA, which are 254.1, 260.2, 257.0 and 259.1 kJ mol^{-1} respectively. The reduction in E_a values of bionanocomposite films may be elucidated by intermolecular distance and enrichment in chain mobility. The evolved gaseous products like hydrocarbons, carbon dioxide, carbon monoxide and cyclic oligomers are successfully identified with TG-FTIR analysis.

1. Introduction

Reuse and recycling is a growing area of research which enhances value to the non-degradable polymeric waste. The environmental impact of degradable conventional synthetic polymers (considering time scale) are increasing continuously due to their huge applications in daily life. Biodegradable polyesters are explored as an alternative to replace the synthetic polymers to improve the environmental balance. One of the potential candidate among biodegradable polymers i.e. Poly lactic acid (PLA) is utilized in various applications due to its origin. PLA, a polymer of 2-hydroxy propanoic acid, is extracted from renewable resources e.g. corn, sweet potato and sugar cane. It is completely biodegradable, biocompostable, bioabsorbable and non-toxic with comparable mechanical properties to those of commercial polymers. It is also acquired much awareness for its use in medical, pharmaceutical and other consumer goods [1]. PLA is hydrophobic in nature with excellent transparency, which is required for food packaging applications. The limitations of PLA are its thermal and photo-stability, which restrict the use of PLA for most engineering applications. The associated reason is that the repeat unit of aliphatic ester in PLA is sensitive to heat and easily breakdown during hydrolysis [1–3]. Hence, thermal degradation analysis is a unique part to understand the thermal behaviour of PLA with its degradation mechanism and formed products in the interest of the improvement in thermal stability of PLA. Various components such as molecular weight distribution, residual oligomers & monomers and metal catalyst influence the thermal degradation of PLA [4]. According to the available literatures, the degradation products of PLA are mainly composed of cyclic oligomers with lactides having other products like acetaldehyde, carbon monoxide, carbon dioxide and ketene [1,5]. Many researchers have performed thermal degradation kinetics study for PLA and its composites films [1,4,5]. Aoyagi et al., has calculated the activation energy (E_a) value in the range of 80–160 kJ mol^{-1} for PLA, which increases with an increase in conversion values and finally concluded that degradation of PLA follows two mechanisms [6]. Wu et al., has studied the deviation in thermal stability of PLA by adding multi-walled carbon nanotubes (MWCNTs) as a filler. They have concluded that the change in thermal stability was very less at the initial degradation stage. However, it has improved slightly at higher degradation level [7]. Another study on thermal degradation was conducted by Wu et al., by using poly lactide/clay nanocomposites (PLACNs) and found the reduction in thermal stability with increasing clay content in PLA matrix [8]. Li et al., has used Flynn-Wall-Ozawa and invariant kinetic parameter (IKP) methods to calculate the E_a values of

* Corresponding author.
E-mail address: vkatiyar@iitg.ernet.in (V. Katiyar).

http://dx.doi.org/10.1016/j.ijbiomac.2016.11.024
0141-8130/

Data in Brief 10 (2017) 304–311

Contents lists available at ScienceDirect

Data in Brief

journal homepage: www.elsevier.com/locate/dib

Data Article

Theoretical and analyzed data related to thermal degradation kinetics of poly (L-lactic acid)/chitosan-*grafted*-oligo L-lactic acid (PLA/CH-g-OLLA) bionanocomposite films

Akhilesh Kumar Pal, Vimal Katiyar*

Department of Chemical Engineering, Indian Institute of Technology Guwahati, Guwahati, Assam 781039, India

ARTICLE INFO

Article history:
Received 11 November 2016
Received in revised form
19 November 2016
Accepted 30 November 2016
Available online 7 December 2016

Keywords:
Poly (lactic acid)
Chitosan
Isoconversional method
Thermal degradation kinetics
Activation energy

ABSTRACT

The theoretical and analyzed data incorporated in this article are related to the recently published research article entitled "Thermal degradation behaviour of nanoamphiphilic chitosan dispersed poly (lactic acid) bionanocomposite films" (http://dx.doi.org/10.1016/j.ijbiomac.2016.11.024) (A.K. Pal, V. Katiyar, 2016) [1]. Supplementary information and data (both raw and analyzed) are related to thermal degradation kinetics and explains various model fitting and is conversional methods, which are used in this research work to enhance the knowledge about degradation behaviour of PLA/CH-g-OLLA bionanocomposite system. Non-isothermal degradation kinetics of such polymeric system was proposed using Kissinger, Kissinger–Akahira–Sunose, Flynn–Wall–Ozawa and Augis and Bennett models to estimate the activation energies (E_α) and R^2 values.

Specifications Table

Subject area	Material Sciences
More specific subject area	Polymer degradation
Type of data	Text file, equations and tables

DOI of original article: http://dx.doi.org/10.1016/j.ijbiomac.2016.11.024
* Corresponding author.
E-mail address: vkatiyar@iitg.ernet.in (V. Katiyar).

http://dx.doi.org/10.1016/j.dib.2016.11.100
2352-3409/

POLYMERS FOR PACKAGING APPLICATIONS

Edited by

Sajid Alavi, PhD, Sabu Thomas, PhD, K. P. Sandeep, PhD, Nandakumar Kalarikkal, PhD, Jini Varghese, and Srinivasarao Yaragalla

Apple Academic Press

TORONTO NEW JERSEY

CONTENTS

Bio-based Plastics for Food Packaging Applications

Editor:
Vimal Katiyar

SMITHERS PIRA

A Smithers Group Company

Shawbury, Shrewsbury, Shropshire, SY4 4NR, United Kingdom
Telephone: +44 (0)1939 250383 Fax: +44 (0)1939 251118
http://www.polymer-books.com

First Published in 2017 by

Smithers Pira
Shawbury, Shrewsbury, Shropshire, SY4 4NR, UK

A catalogue record for this book is available from the British Library.

ISBN: 978-1-91024-258-2 (hardback)
978-1-91108-836-3 (softback)
978-1-91024-259-9 (ebook)

Typeset by Argil Services